Classification of topological quantum matter with symmetries

Ching-Kai Chiu[*]

Department of Physics and Astronomy, University of British Columbia, Vancouver, BC, Canada V6T 1Z1, and Condensed Matter Theory Center and Joint Quantum Institute, Department of Physics, University of Maryland, College Park, Maryland 20742, USA

Jeffrey C. Y. Teo[†]

Department of Physics, University of Virginia, Charlottesville, Virginia 22904, USA

Andreas P. Schnyder[‡]

Max-Planck-Institut für Festkörperforschung, Heisenbergstrasse 1, D-70569 Stuttgart, Germany

Shinsei Ryu[§]

Department of Physics, Institute for Condensed Matter Theory, University of Illinois at Urbana-Champaign, Urbana, Illinois 61801, USA

(published 31 August 2016)

Topological materials have become the focus of intense research in recent years, since they exhibit fundamentally new physical phenomena with potential applications for novel devices and quantum information technology. One of the hallmarks of topological materials is the existence of protected gapless surface states, which arise due to a nontrivial topology of the bulk wave functions. This review provides a pedagogical introduction into the field of topological quantum matter with an emphasis on classification schemes. Both fully gapped and gapless topological materials and their classification in terms of nonspatial symmetries, such as time reversal, as well as spatial symmetries, such as reflection, are considered. Furthermore, the classification of gapless modes localized on topological defects is surveyed. The classification of these systems is discussed by use of homotopy groups, Clifford algebras, K theory, and nonlinear sigma models describing the Anderson (de) localization at the surface or inside a defect of the material. Theoretical model systems and their topological invariants are reviewed together with recent experimental results in order to provide a unified and comprehensive perspective of the field. While the bulk of this article is concerned with the topological properties of noninteracting or mean-field Hamiltonians, a brief overview of recent results and open questions concerning the topological classifications of interacting systems is also provided.

DOI: 10.1103/RevModPhys.88.035005

CONTENTS

[*]chiu7@umd.edu
[†]jteo@virginia.edu
[‡]a.schnyder@fkf.mpg.de
[§]ryuu@illinois.edu

I. INTRODUCTION

In the last decade since the groundbreaking discovery of topological insulators (TIs) induced by strong spin-orbit interactions, tremendous progress has been made in our understanding of topological states of quantum matter. While many properties of condensed matter systems have an analog in classical systems and may be understood without referring to quantum mechanics, topological states and topological phenomena are rooted in quantum mechanics in an essential way: They are states of matter whose quantum mechanical wave functions are topologically nontrivial and distinct from trivial states of matter, i.e., an atomic insulator. The precise meaning of the wave function topology will be elaborated on. The best known example of a topological phase is the integer quantum Hall state, in which protected chiral edge states give rise to a quantized transverse Hall conductivity. These edge states arise due to a nontrivial wave function topology that can be measured in terms of a quantized topological invariant, i.e., the Chern or Thouless–Kohmoto–Nightingale–den Nijs number (Thouless *et al.*, 1982; Kohmoto, 1985). This invariant, which is proportional to the Hall conductivity, remains unchanged under adiabatic

deformations of the system, as long as the bulk gap is not closed. It was long thought that topological states and topological phenomena are rather rare in nature and occur only under extreme conditions. However, with the advent of spin-orbit-induced topological insulators, it became clear that topological quantum states are more ubiquitous than previously thought. In fact, the study of topological aspects has become increasingly widespread in the investigation of insulating and semimetallic electronic structures, unconventional superconductors (SCs), and interacting bosonic and fermionic systems.

Another theme that emerged from spin-orbit-induced topological insulators is the interplay between symmetry and topology. Symmetries play an important role in the Landau-Ginzburg-Wilson framework of spontaneous symmetry breaking for the classification of different states of matter (Wilson and Kogut, 1974; Landau, Lifshitz, and Pitaevskii, 1999). Intertwined with the topology of quantum states, symmetries serve again as an important guiding principle, but in a way that is drastically different from the Landau-Ginzburg-Wilson theory. First, topological insulators cannot be distinguished from ordinary, topologically trivial insulators in terms of their symmetries and their topological nontriviality cannot be detected by a local order parameter. Second, in making a distinction between spin-orbit-induced topological insulators and ordinary insulators, time-reversal symmetry is crucial. That is, in the absence of time-reversal symmetry, it is possible to adiabatically deform spin-orbit-induced topological insulators into a topologically trivial state without closing the bulk gap. For this reason, topological insulators are called symmetry-protected topological (SPT) phases of matter. Roughly speaking, an SPT phase is a short-range entangled gapped phase whose topological properties rely on the presence of symmetries.

A. Overview of topological materials

Let us now give a brief overview of material systems in which topology plays an important role.

First, insulating electronic band structures can be categorized in terms of topology. By now, spin-orbit-induced topological insulators have become classic examples of topological band insulators. In these systems strong spin-orbit interactions open up a bulk band gap and give rise to an odd number of band inversions, thereby altering the wave function topology. Experimentally, this topological quantum state has been realized in HgTe/CdTe semiconductor quantum wells (Bernevig, Hughes, and Zhang, 2006; Konig *et al.*, 2007), in InAs/GaSb heterojunctions sandwiched by AlSb (C. Liu *et al.*, 2008; Knez, Du, and Sullivan, 2011), in BiSb alloys (Hsieh *et al.*, 2008), in Bi_2Se_3 (Hsieh *et al.*, 2009; Xia *et al.*, 2009), and in many other systems (Hasan and Moore, 2011; Ando, 2013). The nontrivial wave function topology of these band insulators manifests itself at the boundary as an odd number of helical edge states or Dirac cone surface states, which are protected by time-reversal symmetry. As first shown by Kane and Mele, the topological properties of these insulators are characterized by a $\mathbb{Z}_2$ invariant (Kane and Mele, 2005a, 2005b; Fu and Kane, 2006, 2007; Fu, Kane, and Mele, 2007; Moore and Balents, 2007; Roy, 2009a, 2009b), in a similar way as the Chern invariant characterizes the integer quantum Hall state. Besides the exotic surface states which completely evade Anderson localization (Bardarson *et al.*, 2007; Nomura, Koshino, and Ryu, 2007; Roushan *et al.*, 2009; Alpichshev *et al.*, 2010), many other novel phenomena have been theoretically predicted to occur in these systems, including axion electrodynamics (Qi, Hughes, and Zhang, 2008; Essin, Moore, and Vanderbilt, 2009), dissipationless spin currents, and proximity-induced topological superconductivity (Fu and Kane, 2008). These novel properties have recently attracted great interest, since they could potentially be used for new technical applications, ranging from spin electronic devices to quantum information technology.

In the case of spin-orbit-induced topological insulators the topological nontriviality is guaranteed by time-reversal symmetry, a nonspatial symmetry that acts locally in position space. However, SPT quantum states can also arise from spatial symmetries, i.e., symmetries that act nonlocally in position space, such as rotation, reflection, or other space-group symmetries (Fu, 2011). One prominent experimental realization of a topological phase with spatial symmetries is the rock-salt semiconductor SnTe, whose Dirac cone surface states are protected by reflection symmetry (Dziawa *et al.*, 2012; Hsieh *et al.*, 2012; Tanaka *et al.*, 2012; Xu *et al.*, 2012).

Second, topological concepts can be applied to unconventional superconductors and superfluids. In fact, there is a direct analogy between TIs and topological superconductors (TSCs). Both quantum states are fully gapped in the bulk, but exhibit gapless conducting modes on their surfaces. In contrast to topological insulators, the surface excitations of topological superconductors are not electrons (or holes), but Bogoliubov quasiparticles, i.e., coherent superpositions of electron and hole excitations. Because of the particle-hole symmetry of superconductors, zero-energy Bogoliubov quasiparticles contain equal parts of electron and hole excitations, and therefore have the properties of Majorana particles. While there exists an abundance of examples of topological insulators, topological superconductors are rare, since an unconventional pairing symmetry is required for a topologically nontrivial state. Nevertheless, topological superconductors have become the subject of intense research, due to their protected Majorana surface states, which could potentially be utilized as basic building blocks of fault-tolerant quantum computers (Nayak *et al.*, 2008). Indeed, there has recently been much effort to engineer topological superconducting states using heterostructures with conventional superconductors (Alicea, 2012; Beenakker, 2013; Stanescu and Tewari, 2013). One promising proposal is to proximity induce p-wave superconductivity in a semiconductor nanowire (Lutchyn, Sau, and Das Sarma, 2010; Oreg, Refael, and von Oppen, 2010; Mourik *et al.*, 2012); another is to use Shiba bound states induced by magnetic adatoms on the surface of an s-wave superconductor (Nadj-Perge *et al.*, 2014). In parallel, there has been renewed interest in the B phase of superfluid ^{3}He, which realizes a time-reversal symmetric topological superfluid. The predicted surface Majorana bound states of ^{3}He-B have been observed using transverse acoustic impedance measurements (Murakawa *et al.*, 2009).

Third, nodal systems, such as semimetals and nodal superconductors, can exhibit nontrivial band topology, even though

the bulk gap closes at certain points in the Brillouin zone (BZ). The Fermi surfaces (superconducting nodes) of these gapless materials are topologically protected by topological invariants, which are defined in terms of an integral along a surface enclosing the gapless points. Similar to fully gapped topological systems, the topological characteristics of nodal materials manifest themselves at the surface in terms of gapless boundary modes. Depending on the symmetry properties and the dimensionality of the bulk Fermi surface, these gapless boundary modes form Dirac cones, Fermi arcs, or flat bands. Topological nodal systems can be protected by nonspatial symmetries (i.e., time-reversal or particle-hole symmetry) as well as spatial lattice symmetries, or a combination of the two. Examples of gapless topological materials include $d_{x^2-y^2}$-wave superconductors (Ryu and Hatsugai, 2002), the A phase of superfluid ^{3}He (Volovik, 2003, 2011), nodal noncentrosymmetric superconductors (Brydon, Schnyder, and Timm, 2011; Schnyder and Ryu, 2011), Dirac materials (Z. Wang *et al.*, 2012; Z. Wang *et al.*, 2013d), and Weyl semimetals (Wan *et al.*, 2011). Recently, it was experimentally shown that the Dirac semimetal is realized in Na_3Bi (Liu *et al.*, 2014b), while the Weyl semimetal is realized in TaAs (Lv *et al.*, 2015; S.-Y. Xu *et al.*, 2015b).

All of the aforementioned topological materials can be understood, at least at a phenomenological level, in terms of noninteracting or mean-field Hamiltonians. While the topological properties of these single-particle theories are reasonably well understood, less is known about the topological characteristics of strongly correlated systems. Recently, a number of strongly correlated materials have been discussed as interacting analogs of topological insulators. Among them are iridium oxide materials (Shitade *et al.*, 2009), transition-metal oxide heterostructures (Xiao *et al.*, 2011), and the Kondo insulator SmB_6 (Dzero *et al.*, 2010, 2012; Wolgast *et al.*, 2013). On the theory side, the Haldane antiferromagnetic spin-1 chain has been identified as an interacting SPT phase. Experimentally, this phase may be realized in some quasi-one-dimensional spin-1 quantum magnets, such as Y_2BaNiO_5 (Darriet and Regnault, 1993) and $Ni(C_2H_8N_2)_2NO_2(ClO_4)$ (Renard *et al.*, 1987).

B. Scope and organization of the review

A major theme of solid-state physics is the classification and characterization of different phases of matter. Many quantum phases, such as superconductors or magnets, can be categorized within the Landau-Ginzburg-Wilson framework, i.e., by the principle of spontaneously broken symmetry. The classification of topological quantum matter, on the other hand, is not based on the broken symmetry, but the topology of the quantum mechanical wave functions (Thouless *et al.*, 1982; Wen, 1990). The ever-increasing number of topological materials and SPT phases, as discussed in the previous section, calls for a comprehensive classification scheme of topological quantum matter.

In this review, we survey recently developed classification schemes of fully gapped and gapless materials and discuss new experimental developments. Our aim is to provide a manual and reference for condensed matter theorists and experimentalists who wish to study the rapidly growing field of topological quantum matter. To exemplify the topological features we discuss concrete model systems together with recent experimental findings. While the main part of this article is concerned with the topological characteristics of quadratic noninteracting Hamiltonians, we will also give a brief overview of established results and open questions regarding the topology of interacting systems.

The outline of the article is as follows. After reviewing symmetries in quantum systems in Sec. II, we start in Sec. III by discussing the topological classification of fully gapped free-fermion systems in terms of nonspatial symmetries, namely, time-reversal symmetry (TRS), particle-hole symmetry (PHS), and chiral symmetry, which define a total of ten symmetry classes (Schnyder *et al.*, 2008; Kitaev, 2009; Ryu, Schnyder *et al.*, 2010). This classification scheme, which is known as the tenfold way, categorizes quadratic Hamiltonians with a given set of nonspatial symmetries into topological equivalence classes. Assuming a full bulk gap, two Hamiltonians are defined to be topologically equivalent, if there exists a continuous interpolation between the two that preserves the symmetries and does not close the energy gap. Different equivalence classes for a given set of symmetries are distinguished by topological invariants, which measure the global phase structure of the bulk wave functions (Sec. III.B). We review how this classification scheme is derived using K theory (Sec. III.C) and nonlinear sigma models describing the Anderson (de)localization at the surface of the material (Sec. III.F). In Sec. III.D we discuss how the classification of gapless modes localized on topological defects can be derived in a similar manner.

Recently, the tenfold scheme has been generalized to include spatial symmetries, in particular, reflection symmetries (Chiu, Yao, and Ryu, 2013; Morimoto and Furusaki, 2013; Shiozaki and Sato, 2014), which is the subject of Sec. IV. In a topological material with spatial symmetries, only those surfaces which are invariant under the spatial symmetry operations can support gapless boundary modes. We review some examples of reflection-symmetry-protected topological systems, in particular, a low-energy model describing the physics of SnTe. This is followed in Sec. V by a description of the topological characteristics of gapless materials, such as semimetals and nodal superconductors, which can be classified in a similar manner as fully gapped systems (Matsuura *et al.*, 2013; Zhao and Wang, 2013; Chiu and Schnyder, 2014; Shiozaki and Sato, 2014). We discuss the topological classification of gapless materials in terms of both nonspatial (Sec. V.A) and spatial symmetries (Sec. V.B).

In Sec. VI, we give a brief overview of various approaches to diagnose and possibly classify interacting SPT phases. Because the field of interacting SPT phases is still rapidly growing, the presentation in this section is less systematic than in the other parts. Interactions can modify the classification in several different ways: (i) Two different phases which are distinct within the free-fermion classification can merge in the presence of interactions, and (ii) interactions can give rise to new topological phases which cannot exist in the absence of correlations. As an example of case (i) we discuss in Sec. VI various topological superconductors in one, two, and three spatial dimensions, where the interaction effects invalidate the

free-fermion classification. Finally, we conclude in Sec. VII, where we give an outlook and mention some omitted topics, such as symmetry-enriched topological phases, fractional topological insulators, and Floquet topological insulators. We also give directions for future research.

Given the constraint of the size of this review and the large literature on topological materials, this article cannot provide a complete coverage of the subject at this stage. For further background and reviews on topological quantum matter beyond the scope of this article, we mention in addition to the Rev. Mod. Phys. articles by Hasan and Kane (2010) and Qi and Zhang (2011), the following works: Volovik (2003), König *et al.* (2008), Moore (2010), Shen (2012), Ando (2013), Bernevig and Hughes (2013), Franz and Molenkamp (2013), Turner and Vishwanath (2013), Witczak-Krempa *et al.* (2014), Zahid Hasan, Xu, and Neupane (2014), Ando and Fu (2015), Hasan, Xu, and Bian (2015), Mizushima *et al.* (2015), Schnyder and Brydon (2015), and Senthil (2015). There are also a number of reviews on the subject of Majorana fermions (Alicea, 2012; Beenakker, 2013; Stanescu and Tewari, 2013; Elliott and Franz, 2015).

II. SYMMETRIES

In this section, we review how different symmetries are implemented in fermionic systems. Let $\{\hat{\psi}_I, \hat{\psi}_I^\dagger\}_{I=1,\ldots,N}$ be a set of fermion annihilation or creation operators. Here we imagine for ease of notation that we have "regularized" the system on a lattice, and $I, J, \ldots$ are combined labels for the lattice sites $i, j, \ldots$, and if relevant, of additional quantum numbers, such as, e.g., a Pauli-spin quantum number [e.g., $I = (i, \sigma)$ with $\sigma = \pm 1/2$]. The creation and annihilation operators satisfy the canonical anticommutation relation $\{\hat{\psi}_I, \hat{\psi}_J^\dagger\} = \delta_{IJ}$.

Let us now consider a general noninteracting system of fermions described by a "second quantized" Hamiltonian $\hat{H}$. For a nonsuperconducting system, $\hat{H}$ is given generically as

$$\hat{H} = \hat{\psi}_I^\dagger H^{IJ} \hat{\psi}_J \equiv \hat{\psi}^\dagger H \hat{\psi}, \tag{2.1}$$

where the $N \times N$ matrix H^{IJ} is the "first quantized" Hamiltonian. In the second expression of Eq. (2.1) we adopt Einstein's convention of summation on repeated indices, while in the last expression in Eq. (2.1) we use matrix notation. [Similarly, a superconducting system is described by a Bogoliubov–de Gennes (BdG) Hamiltonian, for which we use Nambu spinors instead of complex fermion operators, and whose first quantized form is again a matrix H when discretized on a lattice.]

According to the symmetry representation theorem by Wigner, any symmetry transformation in quantum mechanics can be represented on the Hilbert space by an operator that is either linear and unitary, or antilinear and antiunitary. We start by considering an example of a unitary symmetry, described by a set of operators $\{G_1, G_2, \ldots\}$ which form a group. The Hilbert space must then be a representation of this group with $\{\hat{\mathcal{G}}_1, \hat{\mathcal{G}}_2, \ldots\}$ denoting the operators acting on the Hilbert space. For our purposes, it is convenient to introduce the symmetry transformations in terms of their action on fermionic operators. That is, we consider a linear transformation

$$\hat{\psi}_I \to \hat{\psi}'_I \coloneqq \hat{\mathcal{U}} \hat{\psi}_I \hat{\mathcal{U}}^{-1} = U_I{}^J \hat{\psi}_J, \tag{2.2}$$

where $\hat{\mathcal{U}}$ and $\hat{\psi}_I, \hat{\psi}_I^\dagger$ are second quantized operators that act on states in the fermionic Fock space. $U_I{}^J$, however, is "a collection of numbers," i.e., not a second quantized operator. (More general possibilities, where a unitary symmetry operator mixes $\hat{\psi}$ and $\hat{\psi}^\dagger$, will be discussed later.) Now, the system is invariant under $\hat{\mathcal{U}}$ if the canonical anticommutation relation and $\hat{H}$ are preserved, $\{\hat{\psi}_I, \hat{\psi}_J^\dagger\} = \hat{\mathcal{U}}\{\hat{\psi}_I, \hat{\psi}_J^\dagger\}\hat{\mathcal{U}}^{-1}$ and $\hat{\mathcal{U}}\hat{H}\hat{\mathcal{U}}^{-1} = \hat{H}$. The former condition implies that $U_I{}^J$ is a unitary matrix, while the latter leads to $U_K^*{}^I H^{KL} U_L{}^J = H^{IJ}$, or $U^\dagger H U = H$ in matrix notation.

The unitary symmetry operation $\hat{\mathcal{U}}$ is called *spatial* (*nonspatial*) when it acts (does not act) on the spatial part (i.e., the lattice site labels $i, j, \ldots$) of the collective indices $I, J, \ldots$. In particular, when $\hat{\mathcal{U}}$ can be factorized as $\hat{\mathcal{U}} = \prod_i \hat{\mathcal{U}}_i$, i.e., when it acts on each lattice site separately, it is nonspatial and is called on site. A similar definition also applies to antiunitary symmetry operations. In this section, we focus on nonspatial symmetries, i.e., "internal" symmetries, such as time-reversal symmetry. Spatial symmetries are discussed in Sec. IV.

Note that the unitary symmetry of the kind considered in Eq. (2.2) is a global (i.e., nongauge) symmetry. As seen in Sec. VI, local (i.e., gauge) symmetries will play a crucial role as a probe for SPT phases.

A. Time-reversal symmetry

Let us now consider TRS. Time reversal $\hat{\mathcal{T}}$ is an antiunitary operator that acts on the fermion creation and annihilation operators as

$$\hat{\mathcal{T}} \hat{\psi}_I \hat{\mathcal{T}}^{-1} = (U_T)_I{}^J \hat{\psi}_J, \qquad \hat{\mathcal{T}} i \hat{\mathcal{T}}^{-1} = -i. \tag{2.3}$$

[One could in principle have $\hat{\psi}^\dagger$ appearing on the right-hand side of Eq. (2.3). But this case can be treated as a combination of TR and PH.] A system is TR invariant if $\hat{\mathcal{T}}$ preserves the canonical anticommutator and if the Hamiltonian satisfies $\hat{\mathcal{T}}\hat{H}\hat{\mathcal{T}}^{-1} = \hat{H}$. Note that if a Hermitian operator $\hat{O}$, built out of fermion operators, is preserved under $\hat{\mathcal{T}}$, then $\hat{\mathcal{T}}\hat{H}\hat{\mathcal{T}}^{-1} = \hat{H}$ implies that $\hat{\mathcal{T}}\hat{O}(t)\hat{\mathcal{T}}^{-1} = \hat{\mathcal{T}} e^{+i\hat{H}t}\hat{O}e^{-i\hat{H}t}\hat{\mathcal{T}}^{-1} = \hat{O}(-t)$. In noninteracting systems, the condition $\hat{\mathcal{T}}\hat{H}\hat{\mathcal{T}}^{-1} = \hat{H}$ leads to

$$\hat{\mathcal{T}}\colon\ U_T^\dagger H^* U_T = +H. \tag{2.4}$$

Because any given Hamiltonian has many accidental, i.e., nongeneric, symmetries, we consider in the following entire parameter families (i.e., ensembles) of Hamiltonians, whose symmetries are generic. Such an ensemble of Hamiltonians with a given set of generic symmetries is called a *symmetry class*. We now let H run over all possible single-particle Hamiltonians of such a symmetry class with TRS. Applying the TRS condition (2.4) twice, one obtains $(U_T^* U_T)^\dagger H (U_T^* U_T) = H$. Since the first quantized

Hamiltonian H runs over an irreducible representation space, $U_T^* U_T$ should be a multiple of the identity matrix $\mathbb{1}$ due to Schur's lemma, i.e., $U_T^* U_T = e^{i\alpha}\mathbb{1}$. Since U_T is a unitary matrix, it follows that $U_T^* = e^{i\alpha} U_T^\dagger \Rightarrow (U_T)^T = e^{i\alpha} U_T$. Hence, we find $e^{2i\alpha} = 1$, which leads to the two possibilities $U_T^* U_T = \pm\mathbb{1}$. Thus, acting on a fermion operator $\hat{\psi}_I$ with $\hat{\mathcal{T}}^2$ simply reproduces $\hat{\psi}_I$, possibly up to a sign $\hat{\mathcal{T}}^2 \hat{\psi}_I \hat{\mathcal{T}}^{-2} = (U_T^* U_T \hat{\psi})_I = \pm\hat{\psi}_I$. Similarly, for an operator consisting of n fermion creation and annihilation operators $\hat{\mathcal{T}}^2 \hat{O} \hat{\mathcal{T}}^{-2} = (\pm)^n \hat{O}$. To summarize, TR operation $\hat{\mathcal{T}}$ satisfies

$$\hat{\mathcal{T}}^2 = (\pm 1)^{\hat{N}} \quad \text{when } U_T^* U_T = \pm\mathbb{1}, \tag{2.5}$$

where $\hat{N} \coloneqq \sum_I \hat{\psi}_I^\dagger \hat{\psi}_I$ is the total fermion number operator. In particular, when $U_T^* U_T = -\mathbb{1}$, $\hat{\mathcal{T}}$ squares to the fermion number parity defined by

$$\hat{\mathcal{G}}_f \coloneqq (-1)^{\hat{N}}. \tag{2.6}$$

For systems with $\hat{\mathcal{T}}^2 = -1$ (i.e., for systems with an odd number of fermions and $\hat{\mathcal{T}}^2 = \hat{\mathcal{G}}_f$), TR invariance leads to the Kramers degeneracy of the eigenvalues, which follows from the famous Kramers theorem.

B. Particle-hole symmetry

Particle hole $\hat{\mathcal{C}}$ is a unitary transformation that mixes fermion creation and annihilation operators:

$$\hat{\mathcal{C}} \hat{\psi}_I \hat{\mathcal{C}}^{-1} = (U_C^*)_I{}^J \hat{\psi}_J^\dagger. \tag{2.7}$$

$\hat{\mathcal{C}}$ is also called charge conjugation, since in particle-number conserving systems, it flips the sign of the $U(1)$ charge $\hat{\mathcal{C}}\,\hat{Q}\,\hat{\mathcal{C}}^{-1} = -\hat{Q}$, where $\hat{Q} \coloneqq \hat{N} - N/2$ and $N/2$ is half the number of "orbitals," i.e., half the dimension of the single-particle Hilbert space. Requiring that the canonical anticommutation relation is invariant under $\hat{\mathcal{C}}$, one finds that U_C is a unitary matrix. For the case of a noninteracting Hamiltonian $\hat{H}$, PHS leads to the condition $\hat{H} = \hat{\mathcal{C}}\,\hat{H}\,\hat{\mathcal{C}}^{-1} = -\hat{\psi}^\dagger (U_C^\dagger H^T U_C)\hat{\psi} + \mathrm{Tr}H$, which implies

$$\hat{\mathcal{C}}\colon\ U_C^\dagger H^T U_C = -H. \tag{2.8}$$

Observe from Eq. (2.8) it follows that $\mathrm{Tr}H = H^{II} = 0$. Since H is Hermitian, this PHS condition for single-particle Hamiltonians may also be written as $-U_C^\dagger H^* U_C = H$. Inspection of Eq. (2.8) reveals that $\hat{\mathcal{C}}$ when acting on a single-particle Hilbert space, is not a unitary symmetry, but rather a reality condition on the Hamiltonian H modulo unitary rotations. By repeating the same arguments as in the case of TRS, we find that there are two kinds of PH transformations:

$$\hat{\mathcal{C}}^2 = (\pm 1)^{\hat{N}} \quad \text{when } U_C^* U_C = \pm\mathbb{1}. \tag{2.9}$$

In PH symmetric systems $\hat{H}$, where $\hat{\mathcal{C}}\,\hat{H}\,\hat{\mathcal{C}}^{-1} = \hat{H}$, the particle-hole reversed partner $\hat{\mathcal{C}}|\alpha\rangle$ of every eigenstate $|\alpha\rangle$ of $\hat{H}$ is also an eigenstate, since $\hat{\mathcal{C}}\,\hat{H}\,\hat{\mathcal{C}}^{-1}\hat{\mathcal{C}}|\alpha\rangle = E_\alpha \hat{\mathcal{C}}|\alpha\rangle$. Similarly, for single-particle Hamiltonians, it follows that for every eigenwave function u^A of H with single-particle energy ε^A, $H^{IJ} u_J^A = \varepsilon^A u_I^A$, its particle-hole reversed partner $U_C^\dagger (u^A)^*$ is also an eigenwave function, but with energy $-\varepsilon^A$, since $U_C^\dagger H^* U_C U_C^\dagger (u^A)^* = \varepsilon^A U_C^\dagger (u^A)^*$.

As an example of a PH symmetric system, we examine the Hubbard model defined on a bipartite lattice

$$\hat{H} = \sum_{ij}^{i\neq j} \sum_\sigma t_{ij} \hat{c}_{i\sigma}^\dagger \hat{c}_{j\sigma} - \mu \sum_i \sum_\sigma \hat{n}_{i\sigma} + U \sum_i \hat{n}_{i\uparrow} \hat{n}_{i\downarrow}, \tag{2.10}$$

where $\hat{c}_{i\sigma}^\dagger$ is the electron creation operator at lattice site i with spin $\sigma = \uparrow/\downarrow$ and $\hat{n}_{i\sigma} = \hat{c}_{i\sigma}^\dagger \hat{c}_{i\sigma}$. Here $t_{i,j} = t_{ji}^*$, μ, and U denote the hopping matrix element, the chemical potential, and the interaction strength, respectively. Now consider the following PH transformation: $\hat{\mathcal{C}} \hat{c}_{i\sigma} \hat{\mathcal{C}}^{-1} = (-1)^i \hat{c}_{i\sigma}^\dagger$, $\hat{\mathcal{C}} \hat{c}_{i\sigma}^\dagger \hat{\mathcal{C}}^{-1} = (-1)^i \hat{c}_{i\sigma}$, where the sign $(-1)^i$ is $+1$ (-1) for sites i belonging to sublattice A (B). The Hamiltonian (2.10) is invariant under $\hat{\mathcal{C}}$ when the t_{ij}'s connecting sites from the same (different) sublattice are imaginary (real) and $\mu = U/2$.

C. Chiral symmetry

The combination of $\hat{\mathcal{T}}$ with $\hat{\mathcal{C}}$ leads to a third symmetry, the so-called chiral symmetry. That is, one can have a situation where both $\hat{\mathcal{T}}$ and $\hat{\mathcal{C}}$ are broken, but their combination is satisfied

$$\hat{\mathcal{S}} = \hat{\mathcal{T}} \cdot \hat{\mathcal{C}}. \tag{2.11}$$

Chiral symmetry $\hat{\mathcal{S}}$ acts on fermion operators as

$$\hat{\mathcal{S}} \hat{\psi}_I \hat{\mathcal{S}}^{-1} = (U_C U_T)_I{}^J \hat{\psi}_J^\dagger. \tag{2.12}$$

It follows from $\hat{\mathcal{S}}\,\hat{H}\,\hat{\mathcal{S}}^{-1} = \hat{H}$ that the invariance of a quadratic Hamiltonian H under $\hat{\mathcal{S}}$ is described by

$$\hat{\mathcal{S}}\colon\ U_S^\dagger H U_S = -H, \quad \text{where } U_S = U_C^* U_T^*. \tag{2.13}$$

Note that $\mathrm{Tr}H = 0$ follows immediately from Eq. (2.13). Applying the same reasoning that we used to derive $\hat{\mathcal{T}}^2 = \hat{\mathcal{C}}^2 = (\pm)^{\hat{N}}$, we find that $U_S^2 = e^{i\alpha}\mathbb{1}$. By redefining $U_S \to e^{i\alpha/2} U_S$, the chiral symmetry condition for single-particle Hamiltonians simplifies to

$$\hat{\mathcal{S}}\colon \{H, U_S\} = 0, \qquad U_S^2 = U_S^\dagger U_S = \mathbb{1}. \tag{2.14}$$

With this, one infers that the eigenvalues of the chiral operator are ± 1. Additionally, one may impose the condition $\mathrm{Tr}U_S = 0$, which, however, is not necessary (see later for an example). Chiral symmetry gives rise to a symmetric spectrum of single-particle Hamiltonians: if $|u\rangle$ is an eigenstate of H with eigenvalue ε, then $U_S|u\rangle$ is also an eigenstate, but with eigenvalue $-\varepsilon$. In the basis in which U_S is diagonal, the single-particle Hamiltonian H is block off-diagonal,

$$H = \begin{pmatrix} 0 & D \\ D^\dagger & 0 \end{pmatrix}, \tag{2.15}$$

where D is a $N_A \times N_B$ rectangular matrix with $N_A + N_B = N$.

As an example, let us consider a tight-binding Hamiltonian of spinless fermions on a bipartite lattice:

$$\hat{H} = \sum_{m,n} t_{mn} \hat{c}_m^\dagger \hat{c}_n, \qquad t_{mn} = t_{nm}^* \in \mathbb{C}. \tag{2.16}$$

To construct a chiral symmetry we combine the PH transformation discussed in Eq. (2.10) (but drop the spin degree of freedom σ) with TRS for spinless fermions, which is defined as $\hat{\mathcal{T}} \hat{c}_m \hat{\mathcal{T}}^{-1} = \hat{c}_m$, with $\hat{\mathcal{T}} i \hat{\mathcal{T}} = -i$. This leads to the symmetry condition $\hat{\mathcal{S}} \hat{c}_m \hat{\mathcal{S}}^{-1} = (-)^m \hat{c}_m^\dagger$, with $\hat{\mathcal{S}} i \hat{\mathcal{S}}^{-1} = -i$. Hence, $\hat{H}$ is invariant under $\hat{\mathcal{S}}$ when t_{mn} is a bipartite hopping, i.e., when t_{mn} only connects sites on different sublattices. Observe that in this example $\mathrm{Tr} U_S = N_A - N_B$, where $N_{A/B}$ is the number of sites on sublattice A/B.

Besides the bipartite hopping model (Gade and Wegner, 1991; Gade, 1993), chiral symmetry is realized in BdG systems with TRS and S_z conservation (Foster and Ludwig, 2008) and in QCD (Verbaarschot, 1994). Chiral symmetry also appears in bosonic systems (Dyson, 1953; Gurarie and Chalker, 2002, 2003; Kane and Lubensky, 2014) and in entanglement Hamiltonians (Turner, Zhang, and Vishwanath, 2010; Hughes, Prodan, and Bernevig, 2011; Chang, Mudry, and Ryu, 2014).

D. BdG systems

Important examples of systems with PHS and chiral symmetry are BdG Hamiltonians, which we discuss in this section. These BdG examples demonstrate that physically different symmetry conditions at the many-body level may lead to the same set of constraints on single-particle Hamiltonians.

1. Class D

BdG Hamiltonians are defined in terms of Nambu spinors,

$$\hat{\Upsilon} = \begin{pmatrix} \hat{\psi}_1 \\ \vdots \\ \hat{\psi}_N \\ \hat{\psi}_1^\dagger \\ \vdots \\ \hat{\psi}_N^\dagger \end{pmatrix}, \quad \hat{\Upsilon}^\dagger = (\hat{\psi}_1^\dagger, \ldots, \hat{\psi}_N^\dagger, \hat{\psi}_1, \ldots, \hat{\psi}_N), \tag{2.17}$$

which satisfy the canonical anticommutation relation $\{\hat{\Upsilon}_A, \hat{\Upsilon}_B^\dagger\} = \delta_{AB}$ $(A, B = 1, \ldots, 2N)$. It is important to note that $\hat{\Upsilon}$ and $\hat{\Upsilon}^\dagger$ are not independent, but are related to each other by

$$(\tau_1 \hat{\Upsilon})^T = \hat{\Upsilon}^\dagger, \qquad (\hat{\Upsilon}^\dagger \tau_1)^T = \hat{\Upsilon}, \tag{2.18}$$

where the Pauli matrix τ_1 acts on Nambu space. Using Nambu spinors, the BdG Hamiltonian $\hat{H}$ is written as

$$\hat{H} = \tfrac{1}{2} \hat{\Upsilon}_A^\dagger H^{AB} \qquad \hat{\Upsilon}_B = \tfrac{1}{2} \hat{\Upsilon}^\dagger H \hat{\Upsilon}. \tag{2.19}$$

Since $\hat{\Upsilon}$ and $\hat{\Upsilon}^\dagger$ are not independent, the single-particle Hamiltonian H must satisfy a constraint. Using Eq. (2.18), we obtain $\hat{H} = (1/2)(\tau_1 \hat{\Upsilon})^T H (\hat{\Upsilon}^\dagger \tau_1)^T = -(1/2) \hat{\Upsilon}^\dagger (\tau_1 H \tau_1)^T \hat{\Upsilon} + (1/2) \mathrm{Tr}(\tau_1 H \tau_1)$, which yields

$$\tau_1 H^T \tau_1 = -H. \tag{2.20}$$

Thus, every single-particle BdG Hamiltonian satisfies PHS of the form (2.8). However, condition (2.20) does not arise due to an imposed symmetry, but is rather a "built-in" feature of BdG Hamiltonians that originates from Fermi statistics. For this reason, $\tau_1 H^T \tau_1 = -H$ in BdG systems should be called a particle-hole constraint, or Fermi constraint (Kennedy and Zirnbauer, 2016), and not a symmetry. Because of Eq. (2.20), any BdG Hamiltonian can be written as

$$H = \begin{pmatrix} \Xi & \Delta \\ -\Delta^* & -\Xi^T \end{pmatrix}, \qquad \Xi = \Xi^\dagger, \qquad \Delta = -\Delta^T, \tag{2.21}$$

where Ξ represents the "normal" part and Δ is the "anomalous" part (i.e., the pairing term).

BdG Hamiltonians can be thought of as single-particle Hamiltonians of Majorana fermions. The Majorana representation of BdG Hamiltonians is obtained by letting

$$\begin{pmatrix} \hat{\lambda}_I \\ \hat{\lambda}_{I+N} \end{pmatrix} = \begin{pmatrix} \hat{\psi}_I + \hat{\psi}_I^\dagger \\ i(\hat{\psi}_I - \hat{\psi}_I^\dagger) \end{pmatrix}, \tag{2.22}$$

where $\hat{\lambda}$ are Majorana fermions satisfying

$$\{\hat{\lambda}_A, \hat{\lambda}_B\} = 2\delta_{AB}, \qquad \hat{\lambda}_A^\dagger = \hat{\lambda}_A \quad (A, B = 1, \ldots, 2N). \tag{2.23}$$

In this Majorana basis, the BdG Hamiltonian can be written as

$$\hat{H} = i \hat{\lambda}_A X^{AB} \hat{\lambda}_B, \qquad X^* = X, \qquad X^T = -X. \tag{2.24}$$

The $4N \times 4N$ matrix X can be expressed in terms of Ξ and Δ as

$$iX = \frac{1}{2} \begin{pmatrix} R_- + S_- & -i(R_+ - S_+) \\ i(R_+ + S_+) & R_- - S_- \end{pmatrix},$$

where

$$R_\pm = \Xi \pm \Xi^T = \pm R_\pm^T, \qquad S_\pm = \Delta \pm \Delta^* = -S_\pm^T. \tag{2.25}$$

We note that the real skew-symmetric matrix X can be brought into a block diagonal form by an orthogonal transformation, i.e.,

$$X = O\Sigma O^T, \qquad \Sigma = \begin{pmatrix} 0 & \varepsilon_1 & & & \\ -\varepsilon_1 & 0 & & & \\ & & \ddots & & \\ & & & 0 & \varepsilon_N \\ & & & -\varepsilon_N & 0 \end{pmatrix}, \tag{2.26}$$

where O is orthogonal and $\varepsilon_I \geq 0$. In the rotated basis $\hat{\xi} := O^T\hat{\lambda}$, the Hamiltonian takes the form $\hat{H} = i\hat{\xi}^T\Sigma\hat{\xi} = 2\sum_{I=1}^{N}\varepsilon_I\hat{\xi}_{2I-1}\hat{\xi}_{2I}$.

While it is always possible to rewrite a BdG Hamiltonian in terms of Majorana operators, it is quite rare that the Majorana operator is an eigenstate of the Hamiltonian. That is, unpaired or isolated Majorana zero-energy eigenstates are quite rare in BdG systems and appear only in special occasions. Moreover, we note that in general there is no natural way to rewrite a given Majorana Hamiltonian in the form of a BdG Hamiltonian, since in general there does not exist any natural prescription on how to form complex fermion operators out of a given set of Majorana operators. (A necessary condition for such a prescription to be well defined is that the Majorana Hamiltonian must be an even-dimensional matrix.)

To summarize, single-particle BdG Hamiltonians are characterized by the PH constraint (2.20). The ensemble of Hamiltonians satisfying Eq. (2.20) is called symmetry class D. By imposing various symmetries, BdG Hamiltonians can realize five other symmetry classes: DIII, A, AIII, C, and CI, which we discuss next.

2. Class DIII

Let us start by studying how TRS with $\hat{\mathcal{T}}^2 = \hat{\mathcal{G}}_f$ restricts the form of BdG Hamiltonians. For this purpose, we label the fermion operators by the spin index $\sigma = \uparrow/\downarrow$, i.e., we let $\hat{\psi}_I \to \hat{\psi}_{I\sigma}$. We introduce TRS with the condition

$$\hat{\mathcal{T}}\hat{\psi}_{I\sigma}\hat{\mathcal{T}}^{-1} = (i\sigma_2)_{\sigma\sigma'}\hat{\psi}_{I\sigma'}, \tag{2.27}$$

where σ_2 is the second Pauli matrix acting on spin space. The BdG Hamiltonian then satisfies

$$\tau_1 H^T \tau_1 = -H \quad \text{and} \quad \sigma_2 H^* \sigma_2 = H. \tag{2.28}$$

As discussed before, the PH constraint (2.20) and the TRS (2.27) can be combined to yield a chiral symmetry $\tau_1\sigma_2 H\tau_1\sigma_2 = -H$. Observe that in this realization of chiral symmetry, $\mathrm{Tr}U_S = 0$. The ensemble of Hamiltonians satisfying conditions (2.28) is called symmetry class DIII. (Imposing $\hat{\mathcal{T}}^2 = +1$ instead of $\hat{\mathcal{T}}^2 = \hat{\mathcal{G}}_f$ leads to a different symmetry class, namely, class BDI.)

3. Classes A and AIII

Next we consider BdG systems with a $U(1)$ spin-rotation symmetry around the S_z axis in spin space. This symmetry allows us to rearrange the BdG Hamiltonian into a reduced form, i.e.,

$$\hat{H} = \hat{\Psi}_A^\dagger H^{AB}\hat{\Psi}_B, \tag{2.29}$$

up to a constant, where H is an unconstrained $2N \times 2N$ matrix and

$$\hat{\Psi}^\dagger = (\,\hat{\psi}_{I\uparrow}^\dagger \quad \hat{\psi}_{I\downarrow}\,), \qquad \hat{\Psi} = \begin{pmatrix} \hat{\psi}_{I\uparrow} \\ \hat{\psi}_{I\downarrow}^\dagger \end{pmatrix}. \tag{2.30}$$

Observe that, unlike for Υ, $\Upsilon^\dagger$, there is no constraint relating $\hat{\Psi}$ and $\hat{\Psi}^\dagger$. As H is unconstrained, this Hamiltonian is a member of symmetry class A. Since $\hat{\Psi}$ and $\hat{\Psi}^\dagger$ are independent operators, it is possible to rename the fermion operator $\hat{\psi}_\downarrow^\dagger$ as $\hat{\psi}_\downarrow^\dagger \to \hat{\psi}_\downarrow$. With this relabeling, the BdG Hamiltonian (2.29) can be converted to an ordinary fermion system with particle-number conservation. In this process, the $U(1)$ spin-rotation symmetry of the BdG system becomes a fictitious charge $U(1)$ symmetry.

Let us now impose TRS on Eq. (2.29), which acts on $\hat{\Psi}$ as

$$\hat{\mathcal{T}}\,\hat{\Psi}\,\hat{\mathcal{T}}^{-1} = \begin{pmatrix} \hat{\psi}_\downarrow \\ -\hat{\psi}_\uparrow^\dagger \end{pmatrix} = i\rho_2(\hat{\Psi}^\dagger)^T =: \hat{\Psi}^c, \tag{2.31}$$

where $\rho_{1,2,3}$ denote Pauli matrices acting on the particle-hole and spin components of the spinor (2.30). Observe that, if we let $\hat{\psi}_\uparrow^\dagger \to \hat{\psi}_\uparrow$, then $\hat{\mathcal{T}}$ in Eq. (2.31) looks like a composition of $\hat{\mathcal{T}}$ and $\hat{\mathcal{C}}$, i.e., it represents a chiral symmetry. Indeed, the relationship between chiral symmetry $\hat{\mathcal{T}}\,\hat{\mathcal{C}}$ and the $U(1)$ charge $\hat{Q}$ in particle-number conserving systems $(\hat{\mathcal{T}}\,\hat{\mathcal{C}})\hat{Q}(\hat{\mathcal{T}}\,\hat{\mathcal{C}})^{-1} = \hat{Q}$ is isomorphic to the relationship between TRS and $\hat{S}_z$ in BdG systems with S_z conservation $\hat{\mathcal{T}}\hat{S}_z\hat{\mathcal{T}}^{-1} = \hat{S}_z$. That is, by reinterpreting Eq. (2.29) as a particle-number conserving system TRS leads to an effective chiral symmetry. The ensemble of Hamiltonians satisfying a chiral symmetry is called symmetry class AIII. Hence, BdG systems with S_z conservation and TRS belong to symmetry class AIII.

4. Classes C and CI

We now study the constraints due to SU(2) spin-rotation symmetries other than S_z conservation. A spin rotation $\hat{\mathcal{U}}_{\boldsymbol{n}}^{\phi}$ by an angle ϕ around the rotation axis $\boldsymbol{n}$ acts on the doublet $(\hat{\psi}_\uparrow, \hat{\psi}_\downarrow)^T$ as

$$\begin{pmatrix} \hat{\psi}_\uparrow \\ \hat{\psi}_\downarrow \end{pmatrix} \to \hat{\mathcal{U}}_{\boldsymbol{n}}^{\phi}\begin{pmatrix} \hat{\psi}_\uparrow \\ \hat{\psi}_\downarrow \end{pmatrix}, \quad \hat{\mathcal{U}}_{\boldsymbol{n}}^{-\phi} = e^{-i(\phi/2)\boldsymbol{\sigma}\cdot\boldsymbol{n}}\begin{pmatrix} \hat{\psi}_\uparrow \\ \hat{\psi}_\downarrow \end{pmatrix}. \tag{2.32}$$

That is, a spin rotation by ϕ around the S_x or S_y axis transforms $\hat{\Psi}$ into

$$\begin{aligned} \hat{\mathcal{U}}_{S_x}^{\phi}\,\hat{\Psi}\hat{\mathcal{U}}_{S_x}^{-\phi} &= \cos(\phi/2)\hat{\Psi} - i\sin(\phi/2)\hat{\Psi}^c, \\ \hat{\mathcal{U}}_{S_y}^{\phi}\,\hat{\Psi}\hat{\mathcal{U}}_{S_y}^{-\phi} &= \cos(\phi/2)\hat{\Psi} - \sin(\phi/2)\hat{\Psi}^c, \end{aligned} \tag{2.33}$$

respectively. Thus, both $\hat{\mathcal{U}}_{S_x}^{\phi}$ and $\hat{\mathcal{U}}_{S_y}^{\phi}$ rotate $\hat{\Psi}$ smoothly into $\hat{\Psi}^c$. In particular, a rotation by π around S_x or S_y acts as a

discrete PH transformation, $\hat{\Psi} \to -i\hat{\Psi}^c$ or $-\hat{\Psi}^c$. That is, if we interpret Eq. (2.29) as a particle-number conserving system, then $\hat{\mathcal{U}}^{\pi}_{S_i}\hat{S}_z\hat{\mathcal{U}}^{-\pi}_{S_i} = -\hat{S}_z$ for $i = x, y$ can be viewed as a charge conjugation $\hat{\mathcal{C}}\,\hat{Q}\,\hat{\mathcal{C}}^{-1} = -\hat{Q}$. Observe that the π rotations $\hat{\mathcal{U}}^{\pi}_{S_i}$ are examples of PH transformations which square to -1, which is in contrast to the PH constraint of class D. For the single-particle Hamiltonian H the π-rotation symmetries $\hat{\mathcal{U}}^{\pi}_{S_i}$ lead to the condition

$$\rho_2 H^T \rho_2 = -H. \tag{2.34}$$

The ensemble of Hamiltonians satisfying this condition is called symmetry class C. We note that for quadratic Hamiltonians the π-rotation symmetry constrains of $\hat{\mathcal{U}}^{\pi}_{S_i}$ actually correspond to a full $SU(2)$ spin-rotation symmetry. This is because for an arbitrary $SU(2)$ rotation around S_x or S_y, the Hamiltonian $\hat{H}$ is transformed into a superposition of $\hat{\Psi}^\dagger H\hat{\Psi}$ and its conjugate $\hat{\Psi}^{c\dagger}H\hat{\Psi}^c$ [i.e., $\hat{H} \to \alpha\hat{\Psi}^\dagger H\hat{\Psi} + (1-\alpha)\hat{\Psi}^{c\dagger}H\hat{\Psi}^c$, for some α], since $\hat{\Psi}^\dagger H\hat{\Psi}^c = \hat{\Psi}^{c\dagger}H\hat{\Psi} = 0$. It follows from $\hat{\Psi}^\dagger H\hat{\Psi} = \hat{\Psi}^{c\dagger}H\hat{\Psi}^c$ together with the S_z invariance that the BdG Hamiltonian is fully invariant under $SU(2)$ spin-rotation symmetry.

Finally, imposing TRS (2.31) in addition to S_z conservation leads to $\hat{\Psi}^\dagger H\hat{\Psi} \to \hat{\Psi}^T\rho_2 H^*\rho_2(\hat{\Psi}^\dagger)^T = -\hat{\Psi}^\dagger\rho_2 H^\dagger\rho_2\hat{\Psi} = \hat{H}$, i.e., $\rho_2 H^\dagger\rho_2 = -H$. Combined with PHS (2.34), this gives the conditions

$$\rho_2 H^T\rho_2 = -H, \qquad H^* = H, \tag{2.35}$$

which defines symmetry class CI.

E. Symmetry classes of tenfold way

Let us now discuss a general symmetry classification of single-particle Hamiltonians in terms of nonunitary symmetries. Note that unitary symmetries, which commute with the Hamiltonian, allow us to bring the Hamiltonian into a block diagonal form. Here our aim is to classify the symmetry properties of these irreducible blocks, which do not exhibit any unitary symmetries. So far we have considered the following set of discrete symmetries:

$$\begin{aligned} &T^{-1}HT = H, \qquad T = U_T\mathcal{K}, \qquad U_T U_T^* = \pm\mathbb{1}, \\ &C^{-1}HC = -H, \qquad C = U_C\mathcal{K}, \qquad U_C U_C^* = \pm\mathbb{1}, \\ &S^{-1}HS = -H, \qquad S = U_S, \qquad U_S^2 = \mathbb{1}, \end{aligned} \tag{2.36}$$

where $\mathcal{K}$ is the complex conjugation operator. As it turns out, this set of symmetries is exhaustive. That is, without loss of generality we may assume that there is only a single TRS with operator T and a single PHS with operator C. If the Hamiltonian H was invariant under, say, two PH operations C_1 and C_2, then the composition $C_1 \cdot C_2$ of these two symmetries would be a unitary symmetry of the single-particle Hamiltonian H, i.e., the product $U_{C_1} \cdot U_{C_2}^*$ would commute with H. Hence, it would be possible to bring H into block form, such that $U_{C_1} \cdot U_{C_2}^*$ is a constant on each block. Thus, on each block U_{C_1} and U_{C_2} would be trivially related to each other, and therefore it would be sufficient to consider only one of the two PH operations. The product $T \cdot C$, however, corresponds to a unitary symmetry operation for the single-particle Hamiltonian H. But in this case, the unitary matrix $U_T \cdot U_C^*$ does not commute, but anticommutes with H. Therefore, $T \cdot C$ does not represent an "ordinary" unitary symmetry of H. This is the reason why we need to consider the product $T \cdot C$ [i.e., chiral symmetry S in Eq. (2.36)] as an additional crucial ingredient for the classification of the irreducible blocks, besides TR and PH symmetries.

Now it is easy to see that there are only ten possible ways for how a Hamiltonian H can transform under the general nonunitary symmetries (2.36). First we observe that there are three different possibilities for how H can transform under TRS (T): (i) H is not TR invariant, which we denote by $T = 0$ in Table I; (ii) the Hamiltonian is TR invariant and the TR operator T squares to $+\mathbb{1}$, in which case we write $T = +1$; and (iii) H is symmetric under TR and T squares to $-\mathbb{1}$, which we denote by $T = -1$. Similarly, there are three possible ways for how the Hamiltonian H can transform under PHS with PH operator C (again, C can square to $+\mathbb{1}$ or $-\mathbb{1}$). For these three possibilities we write $C = 0, +1, -1$. Hence, there are $3 \times 3 = 9$ possibilities for how H can transform under both TRS and PHS. These are not yet all ten cases, since it is also necessary to consider the behavior of the Hamiltonian under the product $S = T \cdot C$. A moment's thought shows that for eight of the nine possibilities the presence or absence of $S = T \cdot C$ is fully determined by how H transforms under TRS and PHS. (We write $S = 0$ if S is not a symmetry of the Hamiltonian, and $S = 1$ if it is.) But in the case where both TRS and PHS are absent, there exists the extra possibility that S is still conserved, i.e., either $S = 0$ or $S = 1$ is possible. This then yields $(3 \times 3 - 1) + 2 = 10$ possible behaviors of the Hamiltonian.

TABLE I. Periodic table of topological insulators and superconductors; $\delta := d - D$, where d is the space dimension and $D + 1$ is the codimension of defects; the leftmost column (A, AIII, …, CI) denotes the ten symmetry classes of fermionic Hamiltonians, which are characterized by the presence or absence of time-reversal (T), particle-hole (C), and chiral (S) symmetries of different types denoted by ± 1. The entries $\mathbb{Z}$, $\mathbb{Z}_2$, $2\mathbb{Z}$, and 0 represent the presence or absence of nontrivial topological insulators or superconductors or topological defects, and when they exist, types of these states. The case of $D = 0$ (i.e., $\delta = d$) corresponds to the tenfold classification of gapped bulk topological insulators and superconductors.

				δ							
Class	T	C	S	0	1	2	3	4	5	6	7
A	0	0	0	$\mathbb{Z}$	0	$\mathbb{Z}$	0	$\mathbb{Z}$	0	$\mathbb{Z}$	0
AIII	0	0	1	0	$\mathbb{Z}$	0	$\mathbb{Z}$	0	$\mathbb{Z}$	0	$\mathbb{Z}$
AI	+	0	0	$\mathbb{Z}$	0	0	0	$2\mathbb{Z}$	0	$\mathbb{Z}_2$	$\mathbb{Z}_2$
BDI	+	+	1	$\mathbb{Z}_2$	$\mathbb{Z}$	0	0	0	$2\mathbb{Z}$	0	$\mathbb{Z}_2$
D	0	+	0	$\mathbb{Z}_2$	$\mathbb{Z}_2$	$\mathbb{Z}$	0	0	0	$2\mathbb{Z}$	0
DIII	−	+	1	0	$\mathbb{Z}_2$	$\mathbb{Z}_2$	$\mathbb{Z}$	0	0	0	$2\mathbb{Z}$
AII	−	0	0	$2\mathbb{Z}$	0	$\mathbb{Z}_2$	$\mathbb{Z}_2$	$\mathbb{Z}$	0	0	0
CII	−	−	1	0	$2\mathbb{Z}$	0	$\mathbb{Z}_2$	$\mathbb{Z}_2$	$\mathbb{Z}$	0	0
C	0	−	0	0	0	$2\mathbb{Z}$	0	$\mathbb{Z}_2$	$\mathbb{Z}_2$	$\mathbb{Z}$	0
CI	+	−	1	0	0	0	$2\mathbb{Z}$	0	$\mathbb{Z}_2$	$\mathbb{Z}_2$	$\mathbb{Z}$

These ten possible behaviors of the first quantized Hamiltonian H under T, C, and S are listed in the first column of Table I. These are the ten generic symmetry classes (the "tenfold way") which are the framework within which the classification scheme of TIs and TSCs is formulated in Sec. III. We note that these ten symmetry classes were originally described by Altland and Zirnbauer in the context of disordered systems (Zirnbauer, 1996; Altland and Zirnbauer, 1997) and are therefore sometimes called Altland-Zirnbauer (AZ) symmetry classes. The tenfold way extends and completes the well-known "threefold way" scheme of Wigner and Dyson (Dyson, 1962).

III. FULLY GAPPED FREE-FERMION SYSTEMS AND TOPOLOGICAL DEFECTS

In this section we discuss the topological classification of fully gapped noninteracting fermionic systems, such as band insulators and fermionic quasiparticles in fully gapped SCs described by BdG Hamiltonians, in terms of the ten AZ symmetry classes. When considering superconductors, the superconducting pairing potentials will be treated at the mean-field level, i.e., as a fixed background to fermionic quasiparticles. We also discuss in this section the topological classification of zero-energy modes localized at topological defects in insulators and SCs. As shown, gapped topological phases and zero modes bound to topological defects can be discussed in a fully parallel and unified fashion (Teo and Kane, 2010b) by introducing the parameter $\delta \coloneqq d - D$, where d is the space dimension and $D+1$ denotes the codimension of defects (see Sec. III.A.2 for more details). When necessary, by taking $\delta = d$ and $D = 0$, one can easily specialize to the case of gapped topological systems, instead of defects of codimension greater than 1.

A. Tenfold classification of gapped free-fermion systems and topological defects

1. Gapped free-fermion systems

Gapped phases of quantum matter can be distinguished topologically by asking if they are connected in a phase diagram. If two gapped quantum phases can be transformed into each other through an adiabatic or a continuous path in the phase diagram without closing the gap (i.e., without encountering a quantum phase transition), then they are said to be topologically equivalent. In particular, states which are continuously deformable to an atomic insulator, i.e., a collection of independent atoms, are called topologically trivial or trivial, e.g., trivial band insulators. On the other hand, those that cannot be connected to atomic insulators are called topologically nontrivial or topological.

Since physical systems can be characterized by the presence or absence of symmetries (Sec. II), it is meaningful to discuss the topological distinction of quantum phases in the presence of a certain set of symmetry conditions. Let us then consider an ensemble of Hamiltonians within a given symmetry class and for a fix spatial dimension d and ask if there is a topological distinction among ground states of gapped insulators and SCs.[1] In particular, we focus on the classification of topological insulators and superconductors in free-fermion systems, described by quadratic Bloch-BdG Hamiltonians. Namely, we are interested in quadratic Hamiltonians of the form

$$\hat{H} = \sum_{\mathsf{r},\mathsf{r}'} \hat{\psi}_i^\dagger(\mathsf{r}) H^{ij}(\mathsf{r},\mathsf{r}') \hat{\psi}_j(\mathsf{r}'), \tag{3.1}$$

where $\hat{\psi}_i(\mathsf{r})$ is a multicomponent fermion annihilation operator, and index r labels a site on a d-dimensional lattice. Quadratic BdG Hamiltonians defined on a d-dimensional lattice can be treated or discussed similarly. The single-particle Hamiltonians $H^{ij}(\mathsf{r},\mathsf{r}')$ belong to one of the ten AZ symmetry classes and are, in general, subject to a set of symmetry constraints; see Eq. (2.36).

Assuming that the physical system has translation symmetry $H^{ij}(\mathsf{r},\mathsf{r}') = H^{ij}(\mathsf{r}-\mathsf{r}')$ with periodic boundary conditions in each spatial direction, it is convenient to use the corresponding single-particle Hamiltonian in momentum space $H^{ij}(\mathsf{k})$,

$$\hat{H} = \sum_{\mathsf{k}\in \mathrm{BZ}^d} \hat{\psi}_i^\dagger(\mathsf{k}) H^{ij}(\mathsf{k}) \hat{\psi}_j(\mathsf{k}), \tag{3.2}$$

where the crystal momentum k runs over the first BZ. The Fourier components of the fermion operator and the Hamiltonian are given by $\hat{\psi}_i(\mathsf{r}) = \sqrt{V}^{-1} \sum_{\mathsf{k}\in \mathrm{BZ}^d} e^{i\mathsf{k}\cdot\mathsf{r}} \hat{\psi}_i(\mathsf{k})$ and $H^{ij}(\mathsf{k}) = \sum_{\mathsf{r}} e^{-i\mathsf{k}\cdot\mathsf{r}} H^{ij}(\mathsf{r})$, respectively, where V is the total number of sites.[2] TRS, PHS, and chiral symmetry act on the single-particle Hamiltonian $H(\mathsf{k})$ as

$$TH(\mathsf{k})T^{-1} = H(-\mathsf{k}), \tag{3.3}$$

$$CH(\mathsf{k})C^{-1} = -H(-\mathsf{k}), \tag{3.4}$$

$$SH(\mathsf{k})S^{-1} = -H(\mathsf{k}), \tag{3.5}$$

where T, C, and S are the antiunitary TR, PH, and unitary chiral operators, respectively. With this setup, we then ask whether two gapped quadratic Hamiltonians, which belong to the same symmetry class, can be continuously transformed into each other without closing the gap. That is, we classify gapped Hamiltonians of a given symmetry class into different topological equivalence classes. The result of this classification is summarized by the periodic table of TIs and TSCs (Qi, Hughes, and Zhang, 2008; Schnyder *et al.*, 2008, 2009; Kitaev, 2009; Ryu, Schnyder *et al.*, 2010); see Table I. [The case of $D = 0$ (i.e., $\delta = d$) corresponds to the tenfold classification of gapped bulk TIs and TSCs.] Systematic derivations of this classification table are discussed later.

[1] More specifically, we are not interested in systems with genuine topological order, whose existence has nothing to do with the presence or absence of symmetries, but in symmetry-protected topological phases; see Sec. VI.

[2] It should, however, be emphasized that all TIs and TSCs in the ten AZ symmetry classes are stable against disorder, and hence the assumption of translation invariance is not at all necessary (see Sec. III.F).

Here the following comments on noticeable features of the table are in order:

(1) The symmetry classes A and AIII, and the other eight classes are separately displayed. We call the former "the complex symmetry classes," and the latter "the real symmetry classes." The complex symmetry classes do not have TRS nor PHS.

(2) The symbols $\mathbb{Z}$, $\mathbb{Z}_2$, $2\mathbb{Z}$, and 0 indicate whether or not TIs and TSCs exist for a given symmetry class in a given dimension, and if they exist, what kind of topological invariant characterizes the topological phases. For example, $2\mathbb{Z}$[3] indicates that the topological phase is characterized by an even-integer topological invariant, and 0 simply means there is no TI or TSC; i.e., all states in a symmetry class in a given dimension are adiabatically deformable.

(3) In Table I, the so-called weak TIs and TSCs, which are nontrivial topological phases that exist in the presence of lattice-translation symmetries, are not presented. That is, the table shows only the strong TIs and TSCs whose existence does not rely on translation symmetries. However, the presence or absence of weak TIs or TSCs in a given symmetry class can be deduced from the presence or absence of strong TIs or TSCs in lower dimensions in the same symmetry class.

(4) The classification table exhibits a periodicity of 2 and 8 as a function of spatial dimension, for the complex and real symmetry classes, respectively. (The table is shown only up to $d = 7$ for this reason.) In addition, note that the classifications for different symmetry classes are related by a dimensional shift. For this reason it is convenient to label the eight real AZ symmetry classes by an integer s running from 0 to 7, which can be arranged on a periodic *eight-hour clock*, the "Bott clock" (Fig. 1). Denoting the classification of TIs and TSCs in symmetry class s and in space dimension d by $K(s;d,0)$, the periodic table can be summarized as Table II.

(5) Now let us examine the pattern in which the different kinds of topological phases appear in the table. Along the main diagonal of the table the entries appear for topological phases characterized by an integer topological invariant ($\mathbb{Z}$). These topological phases are called the "primary series." Just below the primary series (i.e., to the lower left), there are two sets of diagonal entries for the topological phase characterized by a $\mathbb{Z}_2$ topological invariant. These topological phases are called the "first descendants" and the "second descendants", respectively. There is also a series of topological phases characterized by $2\mathbb{Z}$ invariants, i.e., by an even-integer topological invariant. These entries are called the "even series."

To discuss an observable consequence of having a topologically nontrivial state, let us recall that, by definition, topologically nontrivial and trivial states in the phase diagram are always separated by a quantum phase transition, if the symmetry conditions are strictly enforced. This, in turn, implies that if a TI or TSC is in spatial proximity to a trivial phase, there should be a gapless state localized at the boundary between the two phases. This gapless (i.e., critical) state can be thought of as arising due to a phase transition occurring locally in space, where the parameters of the Hamiltonian change as a function of the direction transverse to the boundary. Such gapless boundary modes are protected in the sense that they are stable against perturbations as long as the bulk gap is not destroyed and the symmetries are preserved. In particular, gapless boundary modes are completely immune to disorder and evade Anderson localization completely (Sec. III.F). The presence of such gapless boundary states is the most salient feature of TIs and TSCs, and in fact can be considered as a definition of TIs and TSCs. This close connection between nontrivial bulk topological properties and gapless boundary modes is known as the bulk-boundary correspondence (Sec. III.D).

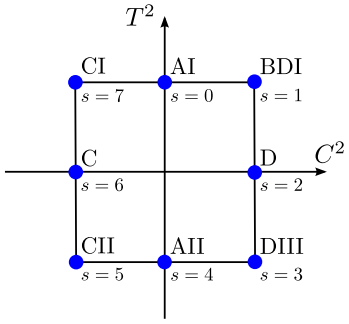

FIG. 1. The eight real symmetry classes that involve the antiunitary symmetries T (time-reversal) and/or C (particle-hole) are specified by the values of $T^2 = \pm 1$ and $C^2 = \pm 1$. They can be visualized on an eight-hour clock. Adapted from Teo and Kane, 2010b.

2. Topological defects

Boundaries separating bulk TIs and TSCs from trivial states of matter, which host topologically protected gapless modes, are codimension one objects, i.e., one dimension less than the bulk. It is possible to discuss general higher codimension topological defects, such as point and line defects introduced in a gapped bulk system, and their topological classification. Topological properties of adiabatic cycles can also be discussed in a similar manner.

TABLE II. The eightfold periodic classification of topological insulators and superconductors and topological defects with time-reversal and/or particle-hole symmetries. s labels the Altland-Zirnbauer symmetry classes (see Fig. 1), $\delta = d - D$ is the topological dimension, and $\mathbb{Z}_2^{(1,2)}$ are the first and second descendant $\mathbb{Z}_2$ classifications.

$s-\delta$	0	1	2	3	4	5	6	7
$K(s;d,D)$	$\mathbb{Z}$	$\mathbb{Z}_2^{(1)}$	$\mathbb{Z}_2^{(2)}$	0	$2\mathbb{Z}$	0	0	0

[3]The label $2\mathbb{Z}$ indicates that the topological invariant is given by an even integer, reflecting the fact that there is an even number of protected gapless surface modes. Note, however, that the group of integers ($\mathbb{Z}$) and the group of even integers ($2\mathbb{Z}$) are isomorphic.

Topological defects were discussed originally in the context of spontaneous symmetry breaking. For example, the quantum flux vortex of a type II SC (de Gennes, 1999) involves the winding of the pairing order parameter, which breaks the charge conserving $U(1)$ symmetry. Dislocations and disclinations (Chaikin and Lubensky, 2000; Nelson, 2002) are crystalline defects that associate discrete torisional and curvature fluxes in a lattice medium, which breaks continuous translation and rotation symmetries. They all involve nontrivial long length scale modulations of some order parameter around the defects.

Topological defects in the context of topological band theories (Teo and Kane, 2010b) have a different origin in that they are not necessarily associated with spontaneous symmetry breaking. For example, the mass gap that inverts between topological and trivial insulators does not break any symmetry. It is nonetheless a parameter in the band theory that controls the topology of the bulk material, and we refer to them as band parameters or topological parameters. Topological defects in insulators and SCs are therefore nontrivial long length scale windings of these topological parameters around the defects.

Topological defects for our interest are described by a defect Hamiltonian, which is a band Hamiltonian $H_{\mathsf{r}}(\mathsf{k}) = H(\mathsf{k},\mathsf{r})$ that is slowly modulated by a parameter r, which includes spatial coordinates and/or a temporal parameter. A defect Hamiltonian describes the long length scale environment surrounding of a defect—far away from it. The modulation is slow enough so that the bulk system well separated from the defect core has microscopic spacetime translation symmetry and hence can be characterized by momentum k. More precisely, we assume $\xi|\nabla_{\mathsf{r}}H(\mathsf{k},\mathsf{r})| \ll \varepsilon_g$, where ξ is a characteristic microscopic length scale similar to the lattice spacing, or a time scale similar to $1/\varepsilon_g$, where ε_g is the bulk energy gap.[4] TR, PH, and chiral symmetry act on a defect Hamiltonian as

$$TH(\mathsf{k},\mathsf{r})T^{-1} = H(-\mathsf{k},\mathsf{r}), \tag{3.6}$$

$$CH(\mathsf{k},\mathsf{r})C^{-1} = -H(-\mathsf{k},\mathsf{r}), \tag{3.7}$$

$$SH(\mathsf{k},\mathsf{r})S^{-1} = -H(\mathsf{k},\mathsf{r}), \tag{3.8}$$

where the spatial (temporal, when discussing adiabatic cycles) parameter r is unaltered, since the symmetries act on local microscopic degrees of freedom, which are independent of the slowly varying modulation.

Different defect Hamiltonians are distinguished by (i) the AZ symmetry class s, (ii) the bulk dimension d, and (iii) the defect codimension d_c defined in terms of the dimension of the defect d_{defect} by $d_c = d - d_{\text{defect}}$. A spatial defect of dimension d_{defect} is wrapped by a D-dimension sphere S^D, where $D = d_c - 1 = d - d_{\text{defect}} - 1$. For example, a point defect in 3D has codimension $d_c = 3 - 0 = 3$ and thus is surrounded by a 2D sphere. Adiabatic cycles are incorporated as topological defects that depend on a cyclic temporal parameter. In this case the defect is enclosed by a sphere S^{D-1} of dimension $D - 1 = d - d_{\text{defect}} - 1$ in d-dimensional real space. Together with the temporal parameter that lives on S^1, the adiabatic cycle is wrapped by a D-dimensional manifold such as $S^{D-1} \times S^1$. A table of low-dimensional defects is presented in Fig. 2.

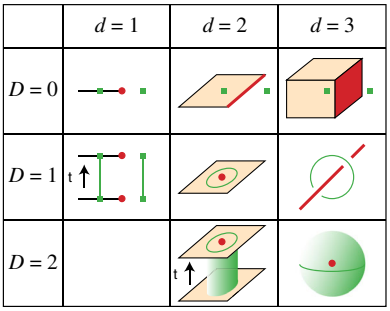

FIG. 2. Topological defects characterized by a D parameter family of d-dimensional Bloch-BdG Hamiltonians. Line defects correspond to $d - D = 2$, while point defects correspond to $d - D = 1$. Temporal cycles for point defects correspond to $d - D = 0$. Adapted from Teo and Kane, 2010b.

For real AZ symmetry classes, it was shown that the classification of topological defects depends only on a single number (Teo and Kane, 2010b; Freedman *et al.*, 2011)

$$s - \delta = s - d + D \quad \text{modulo } 8, \tag{3.9}$$

where $\delta = d - D$ is called the topological dimension that takes the role of the usual dimension d in the case of gapped TIs and TSCs. For spatial defects, the topological dimension is related to the defect dimension by $\delta = d_{\text{defect}} + 1$ and is independent of the bulk dimension d. For instance, point defects always have $\delta = 1$, while line defects always have $\delta = 2$. For adiabatic cycles, the extra temporal parameter in the D-component parameter r reduces the topological dimension by 1. For example, a temporal cycle of point defects has $\delta = 0$. The classification is summarized in Tables I and II. (As in the case of gapped TIs and TSCs, we are interested in the highest dimension strong topologies of the defect that do not involve lower dimensional cycles.)

Topological defects in the two complex AZ classes A and AIII are classified in a similar manner, except that the symmetry classes now live on a periodic two-hour clock, and the topological dimension $\delta = d - D$ as well as the number $d - \delta$ are now integers modulo 2. Topological defects in class A (class AIII) are $\mathbb{Z}$ classified when δ is even (when δ is odd). Otherwise they are trivially classified. By forgetting the antiunitary symmetries, the real AZ classes separate into the two complex classes AI, D, AII, C → A and BDI, DIII, CI, CII → AIII, where the chiral operator S is given by the product of TR and PH (possibly up to a factor of i). This procedure (forgetful functor, see Sec. III.C) relates real and complex classifications. For instance, the $2\mathbb{Z}$ classification for $s - \delta \equiv 4$ modulo 8 in Table II is normalized according to the corresponding complex $\mathbb{Z}$ classification. This means when

[4]Note, however, that the topological classification of topological defects, which is presented in the following, also applies to the cases where this assumption is not satisfied, such as sharp interfaces or domain walls between different gapped bulk phases.

forgetting the antiunitary symmetries, the topological invariants must be even for $s-\delta\equiv 4$.

Like the bulk-boundary correspondence that relates bulk topology to boundary gapless excitations, we have a bulk-defect correspondence that guarantees gapless defect excitations from the nontrivial winding of bulk topological parameters around the defect. This framework unifies numerous TI and TSC defect systems (Sec. III.D).

B. Topological invariants

In this section, we discuss the tenfold classification of gapped TIs and TSCs and topological defects, in terms of bulk topological invariants. A short summary of topological invariants that will be discussed is presented in Table III. Various specific examples of the topological invariants and systems characterized by the topological invariants will be discussed, but we mostly confine ourselves to examples taken from gapped TIs and TSCs. Examples of topological defects are discussed later in Sec. III.D. A systematic derivation of the periodic table and physical consequences of the nontrivial bulk topologies measured by the topological invariants, such as gapless modes localized at boundaries and defects, is discussed in Secs. III.C and III.D, respectively.

The topological invariants introduced in this section are given in terms of the eigenfunction of a Bloch-BdG Hamiltonian. We denote the ath eigenfunction with energy $\varepsilon^a(\mathsf{k},\mathsf{r})$ by $|u^a(\mathsf{k},\mathsf{r})\rangle$, $H(\mathsf{k},\mathsf{r})|u^a(\mathsf{k},\mathsf{r})\rangle=\varepsilon^a(\mathsf{k},\mathsf{r})|u^a(\mathsf{k},\mathsf{r})\rangle$. By assumption, there is a spectral gap at the Fermi energy in the band structure given by $\varepsilon^a(\mathsf{k},\mathsf{r})$. We assume that there are $N_{-/+}$ bands below and above the Fermi energy. The total number of the bands is N_++N_-. We denote the set of filled Bloch wave functions by $\{|u^\alpha_-(\mathsf{k},\mathsf{r})\rangle\}$, or simply $\{|u^\alpha(\mathsf{k},\mathsf{r})\rangle\}$, where the Greek index $\alpha=1,\ldots,N_-$ labels the occupied bands only.

The Bloch wave functions are defined on the base manifold $\mathrm{BZ}^d\times\mathcal{M}^D$, the $(d+D)$-dimensional total phase space parametrized by (k,r). Here the D-dimensional manifold $\mathcal{M}^D$ wraps around the topological defect (Fig. 2). (It deformation retracts from the defect complement of spacetime.) For example, taking away a point defect in real 3-space leaves behind a punctured space, which has the same homotopy type as the 2-sphere S^2. The complement of an infinite defect line in 3-space can be compressed along the defect direction onto a punctured disk, which then can be deformation retracted to the circle S^1. The D manifold $\mathcal{M}^D$ enclosing a more complicated topological defect may not be spherical. For instance, the one surrounding a link in 3-space is a 2-torus. The D manifold of a temporal cycle must contain a noncontractible 1-cycle that corresponds to the periodic time direction. For the bulk of the review, we are interested in the highest dimension strong topologies of defects that do not involve lower dimensional cycles. For this purpose, we compactify the phase space into a sphere

$$(\mathsf{k},\mathsf{r})\in \mathrm{BZ}^d\times\mathcal{M}^D\xrightarrow{\text{compactify}}S^{d+D}$$

by contracting all lower dimensional cycles. Physically this means the defect band theory are assumed to have trivial winding around those low-dimensional cycles.

TABLE III. Strong topological invariants for topological defects. The $\mathbb{Z}$ invariants apply to both complex and real Altland-Zirnbauer classes.

	Nonchiral classes (s even)	Chiral classes (s odd)
$\mathbb{Z}$	Chern number (Ch)	Winding number (ν)
$\mathbb{Z}_2^{(1)}$	CS (CS)	Fu-Kane (FK)
$\mathbb{Z}_2^{(2)}$	Fu-Kane (FK)	CS ($\widetilde{\mathrm{CS}}$)

1. Primary series for s even: The Chern number

For gapped topological phases and topological defects in nonchiral classes (i.e., s is even), the $\mathbb{Z}$-classified topologies are characterized by the Chern number

$$\mathrm{Ch}_n=\frac{1}{n!}\left(\frac{i}{2\pi}\right)^n\int_{\mathrm{BZ}^d\times\mathcal{M}^D}\mathrm{Tr}(\mathcal{F}^n),\tag{3.10}$$

where $n:=(d+D)/2$. The Berry curvature[5]

$$\mathcal{F}=d\mathcal{A}+\mathcal{A}^2\tag{3.12}$$

is given in terms of the non-Abelian Berry connection

$$\begin{aligned}\mathcal{A}^{\alpha\beta}(\mathsf{k},\mathsf{r})&=\langle u^\alpha(\mathsf{k},\mathsf{r})|du^\beta(\mathsf{k},\mathsf{r})\rangle\\&=\langle u^\alpha(\mathsf{k},\mathsf{r})|\nabla_{\mathsf{k}}u^\beta(\mathsf{k},\mathsf{r})\rangle\cdot d\mathsf{k}\\&\quad+\langle u^\alpha(\mathsf{k},\mathsf{r})|\nabla_{\mathsf{r}}u^\beta(\mathsf{k},\mathsf{r})\rangle\cdot d\mathsf{r}.\end{aligned}\tag{3.13}$$

The Chern number is well defined only when $d+D$ is even. Furthermore, it vanishes in the presence of TRS (or PHS) when $\delta=d-D$ is 2 (respectively, 0) mod 4. Moreover it must be even when $s-\delta$ is 4 mod 8.

The Chern number detects an obstruction in defining a set of Bloch wave functions smoothly over the base space $\mathrm{BZ}^d\times\mathcal{M}^D$. Associated with each (k,r), we have a set of wave functions $|u^a(\mathsf{k},\mathsf{r})\rangle$, a collection of which can be thought of as a member of $U(N_++N_-)$. There is, however, a gauge redundancy: $U(N_\pm)$ rotations among unoccupied or occupied Bloch wave functions give rise to the same quantum ground state (the Fermi-Dirac sea) at given (k,r). In other words, the quantum ground state at a given (k,r) is a

[5]As in Eqs. (3.10)–(3.12), we use the differential form notation, e.g.,

$$\begin{aligned}\mathcal{A}^{\alpha\beta}&=A_I^{\alpha\beta}(\mathsf{s})ds^I,\qquad A_I^{\alpha\beta}(\mathsf{s}):=\langle u(\mathsf{s})|\partial_I u(\mathsf{s})\rangle,\\\mathcal{F}^{\alpha\beta}&=d\mathcal{A}^{\alpha\beta}+\mathcal{A}^{\alpha\gamma}\wedge\mathcal{A}^{\gamma\beta}\\&=(\partial_IA_J^{\alpha\beta}+A_I^{\alpha\gamma}A_J^{\gamma\beta})ds^I\wedge ds^J\\&=\tfrac{1}{2}(\partial_IA_J-\partial_JA_I+[A_I,A_J])^{\alpha\beta}ds^I\wedge ds^J,\end{aligned}\tag{3.11}$$

where $\mathsf{s}=(\mathsf{k},\mathsf{r})$ and $I,J=1,\ldots,d+D$. The wedge symbol $\wedge$ is often omitted. When necessary, we use a subscript to indicate that a differential form $\mathcal{A}_n$ is an n-form.

member of the coset space $U(N_+ + N_-)/U(N_-) \times U(N_+)$, the complex Grassmannian. The Fermi-Dirac sea at (k, r) can be conveniently described by the spectral projector:

$$P(\mathsf{k}, \mathsf{r}) = \sum_{\alpha=1}^{N_-} |u^\alpha(\mathsf{k}, \mathsf{r})\rangle\langle u^\alpha(\mathsf{k}, \mathsf{r})| \tag{3.14}$$

[or $P^{ij}(\mathsf{k}, \mathsf{r}) = \sum_{\alpha=1}^{N_-} u_i{}^\alpha(\mathsf{k}, \mathsf{r})[u_j{}^\alpha(\mathsf{k}, \mathsf{r})]^*$ if indices are shown explicitly], which specifies a subspace of the total Hilbert space defined by the set of occupied Bloch wave functions. The projector is gauge invariant and a member of the complex Grassmannian $P(\mathsf{k}, \mathsf{r}) \in U(N_+ + N_-)/U(N_-) \times U(N_+)$. For what follows, it is convenient to introduce the "Q matrix" by

$$Q(\mathsf{k}, \mathsf{r}) = \mathbb{1} - 2P(\mathsf{k}, \mathsf{r}). \tag{3.15}$$

The Q matrix is Hermitian and has the same set of eigenfunctions as $H(\mathsf{k}, \mathsf{r})$, but its eigenvalues are either ± 1 since $Q^2 = \mathbb{1}$.

As we move around in the base space $\mathrm{BZ}^d \times \mathcal{M}^D$, the set of wave functions undergoes adiabatic changes. Such wave functions thus define a fiber bundle, which may be "twisted": It may not be possible to find smooth wave functions that are well defined everywhere over the base space. One quick way to see when the fiber bundle is twisted is to note that the set of Bloch functions (or equivalently the projector) defines a map from the base space to $U(N_+ + N_-)/U(N_+) \times U(N_-)$. Topologically distinct maps of this type can be classified by the homotopy group

$$\pi_{d+D}[U(N_+ + N_-)/U(N_+) \times U(N_-)]. \tag{3.16}$$

For large enough $N_\pm$ and when $d + D$ is even, $\pi_{d+D}[U(N_+ + N_-)/U(N_+) \times U(N_-)] = \mathbb{Z}$. Topologically distinct maps are therefore characterized by an integer topological invariant, namely, by

$$\frac{-1}{2^{2n+1}} \frac{1}{n!} \left(\frac{i}{2\pi}\right)^n \int_{\mathrm{BZ}^d \times \mathcal{M}^D} \mathrm{Tr}[Q(dQ)^{2n}]. \tag{3.17}$$

This, in turn, is nothing but the Chern number.

a. Example: The 2D class A quantum anomalous Hall effect

As an illustration, let us consider band insulators with $N_+ = N_- = 1$ in two spatial dimensions $d = 2$. In general, two-band Bloch Hamiltonians can be written in terms of four real functions $R_{0,1,2,3}(\mathsf{k})$ as

$$H(\mathsf{k}) = R_0(\mathsf{k})\sigma_0 + \boldsymbol{R}(\mathsf{k}) \cdot \boldsymbol{\sigma}, \tag{3.18}$$

where $\boldsymbol{R} = (R_1, R_2, R_3)$. The energy dispersions of the bands are given by $\varepsilon_\pm(\mathsf{k}) = R_0(\mathsf{k}) \pm R(\mathsf{k})$ with $R(\mathsf{k}) \coloneqq |\boldsymbol{R}(\mathsf{k})|$. For band insulators, there is a spectral gap at the Fermi energy, which we take to be zero for convenience. Hence we assume $R_0(\mathsf{k}) + R(\mathsf{k}) > 0 > R_0(\mathsf{k}) - R(\mathsf{k})$, which, in particular, implies $R(\mathsf{k}) > 0$ for all k.

In this two-band example, the Bloch Hamiltonian $H(\mathsf{k})$ or the four vector $R_{\mu=0,1,2,3}(\mathsf{k})$ defines a map from the BZ to the space of the unconstrained four vector R_μ. The Bloch wave functions, however, depend only on the normalized vector $\boldsymbol{n}(\mathsf{k}) \equiv \boldsymbol{R}(\mathsf{k})/R(\mathsf{k})$, as seen easily from (i) $R_0(\mathsf{k})$ in $H(\mathsf{k})$ does not affect the wave functions, and (ii) $\boldsymbol{R}(\mathsf{k}) \cdot \boldsymbol{\sigma} = R(\mathsf{k})\boldsymbol{n}(\mathsf{k}) \cdot \boldsymbol{\sigma}$. [Note that because of the presence of the spectral gap, $R(\mathsf{k}) > 0$ for all k, and the normalized vector $\boldsymbol{n}(\mathsf{k})$ is always well defined.] Thus, from the point of view of the Bloch wave functions, we consider a map from the BZ to the space of the normalized vector $\boldsymbol{n}$, which is simply S^2. The latter is the simplest example of the complex Grassmannian $U(2)/U(1) \times U(1) \simeq S^2$.

Within the two-band model, different band insulators can thus be characterized by different maps $\boldsymbol{n}(\mathsf{k})$. By "compactifying" the BZ T^2 to S^2, topologically distinct maps can be classified by the second homotopy group $\pi_2(S^2)$, which is given by $\pi_2(S^2) = \mathbb{Z}$. For a given map $\boldsymbol{n}$, the integer topological invariant

$$\frac{1}{4\pi} \int_{\mathrm{BZ}} \boldsymbol{n} \cdot d\boldsymbol{n} \times d\boldsymbol{n} \in \mathbb{Z} \tag{3.19}$$

counts the number of times the unit vector $\boldsymbol{n}$ "wraps" around S^2 as we go around the BZ and hence tells us to which topological class the map $\boldsymbol{n}(\mathsf{k})$ belongs.

Let us now construct the Bloch wave functions explicitly. One possible choice is

$$|u^\pm\rangle = \frac{1}{\sqrt{2R(R \mp R_3)}} \begin{pmatrix} R_1 - iR_2 \\ \pm R - R_3 \end{pmatrix}. \tag{3.20}$$

Observe that the occupied Bloch wave function $|u^-\rangle$ has a singularity at $\boldsymbol{R} = (0, 0, -R)$, i.e., at the "south pole." When the topological invariant (3.19) is nonzero, the vector $\boldsymbol{n}(\mathsf{k})$ necessarily maps at least one point in the BZ to the south pole, and hence one encounters a singularity, if one insists on using the wave function (3.20) everywhere in the BZ. There is an obstruction in this sense in defining wave functions that are smooth and well defined globally in the BZ. To avoid the singularity, one can "patch" the BZ and use different wave functions on different patches. For example, near the south pole one can make an alternative choice,

$$|u^\pm\rangle = \frac{1}{\sqrt{2R(R \pm R_3)}} \begin{pmatrix} \pm R + R_3 \\ R_1 + iR_2 \end{pmatrix}, \tag{3.21}$$

which is smooth at the south pole, but singular at the north pole $\boldsymbol{R} = (0, 0, R)$. With the two patches with the wave functions (3.20) and (3.21), one can cover the entire BZ. In those regions where the two patches overlap, the two wave functions are related to each other by a gauge transformation.

With the explicit form of the Bloch wave functions, one can compute the spectral projector or the Q matrix, and check that the different gauge choices (3.20) and (3.21) give rise to the same projector (the projector is gauge invariant), and that it depends only on $\boldsymbol{n}(\mathsf{k})$, i.e., $Q(\mathsf{k}) = \boldsymbol{n}(\mathsf{k}) \cdot \boldsymbol{\sigma}$. From the Bloch wave functions, one can compute the Berry connection and then the Chern number $\mathrm{Ch} = (i/4\pi) \int_{\mathrm{BZ}} \mathrm{Tr}\mathcal{F}$.

The Chern number is, in fact, equal to the topological invariant (3.19), as seen from Eq. (3.17), since $\mathrm{Tr}\mathcal{F}(\mathsf{k}) = (i/2)\epsilon^{ijk} n_i (\partial_\mu n_j)(\partial_\nu n_k) dk^\mu \wedge dk^\nu$.

An explicit example of the two-band model (3.18) with nonzero Chern number is given in momentum space by

$$\boldsymbol{R}(\mathsf{k}) = \begin{pmatrix} -2\sin k_x \\ -2\sin k_y \\ \mu + 2\sum_{i=x,y} \cos k_i \end{pmatrix}. \tag{3.22}$$

There are four phases separated by three quantum critical points at $\mu = 0, \pm 4$, which are labeled by the Chern number as $\mathrm{Ch} = 0$ ($|\mu| > 4$), $\mathrm{Ch} = -1$ ($-4 < \mu < 0$), and $\mathrm{Ch} = +1$ ($0 < \mu < +4$). Band insulators on $d = 2$ dimensional lattices having nonzero Chern number and without net magnetic field are commonly called Chern insulators and exhibit the quantum anomalous Hall effect (Haldane, 1988; Nagaosa *et al.*, 2010), which generalizes the integer quantum Hall effect (QHE) realized in the presence of a uniform magnetic field (Klitzing, Dorda, and Pepper, 1980; Laughlin, 1981; Thouless *et al.*, 1982; Kohmoto, 1985; Prange Girvin, 1990). The Chern number is nothing but the quantized Hall conductance σ_{xy}. Experimental realizations of Chern insulators include Cr-doped $(\mathrm{Bi},\mathrm{Sb})_2\mathrm{Te}_3$ thin films (Yu *et al.*, 2010; Chang *et al.*, 2013; G. Xu *et al.*, 2015), InAs/GaSb and $\mathrm{Hg}_{1-y}\mathrm{Mn}_y\mathrm{Te}$ quantum wells (C.-X. Liu *et al.*, 2008; Q.-Z. Wang *et al.*, 2014), graphene with adatoms (Qiao *et al.*, 2010), and $\mathrm{La}_2\mathrm{MnIrO}_6$ monolayers (Zhang *et al.*, 2014).

2. Primary series for s odd: The winding number

a. Winding number

The Chern number can be defined for Bloch-BdG Hamiltonians in any symmetry class as long as $d + D$ is even (although its allowed value depends on symmetry classes and δ). On the other hand, there are topological invariants which can be defined only in the presence of symmetries. One example is the winding number topological invariant ν, which can be defined only in the presence of chiral symmetry, $\{H(\mathsf{k},\mathsf{r}), U_S\} = 0$, with $U_S^2 = \mathbb{1}$. For simplicity, we focus below on the case of $\mathrm{Tr}U_S = 0$, i.e., $N_+ = N_- = N$.

While in the absence of chiral symmetry the spectral projector is a member of the complex Grassmannian, in the presence of chiral symmetry the relevant space is the unitary group $U(N)$. This can be seen from the block-off-diagonal form of chiral symmetric Hamiltonians,

$$H(\mathsf{k},\mathsf{r}) = \begin{pmatrix} 0 & D(\mathsf{k},\mathsf{r}) \\ D^\dagger(\mathsf{k},\mathsf{r}) & 0 \end{pmatrix}. \tag{3.23}$$

Correspondingly, in this basis, the Q matrix is also block off-diagonal,

$$Q(\mathsf{k},\mathsf{r}) = \begin{pmatrix} 0 & q(\mathsf{k},\mathsf{r}) \\ q^\dagger(\mathsf{k},\mathsf{r}) & 0 \end{pmatrix}, \tag{3.24}$$

where the off-diagonal block $q(\mathsf{k},\mathsf{r})$ is a unitary matrix. Hence, the q matrix defines a map from the base space $\mathrm{BZ}^d \times \mathcal{M}^D$ to the space of unitary matrices $U(N)$. Topologically distinct maps of this type are classified by the homotopy group $\pi_{d+D}[U(N)]$, which is nontrivial when $d + D$ is odd, i.e., $\pi_{d+D}[U(N)] = \mathbb{Z}$ (for large enough N). Topologically distinct maps are characterized by the winding number, which is given by

$$\begin{aligned} \nu_{2n+1}[q] &= \int_{\mathrm{BZ}^d \times \mathcal{M}^D} \omega_{2n+1}[q], \\ \omega_{2n+1}[q] &= \frac{(-1)^n n!}{(2n+1)!} \left(\frac{i}{2\pi}\right)^{n+1} \mathrm{Tr}[(q^{-1}dq)^{2n+1}], \end{aligned} \tag{3.25}$$

where $d + D = 2n + 1$ is an odd integer. For example, when $(d, D) = (1, 0), (3, 0)$, we have

$$\begin{aligned} \nu_1 &= \frac{i}{2\pi} \int_{\mathrm{BZ}} dk \mathrm{Tr}[q^{-1}\partial_k q], \\ \nu_3 &= \int_{\mathrm{BZ}} \frac{d^3\mathsf{k}}{24\pi^2} \epsilon^{\mu\nu\rho} \mathrm{Tr}[(q^{-1}\partial_\mu q)(q^{-1}\partial_\nu q)(q^{-1}\partial_\rho q)], \end{aligned} \tag{3.26}$$

respectively, where $\partial_\mu = \partial_{k_\mu}$.

b. Chern-Simons invariant

We now introduce yet another topological invariant, the Chern-Simons invariant (CS invariant). This invariant can be defined when $d + D =$ odd and is not quantized in general, unlike the Chern number. In the presence of symmetries, however, it may take discrete values. We use the quantized CS invariant later to characterize first and second descendants. Here we show that the CS invariant is also quantized in the presence of chiral symmetry.

The CS invariant is defined in terms of the CS form $\mathcal{Q}_{2n+1}$ in $d + D = 2n + 1$ dimensions, where

$$\begin{aligned} &\mathcal{Q}_{2n+1}(\mathcal{A}) \coloneqq \frac{1}{n!} \left(\frac{i}{2\pi}\right)^{n+1} \int_0^1 dt \mathrm{Tr}(\mathcal{A}\mathcal{F}_t^n), \\ &\text{with} \quad \mathcal{F}_t = td\mathcal{A} + t^2\mathcal{A}^2 = t\mathcal{F} + (t^2 - t)\mathcal{A}^2. \end{aligned} \tag{3.27}$$

Integrating the CS form over the base space yields the CS invariant

$$\mathrm{CS}_{2n+1}[\mathcal{A}] \coloneqq \int_{\mathrm{BZ}^d \times \mathcal{M}^D} \mathcal{Q}_{2n+1}(\mathcal{A}). \tag{3.28}$$

For example, for $n = 0$, 1, 2,

$$\begin{aligned} \mathcal{Q}_1(\mathcal{A}) &= \frac{i}{2\pi} \mathrm{Tr}\mathcal{A}, \\ \mathcal{Q}_3(\mathcal{A}) &= \frac{-1}{8\pi^2} \mathrm{Tr}\left(\mathcal{A}d\mathcal{A} + \frac{2}{3}\mathcal{A}^3\right), \\ \mathcal{Q}_5(\mathcal{A}) &= \frac{-i}{48\pi^3} \mathrm{Tr}\left(\mathcal{A}(d\mathcal{A})^2 + \frac{3}{2}\mathcal{A}^3 d\mathcal{A} + \frac{3}{5}\mathcal{A}^5\right). \end{aligned} \tag{3.29}$$

The CS forms are not gauge invariant. Neither are the integrals of the CS forms. However, for two different choices of gauge $\mathcal{A}$ and $\mathcal{A}^g$, which are connected by a gauge transformation g as

$$\mathcal{A}^g \coloneqq g^{-1}\mathcal{A}g + g^{-1}dg, \qquad \mathcal{F}^g = g^{-1}\mathcal{F}g, \tag{3.30}$$

the difference $\mathcal{Q}_{2n+1}(\mathcal{A}^g) - \mathcal{Q}_{2n+1}(\mathcal{A})$ is given by the winding number density $\omega_{2n+1}[g]$ up to a total derivative term,

$$\mathcal{Q}_{2n+1}(\mathcal{A}^g) - \mathcal{Q}_{2n+1}(\mathcal{A}) = \omega_{2n+1}[g] + d\alpha_{2n+1}(\mathcal{A}, g). \tag{3.31}$$

Thus, for the integral of the CS form,

$$\mathrm{CS}_{2n+1}[\mathcal{A}^g] - \mathrm{CS}_{2n+1}[\mathcal{A}] = \text{integer}, \tag{3.32}$$

and hence the exponential

$$W_{2n+1} \coloneqq \exp\{2\pi i \mathrm{CS}_{2n+1}[\mathcal{A}]\} \tag{3.33}$$

is a well-defined, gauge invariant quantity, although it is not necessarily quantized.

The discussion so far has been general. We now compute the CS invariant in the presence of chiral symmetry. To this end, we first explicitly write down the Berry connection for chiral symmetric Hamiltonians. For a given $q(\mathsf{k},\mathsf{r})$, the eigenfunctions can explicitly be constructed as

$$|u^\alpha_\epsilon(\mathsf{k},\mathsf{r})\rangle_N = \frac{1}{\sqrt{2}}\begin{pmatrix} |n^\alpha\rangle \\ \epsilon q^\dagger(\mathsf{k},\mathsf{r})|n^\alpha\rangle \end{pmatrix}, \qquad \epsilon = \pm, \tag{3.34}$$

where $|n^\alpha\rangle$ are N momentum independent orthonormal vectors. For simplicity we choose $(n^\alpha)_\beta = \delta_{\alpha\beta}$. These wave functions are free from any singularity, i.e., we explicitly demonstrated that there is no obstruction to constructing eigenwave functions globally. The Berry connection is computed as $\mathcal{A}_N = (1/2)q(\mathsf{k},\mathsf{r})dq^\dagger(\mathsf{k},\mathsf{r})$. In this gauge, the CS form $\mathcal{Q}_{2n+1}$ is shown to be one-half of the winding number density, i.e., $\mathcal{Q}_{2n+1}(\mathcal{A}_N) = \omega_{2n+1}[q^\dagger]/2$. We conclude that $\mathrm{CS}_{2n+1}[\mathcal{A}_N] = \nu_{2n+1}[q^\dagger]/2$ and hence

$$W_{2n+1} = \exp\{\pi i \nu_{2n+1}[q]\} = \pm 1. \tag{3.35}$$

That is, for Hamiltonians with chiral symmetry W_{2n+1} can take on only two values $W_{2n+1} = \pm 1$.

When $(d, D) = (1, 0)$ $(n = 0)$, the CS invariant W_1 is a $U(1)$ Wilson loop defined in the $\mathrm{BZ}^{d=1} \simeq S^1$. The logarithm of W_1 represents the electric polarization (King-Smith and Vanderbilt, 1993; Vanderbilt and King-Smith, 1993; Resta, 1994), which can be quantized by chiral symmetry and inversion symmetry (Zak, 1989; Ryu and Hatsugai, 2002). In this context, the noninvariance of $\mathrm{CS}_1[\mathcal{A}]$, Eq. (3.32), is related to the fact that the displacement of electron coordinates in periodic systems has a meaning only within a unit cell, i.e., two coordinates that differ by an integer multiple of the lattice constant should be identified.

When $(d, D) = (3, 0)$ $(n = 1)$, CS_3 represents the quantized magnetoelectric polarizability or "θ angle." The θ angle, which is given in terms of the Chern-Simons integral as

$$\theta = 2\pi \int_{\mathrm{BZ}^3} \mathcal{Q}_3(\mathsf{k}) \mod 2\pi, \tag{3.36}$$

appears in the electrodynamic efffective action through the axion term $\delta S = (\theta\alpha/4\pi)\int d^3\mathsf{r}dt\mathbf{E}\cdot\mathbf{B}$, where α is the fine structure constant. The quantized magnetoelectric polarizability was first noted in the context of 3D TR symmetric TIs (in class AII) (Qi, Hughes, and Zhang, 2008; Essin, Moore, and Vanderbilt, 2009; Xiao *et al.*, 2009). Besides TRS, chiral and inversion symmetries also quantize the CS invariant W_3 (Hosur, Ryu, and Vishwanath, 2010; Ryu, Schnyder *et al.*, 2010; Turner, Zhang, and Vishwanath, 2010; Deng, Wang, and Duan, 2014; S.-T. Wang *et al.*, 2015).

c. Example: The 1D class AIII polyacetylene

Consider the bipartite hopping model (2.16) on the 1D lattice,

$$\hat{H} = t\sum_i (\hat{a}_i^\dagger \hat{b}_i + \mathrm{H.c.}) - t'\sum_i (\hat{b}_i^\dagger \hat{a}_{i+1} + \mathrm{H.c.}), \tag{3.37}$$

where $\hat{a}_i/\hat{b}_i$ are the fermion annihilation operators on sublattice A/B in the ith unit cell. We consider only real-valued nearest neighbor hopping amplitudes in Eq. (2.16), which we denote by t, t', where we assume that t, $t' \geq 0$. This is the Su-Schrieffer-Heeger (SSH) model describing transpolyacetylene (Su, Schrieffer, and Heeger, 1980; Heeger *et al.*, 1988). In momentum space, the Hamiltonian is written as $\hat{H} = \sum_k \hat{\Psi}^\dagger(k)H(k)\hat{\Psi}(k)$, where $\hat{\Psi}(k) = (\hat{a}_k, \hat{b}_k)^T$, $k \in [-\pi, \pi]$, and

$$H(k) = \boldsymbol{R}(k)\cdot\boldsymbol{\sigma}, \qquad \boldsymbol{R}(k) = \begin{pmatrix} t - t'\cos k \\ -t'\sin k \\ 0 \end{pmatrix}. \tag{3.38}$$

The energy dispersion is $\varepsilon(k) = \pm\sqrt{t^2 - 2tt'\cos k + t'^2}$. The Hamiltonian has chiral symmetry as discussed around Eq. (2.16), which in momentum space translates into the condition $\sigma_3 H(k)\sigma_3 = -H(k)$. With this symmetry, the two gapped phases with $t > t'$ and $t < t'$ are topologically distinct and are separated by a quantum critical point at $t = t'$. Ground states in the phase $t > t'$ are adiabatically connected to an atomic insulator (a collection of decoupled lattice sites) realized at $t' = 0$. On the other hand, ground states in the phase $t' > t$ are topologically distinct from topologically trivial, atomic insulators, once chiral symmetry is imposed. These two phases are characterized by the winding number

$$\nu[q] = \frac{i}{2\pi}\int_{\mathrm{BZ}} dk q^\dagger \partial_k q = \begin{cases} 1, & t' > t, \\ 0, & t' < t, \end{cases} \tag{3.39}$$

where the off-diagonal component of the projector is given by $q(k) = (t - t'e^{-ik})/|\varepsilon(k)|$. Correspondingly, the CS invariant also takes two distinct quantized values $\mathrm{CS} = 1(0)$ for $t' > t$ and $t > t'$, respectively. Provided t/t' is close to the critical point, the low-energy physics of the SSH model is captured by the continuum Dirac Hamiltonian

$$H(k) \simeq -t'k\sigma_2 + (t - t')\sigma_1, \tag{3.40}$$

which is obtained from Eq. (3.38) by expanding around $k = 0$. Note that $t - t'$ plays the role of the mass m.

To discuss domain walls, we first simplify the notation by letting $t \to t + m$ and $t' \to t$. Furthermore, we make m position dependent, which defines a defect Hamiltonian in class AIII or BDI:

$$H(k, r) = [t(1 - \cos k) + m(r)]\sigma_1 - t \sin k \sigma_2. \tag{3.41}$$

Let us consider a spatially modulated mass gap $m(r)$ that describes a domain wall profile, i.e., $m(r) = \mathrm{sgn}(r)m_0$ for $|r| \geq R_0$ with $m_0 \neq 0$. From Eq. (3.25), we associate a topological invariant to this domain wall

$$\begin{aligned}\nu_1 &= \frac{i}{2\pi}\int_{\mathrm{BZ}\times S^0} q^\dagger dq \\ &= \frac{i}{2\pi}\int_0^{2\pi} dk[q(k, R_0)^\dagger \partial_k q(k, R_0) \\ &\quad - q(k, -R_0)^\dagger \partial_k q(k, -R_0)] = \pm 1,\end{aligned} \tag{3.42}$$

where $S^0 = \{R_0, -R_0\}$ is the two points that sandwich the point defect at the origin. The defect is also characterized by the CS integral (3.46), which in this case is the electric polarization:

$$\begin{aligned}\mathrm{CS}_1 &= \frac{i}{2\pi}\int_{\mathrm{BZ}\times S^0} \mathcal{A} \\ &= \frac{i}{2\pi}\int_0^{2\pi} dk[A(k, R_0) - A(k, -R_0)] = \frac{1}{2} \mod \mathbb{Z}.\end{aligned} \tag{3.43}$$

The invariants (3.42) and (3.43) tell the difference between the two sides of the domain wall. They are well defined even for the continuum Jackiw-Rebbi analog (Jackiw and Rebbi, 1976)

$$H(k, r) = -tk\sigma_2 + m(r)\sigma_1, \tag{3.44}$$

where the bulk topological invariants on either side do not take integer values without a regularization. Their differences as presented in Eqs. (3.42) and (3.43), however, are regularization independent, and detect the localized zero-energy mode at the domain wall. The properties of these localized modes are further discussed later in Sec. III.D.

d. Example: The 3D class DIII ^{3}He-*B*

Three-dimensional TSCs in class DIII have been discussed in the context of the B phase of superfluid ^{3}He (Volovik, 2003; Schnyder *et al.*, 2008; Wada *et al.*, 2008; Chung and Zhang, 2009; Murakawa *et al.*, 2009, 2011; Qi *et al.*, 2009; Ryu, Schnyder *et al.*, 2010), in superconducting copper doped bismuth selinide (Fu and Berg, 2010; Hor *et al.*, 2010; Wray *et al.*, 2010), and in noncentrosymmetric SCs (Schnyder and Ryu, 2011). Here we consider the Balian-Werthamer state of the B phase of ^{3}He. The BdG Hamiltonian that describes the B phase is given in terms of the Nambu spinor $\hat{\Psi}^\dagger = (\hat{\psi}^\dagger_\uparrow, \hat{\psi}^\dagger_\downarrow, \hat{\psi}_\uparrow, \hat{\psi}_\downarrow)$ composed of the fermion annihilation operator for ^{3}He $\hat{\psi}_{\uparrow,\downarrow}$ as $\hat{H} = (1/2)\sum_{\mathsf{k}} \hat{\Psi}^\dagger(\mathsf{k}) H(\mathsf{k}) \hat{\Psi}(\mathsf{k})$, where

$$\begin{aligned}H(\mathsf{k}) &= \begin{pmatrix} \xi(\mathsf{k}) & \Delta(\mathsf{k}) \\ \Delta^\dagger(\mathsf{k}) & -\xi(\mathsf{k}) \end{pmatrix}, \\ \xi(\mathsf{k}) &= k^2/2m - \mu, \qquad \Delta(\mathsf{k}) = \Delta_0 i\sigma_2 \mathsf{k}\cdot\boldsymbol{\sigma}.\end{aligned} \tag{3.45}$$

The BdG Hamiltonian satisfies $\tau_1 H(-\mathsf{k})^T \tau_1 = -H(\mathsf{k})$ and $\sigma_2 H(-\mathsf{k})^* \sigma_2 = H(\mathsf{k})$, and belongs to class DIII. From the periodic table, class DIII in $d = 3$ dimensions admits topologically nontrivial SCs (superfluid), which are characterized by an integer topological invariant, i.e., the winding number $\nu_3[q]$. The winding number for the BdG Hamiltonian (3.45) is given by $\nu_3 = (1/2)(\mathrm{sgn}\mu + 1)$. Hence, for $\mu > 0$ a topological superfluid is realized. When terminated by a surface, topological superfluids support a topologically stable surface Andreev bound state (Majorana cone). Surface acoustic impedance measurements experimentally detected such a surface Andreev bound state in ^{3}He-B (Wada *et al.*, 2008; Murakawa *et al.*, 2009, 2011).

3. The first $\mathbb{Z}_2$ descendant for s even

While for the primary series the topological phases or topological defects are characterized by an integer-valued Chern number (or winding number), for the first and second descendants the topological phases are characterized by a $\mathbb{Z}_2$ invariant. To discuss these $\mathbb{Z}_2$ indices in a unified framework, we follow two strategies: First, we construct various $\mathbb{Z}_2$ topological invariants by starting from the CS invariants and using symmetry conditions to restrict their possible values (CS and $\widetilde{\mathrm{CS}}$ in Table III). Second, we use both the Chern numbers and CS integrals to construct $\mathbb{Z}_2$ invariants (FK in Table III).

The first $\mathbb{Z}_2$ descendant topologies are characterized by the CS integral

$$\mathrm{CS}_{2n-1} = \int_{\mathrm{BZ}^d\times\mathcal{M}^D} \mathcal{Q}_{2n-1} \in \frac{1}{2}\mathbb{Z}, \tag{3.46}$$

for $n = (d + D + 1)/2$. The CS invariant is well defined only up to an integer. Note that under antiunitary symmetries, the CS invariant can in general take half-integer values. The $\mathbb{Z}_2$ topology is trivial when CS_{2n-1} is an integer or nontrivial when CS_{2n-1} is a half integer.

There is a subtlety when computing the CS integrals (3.46) for a general defect Hamiltonian [this also applies to the Fu-Kane invariant (3.63), which will be discussed later]: they require a set of occupied states defined globally on the base space, which is unnecessary for the definition of the Chern number (3.10) and the winding number (3.25). There may be a topological obstruction to such global continuous basis. In particular, a global valence frame does not exist whenever there are nontrivial weak topologies with nonzero Chern invariants in lower dimensions. In this case, one needs to include artificial Hamiltonians, i.e., $H(\mathsf{k}, \mathsf{r}) \to H(\mathsf{k}, \mathsf{r}) \oplus H_0(\mathsf{k}, \mathsf{r}_0)$, that cancel the weak topologies while at the same time do not affect the highest dimensional strong topology (Teo and Kane, 2010b). This can be achieved by a lower dimensional Hamiltonian $H_0(\mathsf{k}, \mathsf{r}_0)$, where r_0 lives in some proper cycles $\mathcal{N}^{D'} \subsetneq \mathcal{M}^D$ that do not wrap around the defect under consideration; see Sec. III.D.1.b for an example.

a. Class D in $d = 1$

A BdG Hamiltonian in class D in $d = 1$ dimensions satisfies $C^{-1}H(-k)C = -H(k)$, with $C = \tau_1\mathcal{K}$, where $k \in (-\pi, \pi]$ is the 1D momentum. Class D TSCs in $d = 1$ are characterized by the CS integral (3.46). As chiral symmetry, PHS also quantizes $W = \exp(2\pi i \mathrm{CS}[\mathcal{A}])$ to be ± 1 (Qi, Hughes, and Zhang, 2008; Budich and Ardonne, 2013). To see this, we first recall that if $|u^\alpha_-(k)\rangle$ is a negative energy solution with energy $-\varepsilon(k)$, then $|\tau_1 u^{*\alpha}_-(-k)\rangle$ is a positive energy solution with energy $\varepsilon(k)$ (Sec. II.B). Consequently, the Berry connections for negative and positive energy states are related by

$$A^{\alpha\beta}_-(k) = \langle u^\alpha_-(k)|\partial_k u^\beta_-(k)\rangle = A^{\alpha\beta}_+(-k). \tag{3.47}$$

The 1D CS integral is then given by

$$\begin{aligned}\int_{-\pi}^{+\pi} dk \mathrm{Tr} A_- &= \int_0^\pi dk \mathrm{Tr}[A_- + A_+] \\ &= \int_0^\pi dk u_i^{*a}\partial_k u_i^a = \int_0^\pi dk \mathrm{Tr} U^\dagger \partial_k U,\end{aligned} \tag{3.48}$$

where a runs over all the bands, while α runs over half of the bands (i.e., only the negative energy bands). Here we introduced unitary matrix notation with $U^a_i(k) \coloneqq u^a_i(k)$. By noting that $\int_0^\pi dk \mathrm{Tr} U^\dagger \partial_k U = \int_0^\pi dk \partial_k \ln\det[U(k)] = \ln\det U(\pi) - \ln\det U(0)$, the CS invariant reduces to

$$W = [\det U(\pi)]^{-1}[\det U(0)]. \tag{3.49}$$

At the PH symmetric momenta $k = 0, \pi$, the unitary matrix $U(k)$ has special properties. This can be seen most easily by using the Majorana basis (2.22). That is, by the basis change in Eq. (2.22), we obtain from $H(k)$ the Hamiltonian $X(k)$ in the Majorana basis. Remember that at TR invariant momenta $\tau_1 H^*(k)\tau_1 = -H(k)$. Hence, $X(k = 0, \pi)$ is a real skew-symmetric matrix, which can be transformed into its canonical form by an orthogonal matrix $O(k = 0, \pi)$ [see Eq. (2.26)]. W can then be written in terms of $O(k = 0, \pi)$ as

$$W = [\det O(\pi)]^{-1}[\det O(0)]. \tag{3.50}$$

Since $O(k = 0, \pi)$ are orthogonal matrices, their determinants are either $+1$ or -1, and so is the CS invariant $W = \pm 1$. Using a Pfaffian of $2n$-dimensional skew-symmetric matrices

$$\mathrm{Pf}(X) = \frac{1}{2^n n!}\sum_{\sigma\in S_{2n}} (-1)^{|\sigma|} X_{\sigma(1)\sigma(2)}\cdots X_{\sigma(2n-1)\sigma(2n)}, \tag{3.51}$$

where σ runs through permutations of $1, \ldots, 2n$, and noting further the identities $\mathrm{Pf}(OXO^T) = \mathrm{Pf}(X)\det(O)$, and $\mathrm{sgn}(\mathrm{Pf}[X(k)]\det[O(k)]) = 1$, W can also be written as

$$W = \mathrm{sgn}(\mathrm{Pf}[X(0)]\mathrm{Pf}[X(\pi)]), \tag{3.52}$$

which is manifestly gauge invariant (i.e., independent of the choice of wave functions).

b. Example: The class D Kitaev chain

The 1D TSC proposed by Kitaev has stimulated many studies on Majorana physics (Kitaev, 2001; Sau *et al.*, 2010; Alicea, 2012). Evidence for the existence of Majorana modes in 1D chains has been observed in a number of recent experiments (Lutchyn, Sau, and Das Sarma, 2010; Oreg, Refael, and von Oppen, 2010; Cook and Franz, 2011; Das *et al.*, 2012; Deng *et al.*, 2012; Mourik *et al.*, 2012; Churchill *et al.*, 2013; Finck *et al.*, 2013; Lee *et al.*, 2014; Nadj-Perge *et al.*, 2014). The Hamiltonian of the Kitaev chain is given by

$$\begin{aligned}\hat{H} = &\frac{t}{2}\sum_i (\hat{c}_i^\dagger \hat{c}_{i+1} + \hat{c}_{i+1}^\dagger \hat{c}_i) - \mu\sum_i (\hat{c}_i^\dagger \hat{c}_i - 1/2) \\ &+ \frac{1}{2}\sum_i (\Delta^* \hat{c}_i^\dagger \hat{c}_{i+1}^\dagger - \Delta \hat{c}_i \hat{c}_{i+i}).\end{aligned} \tag{3.53}$$

Without loss of generality, Δ can be taken as a real number, since the global phase of the order parameter $\Delta = e^{i\theta}\Delta_0$ can be removed by a simple gauge transformation $\hat{c}_i \to \hat{c}_i e^{i\theta/2}$. In momentum space $\hat{H}$ reads

$$\begin{aligned}&\hat{H} = \frac{1}{2}\sum_k \begin{pmatrix}\hat{c}_k^\dagger & \hat{c}_{-k}\end{pmatrix} H(k) \begin{pmatrix}\hat{c}_k \\ \hat{c}_{-k}^\dagger\end{pmatrix}, \\ &\text{where } H(k) = (t\cos k - \mu)\tau_3 - \Delta_0 \sin k \tau_2.\end{aligned} \tag{3.54}$$

There are gapped phases for $|t| > \mu$ and $|t| < \mu$, which are separated by a line of critical points at $t = \pm\mu$. The Kitaev chain can be written in terms of the Majorana basis

$$\hat{\lambda}_j \coloneqq \hat{c}_j^\dagger + \hat{c}_j, \quad \hat{\lambda}'_j \coloneqq (\hat{c}_j - \hat{c}_j^\dagger)/i, \quad \hat{\Lambda}_j \coloneqq \begin{pmatrix}\hat{\lambda}_j \\ \hat{\lambda}'_j\end{pmatrix}, \tag{3.55}$$

as $\hat{H} = (i/2)\sum_k \hat{\Lambda}^T(k) X(k) \hat{\Lambda}(-k)$, where

$$X(k) = -i(t\cos k - \mu)\tau_2 + i\Delta_0 \sin k \tau_1. \tag{3.56}$$

We read off the CS invariant as $W = \mp 1$ for $|\mu| < |t|$ and $|\mu| > |t|$, respectively.

Similar to the SSH model, we also consider a domain wall by changing μ as a function of space, which traps a localized zero-energy Majorana mode. Properties of the localized zero-energy Majorana mode are discussed in Sec. III.D.

c. Class AII in $d = 3$

We now discuss the topological property of TR invariant insulators in $d = 3$ dimensions (Fu, Kane, and Mele, 2007; Moore and Balents, 2007; Roy, 2009b). The topological characteristics of these band insulators are intimately tied to the invariance of the Hamiltonian under TRS, i.e., $T^{-1}H(-\mathsf{k})T = H(\mathsf{k})$. Because of this relation, the Bloch wave functions at k and those at $-\mathsf{k}$ are related. If $|u^\alpha(\mathsf{k})\rangle$ is an eigenstate at k, then $T|u^\alpha(\mathsf{k})\rangle$ is an eigenstate at $-\mathsf{k}$. Imagine now that we can define $|u^\alpha(\mathsf{k})\rangle$ smoothly for the entire BZ. (This is possible since TRS forces the Chern number to be zero and, hence, there is no obstruction.) We

then compare $|u^\alpha(-\mathsf{k})\rangle$ and $T|u^\alpha(\mathsf{k})\rangle$. Since both $|u^\alpha(-\mathsf{k})\rangle$ and $T|u^\alpha(\mathsf{k})\rangle$ are eigenstates of the same Hamiltonian $H(-\mathsf{k})$, they must be related to each other by a unitary matrix $|u^\alpha(-\mathsf{k})\rangle = [w^{\alpha\beta}(\mathsf{k})]^*|Tu^\beta(\mathsf{k})\rangle$. (The complex conjugation on w here is to comply with a common convention.) Hence, the sewing matrix

$$w^{\alpha\beta}(\mathsf{k}) = \langle u^\alpha(-\mathsf{k})|Tu^\beta(\mathsf{k})\rangle, \tag{3.57}$$

which is given by the overlaps between the occupied eigenstates with momentum $-\mathsf{k}$ and the time reversed images of the occupied eigenstates with momentum k, plays an important role in defining the $\mathbb{Z}_2$ index (Fu, Kane, and Mele, 2007). The matrix elements (3.57) obey

$$w^{\alpha\beta}(-\mathsf{k}) = -w^{\beta\alpha}(\mathsf{k}), \tag{3.58}$$

which follows from the fact that T is antilinear and antiunitary, and $T^2 = -1$. Consequently, there is a relation between the Berry connection at k and at $-\mathsf{k}$:

$$A_\mu(-\mathsf{k}) = -w(\mathsf{k})A_\mu^*(\mathsf{k})w^\dagger(\mathsf{k}) - w(\mathsf{k})\partial_\mu w^\dagger(\mathsf{k}). \tag{3.59}$$

That is, $-A_\mu(-\mathsf{k})$ and $A_\mu^*(\mathsf{k}) = -A_\mu^T(\mathsf{k})$ are related to each other by a gauge transformation.

With this constraint on the Berry connection, we now show that the CS invariant is given in terms of the winding number of the sewing matrix w as

$$\mathrm{CS}[\mathcal{A}] = \frac{1}{2}\int_{\mathrm{BZ}} \omega[w] = \frac{1}{2}\times \text{integer}, \tag{3.60}$$

and hence $W = \exp(2\pi i \mathrm{CS}[\mathcal{A}]) = \pm 1$. To see this, we change variables from k to $-\mathsf{k}$ in the integral $\mathrm{CS}[\mathcal{A}]$, and use Eq. (3.59), $A_\mu(-\mathsf{k}) = -[A_\mu^{g^*}(\mathsf{k})]^*$ with $g = w^\dagger$, to show $\mathrm{CS}[\mathcal{A}] = -\mathrm{CS}[(\mathcal{A}^{g^*})^*] = -(\mathrm{CS}[\mathcal{A}^{g^*}])^* = -\mathrm{CS}[\mathcal{A}^{g^*}]$, where in the last equality we noted that $\mathrm{CS}[\mathcal{A}]$ is real. Using Eq. (3.31),

$$\mathrm{CS}[\mathcal{A}] = -\mathrm{CS}[\mathcal{A}] - \int_{\mathrm{BZ}} \{w[g^*] + d\alpha(\mathcal{A}, g^*)\}, \tag{3.61}$$

and $\int_{\mathrm{BZ}} \omega[g] = \int_{\mathrm{BZ}} \omega[w^\dagger] = -\int_{\mathrm{BZ}} \omega[w]$ proves the quantization of the CS invariant (3.60).

The CS invariant can also be written by using the Pfaffian of the gluing matrix w at TR invariant momenta K in the BZ as (Kane and Mele, 2005a, 2005b; Fu and Kane, 2007)

$$W = \prod_{\mathsf{K}} \frac{\mathrm{Pf}[w(\mathsf{K})]}{\sqrt{\det[w(\mathsf{K})]}}. \tag{3.62}$$

The equivalence between the quantized CS invariant and the Pfaffian invariant (3.62) was shown in Wang, Qi, and Zhang (2010).

4. The second $\mathbb{Z}_2$ descendant for s even

The Fu-Kane (FK) invariant (Fu and Kane, 2006) applies to the second $\mathbb{Z}_2$ descendent for nonchiral symmetry classes and is defined by

$$\mathrm{FK}_n = \frac{1}{n!}\left(\frac{i}{2\pi}\right)^n \int_{\mathrm{BZ}^d_{1/2}\times\mathcal{M}^D} \mathrm{Tr}(\mathcal{F}^n) - \oint_{\partial \mathrm{BZ}^d_{1/2}\times\mathcal{M}^D} \mathcal{Q}_{2n-1}, \tag{3.63}$$

where $n = (d+D)/2$. It involves an open integral of the Berry curvature over half of the Brillouin zone $\mathrm{BZ}^d_{1/2}$, where one of the momentum paramenters, say k_1, runs between $[0,\pi]$ so that the complement of $\mathrm{BZ}^d_{1/2}$ is its TR conjugate. The CS integral over $\partial\mathrm{BZ}^d_{1/2}$, the boundary of the half BZ where $k_1 = 0, \pi$, is gauge dependent and requires special attention in the choice of basis. For TRS systems (classes AI and AII), the occupied states $|u^\alpha(\mathsf{k},\mathsf{r})\rangle$ that build the Berry connection $\mathcal{A}^{\alpha\beta}$ need to satisfy the gauge constraint

$$w^{\alpha\beta}(\mathsf{k},\mathsf{r}) = \langle u^\alpha(-\mathsf{k},\mathsf{r})|Tu^\beta(\mathsf{k},\mathsf{r})\rangle = \text{const}, \tag{3.64}$$

for $(\mathsf{k},\mathsf{r}) \in \partial\mathrm{BZ}^d_{1/2}\times\mathcal{M}^D$. For instance the original FK-invariant characterizing 2D class AII TIs requires $w(\mathsf{k},\mathsf{r}) = i\sigma_2$. For PHS systems (classes D and C), the occupied states $|u^\alpha(\mathsf{k},\mathsf{r})\rangle$ generate the unoccupied ones $|v^\alpha(\mathsf{k},\mathsf{r})\rangle$ by the PH operator C, i.e., $|v^\alpha(\mathsf{k},\mathsf{r})\rangle = |Cu^\alpha(-\mathsf{k},\mathsf{r})\rangle$. The CS form in the FK invariant (3.63) needs to be built from occupied states satisfying

$$\int_{\partial\mathrm{BZ}^d_{1/2}\times\mathcal{M}^D} \mathrm{Tr}[(XdX^\dagger)^{d+D-1}] = 0, \tag{3.65}$$

where $X(\mathsf{k},\mathsf{r}) = (u^1,\ldots,u^N,v^1,\ldots,v^N)$ is the unitary matrix formed by the eigenstates. The gauge constraints (3.64) and (3.65) are essential for the FK invariant in Eq. (3.63). Without them, the CS integral can be changed by any integer value by a large gauge transformation of occupied states $|u^\alpha\rangle \to g_{\alpha\beta}|u^\beta\rangle$. The gauge constraints restrict such transformations so that the CS term can be changed only by an even integer. The FK invariant therefore takes values in $\mathbb{Z}_2 = \{0,1\}$.

a. Class AII in $d = 2$

The topological invariant for 2D time-reversal symmetric TIs is the Fu-Kane invariant (3.63) (Fu and Kane, 2006). As in the case of 3D time-reversal symmetric TIs, this $\mathbb{Z}_2$ invariant has the following alternative expression:

$$W = \prod_{\mathsf{K}} \frac{\mathrm{Pf}[w(\mathsf{K})]}{\sqrt{\det[w(\mathsf{K})]}}, \tag{3.66}$$

where K runs over two-dimensional TR fixed momenta. This topological invariant can also be written in a number of different ways. For example, it can be introduced as TR invariant polarization (Fu and Kane, 2006), which can be written as an $SU(2)$ Wilson loop in momentum space (Lee and Ryu, 2008; Ryu, Mudry *et al.*, 2010; Yu *et al.*, 2011); see also Kane and Mele (2005a, 2005b), Prodan (2011), Soluyanov and Vanderbilt (2011), Freed and Moore (2013), and Fruchart and Carpentier (2013) for different representations of the $\mathbb{Z}_2$ invariant.

5. The first $\mathbb{Z}_2$ descendant for s odd

The first $\mathbb{Z}_2$ descendant for the chiral classes relates isomorphically to the second $\mathbb{Z}_2$ descendant for the nonchiral classes. This relation is discussed in more detail in Sec. III.C.2. The topological invariant for chiral $\mathbb{Z}_2^{(1)}$ is therefore given by the FK invariant (3.63) with the gauge constraint (3.64) for $s = 1$, 5 (classes CI and DIII) or Eq. (3.65) for $s = 3$, 7 (classes BDI and CII).

a. Class DIII in $d = 2$

As in the case of time-reversal symmetric TIs in $d = 2$ (AII), the FK invariant for time-reversal symmetric TSCs in $d = 2$ (DIII) can be written in terms of the Pfaffian formula (3.62). The presence of TRS allows us to define the $\mathbb{Z}_2$ invariant. The Pfaffian formula can also be given in terms of the Q matrix. To see this, we write the BdG Hamiltonian in the off-diagonal basis, i.e., in the form

$$H(\mathsf{k}) = \begin{pmatrix} 0 & D(\mathsf{k}) \\ D^\dagger(\mathsf{k}) & 0 \end{pmatrix}, \qquad D(\mathsf{k}) = -D^T(-\mathsf{k}). \tag{3.67}$$

In this representation, the TR operator is given by $T = U_T\mathcal{K} = i\sigma_2 \otimes \mathbb{1}\mathcal{K}$, and the Q matrix reads

$$Q(\mathsf{k}) = \begin{pmatrix} 0 & q(\mathsf{k}) \\ q^\dagger(\mathsf{k}) & 0 \end{pmatrix}, \qquad q(\mathsf{k}) = -q^T(-\mathsf{k}). \tag{3.68}$$

To compute the $\mathbb{Z}_2$ topological number we choose the basis $|u_\pm^\alpha(\mathsf{k})\rangle_N$, in which the sewing matrix is given by $w^{\alpha\beta}(\mathsf{k}) = -q^{\alpha\beta}(-\mathsf{k})$. The $\mathbb{Z}_2$ topological number can thus be expressed as (Schnyder and Ryu, 2011)

$$W = \prod_{\mathsf{K}} \frac{\mathrm{Pf}[q(\mathsf{K})]}{\sqrt{\det[q(\mathsf{K})]}}, \tag{3.69}$$

where K denotes the four TR invariant momenta of the 2D BZ.

6. The second $\mathbb{Z}_2$ descendant for s odd

The second $\mathbb{Z}_2$ descendant for chiral classes is given by the CS integral CS_{2n-1} in Eq. (3.46) for $n = (d + D + 1)/2$. Similar to the FK invariants, the CS form here needs to be built from occupied states that satisfy the gauge constraint (3.64) for classes CI and DIII or Eq. (3.65) for classes BDI and CII. Together with the antiunitary symmetry, this gauge constraint forces the Chern-Simions invariant (3.46) to be a full integer. The $\mathbb{Z}_2$ topology is trivial if CS_{2n-1} is even, and nontrivial if CS_{2n-1} is odd.

a. Class DIII in $d = 1$

In $d = 1$ the gauge constraint (3.64) is automatically satisfied. The CS integral (3.46) becomes the "polarization" (3.43), which takes value in full integers. By taking the basis where the Hamiltonian and the Q matrix take the form of Eq. (3.68), the CS integral can be simplified into the following $\mathbb{Z}_2$ invariant:

$$(-1)^\nu = \frac{\mathrm{Pf}[q(\pi)]}{\mathrm{Pf}[q(0)]} \frac{\sqrt{\det[q(0)]}}{\sqrt{\det[q(\pi)]}}, \tag{3.70}$$

that relies on information only on the fixed momenta $k = 0, \pi$ (Qi, Hughes, and Zhang, 2010). Note that the branch $\sqrt{\det[q(k)]}$ must be chosen continuously between the two fixed momenta. A proof of the equivalence of the 1D CS integral and Eq. (3.70) can be found in Teo and Kane (2010b). As an example, let us consider the class DIII Hamiltonian in the form of Eq. (3.68) with

$$D(k) = -t \sin k\sigma_1 - i[\Delta + u(1 - \cos k)]\sigma_2, \tag{3.71}$$

where $k \in [-\pi, \pi]$ and $u \gg |\Delta|$. By noting that $\det[q(k)]$ is always real and positive, $\mathrm{Pf}[q(0)]/\sqrt{\det[q(0)]} = \mathrm{sgn}(\Delta)$ while $\mathrm{Pf}[q(\pi)]/\sqrt{\det[q(\pi)]} = 1$. Hence this model is nontrivial according to Eq. (3.70) when the pairing Δ is negative.

Before concluding this section, it is worth mentioning that the topological invariants discussed can be cast in many different forms. Moreover, they can be extended, in certain cases, in a way that they are valid in the presence of disorder and interactions. For example, the Chern invariant can be written in terms of many-body ground state wave functions, which depend on twisting boundary conditions (Niu, Thouless, and Wu, 1985; Wang and Zhang, 2014). All topological invariants discussed can be written in the language of scattering matrices (Akhmerov *et al.*, 2011; Fulga *et al.*, 2011; Fulga, Hassler, and Akhmerov, 2012). Topological invariants can also be written in terms of Green's functions (Ishikawa and Matsuyama, 1987; Volovik, 2003; Gurarie, 2011; Wang, Qi, and Zhang, 2012; Wang and Zhang, 2012) and by using C^* algebra (Bellissard, van Elst, and Schulz-Baldes, 1994; Loring and Hastings, 2010; Hastings and Loring, 2011; Prodan, Leung, and Bellissard, 2013; Prodan, 2014; Prodan and Schulz-Baldes, 2014).

C. K-theory approach

In this section, we derive the classification of gapped topological phases and topological defects, which is summarized in Table I. The classification can be shown either by relating to the homotopy groups of classifying spaces or by a K-theoretical argument (Kitaev, 2009). We also demonstrate the use of the Clifford algebra in identifying classifying spaces of symmetry-allowed Dirac mass terms. This method effectively allows us to translate topological problems into algebraic problems, and makes use of a known connection between K theory and Clifford algebras; the Bott periodicity of K theory is proved by using Clifford algebras (Atiyah, Bott, and Shapiro, 1964; Lawson and Michelsohn, 1990; Hatcher, 2001). For a more complete and precise description of K theory, Clifford algebra, and Bott periodicity see the literature in mathematics (Milnor, 1963; Karoubi, 1978; Lawson and Michelsohn, 1990; Atiyah, 1994) as well as in physics (Stone, Chiu, and Roy, 2011; Abramovici and Kalugin, 2012; Fulga, Hassler, and Akhmerov, 2012; Wen, 2012; Budich and Trauzettel, 2013; Freed and Moore, 2013; Kennedy and Zirnbauer, 2016; Thiang, 2016).

1. Homotopy classification of Dirac mass gaps

We have seen already that many topologically nontrivial phases (as well as trivial phases) have a massive Dirac Hamiltonian representative. One could then be interested in focusing on and classifying Dirac representatives. One may think this is a crude approximation, but as it turns out one does not lose much by narrowing one's focus in this way (see Sec. III.C.2). We thus consider the low-energy description of Bloch-BdG Hamiltonians near the relevant momentum point K_0, which generically takes the Dirac form

$$H(\mathsf{k},\mathsf{r}) = \mathsf{k}\cdot\mathbf{\Gamma} + m\Gamma_0(\mathsf{r}), \tag{3.72}$$

where $\mathsf{k} = (k_1,\ldots,k_d)$ is the momentum deviation from K_0 and $\mathbf{\Gamma} = (\Gamma_1,\ldots,\Gamma_d)$ are Dirac matrices that satisfy the Clifford relation $\{\Gamma_\mu,\Gamma_\nu\} = \Gamma_\mu\Gamma_\nu + \Gamma_\nu\Gamma_\mu = 2\delta_{\mu\nu}$ $(\mu,\nu = 0,\ldots,d)$. The mass term $m\Gamma_0(\mathsf{r})$, which depends on a D-dimensional spatial parameter r, anticommutes with all Dirac matrices in the kinetic term and is responsible for a bulk energy gap. For a stable classification, which is independent of and insensitive to the addition of irrelevant trivial bands, the dimension of the Dirac matrices (the number of bands) are taken to be sufficiently large, $\log[\dim(\Gamma_0)] \gg d + D$, the motivation of which will become clear later. In the presence of symmetries [Eqs. (3.6)–(3.8)], the Dirac matrices satisfy

$$T\Gamma_0(\mathsf{r})T^{-1} = \Gamma_0(\mathsf{r}), \qquad T\mathbf{\Gamma}T^{-1} = -\mathbf{\Gamma}, \tag{3.73}$$

$$C\Gamma_0(\mathsf{r})C^{-1} = -\Gamma_0(\mathsf{r}), \qquad C\mathbf{\Gamma}C^{-1} = \mathbf{\Gamma}, \tag{3.74}$$

$$S\Gamma_0(\mathsf{r})S^{-1} = -\Gamma_0(\mathsf{r}), \qquad S\mathbf{\Gamma}S^{-1} = -\mathbf{\Gamma}. \tag{3.75}$$

For a general TI or TSC, the mass term $m\Gamma_0$ lives in some parameter space $\mathcal{R}$ that has the same topology (or homotopy type) as a certain *classifying space* (Lawson and Michelsohn, 1990; Hatcher, 2001; Freedman *et al.*, 2011), which will be identified shortly. Suppose we have a domain wall sandwiched by two bulk regions A and B. For example, a domain wall separating a Chern insulator and a trivial insulator in 2D can be topologically captured by Eq. (3.72), where the mass term changes its sign across the interface. Now pick arbitrary points r_A in A and r_B in B. The domain wall is topological and carries protected interface modes, if there does not exist any continuous path in the parameter space $\mathcal{R}$ that connects $m\Gamma_0(\mathsf{r}_A)$ and $m\Gamma_0(\mathsf{r}_B)$. The topology is therefore characterized by $\pi_0(\mathcal{R}) = [S^0,\mathcal{R}]$, the 0th-homotopy group of $\mathcal{R}$ that counts the path connected components.

For general topological defects other than domain walls, we first approximate the defect Hamiltonian by the Dirac Hamiltonian, where r is now the modulation parameter that wraps around the defect in spacetime. In this case, we are interested in the highest dimensional strong topologies, where r lives on (or deformation retracts to) the compactified sphere S^D.

The mass term $m\Gamma_0$ belongs to different classifying spaces $\mathcal{R}_{s-d}$ for different symmetry classes s and bulk dimension d. As we will see, the classifying space is determined by the symmetries (3.73). Let us now demonstrate this for a few cases.

a. Class A in $d = 2$ and $d = 1$

As the first example, we identity the classifying space that is relevant for 2D Chern insulators in class A. To this end, let us first recall the lattice model given by Eq. (3.22). By linearizing the spectrum near $\mathsf{K}_0 = 0$, we obtain from Eq. (3.22) a $d = 2$ massive Dirac model $H(\mathsf{k}) = k_x\sigma_1 + k_y\sigma_2 + m\sigma_3$. There are two distinct phases in this model for $m > 0$ and $m < 0$, whose Chern number differs by 1. (Note here that we discuss only the relative Chern number.) To discuss phases with more general values of the Chern number, we enlarge the matrix dimension of the Hamiltonian and consider the following $2N\times 2N$ Dirac Hamiltonian:

$$H(\mathsf{k},\mathsf{r}) = k_x\sigma_1\otimes\mathbb{1}_N + k_y\sigma_2\otimes\mathbb{1}_N + M. \tag{3.76}$$

Since the mass M anticommutes with the kinetic term, M should have the form $M = \sigma_3\otimes A$, where A is a $N\times N$ Hermitian matrix. By considering $A = \mathrm{diag}(m_1,\ldots,m_N)$, $m_i \neq 0$, we can realize band insulators with different values of the (relative) Chern number. These are simply N decoupled copies of different Dirac insulators with different masses. The magnitude of the masses does not matter for the Chern number, while the sign $\mathrm{sgn}m_i$ does. So, without losing generality, we can consider $A = \Lambda_{n,N-n}$, where $\Lambda_{n,m} = \mathrm{diag}(\mathbb{1}_n,-\mathbb{1}_m)$. Starting from $\Lambda_{n,N-n}$, more generic mass terms can be generated by a unitary matrix U as $A = U\Lambda_{n,N-n}U^\dagger$, which share the same Chern number as $\Lambda_{n,N-n}$. Conversely, for a given A, as far as its eigenvalues are properly normalized, one can diagonalize A by a unitary matrix U and write $A = U\Lambda_{n,N-n}U^\dagger$. Thus, A is a member of $U(N)/U(n)\times U(N-n)$. Two masses A_1 and A_2 which have the same canonical form are unitarily related to each other, i.e., $U(N)/U(n)\times U(N-n)$ is simply connected. However, two masses A_1 and A_2 which have different canonical forms (i.e., different n) are not. Summarizing, the set of masses for a given N is $\bigcup_{0\le n\le N} U(N)/[U(n)\times U(N-n)]$.

So far we have fixed N, but this is clearly not enough for the purpose of realizing Dirac representatives for all possible phases since for given N, the (relative) Chern number can be at most N, whereas insulators in class A in $d = 2$ can be characterized by the Chern number which can be any integer. To realize insulators with arbitrary Chern number, we can take N as large as possible, and this leads us to consider

$$\mathcal{C}_0 = \bigcup_{n=0}^{N}\frac{U(N)}{U(n)\times U(N-n)} \xrightarrow{N\to\infty} BU\times\mathbb{Z}. \tag{3.77}$$

The disconnected components of this space $\pi_0(C_0)$ is the space of topologically distinct masses, for which it is known that $\pi_0(\mathcal{C}_0) = \mathbb{Z}$. This agrees with the classification of class A in $d = 2$.

The fact that we take the limit of an infinite number of bands, which can be achieved by adding as many orbitals as we want, is an essential ingredient of K theory. In general, one would expect that the addition of trivial atomic bands should not affect the nontrivial topological properties of gapped phases. Hence, one is interested in general in topological properties that are stable against inclusion of trivial bands. However, there are topological distinctions of gapped phases

that exist only when the number of bands is restricted to be some particular integer. For example, it is known that there does not exist nontrivial class A TIs in 3D with an arbitrary number of bands. However, if we restrict ourselves to 2-band models, nontrivial topologies exist as supported by the nontrivial homotopy $\pi_3(\mathbb{C}P^1)=\mathbb{Z}$ (Moore, Ran, and Wen, 2008; De Nittis and Gomi, 2014, 2015; Kennedy and Zirnbauer, 2016), which is unstable against the addition of trivial bands. By taking the limit of infinitely many bands, we eliminate in the following such unstable or accidental topologies, viz., we are interested in the *stable equivalence* of the ground states of gapped noninteracting systems.

The problem of classifying possible masses can be formulated in an alternative way as follows (Kitaev, 2009; Abramovici and Kalugin, 2012; Morimoto and Furusaki, 2013). First, the Dirac kinetic term (the part without mass) consists of gamma matrices, forming a Clifford algebra. In general, a complex Clifford algebra Cl_n is given in terms of a set of generators $\{e_i\}_{i=1,\ldots,n}$, which satisfy

$$\{e_i,e_j\}=2\delta_{ij}. \tag{3.78}$$

"Complex" here means we allow these generators to be represented by a complex matrix. (More formally, we are interested in a 2^n-dimensional complex vector space $\{C_{p_1p_2\cdots}e_1^{p_1}e_2^{p_2}\cdots\}$, where $p_i=0,1$ and $C_{p_1p_2\cdots}$ is a complex number.) For the present example of the class A TI in $d=2$, the Dirac matrices in the kinetic term satisfy $\{\sigma_i,\sigma_j\}=2\delta_{ij}$ ($i=1,2$), i.e., they form Cl_2. A mass should anticommute with all Dirac matrices in the kinetic term $\{\sigma_i,M\}=0$, $\forall i$, i.e., with the mass, we now have Cl_3. When considering a mass, we are thus extending the algebra from Cl_2 to Cl_3 by adding one generator (mass). Counting different ways to extend the algebra is nothing but counting unitary nonequivalent masses.

In the general case, we first consider a set of symmetry operators (and Dirac kinetic terms). They are represented as Clifford generators. We then consider, in addition to these generators, possible mass terms, which in turn extend the Clifford algebra. That is, for a fixed representation of the symmetry generators, we look for possible representations of a new additional generator (= mass). The set of these representations form a classifying space (Lawson and Michelsohn, 1990; Hatcher, 2001). Topologically distinct states correspond to distinct extensions of the algebra.

As yet another example, let us consider class A insulators in $d=1$ and their Dirac representatives given by $H(k)=k_x\sigma_3\otimes\mathbb{1}_N+M$. As before, the mass must anticommute with the Dirac kinetic term $\{\sigma_3,M\}=0$. The generic solution to this is

$$M=\begin{pmatrix}0 & U^\dagger\\ U & 0\end{pmatrix},\qquad U\in U(N). \tag{3.79}$$

Since $\pi_0(U(N))=0$, for fixed N, all masses can be continuously deformed to each other. That is, there is no topological distinction among gapped phases. As before, this problem can be formulated as an extension problem $Cl_1\to Cl_2$. The space classifying the extension is

$$\mathcal{C}_1=U(N) \tag{3.80}$$

and its homotopy group is given by $\pi_0(\mathcal{C}_1)=0$.

This analysis can be repeated for arbitrary d. One considers the extension $Cl_d\to Cl_{d+1}$. Denoting the corresponding classifying space $\mathcal{C}_d$, we look for $\pi_0(\mathcal{C}_d)$. Because of $Cl_{n+2}\simeq Cl_n\otimes\mathbb{C}(2)$, where $\mathbb{C}(2)$ is an algebra of 2×2 complex matrices (which does not affect the extension problem), we have a periodicity of classifying spaces

$$\mathcal{C}_{n+2}\simeq\mathcal{C}_n, \tag{3.81}$$

from which the twofold dimensional periodicity for the topological classification of class A follows.

b. Class AIII

As seen, the dimensional periodicity of the topological classification problem for a given symmetry class follows directly from the Clifford algebras. Similarly, the dimensional shift in the classification, caused by adding a symmetry, can also be understood using Clifford algebras. As an example, let us consider a zero-dimensional system in symmetry class AIII, whose mass (i.e., the Hamiltonian itself) H satisfies the chiral symmetry relation $\{H,U_S\}=0$. The unitary matrix U_S, like the gamma matrices in the Dirac kinetic term, can be thought of as a Clifford generator. With a proper normalization (spectral flattening), the zero-dimensional Hamiltonian H has eigenvalues ±1 and can be considered as an additional Clifford generator. We then consider an extension problem $Cl_1\to Cl_2$, whose classifying space is $\mathcal{C}_1$ and $\pi_0(\mathcal{C}_1)=0$. Thus, the presence of symmetries can be treated by adding a proper number of Clifford generators, and has effectively the same effect as increasing the space dimension.

c. Class D in d = 0, 1, 2

So far we discussed the use of complex Clifford algebras for the classification of Dirac masses in classes A and AIII. Real Clifford algebras are relevant for the classification of Dirac masses in the eight real symmetry classes, as we now illustrate.

We begin with the class D example in $d=0$, i.e., we consider the Hamiltonian $H(\mathsf{r})=m\Gamma_0(\mathsf{r})$, which anticommutes with $C=\mathcal{K}$. Let $\mathbf{u}_1,\ldots,\mathbf{u}_N$ be the orthonormal positive eigenvectors of Γ_0. By PHS, $\mathbf{u}_1^*,\ldots,\mathbf{u}_N^*$ are negative eigenvectors. Let $\mathbf{a}_j$ and $\mathbf{b}_j$ be the real and imaginary parts of $\mathbf{u}_j$, $\mathbf{u}_j=(\mathbf{a}_j+i\mathbf{b}_j)/\sqrt{2}$. The orthonormal relation $\mathbf{u}_i^\dagger\mathbf{u}_j=\delta_{ij}$ and $\mathbf{u}_i^T\mathbf{u}_j=0$ translates into $\mathbf{a}_i^T\mathbf{a}_j=\mathbf{b}_i^T\mathbf{b}_j=\delta_{ij}$ and $\mathbf{a}_i^T\mathbf{b}_j=0$. Thus we have an $O(2N)$ matrix $A=(\mathbf{a}_1,\ldots,\mathbf{a}_N,\mathbf{b}_1,\ldots,\mathbf{b}_N)$. Note that the same Γ_0 can correspond to different orthogonal matrices A, due to the $U(N)$ basis transformation $\mathbf{u}_j\to\mathbf{u}'_j=U_{jk}\mathbf{u}_k$. Hence, the class D mass term Γ_0 in $d=0$ lives in the classifying space

$$\mathcal{R}_2=O(2N)/U(N). \tag{3.82}$$

Moving on to 1D, we consider $H(k,\mathsf{r})=k\Gamma_1+m\Gamma_0(\mathsf{r})$. By a suitable choice of basis, we can assume that the PH operator has the form $C=\mathcal{K}$ and $\Gamma_1=\tau_3\otimes\mathbb{1}_N$. The mass term is thus

$\Gamma_0(\mathsf{r}) = \tau_2 \otimes \gamma_1(\mathsf{r}) + \tau_1 \otimes i\gamma_2(\mathsf{r})$, where γ_1, γ_2 are the real symmetric and antisymmetric components of an $N \times N$ matrix $\gamma(\mathsf{r}) = \gamma_1(\mathsf{r}) + \gamma_2(\mathsf{r})$. The normalization $\Gamma_0^2 = \mathbb{1}$ implies that γ must be orthogonal. Thus, class D mass terms in 1D belong to the classifying space

$$\mathcal{R}_1 = O(N). \tag{3.83}$$

Finally, we discuss the 2D case, where $H(\mathsf{k},\mathsf{r}) = k_1\Gamma_1 + k_2\Gamma_2 + m\Gamma_0(\mathsf{r})$. We choose the basis such that $C = \mathcal{K}$, $\Gamma_1 = \tau_1 \otimes \mathbb{1}_N$, and $\Gamma_2 = \tau_3 \otimes \mathbb{1}_N$. The mass term must be of the form $\Gamma_0(\mathsf{r}) = \tau_2 \otimes \gamma(\mathsf{r})$, where γ is real symmetric and $\gamma^2 = 1$ in order for Γ_0 to have the appropriate symmetry and square to unity. One can diagonalize γ by an orthogonal matrix $O = (\mathbf{a}_1, \ldots, \mathbf{a}_n, \mathbf{a}_{n+1}, \ldots, \mathbf{a}_N) \in O(N)$, where the first n vectors are positive eigenvectors of γ and the others are negative ones. We observe that the same γ can correspond to different orthogonal matrices, due to $O(n) \times O(N-n)$ basis transformations that do not mix positive and negative eigenvectors. Thus class D mass terms in 2D belong to the classifying space

$$\mathcal{R}_0 = \bigcup_{n=0}^{N} \frac{O(N)}{O(n) \times O(N-n)} \overset{N\to\infty}{\longrightarrow} BO \times \mathbb{Z}. \tag{3.84}$$

As in complex symmetry classes, the relevant classifying spaces can be identified through an extension problem. Similar to complex Clifford algebras, a real Clifford algebra $Cl_{p,q}$ is generated by a set of generators $\{e_i\}$, which satisfy

$$\{e_i, e_j\} = 0, \quad i \neq j,$$
$$e_i^2 = \begin{cases} -1 & 1 \le i \le p, \\ +1 & p+1 \le i \le p+q. \end{cases} \tag{3.85}$$

"Real" here means we are interested in real matrices if these generators are represented by matrices. For real symmetry classes, we use the Majorana representation of quadratic Hamiltonians $\hat{H} = \hat{\Psi}_A^\dagger H^{AB} \hat{\Psi}_B = i\hat{\lambda}_A X^{AB} \hat{\lambda}_B$. The real antisymmetric matrix X can be brought into its canonical form by an orthogonal transformation $X \to O^T X O$, which reveals the condition $X^2 = -1$, the only condition in class D. Thus, we have the extension problem $Cl_{0,0} \to Cl_{1,0}$. Let us denote the classifying space of the extension problem $Cl_{p,q} \to Cl_{p,q+1}$ as $\mathcal{R}_{p,q}$. It then turns out that all other extension problems are described by $\mathcal{R}_{p,q}$. First, since $Cl_{p+1,q+1} \simeq Cl_{p,q} \otimes \mathbb{R}(2)$, $\mathcal{R}_{p,q}$ depends only on $q-p$, $\mathcal{R}_{p,q} \equiv \mathcal{R}_{q-p}$. Second, since $Cl_{p,q} \otimes \mathbb{R}(2) \simeq Cl_{q,p+2}$, the extension problem $Cl_{p,q} \to Cl_{p+1,q}$ is mapped to $Cl_{q,p+2} \to Cl_{q,p+3}$. Thus, the classifying space of $Cl_{p,q} \to Cl_{p+1,q}$ is $\mathcal{R}_{p+2-q}$. Finally, since $Cl_{p+8,q} \simeq Cl_{p,q+8} \simeq Cl_{p,q} \otimes \mathbb{R}(16)$ the Bott periodicity

$$\mathcal{R}_{q+8} \simeq \mathcal{R}_q \tag{3.86}$$

follows. By using these results, the extension problem $Cl_{0,0} \to Cl_{1,0}$ can be mapped to $Cl_{0,2} \to Cl_{0,3}$ and the corresponding classifying space is $\mathcal{R}_{0,2} = \mathcal{R}_2 = O(2N)/U(N)$.

TABLE IV. Classifying spaces for complex ($\mathcal{C}_s$) and real ($\mathcal{R}_s$) classes. The rightmost column shows the corresponding Altland-Zirnbauer symmetry classes for zero-dimensional systems.

	Classifying space	Extension	$\pi_0(*)$	AZ class
$\mathcal{C}_0$	$BU \times \mathbb{Z}$	$Cl_0 \to Cl_1$	$\mathbb{Z}$	A
$\mathcal{C}_1$	$U(N)$	$Cl_1 \to Cl_2$	0	AIII
$\mathcal{R}_0$	$BO \times \mathbb{Z}$	$Cl_{p,p} \to Cl_{p,p+1}$	$\mathbb{Z}$	AI
$\mathcal{R}_1$	$O(N)$	$Cl_{p,p+1} \to Cl_{p,p+2}$	$\mathbb{Z}_2$	BDI
$\mathcal{R}_2$	$O(2N)/U(N)$	$Cl_{p,p+2} \to Cl_{p,p+3}$	$\mathbb{Z}_2$	D
$\mathcal{R}_3$	$U(N)/Sp(N)$	$Cl_{p,p+3} \to Cl_{p,p+4}$	0	DIII
$\mathcal{R}_4$	$BSp \times \mathbb{Z}$	$Cl_{p,p+4} \to Cl_{p,p+5}$	$\mathbb{Z}$	AII
$\mathcal{R}_5$	$Sp(N)$	$Cl_{p,p+5} \to Cl_{p,p+6}$	0	CII
$\mathcal{R}_6$	$Sp(2N)/U(N)$	$Cl_{p,p+6} \to Cl_{p,p+7}$	0	C
$\mathcal{R}_7$	$U(N)/O(N)$	$Cl_{p,p+7} \to Cl_{p,p+8}$	0	CI

d. Summary

One can repeat this process for different symmetry classes and dimensions. The classifying space for symmetry s in d dimension is given by $\mathcal{C}_{s-d}$ for the complex AZ classes, or $\mathcal{R}_{s-d}$ for the real cases (Table IV). The winding of the mass terms $m\Gamma_0(\mathsf{r})$ as the spacetime parameter r wraps once around the defect is classified by the homotopy group (Freedman *et al.*, 2011) $\pi_D(\mathcal{R}_{s-d}) = [S^D, \mathcal{R}_{s-d}]$, which counts the number of topologically distinct nonsingular mass terms as continuous maps $m\Gamma: S^D \to \mathcal{R}_{s-d}$. We recall that classifying spaces are related to each other by looping, i.e., $\mathcal{R}_{p+1} \simeq \Omega\mathcal{R}_p = \mathrm{Map}(S^1, \mathcal{R}_p)$. This implies the following relation between homotopy groups: $\pi_n(\mathcal{R}_{p+1}) = \pi_{n+1}(\mathcal{R}_p)$. Hence

$$\pi_D(\mathcal{R}_{s-d}) = \pi_0(\mathcal{R}_{s-d+D}) \tag{3.87}$$

classifies topological defects in class s with topological dimension $\delta = d - D$. This shows that the classification depends only on the combination $s - d + D$ and proves the classification Table II by use of Table IV.

As a digression, let us briefly mention that Table II can also be derived from a stability analysis of gapless surface Hamiltonians, instead of using the homotopy group classification of mass terms. The first step in this approach is to write down a $(d-1)$-dimensional gapless Dirac Hamiltonian with minimal matrix dimension

$$H_{\mathrm{surf}}(\mathsf{k}) = \sum_{j=1}^{d-1} k_j \gamma_j, \qquad \{\gamma_i, \gamma_j\} = 2\delta_{ij}\mathbb{1}, \tag{3.88}$$

which describes the surface state of a d-dimensional gapped bulk system belonging to a given symmetry class. Note that the form of H_{surf} is restricted by the symmetries of Eqs. (3.3)–(3.5). Second, we ask if there exists a symmetry-allowed mass term $m\gamma_0$, which anticommutes with H_{surf}. If so, the surface mode can be gapped, which indicates that the bulk system has trivial topology labeled by 0 in Table II. On the other hand, if there does not exist any symmetry-allowed mass term $m\gamma_0$, then the surface state is topologically stable (i.e., protected by the symmetries), which indicates that the bulk is topologically nontrivial. To distinguish between a $\mathbb{Z}$ and a

$\mathbb{Z}_2$ classification, one needs to consider multiple copies of the surface Hamiltonian, e.g., $H_{\text{surf}} \otimes \mathbb{1}_N$. If the surface Dirac Hamiltonian is stable for an arbitrary number of copies (i.e., if there does not exist any symmetry-allowed mass term), the corresponding bulk is classified by an integer topological invariant $\mathbb{Z}$. If, however, the surface state is stable only for an odd number of copies, the bulk is classified by a $\mathbb{Z}_2$ invariant.

It is possible to derive the entire classification table in this way. As an example, let us consider classes A, AII, and AIII in $d = 3$ dimensions. A 2D surface Dirac Hamiltonian with minimal matrix dimension can be written as

$$H_{\text{surf}}(\mathsf{k}) = k_1\sigma_1 + k_2\sigma_2. \tag{3.89}$$

For class A, the mass term $m\sigma_z$ gaps out the surface mode, leading to the trivial classification 0 in Table I. For classes AII and AIII, however, $m\sigma_z$, which is the only possible mass term, breaks TRS (3.3) and chiral symmetry (3.5) with $T = \sigma_y\mathcal{K}$ and $S = \sigma_z$, respectively. To further distinguish between a $\mathbb{Z}_2$ and $\mathbb{Z}$ classification, we consider $H_{\text{surf}} \otimes \mathbb{1}_2$, for which the symmetry operators are given by $T = \sigma_y \otimes \mathbb{1}_2\mathcal{K}$ and $S = \sigma_z \otimes \mathbb{1}_2$. There exists only one mass term for this doubled Hamiltonian, namely, $m\sigma_z \otimes \sigma_y$, which preserves TRS but breaks chiral symmetry. Thus, classes AII and AIII are classified by $\mathbb{Z}_2$ and $\mathbb{Z}$ invariants, respectively.

Using a similar approach it is also possible to classify TIs and TSCs in terms of crystalline symmetries; see Sec. IV. Furthermore, this classification strategy can also be applied to topological semimetals and nodal SCs; see Sec. V.

2. Defect K theory

The homotopy group classification of mass terms discussed in the previous section seemingly depends on the fact that the defect Hamiltonian (3.72) is of a Dirac type. However, it actually applies to a general defect Hamiltonian $H(\mathsf{k},\mathsf{r})$ (i.e., not only to Dirac Hamiltonians), as long as there is a finite energy gap separating the occupied bands from unoccupied ones. This general classification can be presented in the language of K theory (Teo and Kane, 2010b). For a fixed AZ symmetry class and dimensions (d, D), the collection of defect Hamiltonians forms a *commutative monoid*—an associative additive structure with an identity—by considering a direct sum

$$H_1 \oplus H_2 = \begin{pmatrix} H_1 & 0 \\ 0 & H_2 \end{pmatrix}, \tag{3.90}$$

where direct sums of symmetry operators $T_1 \oplus T_2$, $C_1 \oplus C_2$ are defined similarly. Clearly, $H_1 \oplus H_2$ has the same symmetries and dimensions as its constituents. The identity element is the 0×0 empty Hamiltonian $H = \emptyset$. Physically, the direct sum operation simply means to put the two systems on top of each other without letting them couple to each other.

As in ordinary K theories, this monoid can be promoted to a group by introducing topological equivalence and applying the Grothendieck construction, which will be explained later. Two defect Hamiltonians $H_1(\mathsf{k},\mathsf{r})$ and $H_2(\mathsf{k},\mathsf{r})$ with the same symmetries and spatial dimensions, but not necessarily with the same matrix dimensions ($\dim H_1 \neq \dim H_2$), are *stably* topologically equivalent,

$$H_1(\mathsf{k},\mathsf{r}) \simeq H_2(\mathsf{k},\mathsf{r}), \tag{3.91}$$

if, for large enough M and N, $H_1(\mathsf{k},\mathsf{r}) \oplus (\sigma_3 \otimes \mathbb{1}_M)$ can be continuously deformed into $H_2(\mathsf{k},\mathsf{r}) \oplus (\sigma_3 \otimes \mathbb{1}_N)$ without closing the energy gap or breaking symmetries. Here $\sigma_3 \otimes \mathbb{1}_M$ is a trivial atomic $2M \times 2M$ Hamiltonian that does not depend on k and r, and $M - N = \dim H_2 - \dim H_1$.

Stable topological equivalence defines equivalent classes of defect Hamiltonians

$$[H] = \{H' : H' \simeq H\}, \tag{3.92}$$

which is compatible with the addition structure $[H_1] \oplus [H_2] = [H_1 \oplus H_2]$. The identity element is $0 = [\emptyset]$ which consists of all topologically trivial Hamiltonians that can be deformed into $\sigma_3 \otimes \mathbb{1}_N$. Each Hamiltonian class now has an additive inverse. By adding trivial bands, we can always assume a Hamiltonian has an equal number of occupied and unoccupied bands. Consider the direct sum $H \oplus (-H)$, where in $(-H)$ the occupied states are inverted to unoccupied ones. This sum is topologically trivial as the states below the gap consist of both the valence and conduction states in H and they are allowed to mix. This shows that $[H] \oplus [-H] = 0$ and $[-H]$ is the additive inverse of $[H]$. We see that the collection of equivalent classes of defect Hamiltonians forms a group and defines a K theory

$$K(s;d,D) = \left\{ [H]: \begin{array}{c} H(\mathsf{k},\mathsf{r}),\ \text{a gapped defect} \\ \text{Hamiltonian of AZ class} \\ s \text{ and dimensions } (d,D) \end{array} \right\}. \tag{3.93}$$

Now we establish group homomorphisms relating K groups with different symmetries and dimensions (Teo and Kane, 2010b)

$$\Phi_+ :\ K(s;d,D) \to K(s+1;d+1,D), \tag{3.94}$$

$$\Phi_- :\ K(s;d,D) \to K(s-1;d,D+1). \tag{3.95}$$

That is, given any defect Hamiltonian $H_s(\mathsf{k},\mathsf{r})$ in symmetry class s, one can define a new gapped Hamiltonian

$$H_{s\pm1}(\mathsf{k},\theta,\mathsf{r}) = \begin{cases} \cos\theta H_s(\mathsf{k},\mathsf{r}) + \sin\theta S, & s \text{ odd}, \\ \cos\theta H_s(\mathsf{k},\mathsf{r}) \otimes \sigma_3 + \sin\theta \mathbb{1} \otimes \sigma_{1,2}, & s \text{ even}. \end{cases} \tag{3.96}$$

Here $\theta \in [-\pi/2, \pi/2]$ is a new variable that extends (k,r), which lives on the sphere S^{d+D}, to the suspension $\Sigma S^{d+D} = S^{d+1+D}$. This is because the new Hamiltonian $H_{s\pm1}$ is independent of (k,r) at the north and south poles where $\theta = \pm\pi/2$.

We first look at the case when s is odd. For real symmetry classes, the chiral operator is set to be the product $S = i^{(s+1)/2}TC$ of the TR and PH operators. The factor of i is to make S Hermitian and square to unity. The addition of the

chiral operator in Eq. (3.96) breaks the chiral symmetry since the Hamiltonian $H_{s\pm1}$ does not anticommute with S anymore. Depending on how the new variable θ transforms under the symmetries $\theta \to \pm\theta$, the new Hamiltonian $H_{s\pm1}$ preserves only either TRS or PHS. If θ is odd (even), it belongs to the symmetry class $s+1$ (respectively, $s-1$). This also applies to complex symmetry classes.

Next we consider the even s cases. For real symmetry classes, H_s has one antiunitary symmetry, say TRS. (The case of PHS can be argued by a similar manner.) The introduction of the σ degree of freedom doubles the number of bands and the new Hamiltonian $H_{s\pm1}$ in Eq. (3.96) has a chiral symmetry $S = \mathbb{1} \otimes \sigma_{2,1}$ which anticommutes with the extra term $\sin\theta \mathbb{1} \otimes \sigma_{1,2}$. For the case when $S = \sigma_2$, there is a new PHS with the operator $C = iT \otimes \sigma_2$ that fixes the new parameter $\theta \to \theta$. For the other case for $S = \sigma_1$, the new PHS operator is $C = T \otimes \sigma_1$ and the new parameter flips $\theta \to -\theta$ under the symmetry. The new Hamiltonian then belongs to the symmetry class $s-1$ for the former case, and $s+1$ for the latter.

To summarize, Eq. (3.96) defines the correspondences

$$\Phi_\pm : [H_s(\mathsf{k},\mathsf{r})] \to [H_{s\pm1}(\mathsf{k},\theta,\mathsf{r})]. \tag{3.97}$$

For the $+$ case, θ is odd under the symmetry and behaves like a new momentum parameter. It increases the dimension $d \to d+1$. For the $-$ case, θ is even under the symmetry. The extra spacelike parameter then increases $D \to D+1$. $\Phi_\pm$ commutes with direct sums $\Phi_\pm[H_1 \oplus H_2] = \Phi_\pm[H_1] \oplus \Phi_\pm[H_2]$ and therefore are group homomorphisms between K theories. These homomorphisms are actually invertible and provide isomorphisms between (Teo and Kane, 2010b)

$$\begin{aligned} K(s;d,D) &\cong K(s+1;d+1,D) \\ &\cong K(s-1;d,D+1). \end{aligned} \tag{3.98}$$

To see this, we begin with an arbitrary defect Hamiltonian $H_{s\pm1}(\mathsf{k},\theta,\mathsf{r})$. It can be shown to be topologically equivalent to one with the particular form in Eq. (3.96). We then consider the artificial action

$$S[\bar{H}(\mathsf{k},\theta,\mathsf{r})] = \int d\theta d^d\mathsf{k} d^D\mathsf{r} \mathrm{Tr}(\partial_\theta \bar{H} \partial_\theta \bar{H}) \tag{3.99}$$

on the moduli space of flat-band Hamiltonians $\bar{H}$ so that $\bar{H}^2 = \mathbb{1}$. By satisfying the Euler-Lagrangian equation

$$\left.\frac{\delta S}{\delta H}\right|_{H^2=1} = \partial_\theta^2 H + H = 0, \tag{3.100}$$

Eq. (3.96) locally minimizes the action. The action also defines a natural minimizing flow direction that deforms an arbitrary Hamiltonian $H(\mathsf{k},\theta,\mathsf{r})$ to the form of Eq. (3.96). This shows the invertibility of $\Phi_\pm$.

The isomorphisms (3.98) prove that the classification of topological defects depends only on the combination $s-d+D$. Furthermore, the defect K theory is related to the classifications of TI and TSC by

$$K(s;d,D) \cong K(s+D;d,0) \cong K(s;d-D,0), \tag{3.101}$$

which classifies class s topological band theories in $\delta = d-D$ dimensions. The equivalence (3.101) extends characteristics of the classification of TIs and TSCs to the classification of topological defects.

Beside Eq. (3.101), there are further relationships among K groups having different s, d, D. For example, topological states in the first and second descendants are related to their "parent" states in primary series, by *dimensional reduction* (Qi, Hughes, and Zhang, 2008; Ryu, Schnyder *et al.*, 2010). This procedure is one way to understand how the $\mathbb{Z}_2$ characterization of the first and second descendants emerge. Let us consider a d-dimensional Bloch Hamiltonian $H(\mathsf{k})$ describing a gapped topological state in the first descendants. One can then consider a $(d+1)$-dimensional Bloch Hamiltonian $\tilde{H}(\mathsf{k},k_{d+1})$ which belongs to the same symmetry class and satisfy $\tilde{H}(\mathsf{k},0) = H(\mathsf{k})$. Furthermore, if there is a spectral gap in $\tilde{H}(\mathsf{k},k_{d+1})$, one can compute the topological invariants introduced above, since $\tilde{H}(\mathsf{k},k_{d+1})$ belongs to the primary series. However, as one immediately notices, there is no unique higher-dimensional Hamiltonian to which the original Hamiltonian can be embedded, nor a unique value for the topological invariant. Nevertheless, the parity of the topological invariant can be shown to be independent of the way we embed the Hamiltonian. This is the origin of the $\mathbb{Z}_2$ classification of the first descendants. Similar arguments apply to the second descendants.

Summarizing, the first and second $\mathbb{Z}_2$ topologies are related to their parent $\mathbb{Z}$ topology of the same symmetry class by the surjections

$$\mathbb{Z}_2^{(2)} \underset{\cong}{\overset{i^*}{\leftarrow}} \mathbb{Z}_2^{(1)} \overset{i^*}{\leftarrow} \mathbb{Z}, \tag{3.102}$$

where $i^* : K(s;d+1,D) \to K(s;d,D)$ is the restriction homomorphism that restricts

$$i^* : H_s(\mathsf{k},k_{d+1},\mathsf{r}) \mapsto H_s(\mathsf{k},\mathsf{r})|_{k_{d+1}=0}, \tag{3.103}$$

where $(\mathsf{k},k_{d+1},\mathsf{r})$ lives on the compactified S^{d+1+D} and (k,r) belongs to the equator S^{d+D}.

As yet another relationship, the first $\mathbb{Z}_2$ descendant for the chiral classes relates isomorphically to the second $\mathbb{Z}_2$ descendant for the nonchiral classes:

$$\begin{array}{ll} \text{chiral class } (s \text{ odd}): & \mathbb{Z}_2^{(1)} \\ & \quad\downarrow f \qquad \searrow^{\Phi_+} \\ & \quad\cong \\ \text{non-chiral class } (s+1): & \mathbb{Z}_2^{(2)} \underset{i^*}{\overset{\cong}{\leftarrow}} \mathbb{Z}_2^{(1)} \end{array} \tag{3.104}$$

Here the map between K theories

$$f : K(s;d,D) \cong \mathbb{Z}_2^{(1)} \to K(s+1;d,D) \cong \mathbb{Z}_2^{(2)} \tag{3.105}$$

is the forgetful functor that ignores either TRS or PHS so that the chiral band theory now belongs to the nonchiral symmetry class $s+1$. It agrees with the composition $f = i^* \circ \Phi_+$, where

Φ_+: $K(s;d,D) \to K(s+1;d+1,D)$ is the isomorphism (3.96) and i^* restricts the Hamiltonian $H_{s+1}(\mathsf{k},\theta,\mathsf{r})$ onto the equator where $\theta = 0$. Since both i^* and Φ_+ are isomorphisms, so is the forgetful map f. The topological invariant for chiral $\mathbb{Z}_2^{(1)}$ is therefore given by the FK invariant (3.63) with the gauge constraint (3.64) for $s = 1, 5$ (classes CI and DIII) or (3.65) for $s = 3, 7$ (classes BDI and CII).

D. Bulk-boundary and bulk-defect correspondence

In this section, we relate the bulk topological invariants discussed in Sec. III.B to the protected gapless excitations localized at boundaries and defects. This will be done by introducing proper indices that "count" the number of zero modes and gapless modes localized at defects (*à la* index theorems), and by identifying these indices as the topological invariants. This bulk-boundary and bulk-defect correspondence unifies numerous TI and TSC defect systems, which we demonstrate in terms of a variety of examples. In addition to the following discussion, we refer the interested reader to the literature of Essin and Gurarie (2011) and Graf and Porta (2013), where different approaches to establish the bulk-boundary and bulk-defect correspondence have been studied.

1. Zero modes at point defects and index theorems

We start by demonstrating the protected zero-energy modes localized at topological point defects ($\delta = d - D = 1$). The simplest examples are given by the SSH and 1D Kitaev models, or their continuum counterparts, the Jackiw-Rebbi model, discussed in Secs. III.B.2.c and III.B.3.b. The domain wall defects in these 1D models trap zero-energy bound states protected by chiral or PH symmetry. The continuum versions of these models (3.44) are given by the differential operator

$$\mathcal{H} = -iv\sigma_2 \frac{d}{dr} + m(r)\sigma_3, \qquad r \in (-\infty, +\infty), \tag{3.106}$$

where the mass $m(r)$, which changes sign at the origin, describes the domain wall. The zero-energy bound state $|\gamma\rangle$, which is exponentially localized at the domain wall (i.e., at the origin), is an eigenstate of the chiral or PH operator $S|\gamma\rangle = \pm|\gamma\rangle$ or $C|\gamma\rangle = |\gamma\rangle$, where $S = \sigma_1$ and $C = \sigma_1\mathcal{K}$. The chiral eigenvalue, called chirality, of the zero mode has a definite sign, depending on the sign of the winding number (3.42). The sign of the PH eigenvalue, on the other hand, is unphysical, since it can be flipped by multiplying $|\gamma\rangle$ by i. Hence, for the zero-energy Majorana bound state (MBS) protected by PHS the PH eigenvalue can always be assumed to be $+1$.

Since the 1D example (3.106) is invariant under chiral or PH symmetry, its energy levels must come in $\pm\varepsilon$ conjugate pairs. The zero mode $|\gamma\rangle$, however, is self-conjugate, and therefore does not have a conjugate partner. Hence, $|\gamma\rangle$ is pinned at zero energy and, as a consequence, is robust against any perturbation that does not close the bulk energy gap. We list in Table V the different symmetry classes that can support zero-energy modes at topological point defects. Depending on the symmetry class, these zero-energy modes are of a different type, as indicated by the last column in Table V.

TABLE V. Symmetry classes supporting nontrivial point topological defects and their associated zero-energy modes.

Symmetry	Topological classes	Bound states at $\varepsilon = 0$
AIII	$\mathbb{Z}$	Chiral Dirac
BDI	$\mathbb{Z}$	Chiral Majorana
D	$\mathbb{Z}_2$	Majorana
DIII	$\mathbb{Z}_2$	Majorana Kramers doublet (= Dirac)
CII	$2\mathbb{Z}$	Chiral Majorana Kramers doublet (= chiral Dirac)

a. Index theorems

In general, if a point defect supports an odd number of zero-energy bound states, only an even number of them can be paired up and gapped out upon inclusion of PH symmetric perturbations. This leaves at least one unpaired zero-energy bound state. The even-odd parity of the number of zero modes is known as a $\mathbb{Z}_2$ analytic index of the differential operator $\mathcal{H}$,

$$\mathrm{ind}_{\mathbb{Z}_2}^{(1)}[\mathcal{H}] = \begin{pmatrix} \text{number of zero-} \\ \text{energy bound states} \end{pmatrix} \mod 2, \tag{3.107}$$

which we claim is identical to the $\mathbb{Z}_2$ topological index,

$$\mathrm{ind}_{\mathbb{Z}_2}^{(1)}[\mathcal{H}] = 2\mathrm{CS}_{2d-1}[H(\mathsf{k},\mathsf{r})], \tag{3.108}$$

given by the Chern-Simons integral in Eq. (3.46) for a point defect in d dimensions. The equality (3.108) is an example of the bulk-boundary correspondence.

For chiral symmetric systems, on the other hand, the chiral operator $\mathcal{S}$ defines in addition an integral quantity

$$\mathrm{ind}_{\mathbb{Z}}[\mathcal{H}] = \mathrm{Tr}(\mathcal{S}), \tag{3.109}$$

which is referred to as the chirality of the point defect. It counts the difference between the number of zero modes with positive and negative chiral eigenvalues. This $\mathbb{Z}$ analytical index is robust against any chiral symmetric perturbation that does not close the bulk gap. This is because all conjugate pairs of energy eigenstates, which can always be related by the chiral symmetry $|-\varepsilon\rangle = \mathcal{S}|+\varepsilon\rangle$, do not contribute to $\mathrm{Tr}(\mathcal{S})$, as $|+\varepsilon\rangle \pm |-\varepsilon\rangle$ must have opposite eigenvalues of $\mathcal{S}$. For a point defect in d dimensions, it is found that the chirality is identical to the $\mathbb{Z}$ topological index, i.e., the winding number given in Eq. (3.25)

$$\mathrm{ind}_{\mathbb{Z}}[\mathcal{H}] = \nu_{2d-1}[H(\mathsf{k},\mathsf{r})]. \tag{3.110}$$

Moreover, Eq. (3.109) also agrees with the $\mathbb{Z}_2$-analytic index

$$\mathrm{ind}_{\mathbb{Z}}[\mathcal{H}] = \mathrm{ind}_{\mathbb{Z}_2}^{(1)}[\mathcal{H}] \mod 2. \tag{3.111}$$

Equation (3.108) applies to general point defects in all symmetry classes in any dimension, while Eq. (3.110) applies to arbitrary chiral ones. For instance, from the defect classification (Tables II and V), we see that the CS invariant for a point defect is nonvanishing only for classes AIII, BDI, and D.

Equation (3.108) then agrees with the fact that only point defects in these AZ classes can support an odd number of zero-energy MBS. All other classes either do not have a PHS or the zero modes must come in Kramers doublets. This also explains the even chirality $\mathrm{ind}_{\mathbb{Z}}[\mathcal{H}]$ for class CII point defects and matches, by the index theorem (3.110), with the $2\mathbb{Z}$ winding number $\nu_{2d-1}[H(\mathsf{k},\mathsf{r})]$.

Last, there is another $\mathbb{Z}_2$-analytic index associated with the second descendants. It applies to point defects with an antiunitary symmetry T or C that squares to -1, so that zero-energy states come in Kramers pairs:

$$\mathrm{ind}^{(2)}_{\mathbb{Z}_2}[\mathcal{H}] = \begin{pmatrix} \text{number of zero-energy} \\ \text{Kramers pairs} \end{pmatrix} \bmod 2. \quad (3.112)$$

This index is identical to the second descendant $\mathbb{Z}_2$-topological index

$$\mathrm{ind}^{(2)}_{\mathbb{Z}_2}[\mathcal{H}] = \mathrm{CS}_{2d-1}[H(\mathsf{k},\mathsf{r})], \quad (3.113)$$

for a d-dimensional point defect, where the Chern-Simons invariant is defined in Eq. (3.46) with the gauge constraint (3.64) for $T^2=-1$ or Eq. (3.65) for $C^2=-1$. The defect classification (Table II) tells us that only point defects in class DIII support protected zero-energy Majorana Kramers pairs. These zero modes cannot be detected by the other indices in Eq. (3.108) or (3.110), since there are an even number of MBSs which necessarily carry opposite chirality, as S and T anticommute.

It is worth noting that the $\mathbb{Z}$-analytic index (3.109) and its identification to the topological index (3.110) is a rendition of the original celebrated index theorem in the mathematics literature (Atiyah and Singer, 1963). A chiral symmetric defect Hamiltonian $\mathcal{H}$, in the form of a differential operator, takes the off-diagonal form

$$\mathcal{H} = \begin{pmatrix} 0 & \mathcal{D}^\dagger \\ \mathcal{D} & 0 \end{pmatrix}, \quad (3.114)$$

where $\mathcal{D}$ is a Dirac operator, which is Fredholm. Equation (3.109) is identical to

$$\mathrm{ind}_{\mathbb{Z}}[\mathcal{H}] = \dim\ \ker(\mathcal{D}) - \dim\ \ker(\mathcal{D}^\dagger), \quad (3.115)$$

which is the original definition of the analytic index of a Dirac operator. The index theorem (3.110) can be proven by means of a *heat kernel* method (Lawson and Michelsohn, 1990; Berline, Getzler, and Vergne, 1992). Several alternative proofs have been derived in the context of both condensed matter and high energy physics (Jackiw and Rebbi, 1976; Jackiw and Rossi, 1981; Weinberg, 1981; Nakahara, 2003; Volovik, 2003; Fukui, 2010; Fukui and Fujiwara, 2010).

In the following, we present some examples of zero-energy bound states at topological point defects in both 2D and 3D. We focus on point defects that trap unpaired zero-energy MBSs or Majorana Kramers doublets. In many cases the topological invariants can be simplified into products of a bulk topological invariant and a defect winding number. MBSs are predicted to exists in many systems, e.g., in quantum flux vortices in chiral p_x+ip_y SCs or in superfluid ^{3}He-A, in TI-SC-ferromagnet (FM) heterostructures in 2D and 3D, and so on. The theory of topological defects unifies the topological origin of all these examples. For instance, the appearance of protected zero-energy MBSs is always a consequence of $K(s;d,D)=\mathbb{Z}_2^{(1)}$ for $s=2$ (class D), while the presence of protected zero-energy Majorana Kramers doublets is a result of $K(s;d,D)=\mathbb{Z}_2^{(2)}$ for $s=3$ (class DIII). For example, the protected zero-energy MBS at a quantum flux vortex of a spinless chiral p_x+ip_y SC turns out to have the same topological origin as a MBS located at a dislocation or disclination of a nonchiral p-wave SC (Teo and Hughes, 2013; Hughes, Yao, and Qi, 2014).

b. Example: 2D class D p_x+ip_y superconductors

We first look at a quantum flux vortex of a spinless chiral p_x+ip_y SC (Anderson and Morel, 1961; Balian and Werthamer, 1963; Leggett, 1975, 2006; Sigrist and Ueda, 1991; Rice and Sigrist, 1995; Luke *et al.*, 1998; Volovik, 1999, 2003; Read and Green, 2000; Ivanov, 2001; Kitaev, 2006; Xia *et al.*, 2006; Gurarie and Radzihovsky, 2007; Tewari *et al.*, 2008). Consider a 2D BdG Hamiltonian on the square lattice

$$H_0(\mathsf{k}) = \Delta(\sin k_x\tau_1 + \sin k_y\tau_2) + [t(\cos k_x + \cos k_y) - \mu]\tau_3, \quad (3.116)$$

where $\tau_{i=1,2}$ acts on the Nambu degrees of freedom $(\hat{c},\hat{c}^\dagger)$, and the PH operator is $C=\tau_1\mathcal{K}$. When the electron hopping strength and Fermi energy are arranged so that $2t>|\mu|>0$, this bulk 2D model has a unit Chern invariant and carries a chiral Majorana edge mode. In the continuum limit, a chiral p_x+ip_y SC can be represented by

$$H_0(\mathsf{k}) = \Delta(k_x\tau_1 + k_y\tau_2) + \left(\frac{\hbar^2k^2}{2m} - \mu\right)\tau_3, \quad (3.117)$$

where the Fermi energy μ is positive. A $\phi=hc/2e$ quantum flux vortex can be described by the defect Hamiltonian

$$H(\mathsf{k},\mathsf{r}) = e^{-i\varphi(\mathsf{r})\tau_3/2}H_0(\mathsf{k})e^{i\varphi(\mathsf{r})\tau_3/2}, \quad (3.118)$$

where the SC pairing phase φ winds by $2\pi\times l$ $(l\in\mathbb{Z})$ around the vortex, and can be taken as the angular parameter $\varphi(\mathsf{r})=\tan^{-1}(y/x)\times l$. The vortex can be shown to carry a protected zero-energy Majorana bound state, so that $\mathrm{ind}^{(1)}_{\mathbb{Z}_2}[\mathcal{H}]=1$. The index theorem (3.108) can be verified by evaluating the Chern-Simons invariant CS_3. [For the technical reason explained following Eq. (3.46), we need to consider the modified defect Hamiltonian $\tilde{H}(\mathsf{k},\mathsf{r})=H(\mathsf{k},\mathsf{r})\oplus(-H_0(\mathsf{k}))$, where the lower block cancels the 2D Chern invariant without contributing to extra point defect states. This modification is to ensure that there is a global continuous basis of occupied states for the CS integral.] The CS 3-form can be simplified (Teo and Kane, 2010b) and decomposed into

$$\mathcal{Q}_3 = \left(\frac{i}{2\pi}\right)^2 \mathrm{Tr}[\mathcal{F}_0(\mathsf{k})] \wedge d\varphi, \tag{3.119}$$

where $\mathcal{F}_0$ is the Berry curvature for the $p+ip$ SC $H_0(\mathsf{k},\mathsf{r})$ without a vortex. The topological index therefore is a simple product of the bulk Chern number and the vorticity l,

$$\begin{aligned} 2\mathrm{CS}_3[H(\mathsf{k},\mathsf{r})] &= \frac{i}{2\pi}\int_{\mathrm{BZ}^2} \mathrm{Tr}(\mathcal{F}_0) \oint_{S^1} d\varphi(\mathsf{r}) \\ &= \mathrm{Ch}_1 \times l. \end{aligned} \tag{3.120}$$

Equations (3.119) and (3.120) apply to a general defect Hamiltonian of the form of Eq. (3.118), and the parity of the number of zero-energy MBSs at a flux vortex can always be read off from (Volovik, 2003; Stone and Roy, 2004; Kitaev, 2006)

$$\mathrm{ind}^{(1)}_{\mathbb{Z}_2}[\mathcal{H}] = \mathrm{Ch}_1[H_0(\mathsf{k})] \times l. \tag{3.121}$$

Physical chiral $p_x + ip_y$ SCs are spinful. Strontium ruthenate (Sr_2RuO_4) is a plausible candidate of a spinful chiral p-wave SC with odd parity spin-triplet pairing (Rice and Sigrist, 1995; Luke *et al.*, 1998; Xia *et al.*, 2006), although its precise pairing nature is still under debate (Maeno, Rice, and Sigrist, 2001; Raghu, Kapitulnik, and Kivelson, 2010; Maeno *et al.*, 2012). A continuum model of a 2D spinful chiral p-wave SC is given by

$$\begin{aligned} H_0(\mathsf{k}) = {} & \Delta(\boldsymbol{\sigma}\cdot\mathbf{d})\sigma_2(k_x\tau_1 + k_y\tau_2) \\ & + \left(\frac{\hbar^2k^2}{2m} - \mu\right)\tau_3, \end{aligned} \tag{3.122}$$

where $\sigma_{i=1,2,3}$ acts on the spin degree of freedom, and the $\mathbf{d}$ vector specifies a special spin direction, say along the x-y plane, in the triplet pairing. The Nambu basis is taken to be $(\hat{c}_\uparrow, \hat{c}_\downarrow, \hat{c}^\dagger_\downarrow, -\hat{c}^\dagger_\uparrow)$ and the PH operator is $C = \sigma_2 \otimes \tau_2\mathcal{K}$. From Eq. (3.121), a full $hc/2e$ quantum vortex (FQV) carries two MBSs $\hat{\gamma}_\uparrow, \hat{\gamma}_\downarrow$, which split by a perturbation $\delta\hat{H} = i\varepsilon\hat{\gamma}_\uparrow\hat{\gamma}_\downarrow$ into a $\pm\varepsilon$ pair, due to spin-orbit coupling (SOC) or an in-plane magnetic field. On the other hand, a half-quantum vortex (HQV) of flux $\phi = hc/4e$ consists of a π rotation of the pairing phase as well as the $\mathbf{d}$ vector about the z axis (Salomaa and Volovik, 1985; Das Sarma, Nayak, and Tewari, 2006; Chung, Bluhm, and Kim, 2007; Jang *et al.*, 2011). The HQV is represented by the defect Hamiltonian

$$H(\mathsf{k},\mathsf{r}) = e^{-i\varphi(\mathsf{r})(\tau_3+\sigma_3)/4} H_0(\mathsf{k}) e^{i\varphi(\mathsf{r})(\tau_3+\sigma_3)/4}, \tag{3.123}$$

where φ is the angular parameter around the vortex. The spatial configuration of the $\mathbf{d}$ vector is shown in Fig. 3(a). Effectively, the HQV acts as a quantum vortex only on one of the two spin sectors where τ_3 and σ_3 have the same sign. This gives a single protected zero-energy MBS as shown in Fig. 3(b).

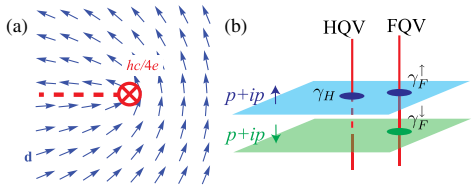

FIG. 3. (a) Spatial configuration of the $\mathbf{d}$ vector around a half-quantum vortex of a $p+ip$ SC. (b) Zero-energy Majorana modes of a half-quantum vortex (HQV) and a full quantum vortex (FQV).

c. Example: 2D class DIII $(p+ip)\times(p-ip)$ superconductors

There exists also an unconventional spinful p-wave SC that preserves TRS (Kitaev, 2009; Schnyder *et al.*, 2009; Zhang, Kane, and Mele, 2013b). It involves an opposite chirality in the two spin species, and the pairing has a $(p_x+ip_y)\uparrow \times (p_x-ip_y)\downarrow$ structure. A continuum BdG Hamiltonian describing this SC is given by

$$H_0(\mathsf{k}) = \Delta(k_x\tau_1 + k_y\sigma_3\tau_2) + \left(\frac{\hbar^2k^2}{2m} - \mu\right)\tau_3, \tag{3.124}$$

where the Nambu basis is chosen to be $(\hat{c}_\uparrow, \hat{c}_\downarrow, \hat{c}^\dagger_\uparrow, \hat{c}^\dagger_\downarrow)$ and the PH operator is $C = \tau_1\mathcal{K}$. $H_0(\mathsf{k})$ has a TRS with $T = \sigma_2\tau_3\mathcal{K}$ and therefore belongs to class DIII. The nontrivial $\mathbb{Z}_2$ topology of $H_0(\mathsf{k})$ corresponds to a gapless helical Majorana edge mode. The Hamiltonian (3.124) is topologically equivalent, by a basis transformation, to the 2D ^{3}He-B model (Volovik, 2003)

$$H_0(\mathsf{k}) = \Delta(k_x\sigma_1 + k_y\sigma_2)\tau_1 + \left(\frac{\hbar^2k^2}{2m} - \mu\right)\tau_3, \tag{3.125}$$

where the Nambu basis is now $(\hat{c}_\uparrow, \hat{c}_\downarrow, \hat{c}^\dagger_\downarrow, -\hat{c}^\dagger_\uparrow)$ with PH operator $C = \sigma_2\tau_2\mathcal{K}$ and TR operator $i\sigma_2\mathcal{K}$. A vortex that respects TRS can be introduced in Eq. (3.125) via

$$H(\mathsf{k},\mathsf{r}) = e^{-i\varphi(\mathsf{r})\sigma_3/2} H_0(\mathsf{k}) e^{i\varphi(\mathsf{r})\sigma_3/2}, \tag{3.126}$$

which consists of a 2π rotation of spin once around the vortex core. One finds that a Majorana Kramers doublet is bound at the vortex core, as guaranteed by the second $\mathbb{Z}_2$ index (3.113).

d. Example: Dislocations and disclinations in crystalline superconductors (class D)

Zero-energy MBSs can also exist in nonchiral media. We have already seen that they appear as boundary modes in a topological 1D p-wave SC [see Eq. (3.41)]. This can be generalized to 2D by stacking the 1D chains into a 2D array. A lattice dislocation (see Fig. 4) binds a zero-energy MBS if the 1D chains are aligned horizontally, so that the MBS is located at the end of a half line (Asahi and Nagaosa, 2012; Juričić *et al.*, 2012; Teo and Hughes, 2013; Benalcazar, Teo, and Hughes, 2014; Hughes, Yao, and Qi, 2014). In general, a nonchiral p-wave SC in 2D can carry a weak $\mathbb{Z}_2$ topology. This is described by weak indices, which originate from the lower dimensional cycles of the 2D BZ, $\mathrm{BZ}^2 = S^1 \times S^1$. The weak indices characterize a homogeneous 2D SC that is

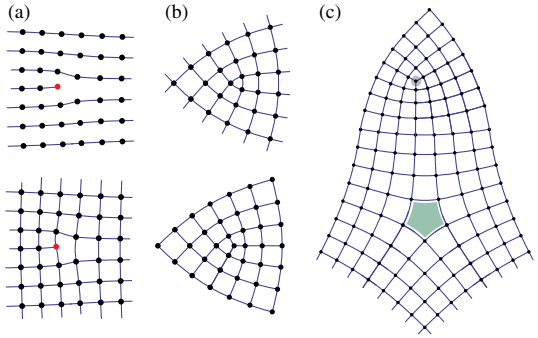

FIG. 4. (a) Dislocation on a square lattice. (b) Two inequivalent $\Omega = -\pi/2$ disclinations. (c) A $\Omega = \pm\pi/2$ disclination dipole.

topologically equivalent to an anisotropic array of p-wave chains. They can be written in the form of a $\mathbb{Z}_2$-valued reciprocal lattice vector

$$\mathbf{G}_\nu = \nu_1 \mathbf{b}_1 + \nu_2 \mathbf{b}_2 \quad \text{with}$$
$$\nu_i = \frac{i}{\pi} \oint_{\mathcal{C}_i} \mathrm{Tr}(\mathcal{A}) \bmod 2, \tag{3.127}$$

where $\mathcal{C}_i = \{\pi \mathbf{b}_i + s\epsilon_{ij}\mathbf{b}_j | s \in (-\pi, \pi]\}$ is the cycle on the boundary of the BZ along the primitive reciprocal lattice direction $\mathbf{b}_i$. On a boundary normal to $\mathbf{G}_\nu$, the weak TSC carries a protected nonchiral Majorana edge mode, where the zero-energy left- and right-moving modes are located at different PH symmetric momenta 0 and π so that backscattering is prohibited by PH and translation symmetry. By the use of Eq. (3.108) together with Eq. (3.127), one finds the following bulk-defect correspondence:

$$\mathrm{ind}^{(1)}_{\mathbb{Z}_2} = \frac{1}{2\pi} \mathbf{B} \cdot \mathbf{G}_\nu \quad \bmod 2, \tag{3.128}$$

where $\mathbf{B}$ is the Burgers vector—the Bravais lattice vector associated with the net translation picked up by a particle going once around the dislocation (Chaikin and Lubensky, 2000; Nelson, 2002). The product in Eq. (3.128) counts the parity of the number of zero-energy MBSs located at a dislocation in a 2D weak TSC. It does not rely on a chiral $p_x + ip_y$ pairing order or a nonvanishing Chern invariant.

Discrete rotation symmetries of a crystalline SC provide further lattice symmetry-protected topologies (Teo and Hughes, 2013; Benalcazar, Teo, and Hughes, 2014); see also Sec. IV. These topological crystalline superconductors (TCSs) possess BdG states $|u^a(\mathsf{K})\rangle$ that behave differently under rotation R at different rotation fixed points K. For example, the fourfold symmetric BdG model (3.116) has at the two fourfold fixed momenta (0,0) and (π, π) inverted occupied states, i.e., $|u(0,0)\rangle = \mathbf{e}_2$ and $|u(\pi,\pi)\rangle = \mathbf{e}_1$. These two eigenstates have distinct rotation eigenvalues $R = e^{i(\pi/4)\tau_3}$, since $\tau_3 = \pm 1$ for these two BdG states. The lattice symmetry-protected bulk topologies can lead to zero-energy MBSs located at disclinations, i.e., at conical point defects. These disclinations correspond to singularities of the curvature that rotate the frame of an orbiting particle by a Frank angle Ω after one cycle. Examples on a square lattice are illustrated in Figs. 4(b) and 4(c). The $\mathbb{Z}_2$ index that counts the parity of the zero-energy MBSs at a disclination takes the form of (Teo and Hughes, 2013; Benalcazar, Teo, and Hughes, 2014)

$$\mathrm{ind}^{(1)}_{\mathbb{Z}_2} = \frac{1}{2\pi} \mathbf{T} \cdot \mathbf{G}_\nu + \frac{\Omega}{2\pi} \left(\mathrm{Ch}_1 + \begin{matrix} \text{rotation} \\ \text{invariant} \end{matrix} \right) \quad \bmod 2, \tag{3.129}$$

where $\mathbf{T}$ is a translation piece of the disclination similar to the Burgers vector of a dislocation. The specific form of the rotation invariant depends on the rotation symmetry and is always a combination involving the rotation eigenvalues of BdG states. Disclination MBSs are proposed to be present in the form of corner states in Sr_2RuO_4 and at grain boundaries in superconducting graphene and silicene.

e. Example: Superconducting heterostructures (class D)

We have seen that MBSs appear in the form of vortex states in chiral $(p + ip)$ SCs and as lattice defects in nonchiral p-wave SCs. Here we review 2D and 3D heterostructures that involve s-wave SCs, but still support robust zero-energy MBSs (Fu and Kane, 2008, 2009; Hasan and Kane, 2010; Teo and Kane, 2010b; Chiu, Gilbert, and Hughes, 2011; Hosur *et al.*, 2011; Qi and Zhang, 2011; Chiu, Ghaemi, and Hughes, 2012; Hung *et al.*, 2013; J.-P. Xu *et al.*, 2014; S.-Y. Xu *et al.*, 2014).

(i) We first look at the gapless helical edge modes of a 2D quantum spin Hall (QSH) insulator consisting of a pair of counterpropagating electronic states (Sec. III.D.2), which couple to a TR-breaking backscattering potential h and a $U(1)$ symmetry breaking SC pairing Δ [Fig. 5(a)]. This setup can be described by the boundary BdG Hamiltonian

$$H_{1d}(k, r) = v_F k \sigma_3 \tau_3 + h(r)\sigma_1 + \Delta(r)\tau_1, \tag{3.130}$$

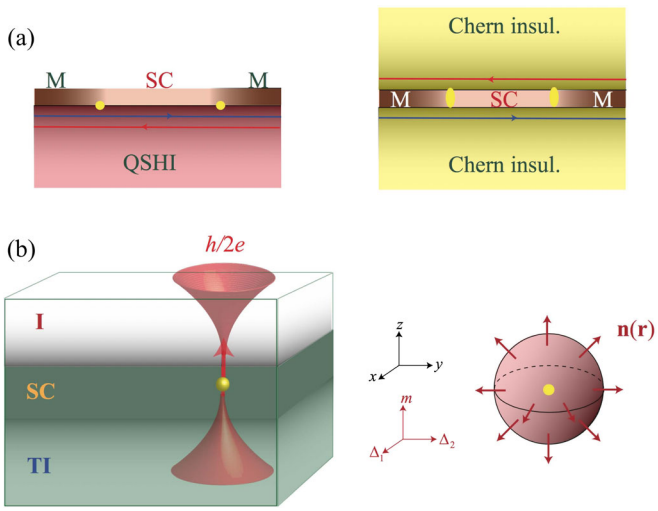

FIG. 5. Zero-energy MBSs (yellow dots) in heterostructures: (a) superconductor (SC)—magnet (M) domain wall along a QSH edge or a Chern insulator interface; (b) a flux vortex across a superconducting interface between a 3D topological (TI) and trivial insulator (I).

where σ_i and τ_i act on spin and Nambu degrees of freedom, respectively. Here the Nambu basis is chosen to be $(\hat{c}_\uparrow, \hat{c}_\downarrow, \hat{c}_\downarrow^\dagger, -\hat{c}_\uparrow^\dagger)$, so that the PH operator is $C = \sigma_2\tau_2\mathcal{K}$ and the TR operator is $T = i\sigma_2\mathcal{K}$. The TR-breaking mass gap h can be generated by magnetic impurities, by a Zeeman field, or by proximity with a ferromagnet (M). The SC pairing Δ, on the other hand, can be induced by proximity coupling with an s-wave SC. The two terms Δ and h commute and correspond to competing orders. An SC-M domain wall, where $|h(r)| - |\Delta(r)|$ changes its sign, traps a zero-energy MBS. This can be seen by decomposing Eq. (3.130) into $H = H^+ \oplus H^-$ by the good quantum number $\sigma_1\tau_1 = \pm 1$, where

$$H_{1d}^{\pm}(k, r) = v_F k\tilde{\sigma}_3 + [h(r) \pm \Delta(r)]\tilde{\sigma}_2, \tag{3.131}$$

where $\tilde{\sigma}$ acts on the two-dimensional subspaces. Assuming both $h(r)$ and $\Delta(r)$ are non-negative throughout the edge, $H^+(k, r)$ always has a gap while the mass term for $H^-(k, r)$ changes its sign across the domain wall. H^- is exactly the Jackiw-Rebbi model (3.44) and therefore traps a zero mode between the SC and M regions.

(ii) Helical modes also occur in an interface between an s-wave SC and two adjacent Chern insulators that have the same unit Chern number [Fig. 5(a)]. For example, consider the spinful band Hamiltonian (3.116) on a square lattice, where τ now acts on the spin degree of freedom. It supports a spin polarized chiral edge mode and has opposite polarizations on opposite edges. A protected MBS therefore is located at the SC-M domain wall of a weakly coupled Chern insulator interface. More exotic parafermionic defects are proposed in SC-M heterostructures in fractional TIs (Cheng, 2012; Lindner *et al.*, 2012; Clarke, Alicea, and Shtengel, 2013; Vaezi, 2013; Zhang and Kane, 2014b).

(iii) The same idea applies to semiconducting nanowires with strong SOC in a magnetic field. This ballistic 1D system can be modeled in the continuum limit by the following spinful Hamiltonian:

$$H_0(k) = \frac{\hbar^2 k^2}{2m}\mathbb{1}_2 + u_{\mathrm{SO}}k\sigma_3 + b\sigma_1. \tag{3.132}$$

The Hamiltonian (3.132) has an energy spectrum, which consists of a spin-filtered pair of counterpropagating modes, provided that the Fermi energy lies within the direct magnetic gap (Fig. 6). These helical modes can be gapped out by a superconducting pairing, which is proximity induced by a bulk s-wave SC. This SC nanowire then behaves like a 1D Kitaev p-wave SC and hosts protected boundary MBSs

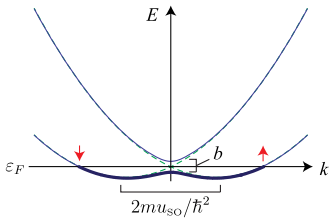

FIG. 6. Energy spectrum of the spin-orbit coupled nanowire (3.132) in a magnetic field.

(Lutchyn, Sau, and Das Sarma, 2010; Oreg, Refael, and von Oppen, 2010; Sau *et al.*, 2010; Alicea *et al.*, 2011). InSb nanowires with a low impurity density which are proximity coupled to an ordinary s-wave SC provide an experimental realization of this 1D p-wave SC. Recently, numerous transport measurements on these systems have observed zero-bias conductance peaks, which were interpreted as evidence of the boundary MBSs (Das *et al.*, 2012; Deng *et al.*, 2012; Mourik *et al.*, 2012; Rokhinson, Liu, and Furdyna, 2012).

(iv) Going back to the SC-M domain wall along a QSH edge, the point defect can be equivalently described in 2D. The defect Hamiltonian that incorporates the 2D bulk takes in the continuum limit the 8-band form of

$$H_{2d}(\mathsf{k}, \mathsf{r}) = [t(k_x\sigma_1 + k_y\sigma_2)\mu_1 + m(\mathsf{r})\mu_3]\tau_3 + h(\mathsf{r})\mu_2 + \Delta(\mathsf{r})\tau_1. \tag{3.133}$$

Here the first line describes the transition between the QSHI and the trivial vacuum as the mass gap $m(\mathsf{r})$ changes its sign along the y axis in Fig. 5(a). The Pauli matrices σ and μ act on spin and orbital degrees of freedom. [Note that the k^2 regularization $m(\mathsf{r}) \to m(\mathsf{r}) - \epsilon k^2$ is not necessary for a defect Hamiltonian, just as in the Jackiw-Rebbi model (3.44).] The TR-breaking $h(r)\mu_2$ term here is actually antiferromagnetic as it also breaks the inversion $P = \mu_3$. It, however, can be replaced by an ordinary ferromagnetic one, like $h(\mathsf{r})\sigma_2$. The magnetic and pairing orders appear only near the interface, the x axis in Fig. 5(a), where $|h(\mathsf{r})| - |\Delta(\mathsf{r})|$ changes its sign across each domain wall point defect. Similar to the boundary Hamiltonian (3.130), the 2D point defect Hamiltonian can be decomposed into $H = H^+ \oplus H^-$ according to the good quantum number $\mu_2\tau_1$. Let us assume that h and Δ are both non-negative. Then H^+ is always gapped and the defect is captured by

$$H_{2d}^{-}(\mathsf{k}, \mathsf{r}) = t(k_x\sigma_1 + k_y\sigma_2)\tilde{\tau}_3 + m(\mathsf{r})\tilde{\tau}_1 + n(\mathsf{r})\tilde{\tau}_2, \tag{3.134}$$

where $n(\mathsf{r}) = h(\mathsf{r}) - \Delta(\mathsf{r})$, and $\tilde{\tau}$ acts on the 2D subspace where $\mu_2\tau_1 = -1$. This Hamiltonian is identical to the 2D Jackiw-Rossi model [cf. Eq. (3.72) (Jackiw and Rossi, 1981; Teo and Kane, 2010b] where the mass terms in $m\Gamma_0(\mathsf{r}) = m(\mathsf{r})\tilde{\tau}_1 + n(\mathsf{r})\tilde{\tau}_2$ can be organized as a vector field $\mathbf{v}(\mathsf{r}) = (m(\mathsf{r}), n(\mathsf{r}))$ that winds once around the defect. This winding mass term represents the nontrivial element in $\pi_1(BO) = \mathbb{Z}_2$, which classifies class D point defects in 2D (Sec. III.C.1). As a consequence of the unit winding, the nontrivial topological index CS_3 in Eq. (3.46) guarantees a protected zero-energy MBS.

(v) The idea generalizes even to 3D (Teo and Kane, 2010a) [Fig. 5(b)]. An SC interface between a bulk TI and a trivial insulator (I) in 3D can be described by the 8-band BdG Hamiltonian

$$H_{3d}(\mathsf{k}, \mathsf{r}) = t(k_x\sigma_1 + k_y\sigma_2 + k_z\sigma_3)\mu_1\tau_3 + m(\mathsf{r})\mu_3\tau_3 + \Delta_x(\mathsf{r})\tau_1 + \Delta_y(\mathsf{r})\tau_2, \tag{3.135}$$

where the TRS mass gap $m(\mathsf{r})$ changes its sign across the TI-I interface, and $\Delta = \Delta_x + i\Delta_y$ is the SC pairing. The model is of the same form as Dirac Hamiltonian (3.72) with spatially

modulated mass term $m\Gamma_0(\mathsf{r}) = m(\mathsf{r})\mu_3\tau_3 + \Delta_x(\mathsf{r})\tau_1 + \Delta_y(\mathsf{r})\tau_2$. A quantum flux vortex brings a unit winding to the pairing phase $\Delta = |\Delta|e^{i\varphi}$. The coefficients in the Dirac mass term can be grouped together into a 3D vector field

$$\mathbf{n}(\mathsf{r}) = (\Delta_x(\mathsf{r}), \Delta_y(\mathsf{r}), m(\mathsf{r})), \tag{3.136}$$

which looks like a "hedgehog" around the vortex core [Fig. 5(b)]. As the vector field is nonsingular except at the point defect, the hedgehog configuration corresponds to a continuous map $\hat{\mathbf{n}}: S^2 \to S^2$ over a 2-sphere spatially enclosing the defect. This map has a unit winding

$$\nu = \frac{1}{4\pi}\int_{S^2} \hat{\mathbf{n}} \cdot d\hat{\mathbf{n}} \times d\hat{\mathbf{n}} = \pm 1 \tag{3.137}$$

and represents the generator in the homotopy group $\pi_2(S^2) = [S^2, S^2] = \mathbb{Z}$. It also represents the nontrivial element in $\pi_2[U(N)/O(N)] = \mathbb{Z}_2$, for instance $\hat{\mathbf{n}}$ wraps the 2-cycle in $U(2)/O(2) \sim U(1) \times S^2$, that classifies class D point defects in 3D. The winding number ν translates into a nontrivial topological index CS_5 in Eq. (3.46) and guarantees a protected zero-energy MBS at the vortex core. The 1D, 2D, and 3D point defect models (3.130), (3.133), and (3.135) are unified by the $K(s; d, D)$ classification (Teo and Kane, 2010b)

$$K(2; 1, 0) \cong K(2; 2, 1) \cong K(2; 3, 2) \cong \mathbb{Z}_2, \tag{3.138}$$

where $s = 2$ for class D.

2. Gapless modes along line defects and index theorems

In this section, we discuss protected gapless modes that propagate along topological line defects ($\delta = d - D = 2$). Relevant symmetry classes and types of gapless modes are summarized in Table VI and Fig. 7. By discussing their transport properties, we introduce proper indices counting the degrees of freedom of the propagating gapless modes, which, by the bulk-boundary correspondence, will be identified with the topological invariants.

a. Edge transports

Here we demonstrate the appearance of protected 1D modes along topological line defects in terms of 1D edges of 2D bulk topological systems. Topological line defects in higher dimensions and their topological origin are discussed later.

The most well-known example is the chiral edge modes [Fig. 7(a)] along the boundary of an integer quantum Hall (QH) fluid (Laughlin, 1981; Halperin, 1982; Volovik, 1992; Hatsugai, 1993; Schulz-Baldes, Kellendonk, and Richter, 2000). A chiral mode is an electronic channel that propagates in a single direction. For example the (spin polarized) lowest Landau level in 2D—despite having a bulk cyclotron gap—carries one conducting gapless chiral edge mode. At zero temperature, each chiral channel carries an electric current

TABLE VI. Symmetry classes that support topologically nontrivial line defects and their associated protected gapless modes.

Symmetry	Topological classes	1D gapless fermion modes
A	$\mathbb{Z}$	Chiral Dirac
D	$\mathbb{Z}$	Chiral Majorana
DIII	$\mathbb{Z}_2$	Helical Majorana
AII	$\mathbb{Z}_2$	Helical Dirac
C	$2\mathbb{Z}$	Chiral Dirac

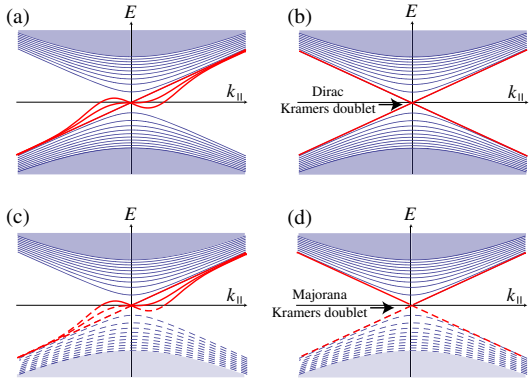

FIG. 7. Gapless spectra inside the bulk gap: (a) chiral Dirac modes, (b) helical Dirac mode, (c) chiral Majorana modes, and (d) helical Majorana mode. From Qi *et al.*, 2009.

$$I_e^1 = \int_{k_{\mathrm{cutoff}}}^{k_F} \frac{dk}{2\pi} e v(k) = \frac{e}{h}(\varepsilon_F - \varepsilon_{\mathrm{cutoff}}), \tag{3.139}$$

where e is the electric charge, ε_F is the Fermi energy, and $v(k) = \partial\varepsilon(k)/\partial k$ is the velocity. In a more general scenario, the 1D boundary may carry multiple chiral channels. Dropping the Fermi energy independent cutoff term, the net electric current takes the form of

$$I_e \approx c_- \frac{e}{h}\varepsilon_F, \tag{3.140}$$

where the integer coefficient is a $\mathbb{Z}$ analytic index that counts the spectral flow (Nakahara, 2003; Volovik, 2003)

$$c_- = \begin{pmatrix} \text{number of forward} \\ \text{propagating Dirac modes} \end{pmatrix} - \begin{pmatrix} \text{number of backward} \\ \text{propagating Dirac modes} \end{pmatrix}. \tag{3.141}$$

The integer QHE (Klitzing, Dorda, and Pepper, 1980) is generated by a transverse bias across the top and bottom edges of a Hall bar. This gives a potential difference $edV_y = d\varepsilon_F = \varepsilon_F^{\mathrm{top}} - \varepsilon_F^{\mathrm{bottom}}$ between the two edges and drives a horizontal current $dI_x = I_e^{\mathrm{top}} - I_e^{\mathrm{bottom}} = \sigma_{xy} dV_y$, where

$$\sigma_{xy} = c_- \frac{e^2}{h} \tag{3.142}$$

is the quantized Hall conductance.

At small temperature T, each chiral Dirac mode also carries an energy (thermal) current (Luttinger, 1964; Kane and Fisher, 1997; Cappelli, Huerta, and Zemba, 2002; Kitaev, 2006)

$$I_T^1 = \int \frac{dk}{2\pi} f(\varepsilon(k)-\mu) v(k) \varepsilon(k) \approx I_0 + \frac{\pi^2 k_B^2}{6h} T^2 + O(T^4), \tag{3.143}$$

where $f(\varepsilon) = (e^{\varepsilon/k_B T}+1)^{-1}$ is the Fermi-Dirac distribution and k_B is the Boltzmann constant. Dropping the T-independent contribution I_0, a general boundary with multiple chiral modes carries the net anomalous energy current

$$I_T \approx c_- \frac{\pi^2 k_B^2}{6h} T^2. \tag{3.144}$$

The QH fluid has a thermal Hall response so that a transverse temperature difference $dT = T^{\text{top}} - T^{\text{bottom}}$ across the Hall bar drives an energy current $dI_T = I_T^{\text{top}} - I_T^{\text{bottom}} = \kappa_{xy} dT$, where

$$\kappa_{xy} = c_- \frac{\pi^2 k_B^2}{3h} T \tag{3.145}$$

is the thermal Hall conductivity, which can be related to the gravitational anomaly (Alvarez-Gaume and Witten, 1984; Volovik, 1990; Wang, Qi, and Zhang, 2011; Nomura *et al.*, 2012; Ryu, Moore, and Ludwig, 2012; Stone, 2012). Thermal response applies to systems that lack $U(1)$ charge conservation, like SCs. A chiral SC hosts chiral Majorana edge modes. These neutral modes do not carry electric currents, but they do carry energy current (3.144). A chiral SC in general has no quantized electric Hall response, but exhibits a thermal Hall response (3.145). Since a Dirac mode is decomposed into two Majorana ones as its real and imaginary components $\psi = (\gamma_1 + i\gamma_2)/2$, the $\mathbb{Z}$ analytic index c_- in Eq. (3.141) translates into

$$c_- = \frac{1}{2}\left(\begin{array}{c}\text{number of forward}\\ \text{Majorana modes}\end{array} - \begin{array}{c}\text{number of backward}\\ \text{Majorana modes}\end{array}\right), \tag{3.146}$$

so that c_- now can take half-integral values. For instance, $c_- = \pm 1/2$ for a chiral spinless $p_x + ip_y$ SC. This quantity extends to many-body systems supporting fractionalization (e.g., fractional QH systems), where the $(1+1)$D gapless boundary can be effectively described by a conformal field theory (CFT) (Francesco, Mathieu, and Senechal, 1997). It corresponds to the chiral central charge $c_- = c_R - c_L$, the difference of the central charges between forward and backward propagating channels of the edge CFT.

Chiral modes necessarily break TRS, as they are not symmetric under $k \leftrightarrow -k$. But in the presence of TRS with $T^2 = -1$ another type of robust gapless edge modes can exist: Helical modes [Figs. 7(b) and 7(d)] are nonchiral, as they have both forward and backward channels. Backscattering is however forbidden by TRS, since the crossing is protected by Kramers theorem. Unlike chiral modes, helical modes are $\mathbb{Z}_2$ classified since a TR symmetric backscattering term can remove a pair of them. The $\mathbb{Z}_2$-analytical index thus counts the (nonchiral) central charge $c = c_R = c_L$

$$c = (\text{number of Dirac helical modes}) \mod 2, \tag{3.147}$$

for $U(1)$ preserving systems, or

$$c = \tfrac{1}{2}(\text{number of Majorana helical modes}) \mod 1, \tag{3.148}$$

for $U(1)$ breaking SCs. These TRS protected modes appear on the boundaries of 2D TIs in class AII (such as a QSH insulator with $c = 1$) and TSCs in class DIII [such as a $(p+ip)\uparrow \times (p-ip)\downarrow$SC with $c = 1/2$].

Along an unequilibrated edge, the pair of counterpropagating channels of a helical mode can have different temperatures, or different chemical potentials, if they are of the Dirac type. This difference can be generated by connecting two charge or heat reservoirs to the 1D boundary. As each Dirac chiral channel carries an electric current (3.139), a potential difference $edV = \varepsilon_F^R - \varepsilon_F^L$ between the forward and backward components of a Dirac helical mode drives a net electric current $dI_e = \sigma_{xx} dV$, where

$$\sigma_{xx} = c\frac{e^2}{h} \mod \frac{2e^2}{h} \tag{3.149}$$

is the longitudinal electric conductance along a single edge. In reality the two charge reservoirs must be connected by a pair of edges, the top and bottom boundaries of a 2D bulk, so that the measured conductance is twice that of Eq. (3.149). A conductance close to $2e^2/h$ is experimentally seen across the QSHI of HgTe/CdTe quantum wells (Konig *et al.*, 2007). On the other hand, a helical Majorana edge mode—in a SC where $U(1)$ symmetry is broken—responds to a thermal difference $dT = T^R - T^L$ between the counterpropagating components and gives the net energy current $dI_T = \kappa_{xx} dT$, where

$$\kappa_{xx} = c\frac{\pi^2 k_B^2}{3h} T \mod \frac{\pi^2 k_B^2}{3h} T \tag{3.150}$$

is the longitudinal thermal conductance along a single edge. Again, the measured conductance must be contributed by two edges and is double of that in Eq. (3.150).

b. Index theorems

We have seen that gapless modes along 1D boundaries of a 2D topological bulk can give rise to anomalous transport signatures. Similar signatures also arise when a line defect in higher dimensions carries these gapless modes. Just like the bulk-boundary correspondence that relates the bulk topology to edge excitations, the gapless excitations along a line defect is guaranteed by the topology of the defect.

The net chirality (3.141) of gapless Dirac modes along a line defect in d dimensions is determined by the Chern invariant

$$c_- = \text{Ch}_{d-1}[H(\mathsf{k},\mathsf{r})] \in \mathbb{Z}, \tag{3.151}$$

where Ch_{d-1} is defined in Eq. (3.10) and the defect Hamiltonian $H(\mathsf{k},\mathsf{r})$ describes the long length scale spatial variation of the insulating band Hamiltonian around the defect. For instance in 2D, the chirality of a QH fluid or Chern insulator is given by the first Chern number. If the

system is superconducting, the line defect carries Majorana instead of Dirac modes. The net chirality is then given by

$$c_- = \tfrac{1}{2}\mathrm{Ch}_{d-1}[H_{\mathrm{BdG}}(\mathsf{k},\mathsf{r})] \in \tfrac{1}{2}\mathbb{Z}, \tag{3.152}$$

where $H(\mathsf{k},\mathsf{r})$ is now the BdG defect Hamiltonian. For example, the edge chirality of a $(p+ip)$ SC is half of the bulk first Chern invariant. Equations (3.151) and (3.152) are consistent with each other, since the band Hamiltonian of an insulator is artificially doubled in the BdG description which has twice the original Chern number.

The defect classification (Table II) allows nontrivial chirality only for the TR-breaking symmetry classes A, D, and C. The PH operator for class C squares to -1, $C^2=-1$. The Kramers theorem applies to zero-energy modes at the symmetric momenta $k_\parallel = 0, \pi$ and requires chiral modes to come in pairs. This agrees with the $2\mathbb{Z}$ defect classification.

The number parity of gapless helical modes along a TRS line defect in d dimensions equates to a Fu-Kane invariant

$$c = \mathrm{FK}_{d-1}[H(\mathsf{k},\mathsf{r})] \mod 2, \tag{3.153}$$

for Dirac systems in bulk insulators, or

$$c = \tfrac{1}{2}\mathrm{FK}_{d-1}[H(\mathsf{k},\mathsf{r})] \mod 1, \tag{3.154}$$

for Majorana systems in bulk SCs. Classes AII and DIII are the only TR symmetric classes that support Kramers degenerated helical modes. For example, the helical Dirac mode along the edge of a 2D TI or QSHI is protected by the original Fu-Kane $\mathbb{Z}_2$ invariant. The helical Majorana edge mode of a 2D TSC, such as ^{3}He-B, has the same topological origin. Similarly, the helical 1D mode along a dislocation line in a 3D weak TI falls under the same classification as the helical edge mode of a 2D QSHI (Ran, 2010).

c. Line defects in three dimensions

We consider various examples of line defects in 3D that host topologically protected gapless modes. The defect Hamiltonian $H(\mathsf{k},\phi)$ is slowly modulated by the spatial angular parameter $\phi \in [0,2\pi]$ that wraps once around the defect line. We begin by looking at heterostructures where the line defect is the trijunction between three different bulk electronic materials (Fig. 8). A finite energy gap is required everywhere away from the trijunction line. This includes the three surface interfaces that separate the three bulk materials. For instance, when the three bulk materials have noncompeting orders, the surface interfaces can be smeared out into the 3D bulk where different orders coexist. The defect Hamiltonian takes the Dirac form (3.72)

$$H(\mathsf{k},\phi) = \hbar v \mathsf{k}\cdot\mathbf{\Gamma} + m\Gamma_0(\phi), \tag{3.155}$$

where the $m\Gamma_0(\phi)$ incorporates coexisting orders as anticommuting mass terms and winds nontrivially around the defect line.

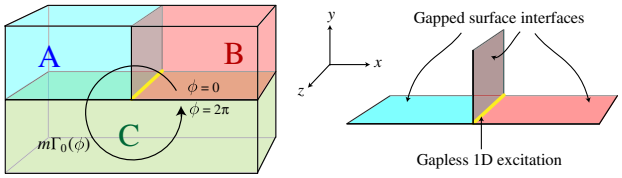

FIG. 8. Line defect (yellow line) at a heterostructure. A, B, and C are different bulk gapped materials put together so that there is no gapless surface modes along interfaces of any pairs. The mass term $m\Gamma_0(\phi)$ wraps nontrivially around the line interface which results in a gapless 1D excitation localized at the line defect.

d. Example: TI-AF heterostructure (class A)

We now explicitly demonstrate the chiral Dirac mode bounded by the TI-AF heterostructure shown in Fig. 9(a). The surface Dirac cone of a TI can be gapped out by a TRS breaking mass term

$$H_{\mathrm{surface}}(k_x,k_z,x) = \hbar v(k_x\sigma_1 + k_z\sigma_2) + m(x)\sigma_3, \tag{3.156}$$

where the surface is parallel to the x-z plane. When the mass term changes its sign $m(x\to\pm\infty)=\pm m_0$, there is a chiral Dirac mode running along the domain wall. Near the line defect the system is described by Eq. (3.156) with k_x replaced by $-id/dx$, i.e., by the differential operator

$$\mathcal{H}_{\mathrm{surface}}(k_z) = \left[-i\hbar v\sigma_1\frac{d}{dx} + m(x)\sigma_3\right] + \hbar v k_z\sigma_2. \tag{3.157}$$

Note that the operator inside the square bracket is exactly the Jackiw-Rebbi model (3.44), which traps a zero mode $|\psi_0\rangle$ for $k_z=0$. As $\sigma_2|\psi_0\rangle = +|\psi_0\rangle$, it has a chiral energy spectrum $\mathcal{H}_{\mathrm{surface}}(k_z)|\psi_0\rangle = +\hbar v k_z|\psi_0\rangle$. This chiral Dirac mode is topologically guaranteed by the Chern invariant (3.151)

$$\begin{aligned} c_- &= \mathrm{Ch}_1[H(k_x,k_y,x)] \\ &= \frac{i}{2\pi}\int_{k_x,k_y} \mathrm{Tr}(\mathcal{F}|_{x>0}) - \mathrm{Tr}(\mathcal{F}|_{x<0}) = 1, \end{aligned} \tag{3.158}$$

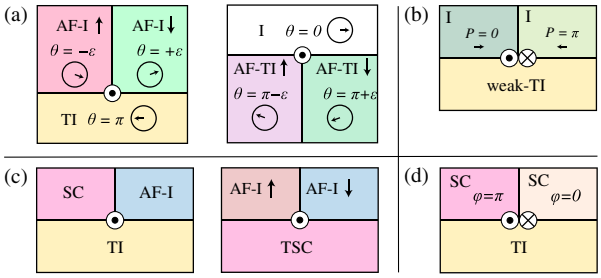

FIG. 9. Heterostructure cross section on the x-y plane. AF = antiferromagnetic, I = trivial insulator, TI = topological insulator, SC = superconductor, and TSC = class DIII topological superconductor. (a) The chiral Dirac mode $\odot$ protected by winding of the magnetoelectric θ angle. (b) The helical Dirac mode $\odot\otimes$ separating opposite polarization insulating domains. (c) The chiral Majorana mode. (d) The helical Majorana mode between SC domains with TRS pairing phase $\varphi = 0, \pi$.

where the integral is taken over k_x, $k_y \in (-\infty, \infty)$. Note that in the defect description, as in the Jackiw-Rebbi model, a εk^2 regularization in Eq. (3.156) is unnecessary.

Alternatively, the TI-AF heterostructure can be described by a 3D defect Hamiltonian in the continuum limit

$$H_{3d}(\mathsf{k}, \phi) = \hbar v \mathsf{k} \cdot \boldsymbol{\sigma} \mu_1 + m_1(\phi)\mu_3 + m_2(\phi)\mu_2, \quad (3.159)$$

or its discrete counterpart obtained by making the replacements $k_i \to \sin k_i$ and $m_1(\phi) \to m_1(\phi) + m_1(\phi) + \varepsilon(3 - \sum_{i=1}^{3} \cos k_i)$, where σ and μ are Pauli matrices acting on spin and orbital degrees of freedom. The Dirac mass $m\Gamma_0(\phi) = m_1(\phi)\mu_3 + m_2(\phi)\mu_2$ incorporates (i) the TRS mass that changes its sign $m_1(y \to \pm\infty) = \pm m_0$ across the horizontal TI surface, and (ii) the AF mass that changes its sign $m_2(x \to \pm\infty) = \pm m_0$ across the vertical y-z plane where the Néel order flips. Here $m_2\mu_2$ corresponds to an AF order as it breaks inversion symmetry $I = \mu_3$. It, however, can be replaced by a ferromagnetic one, i.e., $h\sigma_1$. The mass parameter $\mathbf{m}(\phi) = (m_1(\phi), m_2(\phi))$ is modulated along a circle with radius R_0 far away from the line defect. In the homogeneous limit, m_1 and m_2 coexist and are given by $\mathbf{m}(\phi) \approx (m_0 \sin\phi, m_0 \cos\phi)$. It winds once around the origin. This corresponds to the generator of the homotopy classification $\pi_1(U(N)) = \mathbb{Z}$ of class A line defects in 3D, where $U(N)$ is the classifying space for 3D class A band Hamiltonians. For instance $m\Gamma_0(\phi)$ wraps around the nontrivial cycle in $U(4)$. This nontrivial winding matches with the second Chern invariant (3.151) and (3.10):

$$\begin{aligned} c_- &= \mathrm{Ch}_2[H_{3d}(\mathsf{k}, \phi)] \\ &= \frac{-1}{8\pi^2} \int_{\mathrm{BZ}^3 \times S^1} \mathrm{Tr}[\mathcal{F}(\mathsf{k}, \phi) \wedge \mathcal{F}(\mathsf{k}, \phi)] \\ &= \frac{1}{2\pi} \int_{S^1} d\theta(\phi) = 1, \end{aligned} \quad (3.160)$$

where $\theta(\phi) = 2\pi \int_{\mathrm{BZ}^3} \mathcal{Q}_3(\mathsf{k}, \phi) \pmod{2\pi}$ is the magnetoelectric polarizablility (theta angle) (Sec. III.B.2.b), which in this case is slowly modulated by the spatial angle ϕ and winds once from 0 to 2π around the origin [Fig. 9(a)].

The topology of the long length scale Hamiltonian (3.159) corresponds to the chiral Dirac mode appearing at the heterostructure. Near the line defect the system is effectively described by the differential operator

$$\begin{aligned} \mathcal{H}_{3d}(k_z) = &[-i\hbar v(\partial_x \sigma_1 + \partial_y \sigma_2)\mu_1 + m_1(x, y)\mu_3 + m_2(x, y)\mu_2] \\ &+ \hbar v k_z \sigma_3 \mu_1, \end{aligned} \quad (3.161)$$

which is obtained from Eq. (3.159) by replacing $k_{x/y} \leftrightarrow -i\partial_{x/y}$. Note that the operator inside the square bracket is exactly the 2D Jackiw-Rossi model which has a zero mode $|\psi_0\rangle$ at $k_z = 0$. As the zero mode has positive chirality $S|\psi_0\rangle = +|\psi_0\rangle$ with respect to the chiral operator $S = \sigma_3\mu_1$, it gives a chiral Dirac mode with a linear energy spectrum $\mathcal{H}(k_z)|\psi_0\rangle = +\hbar v k_z |\psi_0\rangle$.

e. Example: Helical modes in heterostructures (class AII)

Heterostructures in symmetry classes AII, D, and DIII can host helical modes. Figure 9(b) shows a helical Dirac mode on the surface of a weak TI, which hosts a pair of Dirac cones at the two TR invariant surface momenta K_1 and K_2. The two cones can be gapped out by a translation breaking TRS perturbation u with a finite wave vector $\mathsf{K}_1 - \mathsf{K}_2$. This density wave u introduces a polarization $P = 0, \pi \pmod{2\pi}$ depending on the sign of u. A domain wall on the surface separating two regions with opposite polarization traps a protected helical Dirac mode (Liu, Qi, and Zhang, 2012; Chiu, 2014).

f. Example: Chiral Majorana modes in heterostructures (class D)

Figure 9(c) shows a chiral Majorana mode realized in two superconducting heterostructures. First, the surface Dirac cone of a TI can be gapped by a TRS or $U(1)$ symmetry breaking order. When restricting the defect momentum to $k_z = 0$ (Tanaka, Yokoyama, and Nagaosa, 2009; Tanaka, Sato, and Nagaosa, 2012). This problem reduces to the previous 2D QSHI-FM-SC heterostructure [Fig. 5(a) and Eq. (3.133)]. The zero-energy MBS now turns into a gapless chiral Majorana mode that disperses linearly in k_z and carries the chiral central charge $c_- = 1/2$. Instead of the SC-AF domain wall on the TI surface, one can also consider a domain wall in the SC phase on the TI surface, which hosts a helical Majorana defect mode [Fig. 9(d)]. Second, the surface of a TSC in class DIII can host multiple ($= n$) copies of Majorana cones, with chiralities $\chi_1, \ldots, \chi_n = \pm 1$. These surface states are sensitive to a TR-breaking perturbation that opens up mass gaps $m_1, \ldots, m_n$. A domain wall where certain mass gaps change their sign hosts chiral Majorana modes with a chiral central charge of

$$c_- = \frac{1}{2} \lim_{x \to \infty} \sum_{a=1}^{n} \chi_a \frac{\mathrm{sgn}[m_a(x)] - \mathrm{sgn}[m_a(-x)]}{2}. \quad (3.162)$$

g. Example: Dislocations in weak TIs and TSCs

Gapless modes can also appear along lattice dislocations in weak TIs and TSCs. The 2D weak topological indices of a 3D bulk TI and TSC is expressed as a reciprocal lattice vector $\mathbf{G}_\nu = \nu_1 \mathbf{b}_1 + \nu_2 \mathbf{b}_2 + \nu_3 \mathbf{b}_3$, where the ith weak index ν_i is evaluated on the 2-cycle $\mathcal{C}_i = \{\mathsf{k} \in \mathrm{BZ}^3 : \mathsf{k} \cdot \mathsf{a}_i = \pi\}$ perpendicular to a_j and a_k on the boundary of the BZ, where $\mathsf{a}_{i,j,k}$ are distinct primitive lattice vectors. Note that the 2-cycles $\mathcal{C}_i$ are invariant under the involution $\mathsf{k} \leftrightarrow -\mathsf{k}$ and restricting the Hamiltonian onto these momentum planes give 2D Hamiltonians with the same symmetries. For example, ν_i are first Chern invariants for classes A, D, and C, or Fu-Kane invariants (or equivalently Pfaffian invariants) for classes AII and DIII. The topological index that characterizes the gapless modes along a dislocation line defect is the product (Ran, Zhang, and Vishwanath, 2009)

$$\mathrm{ind} = \frac{1}{2\pi} \mathbf{B} \cdot \mathbf{G}_\nu, \quad (3.163)$$

where **B** is the Burgers vector, the net amount of translation when a particle circles once around the dislocation line. This integral quantity counts the chiral central charge c_- of Dirac dislocation modes in a weak 3D Chern insulator, or twice the chiral central charge of Majorana dislocation modes in a weak 3D class D SC. For weak class AII TI or class DIII TSC, this index becomes a $\mathbb{Z}_2$ number that counts helical Dirac or Majorana dislocation modes, respectively.

E. Adiabatic pumps

Adiabatic pumps are temporal cycles of defect systems. The Hamiltonian is of the form $H(\mathsf{k},\mathsf{r},t)$, where k lives in the BZ, BZ^d, $\mathsf{r}\in\mathcal{M}^{D-1}$ wraps the defect in real space, and t is the temporal parameter of the adiabatic cyclic. The topological classification is determined by the symmetry class s of the Hamiltonian and the topological dimension $\delta=d-D$, and is given by the classification in Table I. The antiunitary symmetries normally flip $(\mathsf{k},\mathsf{r},t)\to(-\mathsf{k},\mathsf{r},t)$. However, in some cases it can also flip the temporal parameter (Zhang and Kane, 2014a), but this will not be the focus of this review.

The simplest pumps appear in symmetry class A in 1D, known as Thouless pumps (Thouless, 1983) and are classified by an integer topological invariant, the first Chern invariant:

$$\mathrm{Ch}_1=\frac{i}{2\pi}\int_{\mathrm{BZ}^1\times S^1}\mathrm{Tr}[\mathcal{F}(k,t)], \tag{3.164}$$

where $\mathcal{F}$ is the Berry curvature of the occupied states and S^1 parametrizes the temporal cycle. For example,

$$H(k,t)=t\sin k\sigma_1+u\sin t\sigma_2+m(\tfrac{3}{2}-\cos k-\cos t)\sigma_3 \tag{3.165}$$

realizes a nontrivial pump with $\mathrm{Ch}_1=1$, where t runs a cycle in $[0,2\pi]$ so that $H(k,0)=H(k,2\pi)$. The signature of a Thouless pump is the spectral flow of boundary modes: The end of the 1D system does not hold protected bound modes. However, during the adiabatic cycle, a certain number of boundary modes appear and as a function time connect the occupied and unoccupied bands. [See Fig. 7(a), but with $k_\parallel$ replaced by t such that the red midgap bands represent the temporal evolution of the boundary states.] A charge is pumped to (or away from) the boundary when a boundary state is dragged from the unoccupied bands to the occupied ones (respectively, occupied bands to the unoccupied ones) after a cycle. The index theorem relates the Chern invariant and the spectral flow:

$$\mathrm{Ch}_1=(\text{charge accumulated at boundary after 1 cycle}). \tag{3.166}$$

General charge pumps are adiabatic cycles of point defects in d dimensions. The class A Hamiltonian takes the form $H(\mathsf{k},\mathsf{r},t)$ where $(\mathsf{k},\mathsf{r},t)\in\mathrm{BZ}^d\times S^{d-1}\times S^1$. They are characterized by the dth Chern invariant (3.10) defined by the Berry curvature $\mathcal{F}(\mathsf{k},\mathsf{r},t)$ of occupied states. For example, the Laughlin argument (which proves that a $hc/2e$ flux quantum in an integer QH fluid carries charge $h\sigma_{xy}/e$, with σ_{xy} the Hall conductance) can be rephrased as an adiabatic pump of a 2D point defect (Laughlin, 1981).

Adiabatic pumps can also appear in superconducting class D or BDI systems. They are $\mathbb{Z}_2$ classified and are characterized by the Fu-Kane invariant (3.63) with the gauge constraint (3.65). The simplest example is the fermion parity pump realized along a 1D p-wave SC wire (Kitaev, 2001; Fu and Kane, 2009; Teo and Kane, 2010b). The bulk BdG Hamiltonian is of the form of

$$\begin{aligned}H(k,t)&=e^{-it\sigma_3/2}[\Delta\sin k\sigma_1+(u\cos k-\mu)\sigma_3]e^{it\sigma_3/2}\\&=\Delta\sin k(\cos t\sigma_1+\sin t\sigma_2)+(u\cos k-\mu)\sigma_3,\end{aligned} \tag{3.167}$$

where t evolves from 0 to 2π in a cycle. Note that $H(k,0)=H(k,2\pi)$. At all time $H(k,t)$ is a p-wave SC with a nontrivial $\mathbb{Z}_2$ index when $|u|>|\mu|$ and, hence, supports protected boundary Majorana zero modes. The SC pairing phase winds by 2π as the system goes through a cycle. The evolution operator $e^{-it\sigma_3/2}$, however, is not cyclic as it has a period of 4π. Hence, since $|\gamma_t\rangle=e^{-it\sigma_3/2}|\gamma_0\rangle$, the Majorana zero mode γ at the wire end changes its sign after a cycle.

Consider a weak link along a topological p-wave SC wire. At the completely cutoff limit, there are two uncoupled Majorana zero modes $\hat\gamma_1$, $\hat\gamma_2$ sitting at the two sides of the link. They form a fermionic degree of freedom $\hat c=(\hat\gamma_1+i\hat\gamma_2)/2$, which realizes a two-level system $|0\rangle$ and $|1\rangle=\hat c^\dagger|0\rangle$. Electron tunneling across the link splits the zero modes with an energy gap proportional to the tunneling strength, where the ground state has now a definite fermion parity $|0\rangle$ or $|1\rangle$. A phase slip $\delta\varphi=\varphi_R-\varphi_L$ is a discontinuity of the SC pairing phase across the weak link, where $\varphi_{R/L}$ are the phases of the two disconnected SC wires on the two sides of the weak link. In the scenario where the phase slip adiabatically winds by 2π, the fermion parity operator $(-1)^{\hat N(\delta\varphi)}=i\hat\gamma_1(\delta\varphi)\hat\gamma_2(\delta\varphi)$ evolves and acquires an extra sign after a cycle, i.e., $(-1)^{\hat N(2\pi)}=-(-1)^{\hat N(0)}$. In other words, this flips $\hat c\leftrightarrow\hat c^\dagger$ [up to a $U(1)$ phase]. Physically, although there is an energy gap when $\delta\varphi=0$, this gap has to close and reopen as the two-level system undergoes a level crossing during the adiabatic cycle. The single (or in general odd number of) level crossing cannot be removed and is protected by the nontrivial $\mathbb{Z}_2$ bulk topology. The fractional Josephson effect is a consequence of such a nontrivial topology (Kitaev, 2001; Fu and Kane, 2009; Zhang and Kane, 2014b), which can also arise in TR symmetric systems (Keselman *et al.*, 2013; Zhang and Kane, 2014a). Unconventional Josephson effects that may have a topological origin have recently been observed in certain experimental systems (Williams *et al.*, 2012; Yamakage, Sato *et al.*, 2013; Kurter *et al.*, 2014).

F. Anderson "delocalization" and topological phases

So far TIs and TSCs were described from the bulk point of view and by establishing a bulk or defect-boundary correspondence. Here we show that it is also possible to identify TIs and TSCs from the boundary point of view, i.e., by

studying the effects of disorder on the boundary modes (Schnyder *et al.*, 2008).

Let us recall how the bulk topological properties of TIs and TSCs manifest themselves at the boundary of the system: TIs and TSCs are always accompanied by gapless excitations localized at their boundaries. These boundary states are stable against perturbations which respect the symmetries of the system (Sec. III.D). As a deformation of the system let us consider spatially inhomogeneous perturbations, i.e., disorder. As it turns out, the bulk or defect-boundary correspondence holds even in the presence of disorder, and hence gapless boundary and defect excitations are stable against disorder. That is, the boundary modes do not *Anderson localize* even in the presence of disorder, as long as the symmetry conditions are preserved (enforced), and as long as the inhomogeneous perturbations due to disorder do not close the bulk gap.

Adding sufficiently strong disorder in an ordinary metal almost always leads to an (Anderson) insulator.[6] In his seminal paper Anderson (1958) showed by the so-called "locator expansion" that, if one starts from the atomic limit, the presence of sufficiently strong impurities leads to the absence of electron diffusion (i.e., to Anderson localization). If we follow Anderson's analysis, we expect Anderson localization in any system with sufficiently strong disorder, as long as Anderson's assumption applies, i.e., that the system is connected to the atomic limit. Reversing this logic, the absence of Anderson localization implies the absence of an atomic limit, or the impossibility of discretizing the system on a lattice. The absence of Anderson localization (i.e., "Anderson delocalization"), can thus be used as a criterion to identify theories that cannot be discretized on a lattice—lattice versions of such theories can be realized only as a boundary of some topological bulk system. Historically, Anderson delocalization at boundaries was hypothesized to be the defining property of TIs and TSCs. Adopting this hypothesis, it was shown that the Anderson delocalization approach is powerful enough to establish the tenfold classification of TIs and TSCs (Schnyder *et al.*, 2008).

In this section, we review Anderson delocalization and the tenfold classification of TIs and TSCs mainly by using effective field theories, i.e., nonlinear sigma models (NLσMs) (Wegner, 1979; Efetov, Larkin, and Kheml'Nitskiĭ, 1980; Efetov, 1983; Evers and Mirlin, 2008)—a convenient framework to discuss the physics of Anderson localization and delocalization in various dimensions and in the presence of various symmetry conditions. We also briefly touch upon the effects of disorder on bulk TIs and TSCs.

1. Nonlinear sigma models

The NLσMs for the Anderson localization problem are effective field theories that describe the properties of (disorder-averaged) single-particle Green's functions and products thereof. Using the NLσM framework, one can compute all essential properties of single-particle Green's functions, and hence of single-particle Hamiltonians.

The basic concepts that underlie the framework of NLσMs can be illustrated by taking a classical magnet as an example. The classical Heisenberg ferromagnet in d space dimensions can be described, in the long-wave-length limit, by an $O(3)$ NLσM. Its action is given by

$$S[\mathbf{n}] = \frac{1}{t}\int d^d\mathsf{r}\partial_\mu \mathbf{n}\cdot\partial_\mu\mathbf{n}, \tag{3.168}$$

where $\mathbf{n}$ is a three-component unit vector and t is the coupling constant, which is proportional to the temperature, the magnitude of spin, and the magnetic exchange interaction. The partition function is given by the functional integral $Z=\int\mathcal{D}[\mathbf{n}]\exp(-S[\mathbf{n}])$, where the sum runs over all maps $\mathbf{n}(\mathsf{r})$ from the d-dimensional space to the space of the order parameter $S^2\simeq O(3)/O(2)$. The space of the order parameter is called the *target space*. Here $O(3)(=G)$ is the symmetry of the classical Heisenberg ferromagnet, and $O(2)(=H)$ is the residual symmetry when the $O(3)$ is spontaneously broken. The Nambu-Goldstone theorem tells us that $G/H=O(3)/O(2)$ is the target manifold representing the fluctuations of the order parameter.

The Nambu-Goldstone modes that are relevant to the physics of Anderson localization correspond to the diffusive motion of electrons or Bogoliubov quasiparticles. These modes are called "diffusons" and "Cooperons" and their dynamics can be described by NLσMs, whose action and path integral are given by (Friedan, 1985)

$$S[X]=\frac{1}{t}\int d^d\mathsf{r}G_{AB}[X]\partial_\mu X^A\partial_\mu X^B,$$
$$Z=\int\mathcal{D}[X]\exp(-S[X]), \tag{3.169}$$

respectively. Here $X^A(\mathsf{r})\colon\mathbb{R}^d\to G/H$ are coordinates on a suitably chosen target manifold G/H, which represents a map from d-dimensional physical space to the target manifold G/H. $G_{AB}[X]$ denotes the metric of the target space. In the context of Anderson localization and delocalization, the coupling constant t in the NLσMs is inversely proportional to the conductivity. For our discussion, d either can be the spatial dimension of the boundary of a $(d+1)$-dimensional (topological) insulator or SC or can be the bulk dimension of a TIs or TSCs. (Technically, the NLσMs in Anderson localization physics are derived by using the replica trick to handle quenched disorder averaging. In the following, we use the fermionic replica trick.) Two typical phases described by NLσMs, ordered and disordered phases, correspond, in the context of Anderson localization, to a metallic and an insulator phase, respectively.

In the NLσM description of Anderson localization, the differences between symmetry classes are encoded by different target manifolds. (See Table VII, which lists the target manifolds.) While generic NLσMs can have more than one coupling constant, the action (3.169) has only one coupling constant t. This is a crucial feature of NLσMs relevant to Anderson localization. This fact is nothing but a reincarnation

[6]There are a few exceptions to this rule, but even in such cases, homogeneous but lattice-translation symmetry breaking perturbations (i.e., charge density wave or dimerization) can turn the system into a band insulator.

TABLE VII. The NLσM target manifolds (in the fermionic replica approach) for the symmetry classes of the tenfold way.

AZ class	NLσM target space
A	$U(2N)/U(N)\times U(N)$
AI	$Sp(2N)/Sp(N)\times Sp(N)$
AII	$O(2N)/O(N)\times O(N)$
AIII	$U(N)\times U(N)/U(N)$
BDI	$U(2N)/Sp(N)$
CII	$U(N)/O(N)$
D	$O(2N)/U(N)$
C	$Sp(N)/U(N)$
DIII	$O(N)\times O(N)/O(N)$
CI	$Sp(N)\times Sp(N)/Sp(N)$

of the single parameter scaling hypothesis by Abrahams *et al.* (1979). The target spaces of the NLσMs which allow only one coupling constant are called symmetric spaces. These have been fully classified by the mathematician E. Cartan (Helgason, 1978). Ignoring those symmetric spaces which involve exceptional Lie groups, there are only ten (families of) symmetric spaces.

To summarize, the action (3.169) depends only on spatial dimension, the choice of target manifolds, and the conductivity. (This fact indicates universality in the physics of Anderson localization.) According to the scaling theory (and also the locator theory of Anderson), if one starts from sufficiently strong disorder, then, by the renormalization group, disorder will be renormalized and become stronger. In other words, Anderson localization is inevitable. Using the analogy to the classical magnet, this means that at infinite temperature a "paramagnetic phase" is always realized, i.e., the NLσMs universally predict Anderson localization at $t=\infty$. We are thus led to conclude that the NLσMs cannot describe the physics at the boundaries of TIs and TSCs.

How can Anderson delocalization possibly happen then? We need a mechanism that prevents Anderson localization. What has escaped from our attention is the effects of topology of the target manifolds. When the target manifolds have nontrivial topology, one can add a topological term to the action of the NLσM:

$$Z=\int \mathcal{D}[X]\exp(-S[X]-iS_{\mathrm{top}}[X]). \tag{3.170}$$

The topological term $S_{\mathrm{top}}[X]$ is an imaginary part of the action and depends only on global information of field configurations. If there is a topological term, there are interferences (cancellations) in the functional integral among different field configurations, and there is a possibility that different physics may emerge.

A famous example of topological terms is the so-called theta terms. They can appear when $\pi_d(G/H)=\mathbb{Z}$. Taking again an example from magnetic systems, consider the Haldane topological term in quantum spin chains. Similar to the classical Heisenberg ferromagnet in 2D, the quantum Heisenberg antiferrmagnet in $(1+1)$D can be described at low energies and long wavelengths by the $O(3)$ NLσM, Eq. (3.168) (Haldane, 1983a, 1983b). However, an important twist in the quantum case is the possible presence of a topological term, whose presence or absence crucially affects the structure of the low-energy spectrum (i.e., it leads to the presence or absence of the "Haldane gap"). The theta term in this case is given by $S_{\mathrm{top}}[\mathbf{n}]=\theta\times(\text{integer})$ with $\theta=2\pi S$, where S is the spin magnitude, and the integer is a topological invariant defined for a given texture $\mathbf{n}(\mathrm{r})$. The low-energy properties of the system are dramatically different for integer spin S than for half-odd integer spin S.

2. Anderson delocalization at boundaries

For the application of NLσMs to the boundary physics of TIs and TSCs, Wess-Zumino-Novikov-Witten (WZNW) terms and $\mathbb{Z}_2$ topological terms (Fendley, 2000; Ostrovsky, Gornyi, and Mirlin, 2007; Ryu *et al.*, 2007) are important, rather than theta terms. In contrast to theta terms, for which the coefficient (the "theta angle") can be tuned continuously as one changes microscopic details (Affleck, 1988), the coefficients of WZNW or $\mathbb{Z}_2$ topological terms are not tunable. Furthermore, when these terms are present, it is expected that, as in the case of theta terms with $\theta=\pi\times$ odd integer, systems are at their critical points. In the context of Anderson localization, critical Nambu-Goldstone bosons indicate that the localization length is diverging and hence the system delocalizes. Hence, in NLσMs with WZNW or $\mathbb{Z}_2$ terms, Anderson delocalization is unavoidable.

From the mathematical point of view, $\mathbb{Z}_2$ topological terms and WZNW terms exist when $\pi_d(G/H)=\mathbb{Z}_2$ and $\pi_{d+1}(G/H)=\mathbb{Z}$, respectively. Thus, by merely looking at the homotopy group of the target manifolds, one can infer if Anderson delocalization can occur or not. In turn, such delocalized states that cannot be Anderson localized must be realized as a boundary state of some bulk TIs or TSCs. Hence, the bulk topological classification of $\mathbb{Z}_2$ or $\mathbb{Z}$ type corresponds to the type of topological terms ($\mathbb{Z}_2$ or WZNW) at the boundary. Combining these considerations all together, one derives the periodic table of TIs and TSCs. For Dirac models of boundary modes of TIs and TSCs, one can explicitly check (i.e., one by one) the existence of these topological terms in the NLσM description (Bocquet, Serban, and Zirnbauer, 2000; Altland, Simons, and Zirnbauer, 2002; Bernard and LeClair, 2002; Ostrovsky, Gornyi, and Mirlin, 2007; Ryu *et al.*, 2007, 2012).

Generically, however, it is difficult to quantify the precise effects of topological terms in NLσMs in a controlled way when the boundary is of dimension larger than 1. Only general arguments are then available (Xu and Ludwig, 2013). When the boundary is 0D or 1D, it is possible to decide in a controlled way if the boundary state is immune to disorder. For example, along the 1D boundary of a TI in the symmetry class AII, by using the Dorokov-Mello-Pereyra-Kumar equations for the transmission eigenvalues of quasi-1D disordered wires, it is possible to show that the edge states contribute a longitudinal conductance of order 1 in the thermodynamic limit (Takane, 2004a, 2004b, 2004c). Historically, this problem was also studied by using the NLσM which can be augmented by the $\mathbb{Z}_2$ topological term (Zirnbauer, 1992; Brouwer and Frahm, 1996), but the connection to bulk

topology phases was only realized after the discovery of the quantum spin Hall effect.

In 2D, some Dirac fermion models in the presence of disorder can be solved exactly (Ludwig *et al.*, 1994; Nersesyan, Tsvelik, and Wenger, 1994; Tsvelik, 1995; Mudry, Chamon, and Wen, 1996). 2D Dirac modes with disorder, realized on the surface of 3D TR symmetric TIs, can be studied numerically to demonstrate Anderson delocalization (Bardarson *et al.*, 2007; Nomura, Koshino, and Ryu, 2007). For the latter, the complete absence of backscattering (Ando, Nakanishi, and Saito, 1998) was later confirmed in experiments on the surface of 3D TR symmetric TIs (Roushan *et al.*, 2009; Alpichshev *et al.*, 2010). The combined effects of disorder and interactions in 2D boundaries of 3D TI and TSCs have also been studied (Ostrovsky, Gornyi, and Mirlin, 2010; Foster and Yuzbashyan, 2012; Foster, Xie, and Chou, 2014; Xie, Chou, and Foster, 2015).

3. Effects of bulk disorder

Before concluding this section, let us briefly discuss the effects of bulk disorder in TIs and TSCs. The effects of disorder in the most famous example of TIs, the integer QHE, manifest themselves by quantized plateaus of the Hall conductivity separated by a continuous phase transitions. If this is the case, the bulk phase diagrams of TIs and TSCs can be understood qualitatively by a NLσM augmented by a theta term, e.g., the so-called Pruisken term for the integer QHE (Pruisken, 1984). From this NLσM which now has two coupling constants, t and the theta term, one then expects that the phase diagram of the integer QH system is described in terms of two parameters, i.e., the longitudinal and transverse conductivities (Khmel'Nitskiĭ, 1983; Pruisken, 1984). Transitions in the presence of disorder between topologically distinct phases were also studied in 2D bulk TSCs (Senthil *et al.*, 1998; Gruzberg, Ludwig, and Read, 1999; Senthil, Marston, and Fisher, 1999; Read and Green, 2000), in 3D TIs and TSCs (Ryu and Nomura, 2012), and in (quasi-)1D by scattering matrix approaches (Brouwer *et al.*, 1998, 2000; Brouwer, Mudry, and Furusaki, 2000; Titov *et al.*, 2001; Gruzberg, Read, and Vishveshwara, 2005; Akhmerov *et al.*, 2011; Rieder and Brouwer, 2014) and by using NLσMs (Altland *et al.*, 2014; Altland, Bagrets, and Kamenev, 2015). For the effects of disorder on TR symmetric $\mathbb{Z}_2$ TIs, see, for example, Obuse *et al.* (2007, 2008), Shindou and Murakami (2009), Shindou, Nakai, and Murakami (2010), Goswami and Chakravarty (2011), Ryu and Nomura (2012), and K. Kobayashi *et al.* (2014) and, in particular, for topological Anderson insulators (i.e., disorder-driven transitions from a trivial insulator into a TI), see Groth *et al.* (2009), Li *et al.* (2009), Guo *et al.* (2010), Yamakage *et al.* (2011), and Yamakage, Nomura *et al.* (2013). Phase diagrams for disordered TIs and TSCs can also be studied by using noncommutative geometry (Bellissard, van Elst, and Schulz-Baldes, 1994; Loring and Hastings, 2010; Hastings and Loring, 2011; Prodan, Leung, and Bellissard, 2013; Prodan and Schulz-Baldes, 2014) and by K theory (Morimoto, Furusaki, and Mudry, 2015a).

IV. TOPOLOGICAL CRYSTALLINE MATERIALS

We have so far focused on topological phases and topological phenomena protected only by nonspatial AZ symmetries. In this section, we introduce additional spatial symmetries and discuss how these modify the topological distinction of gapped phases. There are two possible effects upon imposing additional symmetries. First, additional symmetries may not change the topological classification, but lead to simplified expressions for the topological invariants of the tenfold classification (Dzero *et al.*, 2010, 2012; Fang, Gilbert, and Bernevig, 2012; Ye, Allen, and Sun, 2013). For example, the $\mathbb{Z}_2$ invariant of 3D TR symmetric TIs in the presence of inversion symmetry can be computed from the parity eigenvalues at TR invariant momenta (Fu and Kane, 2007). Second, additional spatial symmetries can modify the topological classification (Fu, 2011). Examples of this case include weak TIs and TSCs, whose existence relies on the presence of a lattice-translation symmetry; see Sec. III.A (Fu, Kane, and Mele, 2007; Ran, Zhang, and Vishwanath, 2009; Ran, 2010; Teo and Hughes, 2013; Hughes, Yao, and Qi, 2014). Besides translation symmetries, point-group symmetries, such as reflection and rotation, can lead to new topological phases, giving rise to an enrichment of the tenfold classification of TIs and TSCs (Ando and Fu, 2015). These TIs and TSCs which are protected by crystalline symmetries are called topological crystalline insulators and superconductors (TCIs and TCSs).

A. Spatial symmetries

Spatial symmetries of a crystal or a lattice are described by space groups. Operations in space groups are composed of translations, including, in particular, lattice translations, and point-group operations that leave at least one point in space unchanged. The latter includes reflection, inversion, proper, and improper rotations. By the crystallographic restriction theorem, only rotations with 1-, 2-, 3-, 4-, and 6-fold axes are compatible with lattice-translation symmetries. A space-group operation G maps the mth site in the unit cell at r to the m'th site in the unit cell at $u_G\mathsf{r}+\mathsf{R}_m$, where u_G is a $d\times d$ orthogonal matrix and R_m is a lattice vector. Correspondingly, fermion annihilation operators in real space $\hat{\psi}_i(\mathsf{r})$ are transformed by a unitary operator $\hat{\mathcal{G}}$ acting on the electron field operator as

$$\hat{\mathcal{G}}\hat{\psi}_i(\mathsf{r})\hat{\mathcal{G}}^{-1}=(U_G)_i{}^j\hat{\psi}_j(u_G\mathsf{r}+\mathsf{R}_i), \tag{4.1}$$

where U_G is a unitary matrix, and i and j are combined indices labeling the sites within a unit cell as well as internal degrees of freedom, such as spin (summation over the index j is implied). It is known that one can always choose the lattice-translation operators to be diagonal in an irreducible representation. In other words, one can always use momentum-space Bloch functions as the basis functions in generating irreducible representations of a space group. The fermion annihilation operators in momentum space transform as

$$\hat{\mathcal{G}}\hat{\psi}_i(\mathsf{k})\hat{\mathcal{G}}^{-1}=(U_G(u_G\mathsf{k}))_i{}^j\hat{\psi}_j(u_G\mathsf{k}), \tag{4.2}$$

where $(U_G(u_G\mathsf{k}))_i{}^j = (U_G)_i{}^j e^{-iu_G\mathsf{k}\cdot\mathsf{R}_i}$ (i is not summed over). For example, for a 1D chain with two different sublattices A and B (i.e., two atoms in the unit cell) reflection $\hat{\mathcal{R}}$ about the A atom in the $j=0$th unit cell is given by $\hat{\mathcal{R}}$: $\hat{a}_j \to \hat{a}_{-j}$ and $\hat{b}_j \to \hat{b}_{-j-1}$ (see the example discussed in Sec. III.B.2.c). In momentum space reflection acts as $\hat{\mathcal{R}}$: $\hat{a}(k) \to \hat{a}(-k)$ and $\hat{b}(k) \to e^{-ik}\hat{b}(-k)$.

In the presence of the crystalline symmetry $\hat{\mathcal{G}}\hat{H}\hat{\mathcal{G}}^{-1} = \hat{H}$, the Bloch-BdG Hamiltonian obeys

$$H(\mathsf{k}) = U_G^\dagger(\mathsf{k})H(u_G^{-1}\mathsf{k})U_G(\mathsf{k}). \tag{4.3}$$

For crystalline symmetry operations, which leave at least one point fixed (k_0, say), we have $[H(\mathsf{k}_0), U_G(\mathsf{k}_0)] = 0$. It is thus possible to define topological invariants at k_0 in each eigenspace of $U_G(\mathsf{k}_0)$. Crystalline symmetries are either *symmorphic* or *nonsymmorphic* space-group symmetries. In the following, we mainly focus on reflection symmetry, which is symmorphic. Topological phases and gapless surface states protected by nonsymmorphic space-group symmetries have recently been discussed by Roy (2012), Parameswaran *et al.* (2013), Liu, Zhang, and VanLeeuwen (2014), Fang and Fu (2015), Shiozaki, Sato, and Gomi (2015), Young and Kane (2015), Dong and Liu (2016), and Lu *et al.* (2016).

Let us consider a reflection symmetry in the r_l direction, $\hat{\mathcal{R}}_l\hat{\psi}_i(\mathsf{r})\hat{\mathcal{R}}_l^{-1} = (U_{R_l})_i^j\hat{\psi}_j(\bar{\mathsf{r}}+\mathsf{R}_i)$, where $\bar{\mathsf{r}} = (r_1, \ldots, r_{l-1}, -r_l, r_{l+1}, \ldots, r_d)$. This reflection symmetry acts on the Bloch Hamiltonian as

$$H(\mathsf{k}) = U_{R_l}^\dagger(\mathsf{k})H(\bar{\mathsf{k}})U_{R_l}(\mathsf{k}), \tag{4.4}$$

where $\bar{\mathsf{k}} = (k_1, \ldots, k_{l-1}, -k_l, k_{l+1}, \ldots, k_d)$. For particles with spin, spatial symmetries also transform the spin degrees of freedom. For example, reflection flips the sign of orbital angular momentum, and hence, the sign of spin, i.e., $\hat{\mathcal{R}}_x\hat{S}_x\hat{\mathcal{R}}_x^{-1} = \hat{S}_x$ and $\hat{\mathcal{R}}_x\hat{S}_{y,z}\hat{\mathcal{R}}_x^{-1} = -\hat{S}_{y,z}$. Hence, for spin-1/2 particles, U_{R_l} is given by $U_{R_l} = is_l$. The reason to include the factor of i here is to ensure $U_R^2 = -1$, since $\mathcal{R}_l^{-1}$ effectively corresponds to a spin rotation by 2π. In general, pure spin reflection operation is often combined with some internal symmetry operation. To allow for this possibility we loosely call any symmetry that involves $\mathsf{r} \to \bar{\mathsf{r}}$ a reflection symmetry.

B. Classification of topological insulators and superconductors in the presence of reflection symmetry

We now discuss the classification of TCIs and TCSs in the presence of reflection symmetry. Consider a d-dimensional Bloch Hamiltonian $H(\mathsf{k})$, which is invariant under reflection in the r_1 direction:

$$R_1^{-1}H(-k_1, \tilde{\mathsf{k}})R_1 = H(k_1, \tilde{\mathsf{k}}), \tag{4.5}$$

where $\tilde{\mathsf{k}} = (k_2, \ldots, k_d)$, and the reflection operator R_1 is unitary and can depend only on k_1, since it is symmorphic. (For simplicity, we drop the subscript 1 in R_1 henceforth.) With a proper choice of the phase of R, R satisfies on a given reflection plane,

$$R^\dagger = R, \qquad R^2 = \mathbb{1}. \tag{4.6}$$

Thus, all eigenvalues of R are either $+1$ or -1. The algebraic relations obeyed by R and the AZ symmetry operators T, C, and S can be summarized as

$$SR = \eta_S RS, \qquad TR = \eta_T RT, \qquad CR = \eta_C RC, \tag{4.7}$$

where $\eta_{S,T,C} = \pm 1$ specify whether R commutes ($+1$) or anticommutes (-1) with S, T, and C. These different possibilities are labeled by R_{η_T}, R_{η_S}, and R_{η_C} for the nonchiral symmetry classes AI, AII, AIII, C, and D, and by $R_{\eta_T\eta_C}$ for the chiral symmetry classes BDI, CI, CII, and DIII. Hence, we distinguish a total of 27 different symmetry classes in the presence of AZ and reflection symmetries (Table VIII and Fig. 10). [Note that the physical reflection operator always commutes with nonspatial symmetries (e.g., TRS). However, due to the phase convention adopted in Eq. (4.6), Hermitian R may fail to commute with T. For example, for spin-1/2 fermions R anticommutes with T since, in order to fulfill Eq. (4.6), R is defined as the physical reflection operator multiplied by $-i$. On the other hand, for spinless fermions, R commutes with T.]

The classification of TCIs and TCSs in the 27 symmetry classes with reflection symmetry is summarized in Table VIII (Chiu, Yao, and Ryu, 2013; Morimoto and Furusaki, 2013; Shiozaki and Sato, 2014). In even (odd) spatial dimension d, 10 (17) out of the 27 symmetry classes allow for the existence of nontrivial TCIs and TCSs, which are characterized and labeled by the following topological invariants: (i) integer or $\mathbb{Z}_2$ topological invariants ($\mathbb{Z}$ or $\mathbb{Z}_2$) of the original tenfold classification of TIs and TSCs without reflection symmetry; (ii) mirror Chern or winding numbers ($M\mathbb{Z}$) (Teo, Fu, and Kane, 2008), or mirror $\mathbb{Z}_2$ invariants ($M\mathbb{Z}_2$); (iii) $\mathbb{Z}_2$ invariants with translation symmetry ($T\mathbb{Z}_2$); (iv) a combined invariant $M\mathbb{Z}\oplus\mathbb{Z}$ (or $M\mathbb{Z}_2\oplus\mathbb{Z}_2$), which consists of an integer $\mathbb{Z}$ number (or $\mathbb{Z}_2$ quantity) and a mirror Chern or winding number $M\mathbb{Z}$ (or mirror $\mathbb{Z}_2$ quantity $M\mathbb{Z}_2$). Let us now give a more precise description of these invariants and of the boundary modes that arise as a consequence.

(i) $\mathbb{Z}$ and $\mathbb{Z}_2$ invariants: For symmetry classes with at least one AZ symmetry that anticommutes with R, the topological invariants ($\mathbb{Z}$ or $\mathbb{Z}_2$) of the original tenfold classification continue to exist in certain cases, even in the presence of reflection. These topological invariants protect gapless boundary modes, independent of the orientation of the boundary.

(ii) $M\mathbb{Z}$ and $M\mathbb{Z}_2$ invariants: The mirror Chern numbers, the mirror winding numbers, and the mirror $\mathbb{Z}_2$ invariants, denoted by $M\mathbb{Z}$ and $M\mathbb{Z}_2$, respectively, are defined on the hyperplanes in the BZ that are symmetric under reflection. For concreteness, let us consider space groups possessing the two reflection hyperplanes $k_1 = 0$ and $k_1 = \pi$. Since the Bloch Hamiltonian at $k_1 = 0$ and $k_1 = \pi$, $H(\mathsf{k})|_{k_1=0,\pi}$, commutes with R, it can be block diagonalized with respect to the two eigenspaces $R = \pm 1$ of the reflection operator. Note that each of the two blocks of $H(\mathsf{k})|_{k_1=0,\pi}$ is invariant under only those

TABLE VIII. Classification of reflection-symmetry-protected topological crystalline insulators and superconductors (TCI and TCS) as well as of stable Fermi surfaces (FS1 and FS2) in terms of the spatial dimension d of the TCIs and TCSs, and the codimension p of the Fermi surfaces. FS1 denotes Fermi surfaces that are located at high-symmetry points within mirror planes. FS2 stands for Fermi surfaces that are within mirror planes but away from high-symmetry points. Note that for gapless topological materials the presence of translation symmetry is always assumed. Hence, there is no distinction between $T\mathbb{Z}_2$ and $\mathbb{Z}_2$ for the classification of stable Fermi surfaces. Furthermore, we remark that $\mathbb{Z}_2$, $M\mathbb{Z}_2$, and $T\mathbb{Z}_2$ invariants can protect Fermi surfaces of only dimension zero ($d_{\mathrm{FS}}=0$) at high-symmetry points of the Brillouin zone (FS1). For the entries labeled by the superscript a, there can exist surface states and bulk Fermi surfaces of type FS2 that are protected by $\mathbb{Z}$ and $M\mathbb{Z}$ invariants inherited from classes A or AIII. That is, in these cases TRS or PHS does not trivialize these topological invariants.

Reflection	TCI/TCS FS1 in mirror FS2 in mirror	$d=1$ $p=8$ $p=2$	$d=2$ $p=1$ $p=3$	$d=3$ $p=2$ $p=4$	$d=4$ $p=3$ $p=5$	$d=5$ $p=4$ $p=6$	$d=6$ $p=5$ $p=7$	$d=7$ $p=6$ $p=8$	$d=8$ $p=7$ $p=1$
R	A	$M\mathbb{Z}$	0	$M\mathbb{Z}$	0	$M\mathbb{Z}$	0	$M\mathbb{Z}$	0
R_+	AIII	0	$M\mathbb{Z}$	0	$M\mathbb{Z}$	0	$M\mathbb{Z}$	0	$M\mathbb{Z}$
R_-	AIII	$M\mathbb{Z}\oplus\mathbb{Z}$	0	$M\mathbb{Z}\oplus\mathbb{Z}$	0	$M\mathbb{Z}\oplus\mathbb{Z}$	0	$M\mathbb{Z}\oplus\mathbb{Z}$	0
R_+, R_{++}	AI	$M\mathbb{Z}$	0	0^a	0	$2M\mathbb{Z}^a$	0	$M\mathbb{Z}_2^a$	$M\mathbb{Z}_2$
	BDI	$M\mathbb{Z}_2$	$M\mathbb{Z}$	0	0^a	0	$2M\mathbb{Z}^a$	0	$M\mathbb{Z}_2^a$
	D	$M\mathbb{Z}_2^a$	$M\mathbb{Z}_2$	$M\mathbb{Z}$	0	0^a	0	$2M\mathbb{Z}^a$	0
	DIII	0	$M\mathbb{Z}_2^a$	$M\mathbb{Z}_2$	$M\mathbb{Z}$	0	0^a	0	$2M\mathbb{Z}^a$
	AII	$2M\mathbb{Z}^a$	0	$M\mathbb{Z}_2^a$	$M\mathbb{Z}_2$	$M\mathbb{Z}$	0	0^a	0
	CII	0	$2M\mathbb{Z}^a$	0	$M\mathbb{Z}_2^a$	$M\mathbb{Z}_2$	$M\mathbb{Z}$	0	0^a
	C	0^a	0	$2M\mathbb{Z}^a$	0	$M\mathbb{Z}_2^a$	$M\mathbb{Z}_2$	$M\mathbb{Z}$	0
	CI	0	0^a	0	$2M\mathbb{Z}^a$	0	$M\mathbb{Z}_2^a$	$M\mathbb{Z}_2$	$M\mathbb{Z}$
R_-, R_{--}	AI	0^a	0	$2M\mathbb{Z}^a$	0	$T\mathbb{Z}_2^a$	$\mathbb{Z}_2$	$M\mathbb{Z}$	0
	BDI	0	0^a	0	$2M\mathbb{Z}^a$	0	$T\mathbb{Z}_2^a$	$\mathbb{Z}_2$	$M\mathbb{Z}$
	D	$M\mathbb{Z}$	0	0^a	0	$2M\mathbb{Z}^a$	0	$T\mathbb{Z}_2^a$	$\mathbb{Z}_2$
	DIII	$\mathbb{Z}_2$	$M\mathbb{Z}$	0	0^a	0	$2M\mathbb{Z}^a$	0	$T\mathbb{Z}_2^a$
	AII	$T\mathbb{Z}_2^a$	$\mathbb{Z}_2$	$M\mathbb{Z}$	0	0^a	0	$2M\mathbb{Z}^a$	0
	CII	0	$T\mathbb{Z}_2^a$	$\mathbb{Z}_2$	$M\mathbb{Z}$	0	0^a	0	$2M\mathbb{Z}^a$
	C	$2M\mathbb{Z}^a$	0	$T\mathbb{Z}_2^a$	$\mathbb{Z}_2$	$M\mathbb{Z}$	0	0^a	0
	CI	0	$2M\mathbb{Z}^a$	0	$T\mathbb{Z}_2^a$	$\mathbb{Z}_2$	$M\mathbb{Z}$	0	0^a
R_{-+}	BDI, CII	$2\mathbb{Z}^a$	0	$2M\mathbb{Z}^a$	0	$2\mathbb{Z}^a$	0	$2M\mathbb{Z}^a$	0
R_{+-}	DIII, CI	$2M\mathbb{Z}^a$	0	$2\mathbb{Z}^a$	0	$2M\mathbb{Z}^a$	0	$2\mathbb{Z}^a$	0
R_{+-}	BDI	$M\mathbb{Z}\oplus\mathbb{Z}$	0	0^a	0	$2M\mathbb{Z}\oplus2\mathbb{Z}^a$	0	$M\mathbb{Z}_2\oplus\mathbb{Z}_2^a$	$M\mathbb{Z}_2\oplus\mathbb{Z}_2$
R_{-+}	DIII	$M\mathbb{Z}_2\oplus\mathbb{Z}_2^a$	$M\mathbb{Z}_2\oplus\mathbb{Z}_2$	$M\mathbb{Z}\oplus\mathbb{Z}$	0	0^a	0	$2M\mathbb{Z}\oplus2\mathbb{Z}^a$	0
R_{+-}	CII	$2M\mathbb{Z}\oplus2\mathbb{Z}^a$	0	$M\mathbb{Z}_2\oplus\mathbb{Z}_2^a$	$M\mathbb{Z}_2\oplus\mathbb{Z}_2$	$M\mathbb{Z}\oplus\mathbb{Z}$	0	0^a	0
R_{-+}	CI	0^a	0	$2M\mathbb{Z}\oplus2\mathbb{Z}^a$	0	$M\mathbb{Z}_2\oplus\mathbb{Z}_2^a$	$M\mathbb{Z}_2\oplus\mathbb{Z}_2$	$M\mathbb{Z}\oplus\mathbb{Z}$	0

nonspatial symmetries that commute with the reflection operator R. Therefore, depending on the nonspatial symmetries of the $R=\pm1$ blocks of $H(\mathsf{k})|_{k_1=0,\pi}$, each block can be characterized by topological invariants of the original tenfold classification in $d-1$ dimension. For instance, when the $R=+1$ block of $H(\mathsf{k})|_{k_1=0(\pi)}$ is characterized by the Chern or winding number $\nu_{k_1=0(\pi)}$, we introduce a mirror Chern or winding invariant by (Chiu, Yao, and Ryu, 2013)

$$n_{M\mathbb{Z}}=\mathrm{sgn}(\nu_{k_1=0}-\nu_{k_1=\pi})(|\nu_{k_1=0}|-|\nu_{k_1=\pi}|). \tag{4.8}$$

Similarly, when the $R=+1$ block of $H(\mathsf{k})|_{k_1=0(\pi)}$ is characterized by a $\mathbb{Z}_2$ invariant $n_{k_1=0(\pi)}=\pm1$, the mirror $\mathbb{Z}_2$ invariant $M\mathbb{Z}_2$ is defined by

$$n_{M\mathbb{Z}_2}=1-|n_{k_1=0}-n_{k_1=\pi}|. \tag{4.9}$$

A nontrivial value of these mirror indices indicates the appearance of protected boundary modes at reflection-symmetric surfaces, i.e., at surfaces that are perpendicular to the reflection hyperplane $x_1=0$. Surfaces that break reflection symmetry, however, are gapped in general.

(iii) $T\mathbb{Z}_2$ invariant: In symmetry classes where R anticommutes with TR and PH operators (R_- and R_{--} in Table VIII), the second descendant $\mathbb{Z}_2$ invariants are well defined only in the presence of translation symmetry. That is,

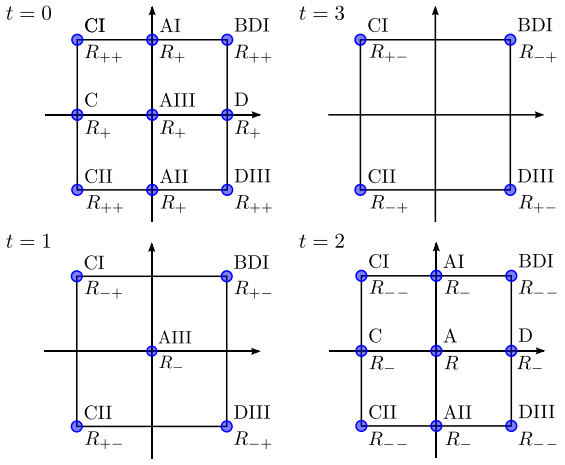

FIG. 10. The 27 symmetry classes with reflection symmetry can be visualized as "the extended Bott clock."

boundary modes of these phases can be gapped out by density-wave-type perturbations, which preserve reflection and AZ symmetries but break translation symmetry. Hence, protected TCIs and TCSs can exist when reflection, translation, and AZ antiunitary symmetries are all there.

(iv) $M\mathbb{Z}\oplus\mathbb{Z}$ and $M\mathbb{Z}_2\oplus\mathbb{Z}_2$ invariants: In some cases, topological properties of reflection-symmetric insulators (SCs) with chiral symmetry are described both by a global $\mathbb{Z}$ or $\mathbb{Z}_2$ invariant and by a mirror index $M\mathbb{Z}$ or $M\mathbb{Z}_2$, which are independent of each other. At boundaries which are perpendicular to the mirror plane, the number of protected gapless states is given by $\max\{|n_{\mathbb{Z}}|,|n_{M\mathbb{Z}}|\}$ (Chiu, Yao, and Ryu, 2013), where $n_{\mathbb{Z}}$ denotes the global $\mathbb{Z}$ invariant, whereas $n_{M\mathbb{Z}}$ is the mirror $\mathbb{Z}$ invariant.

The classification of reflection-symmetric TIs and TSCs (Table VIII) can be generalized to any order-two symmetry ($\mathbb{Z}_2$ symmetry) and, moreover, to include the presence of topological defects (cf. Sec. III.C.2). The generalized classification can be inferred from K groups labeled by six integers $K(s,t,d,d_\parallel,D,D_\parallel)$, where $d_\parallel$ ($D_\parallel$) is the number of momentum (spatial) coordinates that are flipped by the $\mathbb{Z}_2$ operation, s denotes the AZ symmetry class, $t=0$, 1, 2, and 3 labels the reflection Bott clock (Fig. 10), and (d,D) are the dimensions of the defect Hamiltonian. It was shown by Shiozaki and Sato (2014) that the generalized classification follows from the relation $K(s,t,d,d_\parallel,D,D_\parallel)=K(s-d+D,t-d_\parallel+D_\parallel,0,0,0,0)$. For reflection-symmetric TIs and SCs, we have $d_\parallel=1$, $D_\parallel=0$, and $D=0$, which reproduces Table VIII.

1. Bulk-boundary correspondence in topological crystalline systems

While gapless topological surface states exist at any boundary of TIs and TSCs protected by nonspatial AZ symmetries (cf. Sec. III.D), this is not the case for topological crystalline materials. TCIs and TCSs exhibit gapless modes on only those surfaces that are left invariant by the crystal symmetries. In other words, the absence of gapless modes at boundaries that break the spatial symmetries does not indicate trivial bulk topology and therefore cannot be used to infer the topology of TCIs and TCSs. However, for topological crystalline materials one can use the midgap states in the entanglement spectrum or in the entanglement Hamiltonian as a generic way to distinguish between topological trivial and nontrivial phases (Ryu and Hatsugai, 2006; Fidkowski, 2010; Fang, Gilbert, and Bernevig, 2013; Chang, Mudry, and Ryu, 2014). For example, for TCIs and TCSs protected by inversion symmetry, for which there is no boundary that respects the inversion, and hence no gapless topological state at physical surfaces, stable gapless boundary modes in the entanglement spectrum indicate the nontriviality of the bulk topology (Turner, Zhang, and Vishwanath, 2010; Hughes, Prodan, and Bernevig, 2011; Turner *et al.*, 2012).

Another difference between the boundary modes of TCIs and TCSs and those of ordinary TIs and TSCs exists with regard to disorder. While the surface modes of TIs and TSCs with AZ symmetries are robust to spatial disorder (Sec. III.F), the protection of the delocalized surface modes of topological crystalline materials relies crucially on spatial symmetries, which typically are broken by disorder. However, the gapless surface modes of TCIs and TCSs may evade Anderson localization when the disorder respects the spatial symmetries on average. This is the case, for example, for the surface states of weak TIs in class AII in $d=3$, which can be gapped out by charge-density-wave perturbations that preserve TRS but break translation symmetry. However, inhomogeneous perturbations due to disorder which respect translation symmetry on average do not lead to Anderson localization of the surface states (Mong, Bardarson, and Moore, 2012; Ringel, Kraus, and Stern, 2012; Diez *et al.*, 2014; Fulga *et al.*, 2014; Obuse *et al.*, 2014). Similarly, for class AII + R_- in $d=3$ the surface modes remain delocalized in the presence of disorder which preserves TRS and respects reflection symmetry on average (Fu and Kane, 2012). The quantum spin Hall effect with spin S_z conservation is another similar case: When spin S_z rotation symmetry is preserved only on average due to disorder, the spin Chern number remains well defined (Prodan, 2009) and leads to delocalized edge modes even if TRS is broken. Whether the surface states of TCIs and TCSs remain delocalized in the presence of disorder that respects the spatial symmetries only on average depends, in general, on the symmetry class and the spatial dimension of the system. A more detailed discussion of this topic can be found in Diez *et al.* (2015) and Morimoto, Furusaki, and Mudry (2015b).

2. Example: 3D reflection-symmetric topological crystalline insulators (class A + R and class AII + R_-)

Using angle-resolved photoemission spectroscopy (ARPES), SnTe, $Pb_{1-x}Sn_x$, and $Pb_{1-x}Sn_xTe$ have been experimentally identified as TCIs protected by reflection symmetry (Dziawa *et al.*, 2012; Hsieh *et al.*, 2012; Tanaka *et al.*, 2012; Xu *et al.*, 2012). The topology of these materials is characterized by nonzero mirror Chern numbers, which leads to four surface Dirac cones that are protected by reflection symmetry (TRS in not necessary). For example, on the (001) surface of SnTe, the low-energy Hamiltonian near the high-symmetry point $\bar{X}_1=(0,\pi)$ in the surface BZ is given by (Fang *et al.*, 2013; Liu, Duan, and Fu, 2013)

$$H_{\bar{X}_1}(\mathsf{k})=(v_xk_xs_2-v_yk_ys_1)\tau_0+ms_0\tau_3+\delta s_1\tau_2, \quad (4.10)$$

where $v_{x,y}$ are Fermi velocities, s_i and τ_i are Pauli matrices acting on spin and A/B sublattice degrees of freedom, respectively, and δ, m are small parameters. The Hamiltonian (4.10) preserves TRS with $T=is_2\mathcal{K}$ and reflection symmetry in the x direction. The reflection operator in the entire surface BZ is k dependent due to the rock-salt structure of SnTe, i.e., $U_{R_x}=is_1\otimes\mathrm{diag}(1,e^{-ik_x})$. Near $\bar{X}_1=(0,\pi)$ the reflection operator reduces to $U_{R_x}\approx is_1\tau_0$. One verifies that the low-energy Hamiltonian (4.10) is indeed invariant under R_x, i.e., $U_{R_x}^\dagger H_{\bar{X}_1}(-k_x,k_y)U_{R_x}=H_{\bar{X}_1}(k_x,k_y)$. It can be checked that all gap opening perturbations are forbidden by R_x. [Note that on the (001) surface of SnTe there are two additional Dirac cones located near $\bar{X}_2=(\pi,0)$, which are protected by reflection in the y direction.]

The fact that the bulk Hamiltonian of SnTe is characterized by $\mathbb{Z}$ topological invariants (i.e., mirror Chern numbers) can be inferred by considering n identical copies of the surface Hamiltonian $H_{\bar{X}_1} \otimes \mathbb{1}_n$ and by checking that all perturbations that (partially) gap out the enlarged surface Hamiltonian are prohibited by reflection symmetry with the operator $U_{R_x} \otimes \mathbb{1}_n$. Furthermore, one finds that TRS breaking perturbations that respect reflection symmetry do not remove the gapless surface states. In the absence of TRS, the Hamiltonian for SnTe belongs to class $\mathrm{A} + R$. In the presence of TRS, we redefine $U_{R_x} \to iU_{R_x}$ to make U_{R_x} Hermitian. Hence $\{U_{R_x}, T\} = 0$, which corresponds to class $\mathrm{AII} + R_-$. As shown in Table VIII, classes $\mathrm{A} + R$ and $\mathrm{AII} + R_-$ in 3D are both classified by $M\mathbb{Z}$.

In the presence of TRS (i.e., class $\mathrm{AII} + R_-$) the surface states of SnTe are robust against disorder which respects reflection symmetry on average. To gain some insight into this, consider the mass perturbation $ms_3\tau_2$ in Eq. (4.10), which preserves TRS but breaks reflection. As shown in Hsieh *et al.* (2012), Liu, Qi, and Zhang (2012), and Chiu (2014), domain walls in $ms_3\tau_2$ support protected helical 1D modes. When the mass m varies randomly over the surface, but in a way such that reflection symmetry is preserved on average, domain walls and their associated helical modes appear on the entire surface, leading to a gapless (i.e., conducting) surface. Further interesting features of the surface states of these TCIs, such as instabilites toward symmetry-broken phases, Lifishitz transitions, and Landau level spectroscopy, etc., have been investigated by Hsieh *et al.* (2012), Fang *et al.* (2013), Liu, Duan, and Fu (2013), Okada *et al.* (2013), Safaei, Kacman, and Buczko (2013), Wojek *et al.* (2013), Drüppel, Krüger, and Rohlfing (2014), Fang, Gilbert, and Bernevig (2014a), J. Liu *et al.* (2014), Pletikosić, Gu, and Valla (2014), Serbyn and Fu (2014), and J. Wang *et al.* (2014).

Recently, it was proposed that the antiperovskite materials Ca_3PbO and Sr_3PbO also realize a reflection-symmetric TCI (Kariyado and Ogata, 2011; Hsieh, Liu, and Fu, 2014). Furthermore, it was shown that $TlBiS_2$ turns into a TCI with mirror symmetry upon applying pressure (Zhang, Cheng, and Schwingenschlogl, 2015).

C. TCIs and TCSs protected by other point-group symmetries

Besides reflection symmetry, other point-group symmetries can also give rise to new TCIs. For example, TCIs protected by C_n point-group symmetries (Fu, 2011; Fang, Gilbert, and Bernevig, 2012, 2013; Liu, He, and Law, 2014) and C_{nv} point-group symmetries (Alexandradinata *et al.*, 2014) have recently been discussed. It was argued that graphene on a BN substrate is a possible candidate for a TCI protected by C_3 rotation symmetry (Jadaun *et al.*, 2013). A monolayer of PbSe was proposed to realize a TCI protected by a combination of mirror and C_2 rotation symmetry (Wrasse and Schmidt, 2014). Inversion-symmetric TCIs have been considered by Lu and Lee (2014a). TCIs protected by magnetic symmetry groups have been investigated by Zhang and Liu (2015). A partial classification of TCIs protected by space-group symmetries has been developed by Slager *et al.* (2013). The classification of 2D gapless surfaces on 3D TCIs has been completed by Dong and Liu (2016) by investigating all 17 2D space groups.

As for TCSs, TCSs in 2D with discrete rotation symmetries have been discussed by Teo and Hughes (2013) and Benalcazar, Teo, and Hughes (2014). TCSs protected by magnetic symmetry groups (Fang, Gilbert, and Bernevig, 2014b) and by C_3 symmetry (Mendler, Kotetes, and Schön, 2015) have also been studied. Finally, there are also TCSs which are protected by a combination of PHS and reflection symmetry (Kotetes, 2013; Ueno *et al.*, 2013; Yao and Ryu, 2013; Zhang, Kane, and Mele, 2013a; Sato, Yamakage, and Mizushima, 2014); cf. Table VIII. Majorana gapless modes on the surfaces of these TCSs are protected by reflection.

V. GAPLESS TOPOLOGICAL MATERIALS

By definition, Fermi surfaces, Fermi points, and nodal lines are sets of zeros of the energy dispersion $\varepsilon(\mathsf{k}) = \text{const}$ in momentum space. For simplicity, all these objects will be collectively called Fermi surfaces (FSs) in the following. When an FS exists at any energy, the (bulk) system is gapless. FSs are said to be topologically stable (or simply "stable"), when they cannot be fully gapped by perturbations that are local in momentum space and small, such that the bulk gap remains intact sufficiently far away from the FS. (The precise meaning of "local" here will be elaborated on shortly.) In this section, we review topological classifications of stable FSs that appear in gapless (semi)metals and nodal SCs (Volovik, 2003, 2013; Hořava, 2005; Matsuura *et al.*, 2013; Zhao and Wang, 2013; Chiu and Schnyder, 2014; Shiozaki and Sato, 2014; Yang, Pan, and Zhang, 2014; Zhao and Wang, 2014). As seen, the classification of gapless topological materials and fully gapped TIs and TSCs can be developed along parallel lines.

Note that in lattice systems it is only meaningful to discuss the stability for a "single" FS (i.e., of one FS that is "isolated" from the other FSs in the BZ). That is, we consider FSs that are located only within a part of the BZ, but do not include all FSs in the entire BZ. This is so since, for any lattice system, it is expected that FSs can be gapped pairwise by *nesting*, i.e., by including perturbations that connect different FSs. Thus, FSs are at best only locally stable in momentum space, i.e., robust against perturbations that are smooth in real space and slowly varying on the scale of the lattice. This is closely related to the fermion doubling theorem (Nielsen and Ninomiya, 1981), from which it follows that FSs with nontrivial topological charges in any lattice system are always accompanied by "partners" with opposite topological charges. Hence, the sum of the topological charges of all FSs in a compact BZ adds up to zero. As a consequence of this, the topological invariants for FSs are defined in terms of an integral along a submanifold of the BZ, and not in terms of an integral over the entire BZ as in the case of TIs and TSCs.

We start by reviewing the classification of stable FSs protected by nonspatial AZ symmetries and then describe how this classification is modified and extended in the presence of additional crystal symmetries, such as reflection. The properties of these topologically stable FSs are illustrated by selected examples.

A. Tenfold classification of gapless topological materials

The topological classification of gapless materials depends on the symmetry class of the Hamiltonians and the codimension p of the FS,

$$p = d - d_{\mathrm{FS}}, \tag{5.1}$$

where d and d_{FS} denote the dimension of the BZ and the "minimal" dimension of the FS, respectively. Since the dimension of the FS can be different for different Fermi energies, we define here d_{FS} as the dimension of the band crossing, which is independent of the Fermi energy. In other words, d_{FS} is the smallest possible dimension (i.e., the "minimal dimension") of the Fermi surface, as the Fermi energy is varied.[7] For example, for Weyl semimetals $d_{\mathrm{FS}} = 0$, since the Fermi surface is either 0D (when the Fermi energy is at the Weyl node) or 2D (when the Fermi energy is away from the band crossing). Furthermore, we note that $p \leq d$ since d_{FS} cannot be negative.

For the classification of topological FSs, we need to distinguish whether or not the FSs are left invariant by the nonspatial AZ symmetries (Matsuura *et al.*, 2013), i.e., two different cases have to be examined (Fig. 11): (i) each individual FS is left invariant under antiunitary AZ symmetries (FS1) (Zhao and Wang, 2013, 2014; Shiozaki and Sato, 2014), and (ii) different FSs are pairwise related to each other by AZ symmetries (FS2) (Matsuura *et al.*, 2013; Chiu and Schnyder, 2014). Note that in case (i) the FSs must be located at high-symmetry points of the BZ, which are invariant under $\mathsf{k} \to -\mathsf{k}$.

1. Fermi surfaces at high-symmetry points (FS1)

The complete tenfold classification of stable FSs that are located at high-symmetry points (i.e., of FSs which are left invariant under AZ symmetries) is shown in Table IX, where the first row (FS1) indicates the codimension p of the FS (Hořava, 2005; Matsuura *et al.*, 2013; Zhao and Wang, 2013; Chiu and Schnyder, 2014; Shiozaki and Sato, 2014; Zhao and Wang, 2014). We observe that this classification is related to the periodic table of gapped TIs and TSCs (Table I) by a dimensional shift. It is important to point out that for a given symmetry class and codimension p, a $\mathbb{Z}$-type topological invariant guarantees the stability of the FS independent of d_{FS}. A $\mathbb{Z}_2$-type topological number, on the other hand, protects FSs only with $d_{\mathrm{FS}} = 0$, i.e., Fermi points. By the bulk-boundary correspondence, gapless topological materials support protected boundary states, which, depending on the case, are either Dirac or Majorana cones, dispersionless flat bands, or Fermi arc surface states, etc. (see example a in Sec. V.A.1).

[7]If necessary, the energy bands should be adjusted without changing the topology to reach the minimal dimension of the FS. For example, although a type II Weyl node does not possess a 0D FS (Soluyanov *et al.*, 2015; Xu, Zhang, and Zhang, 2015), the node can be continuously deformed into a type I Weyl node. Hence, $d_{\mathrm{FS}} = 0$.

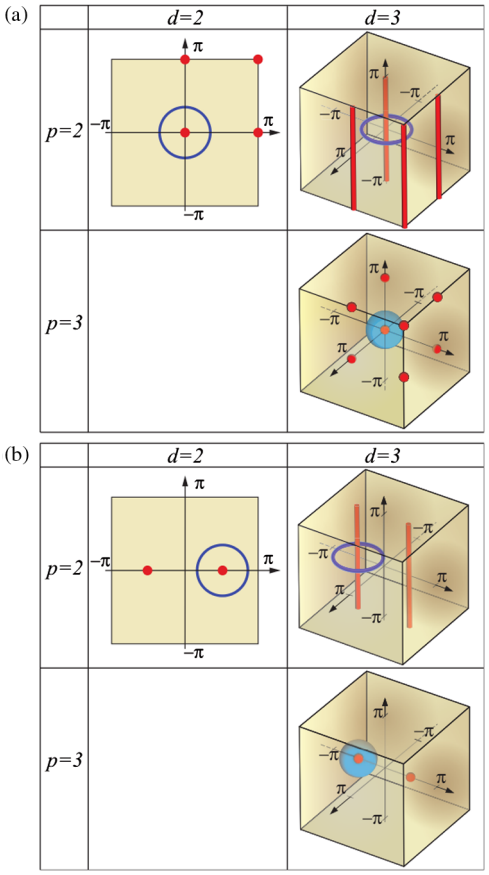

FIG. 11. The classification of stable Fermi surfaces depends on how the Fermi surfaces transform under nonspatial antiunitary symmetries and hence their location in the Brillouin zone. Here d denotes the spatial dimension (the dimension of the Brillouin zone) and p is the codimension of the Fermi surface. The blue circles and spheres represent the contour on which the topological invariant is defined. (a) Each Fermi surface (red points and lines) is left invariant under nonspatial symmetries. (b) Different Fermi surfaces are pairwise related by the nonspatial symmetries which map $\mathsf{k} \leftrightarrow -\mathsf{k}$. Adapted from Chiu and Schnyder, 2014.

a. Example: 2D nodal SC with TRS ($p = 2$, class DIII)

As an example of stable point nodes in a SC, let us consider the following 2D Hamiltonian on the square lattice:

$$H(\mathsf{k}) = \sin k_x \sigma_1 + \sin k_y \sigma_2, \tag{5.2}$$

which belongs to class DIII, since it preserves TRS and PHS with $T = \sigma_2 \mathcal{K}$ and $C = \sigma_1 \mathcal{K}$ ($T^2 = -\mathbb{1}$ and $C^2 = +\mathbb{1}$). This SC exhibits four point nodes ($d_{\mathrm{FS}} = 0$, $p = 2$) at the four TR invariant momenta (0,0), $(0, \pi)$, $(\pi, 0)$, and (π, π). According to Table IX, these point nodes are protected by an integer topological invariant, which takes the form of the winding number (3.26), $\nu = (i/2\pi) \int_{\mathcal{C}} q^* dq$, where the closed contour $\mathcal{C}$ encircles one of the four nodal points and $q(\mathsf{k}) = (\sin k_x - i \sin k_y)/\sqrt{\sin^2 k_x + \sin^2 k_y}$. One finds that $\nu = +1$ for the nodes at (0,0) and (π, π), whereas $\nu = -1$ for the nodes at $(0, \pi)$ and $(\pi, 0)$. (The contour integral is performed counterclockwise.) The topological nature of these point nodes results in the appearance of protected flat-band edge

states at all surfaces, except the (10) and (01) faces. These flat-band states connect two nodal points with opposite winding numbers in the boundary BZ.

2. Fermi surfaces off high-symmetry points (FS2)

The classification of stable FSs that are located away from high-symmetry points of the BZ is shown in Table IX, where the second row (FS2) gives the codimension p of the FS. We remark that only $\mathbb{Z}$ invariants can guarantee the stability of FSs away from high-symmetry points. $\mathbb{Z}_2$ indices, on the other hand, cannot protect these FSs, but they may lead to the appearance of zero-energy surface states at high-symmetry points of the boundary BZ (Chiu and Schnyder, 2014). It is important to note that, in contrast to the classification of fully gapped systems, the label 0 in Table IX does not always indicate trivial topology. That is, for entries with the superscript a there can exist surface states and stable bulk FSs that are protected by the $\mathbb{Z}$ invariants inherited from classes A and AIII, i.e., in these cases, the $\mathbb{Z}$ invariants are not required to be zero in the presence of TRS or PHS.

In experimental systems, the FSs are usually positioned away from the high-symmetry points of the BZ. Indeed, there are numerous experimental examples of protected FSs off high-symmetry points, such as Weyl point nodes protected by a Chern number in superfluid ^{3}He-A phase (class A) (Volovik, 2011) and in chiral $(d \pm id)$-wave SCs (Goswami and Balicas, 2013; Fischer *et al.*, 2014), point nodes in $d_{x^2-y^2}$-wave SCs protected by a winding number (Ryu and Hatsugai, 2002), and line nodes in nodal noncentrosymmetric SCs protected by a winding number (Sato, 2006; Béri, 2010; Brydon, Schnyder, and Timm, 2011; Schnyder and Ryu, 2011). In order to illustrate some of the properties of these gapless topological materials let us consider two examples in more detail, namely, protected point nodes in Weyl semimetals and unprotected Dirac nodes in a 3D TR symmetric semimetal.

TABLE IX. Classification of stable Fermi surfaces in terms of the ten AZ symmetry classes, which are listed in the first column. The first and second rows (FS1 and FS2) give the codimension $p = d - d_{\mathrm{FS}}$ for Fermi surfaces at high-symmetry points [Fig. 11(a)] and away from high-symmetry points of the BZ [Fig. 11(b)], respectively. The classification of stable Fermi surfaces is related to the classification of gapped topological insulators and superconductors (the third row) by a simple dimensional shift. For entries labeled with the superscript a, there can exist surface states and bulk Fermi surfaces of type FS2 that are protected by $\mathbb{Z}$ invariants inherited from classes A or AIII, since in these cases TRS or PHS does not trivialize the $\mathbb{Z}$ invariants. Also note that $\mathbb{Z}_2$ topological invariants protect only Fermi surfaces of dimension zero at high-symmetry points. That is, $\mathbb{Z}_2$ topological numbers cannot protect Fermi surfaces located away from high-symmetry points. This is indicated by the superscript b.

FS1	$p=8$	$p=1$	$p=2$	$p=3$	$p=4$	$p=5$	$p=6$	$p=7$
FS2	$p=2$	$p=3$	$p=4$	$p=5$	$p=6$	$p=7$	$p=8$	$p=1$
TI/TSC	$d=1$	$d=2$	$d=3$	$d=4$	$d=5$	$d=6$	$d=7$	$d=8$
A	0	$\mathbb{Z}$	0	$\mathbb{Z}$	0	$\mathbb{Z}$	0	$\mathbb{Z}$
AIII	$\mathbb{Z}$	0	$\mathbb{Z}$	0	$\mathbb{Z}$	0	$\mathbb{Z}$	0
AI	0	0^a	0	$2\mathbb{Z}$	0	$\mathbb{Z}_2^{a,b}$	$\mathbb{Z}_2^b$	$\mathbb{Z}$
BDI	$\mathbb{Z}$	0	0^a	0	$2\mathbb{Z}$	0	$\mathbb{Z}_2^{a,b}$	$\mathbb{Z}_2^b$
D	$\mathbb{Z}_2^b$	$\mathbb{Z}$	0	0^a	0	$2\mathbb{Z}$	0	$\mathbb{Z}_2^{a,b}$
DIII	$\mathbb{Z}_2^{a,b}$	$\mathbb{Z}_2^b$	$\mathbb{Z}$	0	0^a	0	$2\mathbb{Z}$	0
AII	0	$\mathbb{Z}_2^{a,b}$	$\mathbb{Z}_2^b$	$\mathbb{Z}$	0	0^a	0	$2\mathbb{Z}$
CII	$2\mathbb{Z}$	0	$\mathbb{Z}_2^{a,b}$	$\mathbb{Z}_2^b$	$\mathbb{Z}$	0	0^a	0
C	0	$2\mathbb{Z}$	0	$\mathbb{Z}_2^{a,b}$	$\mathbb{Z}_2^b$	$\mathbb{Z}$	0	0^a
CI	0^a	0	$2\mathbb{Z}$	0	$\mathbb{Z}_2^{a,b}$	$\mathbb{Z}_2^b$	$\mathbb{Z}$	0

a. Example: Weyl semimetal ($p = 3$, class A)

The point nodes of 3D Weyl semimetals are a canonical example of gapless topological bulk modes located away from high-symmetry points. These bulk modes are linearly dispersing Weyl fermions, which are robust without requiring any symmetry protection (Murakami, 2007; Burkov and Balents, 2011; Burkov, Hook, and Balents, 2011; Wan *et al.*, 2011; Vafek and Vishwanath, 2014). The generic low-energy Hamiltonian for a Weyl node located at $\mathsf{k}^0 = (k_x^0, k_y^0, k_z^0)$ is given by

$$H_{\mathrm{Weyl}}(\mathsf{k}) = \sum_{i,j=1,2,3} v_{ij}(k_i - k_i^0)\sigma_j, \tag{5.3}$$

where v_{ij} denotes the Fermi velocity. Weyl nodes cannot be gapped out, since there exists no "fourth Pauli matrix" that anticommutes with H_{Weyl}. A Weyl node is characterized by its chirality $\chi_{\mathsf{k}^0} = \mathrm{sgn}[\det(v_{ij})] = \pm 1$, which measures the relative handedness of the three momenta $\mathsf{k} - \mathsf{k}_i^0$ with respect to the Pauli matrices σ_j in Eq. (5.3).

In a lattice model, Weyl nodes must come in pairs with opposite chiralities (Nielsen and Ninomiya, 1981). Let us demonstrate how Weyl nodes arise in a simple four-band lattice model, and show that Weyl semimetals support Fermi arc surface states, which connect the projected bulk Weyl nodes with opposite chiralities in the surface BZ. To that end, consider the following cubic-lattice Hamiltonian describing a four-band semimetal with two Dirac points:

$$H(\mathsf{k}) = \sin k_x \tau_1 s_1 + \sin k_y \tau_1 s_2 + M(\mathsf{k})\tau_3 s_0, \tag{5.4}$$

where the two sets of Pauli matrices τ_α and s_α operate in spin and orbital spaces, respectively, and $M(\mathsf{k}) = \cos k_x + \cos k_y + \cos k_z - m$. For concreteness, we set $m = 2$. With this choice, the bulk Dirac points of $H(\mathsf{k})$ are located at $\mathsf{k}_\pm = (0, 0, \pm\pi/2)$. The Dirac semimetal (5.4) preserves TRS and inversion symmetry with $T = \tau_0 s_2 \mathcal{K}$ and $U_I = \tau_0 s_3$, respectively. When one of these two symmetries is broken, a Dirac node can be separated into two Weyl nodes. For example, a Zeeman term $\Delta\tau_0 s_3$ (with $\Delta = 1/2$ for simplicity), which breaks TRS, separates the two Dirac cones into four Weyl nodes located at $\mathsf{k}^0 = (0, 0, \pm\pi/3)$ and $\mathsf{k}^0 = (0, 0, \pm 2\pi/3)$. These Weyl points realize (anti)hedgehog defects of the vector of the Berry curvature $[\mathrm{Tr}(\mathcal{F}_{ij})\epsilon^{ijl} dk^l]$ [see the right part of Fig. 5(b)], and are protected by the nonzero Chern number

$$\mathrm{Ch}(\mathcal{N}_{\mathsf{k}^0}) := \frac{i}{2\pi}\int_{\mathcal{N}_{\mathsf{k}^0}} \mathrm{Tr}(\mathcal{F}) = \begin{cases} +1, & \text{for } \mathsf{k}^0 = (0,0,-\frac{\pi}{3}), (0,0,\frac{2\pi}{3}), \\ -1, & \text{for } \mathsf{k}^0 = (0,0,-\frac{2\pi}{3}), (0,0,\frac{\pi}{3}), \end{cases} \tag{5.5}$$

where the integral is over a small closed surface $\mathcal{N}_{\mathsf{k}^0}$ surrounding the Weyl node at k^0. We observe that the chiralities χ_{k^0} of the Weyl nodes, which can be computed from the low-energy description (5.3), are identical to the topological invariant, i.e., $\mathrm{Ch}(\mathcal{N}_{\mathsf{k}^0}) = \chi_{\mathsf{k}^0}$, where $\mathcal{N}_{\mathsf{k}^0}$ encloses a single Weyl point. In general, the integral topological invariant $\mathrm{Ch}(\mathcal{N}_{\mathsf{k}^0})$ counts the number of Weyl points within $\mathcal{N}_{\mathsf{k}^0}$ weighted by their chiralities. Two Weyl nodes with opposite chiralities at the same momentum in the BZ can be easily gapped out by local perturbations. However, when the two Weyl nodes are located at different momenta, nesting instabilities that gap out the Weyl nodes carry finite momentum, and hence necessarily break translation symmetry. Therefore, as long as translation symmetry is preserved, Weyl nodes are robust. Even in the presence of disorder which is sufficiently smooth on the scale of the lattice and does not induce scattering between Weyl nodes with opposite chiralities, the Weyl points are protected and do not Anderson localize.

As seen from Eq. (5.5), Weyl nodes are sources and drains of Berry flux, i.e., there is a Berry flux of 2π flowing from one Weyl node to another along the k_z direction, which is measured by the Chern number (5.5). To exemplify this, consider a family of planes $\{\mathcal{N}(k_z)\}$, which are perpendicular to the k_z axis and parametrized by k_z. When k_z is in between a pair of Weyl nodes with opposite chiralities, $\mathcal{N}(k_z)$ has a nonzero Chern number

$$\mathrm{Ch}(k_z) := \frac{i}{2\pi}\int_{\mathcal{N}(k_z)} \mathrm{Tr}[\mathcal{F}(k_z)] = \begin{cases} -1, & \text{for } \pi/3 < |k_z| < 2\pi/3, \\ 0, & \text{for } |k_z| < \pi/3 \text{ and } 2\pi/3 < |k_z|. \end{cases} \tag{5.6}$$

Each of these planes can be interpreted as a 2D fully gapped Chern insulator with a chiral edge mode. Hence, the surface states of the Weyl semimetal form a 1D open Fermi arc in the surface BZ, connecting the projected bulk Weyl nodes with opposite chiralities; see Fig. 12. These chiral surface states give rise to a quantum anomalous Hall effect, with the Hall conductivity proportional to the separation of Weyl nodes with opposite chiralities in momentum space. A number of other exotic transport phenomena have also been discussed for Weyl semimetals, including negative magnetoresistance, nonlocal transport, and chiral magnetic and vortical effects (Zyuzin and Burkov, 2012; Hosur and Qi, 2013; Liu, Ye, and Qi, 2013; Vazifeh and Franz, 2013; Parameswaran *et al.*, 2014).

An alternative way to create Weyl nodes in the Hamiltonian (5.4) is to break inversion symmetry by adding $\sin k_z \tau_1 s_3$ (which, however, preserves reflection symmetry and TRS). The resulting four Weyl nodes are located at $(0, 0, \pm\pi/4)$ and $(0, 0, \pm 3\pi/4)$ and are robust in the absence of scattering between these nodes. The Weyl nodes are protected by a $\mathbb{Z}$ topological invariant, even though the Hamiltonian (5.4) itself belongs to class AII with $p = 3$ (see footnote *a* in Table IX for more details). In the presence of TRS the number of Weyl nodes with chirality ± 1 is always a multiple of 4 due to the vanishing Chern numbers on TR symmetric planes. Note that this TR symmetric Weyl semimetal exhibits besides the arc surface states also Dirac surface states at $k_z = 0, \pi$ which are protected by a $\mathbb{Z}_2$ topological invariant (cf. discussion in the following example). Thus, this is an example of a gapless topological material with surface states that are protected by a different invariant than the bulk nodes.

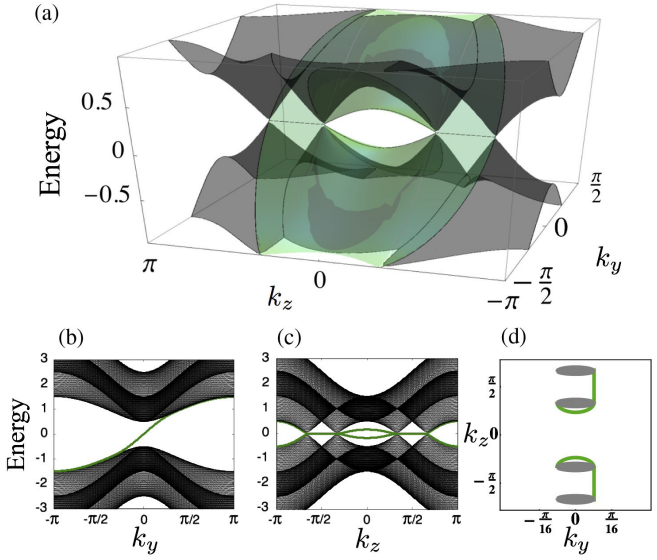

FIG. 12. Surface spectrum of the Weyl semimetal (5.4) for the (100) face in the presence of the Zeeman term $\Delta\tau_0 s_3$. The surface and bulk states are colored in green and gray, respectively. (a) Surface spectrum as a function of surface momenta (k_y, k_z). (b), (c) Surface spectrum as a function of surface momentum k_y and k_z with fixed $k_z = \pi/4$ and $k_y = 0$, respectively. (d) Bulk Fermi surface and surface Fermi arc at the energy $E = 0.1$. The Fermi arcs located within the interval $\pi/3 < |k_z| < 2\pi/3$ are protected by the nonzero Chern number $\mathrm{Ch}(k_z) = -1$; see Eq. (5.6). The surface modes with $|k_z| < \pi/3$ are unstable and can be gapped out by surface perturbations [e.g., by the term $\cos(3k_z/2)\tau_1 s_3$].

Over the last few years a number of materials with Weyl nodes in their band structure have been investigated. For example, the transition-metal monophosphide TaAs is an experimental realization of a TR symmetric Weyl semimetal. Based on first-principle calculations, this material was theoretically identified to be an inversion-symmetric Weyl semimetal (S.-M. Huang *et al.*, 2015; Weng, Fang *et al.*, 2015), which was later confirmed by ARPES experiments (Lv *et al.*, 2015; S.-Y. Xu *et al.*, 2015b). Magnetotransport measurements on TaAs have revealed a negative megnetoresistance, which is a signature of the chiral anomaly of Weyl semimetals (X. Huang *et al.*, 2015; Zhang *et al.*, 2015). Other experimental realizations of TR symmetric Weyl semimetals are TaP, NbAs, and NbP (Shekhar *et al.*, 2015; Weng, Fang *et al.*, 2015; S.-Y. Xu *et al.*, 2015a). A Weyl phase with broken TRS has been theoretically proposed to exist in pyrochlore iridates (Wan *et al.*, 2011; Chen and Hermele, 2012; Witczak-Krempa and Kim, 2012), magnetically doped TIs, and TI multilayers (Burkov and Balents, 2011). However, these TRS breaking Weyl semimetals have not yet been discovered experimentally. A double Weyl semimetal, where the Weyl nodes have chiralities $\chi_{\mathsf{k}^0} = \pm 2$, has been predicted to be realized in the ferromagnetic spinel $HgCr_2Se_4$ (Xu *et al.*, 2011). The

conditions for the existence of double Weyl nodes were recently discussed by Fang *et al.* (2012). Furthermore, the band structure of photonic crystals can be designed in such a way that it exhibits Weyl nodes (Lu *et al.*, 2013, 2015).

b. Example: 3D Dirac semimetal ($p = 3$, class AII)

As a second example we consider the Hamiltonian (5.4) with two Dirac points, which are located away from high-symmetry momenta in the BZ, i.e., at $(0, 0, \pm\pi/2)$, and impose TRS with $T = \tau_0 s_2 \mathcal{K}$. Although a $\mathbb{Z}_2$ invariant can be defined for this case, these Dirac points are not protected by TRS (Table IX), since there exists a TRS preserving mass term, namely, $\sin k_z \tau_2 s_0$. While the class AII $\mathbb{Z}_2$ invariant does not guarantee the stability of the bulk Dirac points, it nevertheless leads to protected gapless surface states at high-symmetry momenta of the surface BZ. To see this, we first need to remove some accidental symmetries of Eq. (5.4) that also give rise to protected surface states (see the discussion in Sec. V.B.2.a). These accidental symmetries are reflections with $R_y = \tau_3 s_2$ [cf. Eq. (5.7)] and chiral symmetry with $S = \tau_1 s_3$. Both of these accidental symmetries can be broken on the surface by adding the perturbation $+g \sin k_z \tau_1 s_3$ on the (100) and $(\bar{1}00)$ faces. In the presence of this perturbation the surface states are gapped except at $k_z = 0$, where there exists a helical mode protected by TRS and the $\mathbb{Z}_2$ invariant of class AII; see Figs. 13(a)–13(c). This type of helical surface mode was observed by ARPES in the Dirac semimetal Na_3Bi (S.-Y. Xu *et al.*, 2015c).

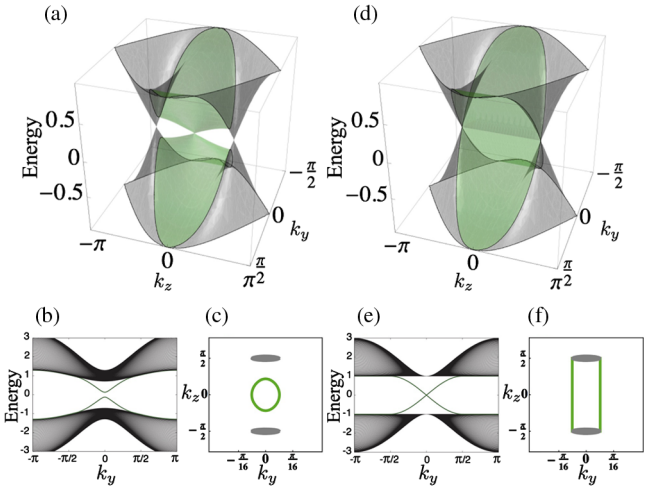

FIG. 13. Surface spectrum of the time-reversal symmetric (i.e., without Zeeman term) Dirac semimetal (5.4) for the (100) face. The surface and bulk states are colored in green and gray, respectively. (a)–(c), (d)–(f) The surface spectrum in the presence and absence of the surface perturbation $+g \sin k_z \tau_1 s_3$, respectively, which breaks reflection and chiral symmetry. (b), (e) The surface bands as a function of surface momentum k_y with fixed $k_z = \pi/4$ and $k_z = 0$, respectively. (c), (f) The bulk and surface states for a fixed energy $\varepsilon = 0.1$. The surface Dirac cone of (a) is protected by a $\mathbb{Z}_2$ invariant, while the surface Fermi arc of (d) is protected by the mirror winding number ν^+ (see Sec. V.B.2.a).

B. Topological semimetals and nodal superconductors protected by reflection symmetry

Let us now discuss how the classification of stable FSs is enriched by the presence of reflection symmetry (Chiu and Schnyder, 2014). Similar to the classification of fully gapped TCIs and TCSs (cf. Sec. IV.B), one needs to distinguish whether the reflection operator commutes or anticommutes with the operators of the AZ symmetries (Chiu and Schnyder, 2014). The classification of reflection-symmetry-protected semimetals and nodal SCs also depends on the codimension of the FSs, $p = d - d_{\mathrm{FS}}$, and on how the FSs transform under reflection and AZ symmetries. In general, one distinguishes the following three different situations: (i) Each FS is left invariant by both reflection and AZ symmetries; (ii) FSs are invariant under reflection symmetry, but are pairwise related to each other by the internal symmetries; and (iii) different FSs are pairwise related to each other by both reflection and AZ symmetries. In cases (i) and (ii), the FSs are located within a reflection plane, whereas in case (iii) they lie outside the reflection plane. For brevity we focus here only on cases (i) and (ii). Case (iii) was discussed extensively by Chiu and Schnyder (2014) and Morimoto and Furusaki (2014).

1. Fermi surfaces at high-symmetry points within mirror plane (FS1 in mirror)

First we consider case (i), where the FSs are located within a reflection plane and at high-symmetry points in the BZ. In this situation the classification of stable FSs with $d_{\mathrm{FS}} = 0$ can be inferred from the classification of TIs and TSCs protected by reflection by a dimensional reduction procedure. Namely, the surface states of reflection-symmetric d-dimensional TIs and TSCs can be viewed as reflection-symmetry-protected FSs in $d - 1$ dimensions. It then follows that the classification of stable Fermi points ($d_{\mathrm{FS}} = 0$) is obtained from the classification of reflection-symmetric TIs and TSCs by a dimensional shift $d \to d - 1$; see Table VIII. This logic also works for FSs with $d_{\mathrm{FS}} > 0$, if their stability is guaranteed by an $M\mathbb{Z}$ or $2M\mathbb{Z}$ topological number. However, $\mathbb{Z}_2$ and $M\mathbb{Z}_2$ topological numbers ensure only the stability of Fermi points, i.e., FSs with $d_{\mathrm{FS}} = 0$. Derivations based on Clifford algebras and K theory (Chiu and Schnyder, 2014; Shiozaki and Sato, 2014) corroborate these findings.

2. Fermi surfaces within mirror plane but off high-symmetry points (FS2 in mirror)

In case (ii), the FSs transform pairwise into each other by AZ symmetries, which relate k and $-\mathsf{k}$. Using an analysis based on the minimal-Dirac-Hamiltonian method (Chiu and Schnyder, 2014) it was shown that only $M\mathbb{Z}$ and $2M\mathbb{Z}$ topological numbers can ensure the stability of reflection-symmetric FSs off high-symmetry points. $\mathbb{Z}_2$ and $M\mathbb{Z}_2$ invariants, on the other hand, do not give rise to stable FSs. Nevertheless, $\mathbb{Z}_2$ or $M\mathbb{Z}_2$ invariants may lead to protected zero-energy surface states at TR invariant momenta of the surface BZ. We observe that the classification of reflection-symmetric FSs located away from high-symmetry points with codimension p is related to the classification of reflection-symmetric TIs and TSCs with spatial dimension $d = p - 1$; see Table VIII.

Reflection-symmetry-protected FSs in most experimental systems are of type FS2. Let us in the following illustrate the properties of these FSs using two examples.

a. Example: FS2 with $p = 3$ in DIII $+ R_{--}$

We consider a topological nodal SC with point nodes, described by the Hamiltonian (5.4). It preserves TRS with $T = \tau_0 s_2 \mathcal{K}$ and PHS with $C = i\tau_1 s_1 \mathcal{K}$. In addition, it is symmetric under reflection,

$$R_y^{-1} H(k_x, -k_y, k_z) R_y = H(k_x, k_y, k_z), \tag{5.7}$$

with $R_y = \tau_3 s_2$. The reflection operator R_y anticommutes with T and C, and hence the Hamiltonian (5.4) is a member of symmetry class DIII $+ R_{--}$. According to Table VIII, the Dirac nodes in Eq. (5.4) [Fig. 13(d)] are protected by an $M\mathbb{Z}$ invariant, i.e., the mirror winding number ν^+. The mirror invariant is defined by a 1D integral along a contour that lies within the mirror plane $k_y = 0$. Within the $k_y = 0$ mirror plane the Hamiltonian can be block diagonalized with respect to R_y. For the block with mirror eigenvalue $R_y = +1$ by choosing a one-parameter family of contours $\mathcal{C}(k_z)$ that are parallel to the k_x axis with fixed k_z, the mirror winding number is given by $\nu^+(k_z) = -1$ for $|k_z| < \pi/2$ whereas $\nu^+(k_z) = 0$ for $|k_z| > \pi/2$. This indicates that there exists a gapless Fermi arc state on the (100) surface, connecting the projection of the bulk Dirac nodes at $\mathsf{k}_\pm = (0, 0, \pm\pi/2)$; see Figs. 13(d)–13(f). Other types of topological nodal SCs with crystal symmetries have been studied by Schnyder, Brydon, and Timm (2012), S. Kobayashi *et al.* (2014), and Schnyder and Brydon (2015).

b. Example: FS2 with $p = 2$ in class AI + R_+ ("spinless graphene")

As a second example we discuss spinless fermions hopping on the honeycomb lattice. Provided one neglects the spin degrees of freedom, this model describes the electronic properties of graphene (Castro Neto *et al.*, 2009). The Dirac cones of spinless graphene are protected by TR, reflection, and translation symmetry. [Note that the Dirac cones are also stable in the presence of inversion symmetry instead of reflection symmetry (Mañes, Guinea, and Vozmediano, 2007).] The tight-binding Hamiltonian is given by $\hat{H} = \sum_{\mathsf{k}} \hat{\Psi}_{\mathsf{k}}^\dagger H(\mathsf{k}) \hat{\Psi}_{\mathsf{k}}$ with the spinor $\hat{\Psi}_{\mathsf{k}} = (\hat{a}_{\mathsf{k}}, \hat{b}_{\mathsf{k}})^T$ and

$$H(\mathsf{k}) = \begin{pmatrix} \Theta_{\mathsf{k}} & \Phi_{\mathsf{k}} \\ \Phi_{\mathsf{k}}^* & \Theta_{\mathsf{k}} \end{pmatrix},$$
$$\Phi_{\mathsf{k}} = t_1 \textstyle\sum_{i=1}^{3} e^{i\mathsf{k}\cdot\mathbf{s}_i}, \qquad \Theta_{\mathsf{k}} = t_2 \textstyle\sum_{i=1}^{6} e^{i\mathsf{k}\cdot\mathbf{d}_i}, \tag{5.8}$$

where $\hat{a}_{\mathsf{k}}$ and $\hat{b}_{\mathsf{k}}$ denote the fermion annihilation operators with momentum k on sublattices A and B, respectively, $\mathbf{s}_i$ and $\mathbf{d}_i$ are the nearest- and second-neighbor bond vectors, respectively [Fig. 14(a)], and the hopping integrals $t_{1,2}$ are assumed to be positive. The Hamiltonian (5.8) is invariant under TR with $T = \sigma_0 \mathcal{K}$ and reflection $k_x \to -k_x$ with $R = \sigma_1$. [Incidentally, the Hamiltonian (5.8) is also symmetric under $k_y \to -k_y$, which, however does not play any role for the protection of the Dirac points.] Since $T^2 = +\mathbb{1}$ and $[R, T] = 0$, the Hamiltonian (5.8) belongs to symmetry class AI $+ R_+$.

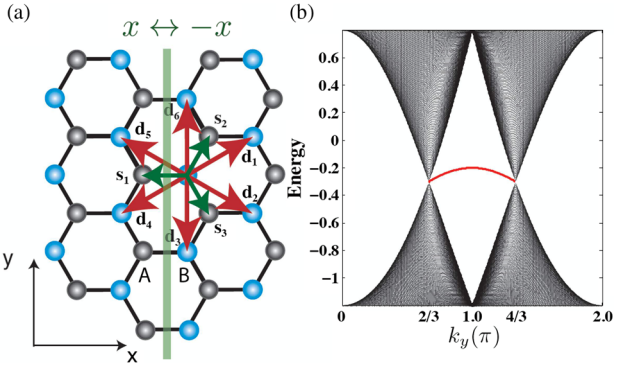

FIG. 14. (a) The honeycomb lattice is a bipartite lattice composed of two interpenetrating triangular sublattices A (black dots) and B (blue dots). The vectors connecting nearest-neighbor and next-nearest-neighbor sites are denoted by $\mathbf{s}_i$ (green) and $\mathbf{d}_i$ (red), respectively, where $\mathbf{s}_1 = (-1, 0)$, $\mathbf{s}_2 = \frac{1}{2}(1, \sqrt{3})$, $\mathbf{s}_3 = \frac{1}{2}(1, -\sqrt{3})$, and $\mathbf{d}_1 = -\mathbf{d}_4 = \frac{1}{2}(3, \sqrt{3})$, $\mathbf{d}_2 = -\mathbf{d}_5 = \frac{1}{2}(3, -\sqrt{3})$, $\mathbf{d}_3 = -\mathbf{d}_6 = (0, -\sqrt{3})$. The mirror line $x \to -x$ is indicated by the green line. (b) Energy spectrum of a graphene ribbon with (10) edges (i.e., zigzag edges) and $(t_1, t_2) = (1.0, 0.1)$. A linearly dispersing edge state (red trace) connects the Dirac points at $k_y = 2\pi/3$ and $k_y = 4\pi/3$ in the edge BZ. Adapted from Chiu and Schnyder, 2014.

The energy spectrum of Eq. (5.8), $\varepsilon_{\mathsf{k}}^\pm = \Theta_{\mathsf{k}} \pm |\Phi_{\mathsf{k}}|$, exhibits two Dirac points, which are located on the mirror line $k_x = 0$, i.e., at $(k_x, k_y) = (0, \pm k_0)$ with $k_0 = 4\pi/(3\sqrt{3})$. These two Dirac points transform pairwise into each other under TRS. Any gap opening term is forbidden by TRS and reflection symmetry, and the Dirac points are topologically stable. In particular, the TRS preserving mass term σ_3 is forbidden by reflection symmetry R. This finding is consistent with the classification in Table VIII, which indicates that the stability of the Dirac points is guaranteed by an $M\mathbb{Z}$-type invariant.

The mirror invariant $n_{M\mathbb{Z}}$ can be computed from the eigenstates $\psi_{\mathsf{k}}^\pm$ of $H(\mathsf{k})$ with energy $\varepsilon_{\mathsf{k}}^\pm$, $\psi_{\mathsf{k}}^\pm = (\pm e^{i\varphi_{\mathsf{k}}}, 1)^T/\sqrt{2}$, where $\varphi_{\mathsf{k}} = \arg(\Phi_{\mathsf{k}})$. Noting $e^{i\varphi_{(0,k_y)}} = +1$ (-1) for $|k_y| < k_0$ $(|k_y| > k_0)$, $\psi_{(0,k_y)}^\pm$ are simultaneous eigenstates of the reflection operator with opposite eigenvalues $(+1$ and $-1)$, and do not hybridize. The mirror invariant $n_{M\mathbb{Z}}$ is given in terms of the number of states with energy $\varepsilon_{\mathsf{k}}^-$ and reflection eigenvalue $R = +1$, $n_{\mathrm{neg}}(k_y)$, as

$$n_{M\mathbb{Z}} = n_{\mathrm{neg}}(|k_y| > k_0) - n_{\mathrm{neg}}(|k_y| < k_0) = +1. \tag{5.9}$$

Because of the bulk-boundary correspondence, the nontrivial topology of the Dirac points leads to a linearly dispersing edge mode, which connects the projected Dirac points in the (10) edge BZ [Fig. 14(b)].

C. Dirac semimetals protected by other point-group symmetries

Besides reflection symmetry, other point-group symmetries, such as rotation or inversion, can give rise to topologically stable FSs (Z. Wang *et al.*, 2012, 2013d; Young *et al.*, 2012; Kim *et al.*, 2015; Yu *et al.*, 2015).

1. 3D semimetals with $p=3$

First, let us briefly illustrate how rotation symmetry can lead to protected Dirac points by using the Hamiltonian (5.4) again as a simple example. As discussed, the Dirac points of Eq. (5.4), located at $(0,0,\pm\pi/2)$, are not protected by TRS. However, spatial symmetries can protect these Dirac cones. One example is chiral symmetry together with mirror symmetry (5.7), which was described before; another example is the fourfold C_4 rotation symmetry along the z axis, which acts on $H(\mathsf{k})$ as

$$R_{C_4}^{-1}H(-k_y,k_x,k_z)R_{C_4}=H(k_x,k_y,k_z), \tag{5.10}$$

where $R_{C_4}=\tau_3(s_0+is_3)/\sqrt{2}$. We find that there exist two mass terms that can gap out the Dirac nodes, namely, $f_1(k_z)\tau_2 s_0$ and $f_2(k_z)\tau_1 s_3$, since these are the terms that anticommute with $H(\mathsf{k})$. Here $f_1(k_z)$ and $f_2(k_z)$ represent k_z dependent masses. However, these two gap opening terms break the C_4 rotation symmetry (5.10), since they anticommute with R_{C_4}. However, each Dirac point can be decomposed into two Weyl nodes along the z direction in the presence of the C_4-preserving term $\tau_0 s_3$. (The additional inversion symmetry and TRS forbid this term.) Thus, the gapless nature of the Hamiltonian (5.4) is protected by the C_4 rotation symmetry (5.10), and the Dirac points are protected by the full point group D_{6h}. Note that similar arguments can be used to explain the gapless stability of the bulk Dirac points of Na_3Bi and Cd_3As_2, which possess C_3 and C_4 rotation symmetries, respectively (Yang and Nagaosa, 2014; Chiu and Schnyder, 2015; Yang, Morimoto, and Furusaki, 2015).

Recently, several materials were experimentally identified as topological semimetals protected by crystalline symmetry. Among them are the Dirac materials Cd_3As_2 (Borisenko *et al.*, 2014; Jeon *et al.*, 2014; Liu *et al.*, 2014a; Neupane *et al.*, 2014; Liang *et al.*, 2015) and Na_3Bi (Z. Wang *et al.*, 2012; Liu *et al.*, 2014b; S.-Y. Xu *et al.*, 2015c), whose gapless spectrum is protected by rotation symmetry. The Fermi arc states of Na_3Bi were recently observed by ARPES (S.-Y. Xu *et al.*, 2015c). Unusual magnetoresistence was also reported in these Dirac systems (Liang *et al.*, 2015; Novak *et al.*, 2015; Li *et al.*, 2016). Superconducting Dirac semimetals were theoretically investigated by Kobayashi and Sato (2015).

2. 3D semimetals with $p=2$

Topological nodal lines with $p=2$, i.e., 1D FSs in a 3D BZ, were theoretically proposed to exist in several materials. For semimetals with negligible spin-orbit coupling, it was shown that topological nodal lines are typically protected by either reflection symmetry or the combination of TRS and inversion symmetry (Chan *et al.*, 2015; Fang *et al.*, 2015). There are two different types of topological line nodes, namely, Weyl and Dirac line nodes. While for the stability of Weyl line nodes the presence of just a single symmetry (e.g., reflection or chiral symmetry) is usually sufficient (Fang *et al.*, 2012; Chiu and Schnyder, 2014), Dirac line nodes, which can be viewed as two copies of Weyl line nodes, need additional symmetries for their protection. For example, the compound Ca_3P_2 (Chan *et al.*, 2015; Xie *et al.*, 2015) possesses a stable Dirac line protected by reflection symmetry together with $SU(2)$ spin-rotation symmetry. In Ca_3P_2 the nodal line is located at the Fermi level, which makes it an ideal system to study the unconventional transport properties of nodal line semimetals. Besides Ca_3P_2, CaAgP, CaAgAs (Yamakage *et al.*, 2015), and rare-earth monopnictides LaX ($X=$ N, P, As, Sb, Bi) (Zeng *et al.*, 2015) have been proposed to possess Dirac nodal lines protected by reflection symmetry and $SU(2)$ spin-rotation symmetry. Dirac line nodes also appear in the band structure of some orthorhombic perovskite iridates (Chen, Lu, and Kee, 2015). Examples of Dirac line nodes protected by inversion, TRS, and $SU(2)$ spin-rotation symmetry include Cu_3N (Kim *et al.*, 2015), Cu_3PbN (Yu *et al.*, 2015), and all-carbon Mackay-Terrones crystals (Weng, Liang *et al.*, 2015).

Weyl line nodes protected by reflection symmetry exist in the band structure of $PbTaSe_2$ (Bian *et al.*, 2016) and $TlTaSe_2$ (Bian *et al.*, 2016). These materials belong to symmetry class AII $+ R_-$ in Table VIII. Their Weyl lines, which are located away from high-symmetry points, are protected by the $M\mathbb{Z}$ invariant that is inherited from class A $+ R$ (compare with the discussion about Weyl nodes in Sec. V.A.2.a).

VI. EFFECTS OF INTERACTIONS: THE COLLAPSE OF NONINTERACTING CLASSIFICATIONS

A. Introduction

In this section we present a brief overview of topics that go beyond the classification of noninteracting fermionic systems. Interactions can affect or modify topological classifications of noninteracting fermion systems in various ways. For example, interactions can "destroy" noninteracting topological phases—a would-be topological state of a single-particle Hamiltonian, characterized by a topological invariant built out of single-particle wave functions, can be adiabatically deformable to a topologically trivial state, once interactions are included. To describe such situations, we say the noninteracting classification "collapses" or "reduces." Another possibility is that interactions can create new topological states which are topologically distinct from trivial states.

Examples of the latter case include, e.g., interaction-enabled symmetry-protected topological phases in 1D (Lapa, Teo, and Hughes, 2016), topological insulating phases in 3D that arise only in the presence of interactions (together with topological band insulators, these fall into a $\mathbb{Z}_2\times\mathbb{Z}_2$ classification of 3D gapped insulating phases) (Wang, Potter, and Senthil, 2014), and fractional topological insulators in $(2+1)$D and $(3+1)$D (Young, Lee, and Kallin, 2008; Levin and Stern, 2009; Maciejko *et al.*, 2010; Neupert *et al.*, 2011, 2014; Sheng *et al.*, 2011; Swingle *et al.*, 2011; Parameswaran, Roy, and Sondhi, 2012; Bergholtz and Liu, 2013; Chan *et al.*, 2013; Repellin, Bernevig, and Regnault, 2014; Maciejko and Fiete, 2015).

Even when interactions do not destroy a noninteracting topological phase (i.e., it exists irrespective of the absence or presence of interactions), characterizing such states without relying on the single-particle picture is often nontrivial. Because of the rapidly developing nature of the field of

strongly interacting topological phases, we do not aim to give a complete review of this field here, but focus our discussion instead on the collapse of the classification of noninteracting fermionic systems. More specifically, we discuss the classification of interacting TSCs [fermionic phases which lack $U(1)$ charge conservation] with various symmetries (such as TRS, spin parity conservation, and reflection symmetry) in one, two, and three spatial dimensions.

1. Symmetry-protected topological phases, short-range and long-range entanglement

Before discussing examples of interacting fermionic systems, let us first introduce a few concepts and common terminologies, which are useful in discussing general interacting (topological) phases. In the previous sections, we discussed TIs and TSCs within noninteracting band theories, described by quadratic Bloch or BdG Hamiltonians. In a broader context, including bosonic systems, and, in particular, in the presence of interactions, the terminology symmetry-protected topological (SPT) phases is used (Gu and Wen, 2009). In the absence of symmetry conditions these phases are trivial states of matter which are continuously deformable to, e.g., an atomic insulator. On the other hand, in the presence of a set of symmetry conditions, they are topologically distinct from trivial states and are separated from trivial states by a quantum phase transition.

SPT phases are also called states with short-range entanglement or short-range entangled (SRE) states. To be more precise, SRE states are states that can be transformed, by applying a finite-depth local unitary quantum circuit, into a product state. In contrast, those states which cannot be disentangled into a product state by a finite-depth local unitary quantum circuit are called states with long-range entanglement, or long-range entangled (LRE) states (Chen, Gu, and Wen, 2010). Note that in this definition noninteracting, integer QH states are examples of LRE states, even though they do not have topological order as measured by the topological entanglement entropy (Kitaev and Preskill, 2006) or by the nontrivial topological ground state degeneracy (Wen and Niu, 1990). Because of the lack of topological order, SPT phases are also sometimes called symmetry-protected trivial phases (Wen, 2014).

There exists an alternative definition for short-range entanglement in the literature, where SRE states are defined as systems with gapped and nondegenerate bulk spectra, namely, as having no topological entanglement order (Kitaev, 2015). In this definition, SRE states include SPT states as a subset. SRE states of this kind are also called invertible or having invertible topological order (Freed, 2014; Kong and Wen, 2014).

While LRE states are not adiabatically deformable to trivial states even in the absence of any symmetry, symmetries can coexist and intertwine with topological orders and can lead to a distinction between states which share the same topological order. To discuss such distinctions between topologically ordered states with symmetries, the terminology symmetry-enriched topological (SET) phases is used (Chen *et al.*, 2013), while in other contexts the term weak symmetry breaking or projective symmetry groups (Wen, 2002; Kitaev, 2006) is used. In the following, we focus on fermionic SPT phases, although some of the techniques and concepts discussed are also applicable to SET phases.

B. Example in $(1+1)$D: Class BDI Majorana chain

The first example of a collapse of a noninteracting classification was shown by Fidkowski and Kitaev for a $(1+1)$D TSC (Fidkowski and Kitaev, 2010, 2011). To discuss this example we use as our starting point the Kitaev chain defined in Eq. (3.53) in terms of spinless fermions. The Kitaev chain is a member of symmetry class D and its different phases are classified by the $\mathbb{Z}_2$ topological index discussed in Sec. III.B.3.a. To impose on this 1D model TRS, we recall that TRS acts on spinless fermions as

$$\hat{\mathcal{T}}\hat{c}_j\hat{\mathcal{T}}^{-1}=\hat{c}_j,\qquad \hat{\mathcal{T}}\hat{c}_j^\dagger\hat{\mathcal{T}}^{-1}=\hat{c}_j^\dagger,\qquad \hat{\mathcal{T}}^2=1. \tag{6.1}$$

[In the Majorana fermion basis (3.55), TRS acts as $\hat{\mathcal{T}}\hat{\lambda}_j\hat{\mathcal{T}}^{-1}=-\hat{\lambda}_j$ and $\hat{\mathcal{T}}\hat{\lambda}'_j\hat{\mathcal{T}}^{-1}=\hat{\lambda}'_j$.] While particle-number conservation is broken in BdG systems, the fermion number parity $\hat{\mathcal{G}}_f$ remains conserved. $\hat{\mathcal{G}}_f$ acts on the fermion operators as

$$\hat{\mathcal{G}}_f\hat{c}_j\hat{\mathcal{G}}_f^{-1}=-\hat{c}_j,\qquad \hat{\mathcal{G}}_f\hat{c}_j^\dagger\hat{\mathcal{G}}_f^{-1}=-\hat{c}_j^\dagger. \tag{6.2}$$

The symmetry operations $\hat{\mathcal{T}}$ and $\hat{\mathcal{G}}_f$ constitute the full symmetry group of the example at hand. These operators satisfy $\hat{\mathcal{T}}\hat{\mathcal{G}}_f=\hat{\mathcal{G}}_f\hat{\mathcal{T}}$ and $\hat{\mathcal{T}}^2=\hat{\mathcal{G}}_f^2=1$. Hence, since $\hat{\mathcal{T}}^2=1$, the relevant symmetry class is BDI, whose topologically distinct ground states in 1D are distinguished by a winding number ν; see Sec. III.B.2.c. For Eq. (3.53) we find that $\nu=0$ for $|t|<|\mu|$, whereas $\nu=1$ for $|t|>|\mu|$. In the topologically nontrivial phases with $\nu\neq 0$ there appear ν isolated Majorana zero modes localized at the end. These Majorana end states are stable against quadratic perturbations which preserve the symmetries. Phases with higher winding number $\nu=N_f$ can be realized by taking N_f identical copies of the Majorana chain $\sum_{a=1}^{N_f}\hat{H}_0(\hat{c}^{a\dagger},\hat{c}^a)$, where $\hat{H}_0(\hat{c}^{a\dagger},\hat{c}^a)$ is the quadratic Hamiltonian of the Kitaev chain for the ath copy (flavor), and the fermion creation and annihilation operators for different copies are denoted by $\hat{c}_j^{a\dagger}$, $\hat{c}_j^a$ with $a=1,\ldots,N_f$.

Fidkowski and Kitaev demonstrated that when $N_f=0$ (mod 8), the noninteracting topological phase with the winding number $\nu=N_f$ can be adiabatically connected to the topologically trivial phase, once interactions are included (Fidkowski and Kitaev, 2010, 2011). Specifically, they considered the following interacting Hamiltonian for the case of $N_f=8$:

$$\hat{H}=\sum_{a=1}^{N_f}\hat{H}_0(\hat{c}^{a\dagger},\hat{c}^a)+w\sum_j[\hat{W}(\hat{\lambda}_j^a)+\hat{W}(\hat{\lambda}_j'^a)], \tag{6.3}$$

where $\hat{W}(\hat{\lambda}^a)$ can be given, conveniently and suggestively, in terms of two species of spin-full complex fermion operators,

$\hat{c}_{1\uparrow}=(\hat{\lambda}^1+i\hat{\lambda}^2)/2$, $\hat{c}^\dagger_{1\downarrow}=(\hat{\lambda}^3+i\hat{\lambda}^4)/2$, $\hat{c}_{2\downarrow}=(\hat{\lambda}^5+i\hat{\lambda}^6)/2$, $\hat{c}^\dagger_{2\uparrow}=(\hat{\lambda}^7+i\hat{\lambda}^8)/2$, as $\hat{W}=16\hat{\mathbf{S}}_1\cdot\hat{\mathbf{S}}_2+2(\hat{n}_1-1)^2+2(\hat{n}_2-1)^2-2$, where $\hat{\mathbf{S}}_i=c^\dagger_{i\alpha}(\boldsymbol{\sigma}_{\alpha\beta}/2)c_{i\beta}$ and $\hat{n}_i=\hat{n}_{i\uparrow}+\hat{n}_{i\downarrow}$. This interaction preserves an $SO(7)$ subgroup of the $SO(8)$ acting on the flavor index. Since the Hamiltonian now depends on three parameters, i.e., on (t,μ,w) (we set $\Delta_0=t$ for simplicity), it is possible to construct a path that connects the noninteracting topological phase ($|t|>|\mu|$ and $w=0$) to the noninteracting trivial phase ($|t|<|\mu|$ and $w=0$) via the interacting phase ($w\neq 0$) without gap closing. To explicitly construct this path, we start from $(t,\mu,0)$ with $|t|>|\mu|$ and switch off μ, $(t,\mu,0)\to(t,0,0)$. Along this deformation, we stay in the topological phase. At the point $(t,0,0)$, the system is a collection of decoupled dimers. We then switch on w and let $t\to 0$, $(t,0,0)\to(0,0,w)$. The interaction term $\hat{W}$ is designed so that the system remains gapped throughout this path. Finally, we switch on μ and let $w\to 0$, $(0,0,w)\to(0,\mu,0)$, which brings us to the noninteracting trivial phase without closing the gap. This completes the construction of a path in the phase diagram connecting the noninteracting topological phase to the trivial phase and proves the triviality of the $\nu=0$ (mod 8) phase. Thus, the noninteracting classification reduces from $\mathbb{Z}$ to $\mathbb{Z}_8$. Similar interaction effects on other 1D fermionic topological phases have been studied by Rosch (2012), Tang and Wen (2012), Ning, Jiang, and Liu (2015), and Lapa, Teo, and Hughes (2016). Proposals on how to realize 1D interaction enable topological phases in experiments were discussed by Chiu, Pikulin, and Franz (2015a, 2015b).

1. Projective representation analysis

More insight into the underlying "mechanism" of the collapse of the classification can be gained by considering the symmetry properties of the boundary Majorana fermion modes of the Kitaev chain. When $\nu=N_f$, there are N_f zero-energy Majorana bound states at the end of the Kitaev chain, which are described by N_f dangling Majorana fermion operators $\hat{\eta}_1,\hat{\eta}_2,\ldots,\hat{\eta}_{N_f}$. As emphasized in Sec. II.D.1, these bound states are *unpaired* (i.e., *isolated*) Majorana zero-energy modes, which are different from the ones that appear in the bulk BdG Hamiltonian, i.e., $\hat{\lambda}$ and $\hat{\lambda}'$, which always come in pairs. While the symmetry operators $\hat{\mathcal{T}}$ and $\hat{\mathcal{G}}_f$ act on the full Hilbert space of fermion operators $\hat{c}^\dagger_j$, $\hat{c}_j$ in a way such that the standard group multiplication laws $\hat{\mathcal{T}}\hat{\mathcal{G}}_f=\hat{\mathcal{G}}_f\hat{\mathcal{T}}$ and $\hat{\mathcal{T}}^2=\hat{\mathcal{G}}_f^2=1$ are satisfied, these symmetries act on the Hilbert space of the dangling Majorana fermions $\hat{\eta}_i$ in a way such that the group composition and multiplication law is respected only up to a phase. That is, the symmetries in the Hilbert space of the dangling Majorana fermions are realized only *projectively* or *anomalously*. The group structure of the symmetry generators $\hat{\mathcal{T}}$ and $\hat{\mathcal{G}}_f$ acting on the Hilbert space of the dangling Majorana fermions was calculated by Fidkowski and Kitaev (2011) and Turner, Pollmann, and Berg (2011). The result of this calculation is summarized as follows:

$$\begin{array}{cccccccccc}\nu(\text{mod }8) & 0 & 1 & 2 & 3 & 4 & 5 & 6 & 7\\ a & +1 & +1 & -1 & -1 & +1 & +1 & -1 & -1\\ \hat{\mathcal{T}}^2 & +1 & +1 & +1 & -1 & -1 & -1 & -1 & +1\end{array}, \tag{6.4}$$

where a specifies the (anti)commutation relation between $\hat{\mathcal{T}}$ and $\hat{\mathcal{G}}_f$ as $\hat{\mathcal{T}}\hat{\mathcal{G}}_f\hat{\mathcal{T}}^{-1}=a\hat{\mathcal{G}}_f$. From the eightfold periodicity of Eq. (6.4), we see that the noninteracting classification collapses from $\mathbb{Z}$ to $\mathbb{Z}_8$. Note that this result can also be derived in terms of Green's functions (Gurarie, 2011; BenTov, 2015) and in terms of nonlinear sigma models (You and Xu, 2014; Morimoto *et al.*, 2015b).

a. Matrix product states

The analysis of the projective symmetry group realized at the boundary of the Kitaev chain can be generalized to arbitrary SPT phases in $(1+1)$D. Besides the interacting Kitaev chain, another well-known example of a 1D interacting SPT phase is the Haldane antiferromagnetic spin-1 chain (Haldane, 1983a, 1983b), which has an $SO(3)$ spin-rotation symmetry. The Haldane spin-1 chain exhibits dangling spin-1/2 moments at its ends, which transform according to a half-integer projective representation of the $SO(3)$ group.

A convenient and unifying way to describe generic SPT phases in $(1+1)$D is provided by the matrix product state (MPS) representation of ground states of $(1+1)$D systems (Pollmann *et al.*, 2010, 2012; Chen, Gu, and Wen, 2011a; Schuch, Perez-Garcia, and Cirac, 2011). In the MPS representation, a quantum state $|\Psi\rangle$ defined on a 1D lattice is written as

$$\begin{aligned}|\Psi\rangle &= \sum_{s_1,s_2,\ldots} A^{s_1}_{ij}A^{s_2}_{jk}\cdots|s_1s_2\cdots\rangle\\ &= \sum_{s_1,s_2,\ldots}\mathrm{Tr}_\chi[A^{s_1}A^{s_2}\cdots]|s_1s_2\cdots\rangle,\end{aligned} \tag{6.5}$$

where $|s_1s_2\cdots\rangle$ is a basis ket of the many-body Hilbert space, which is composed of the basis kets $|s_j\rangle$ at each site j of the 1D lattice, e.g., $|s_j\rangle=|\uparrow\rangle,|\downarrow\rangle$ for a spin 1/2 chain. The A^s_{ij}'s are $\chi\times\chi$ matrices on site s, with $i,j,k,\ldots=1,\ldots,\chi$, and χ is the bond dimension of the MPS. For simplicity, periodic boundary conditions are assumed. By suitably choosing the matrix elements of the A^s_{ij}'s (using a variational approach, say) and by making the bond dimension χ large enough, an MPS is in many cases a good approximation to the true ground state. In fact, it has been shown that the ground state of any gapped (local) 1D Hamiltonian can efficiently and faithfully be represented by an MPS with sufficiently large, but finite, bond dimension χ (Hastings, 2007; Schuch *et al.*, 2008; Gottesman and Hastings, 2010).

In order to describe SPT phases using MPSs, one needs to examine how the symmetries act on the matrices A^s_{ij} that constitute the MPS. To that end, it is crucial to distinguish between the "physical" indices s_i and the "auxiliary" indices i, j. Physical indices represent physical degrees of freedom. The way they transform under symmetries is fully determined

by the microscopic physical laws. The symmetry transformations of the auxiliary indices (or the auxiliary Hilbert space), on the other hand, are not entirely fixed by the symmetries of the physical system. Instead, MPSs representing different phases with the same physical symmetries may transform differently under the symmetries. More precisely, the symmetries may be realized projectively within the auxiliary Hilbert space of the MPS.

To make this more explicit, let us consider a system with the symmetry group $G = \{g, h, \ldots\}$. For simplicity, we consider only unitary and on-site symmetry operations here. For the physical degrees of freedom there exists a unitary representation of G with unitary operators $\hat{U}(g)$ that act on the local physical degrees of freedom as $|s\rangle \to \hat{U}(g)^{s'}_{s}|s'\rangle$. Now, since the quantum state $|\Psi\rangle$ is left invariant by the symmetries G up to an overall phase θ_g, we find that the symmetry transformation $\hat{U}(g)$ induces a corresponding transformation on the auxiliary space as

$$\hat{U}(g)^{s'}_{s} A^{s} = \hat{V}^{-1}(g) A^{s'} \hat{V}(g) e^{i\theta_g}, \tag{6.6}$$

where $\hat{V}(g)$ operates on the auxiliary space indices i and j. While the transformations on the physical index s form a linear representation of the group G, i.e., $\hat{U}(g)\hat{U}(h) = \hat{U}(gh)$, the operations $\hat{V}(g)$ form, in general, a projective representation of G, i.e.,

$$\hat{V}(g)\hat{V}(h) = e^{i\alpha(g,h)}\hat{V}(gh). \tag{6.7}$$

The phase $\alpha(g, h)$ distinguishes between different projective representations of G which, as it turns out, correspond to different SPT phases. In particular, when $e^{i\alpha(g,h)} \neq 1$ the corresponding SPT phase is topologically nontrivial.

C. Examples in $(2+1)$D: TSCs with $\mathbb{Z}_2$ and reflection symmetry

In this section, we present two examples of 2D TSCs, for which the noninteracting classification collapses due to interactions. Furthermore, we show that the collapse of these classifications can be inferred from (i) the absence of a global gravitational anomaly and (ii) the braiding statistics of the quasiparticles of the SPT phase with gauged global symmetry.

a. Example: $\mathbb{Z}_2$ symmetric TSC.—The first example is a 2D TSC with N_f left- and right-moving Majorana edge modes, protected by a $\mathbb{Z}_2$ symmetry in addition to the fermion number parity conservation (Ryu and Zhang, 2012; Qi, 2013). To introduce this TSC we first consider a spin-$1/2$ system with two conserved $U(1)$ charges, given by the total fermion number $N_\uparrow + N_\downarrow$ and the total spin S_z quantum number $N_\uparrow - N_\downarrow$, respectively. By introducing an SC pair potential, we break the electromagnetic $U(1)$ symmetry down to $\mathbb{Z}_2$, such that only the fermion number parity $(-1)^{N_\uparrow + N_\downarrow}$ is conserved. To generate a second $\mathbb{Z}_2$ symmetry, we relax the conservation of total S_z and demand that only the parity $(-1)^{N_\uparrow}$ [and consequently $(-1)^{N_\downarrow}$] is conserved. Observe that in the presence of these two $\mathbb{Z}_2$ symmetries it is possible to block diagonalize the single-particle BdG Hamiltonian into a spin-up and a spin-down block, since the $\mathbb{Z}_2 \times \mathbb{Z}_2$ symmetry does not allow any spin flip terms, i.e., any bilinears connecting the spin-up and spin-down sectors. These two sub-blocks belong to symmetry class A (cf. Sec. II.D.3) and their topological properties are characterized by Chern numbers, i.e., by $\mathrm{Ch}_\uparrow$ and $\mathrm{Ch}_\downarrow$ for the spin-up and spin-down blocks, respectively. When $\mathrm{Ch}_\uparrow + \mathrm{Ch}_\downarrow \neq 0$, TRS is necessarily broken, which corresponds to a class D TSC with $\mathrm{Ch}_{\mathrm{tot}} := \mathrm{Ch}_\uparrow + \mathrm{Ch}_\downarrow$ chiral Majorana edge modes. The class D TSC is robust against interactions as well as disorder for any $\mathrm{Ch}_{\mathrm{tot}}$.

Here, however, we are interested in the case where the total Chern number is vanishing, $\mathrm{Ch}_{\mathrm{tot}} = 0$, but the spin Chern number is nonzero, $\mathrm{Ch}_s := (\mathrm{Ch}_\uparrow - \mathrm{Ch}_\downarrow)/2 \neq 0$. A lattice model that realizes this situation can be constructed by combining two copies of chiral p-wave SCs with opposite chiralities. This TSC supports $\mathrm{Ch}_s = N_f$ nonchiral (i.e., helical) edge modes, which are described by

$$\hat{H} = \int dx \sum_{a=1}^{N_f} [\hat{\psi}^a_L i v \partial_x \hat{\psi}^a_L - \hat{\psi}^a_R i v \partial_x \hat{\psi}^a_R], \tag{6.8}$$

where x is the spatial coordinate along the edge of the TSC, $\hat{\psi}^a_L$ ($\hat{\psi}^a_R$) denote the left- (right-) moving $(1+1)$D Majorana fermions with flavor index a, and v is the Fermi velocity. The generators of the $\mathbb{Z}_2 \times \mathbb{Z}_2$ symmetry of the bulk TSC are realized within the edge theory (6.8) as $\hat{\mathcal{G}}_L = (-)^{\hat{N}_L}$ and $\hat{\mathcal{G}}_R = (-)^{\hat{N}_R}$, where $\hat{N}_L (= \hat{N}_\uparrow)$ [$\hat{N}_R (= \hat{N}_\downarrow)$] is the total left-moving (right-moving) fermion number at the edge. The $\mathbb{Z}_2 \times \mathbb{Z}_2$ symmetry prohibits all mass terms $\hat{\psi}^a_L \hat{\psi}^b_R$ at the edge, since they are odd under the left- or right-$\mathbb{Z}_2$ parity ($\hat{\mathcal{G}}_L$ or $\hat{\mathcal{G}}_R$). Hence, this noninteracting TCS is classified by a $\mathbb{Z}$ invariant, which is simply the number of flavors of the (nonchiral) modes N_f.

Now, to study the effects of interactions we consider quartic interaction terms of the form $\hat{\psi}^a_L \hat{\psi}^b_L \hat{\psi}^c_R \hat{\psi}^d_R$ that preserve the $\mathbb{Z}_2 \times \mathbb{Z}_2$ symmetries. As it turns out, when $N_f \equiv 0 \bmod 8$, one can construct an interaction of this form that destabilizes the edge, i.e., that gaps out the edge without breaking the symmetries (neither explicitly nor spontaneously). This interaction term takes the form of the $SO(7)$ Gross-Neveu interaction and is given essentially by the continuum-limit version of the interaction $\hat{W}$ in Eq. (6.3). We note that this interaction can also be constructed in terms of *twist operators*, which twist the boundary conditions of the Majorana fermion fields when inserted in the path integral (see Sec. VI.C.3). To conclude, in the presence of interactions the classification of the $\mathbb{Z} \times \mathbb{Z}$ symmetric TSC collapses from $\mathbb{Z}$ to $\mathbb{Z}_8$.

b. Example: TCS in DIII $+ R_{--}$.—The second example is a 2D topological crystalline superconductor belonging to class DIII $+ R_{--}$ (Yao and Ryu, 2013); see Sec. IV.B. [Note that this example and the $\mathbb{Z}_2$ symmetric TSCs discussed previously are related by the *CPT* theorem (i.e., by the combined charge, parity, and time-reversal symmetry) (Hsieh, Morimoto, and Ryu, 2014).] According to the noninteracting classification of Table VIII, TCSs in this symmetry class are characterized by an integer topological invariant, i.e., the mirror winding number. Hence, in the absence of interactions this TCS supports an integer number of stable gapless nonchiral edge states, provided that the edge is symmetric under

reflection. These edge states are described by Hamiltonian (6.8). Time reversal $\hat{\mathcal{T}}$ and reflection $\hat{\mathcal{R}}$ act on the Majorana fields in the edge theory (6.8) as

$$\begin{aligned}
&\hat{\mathcal{T}}\hat{\psi}_L^a(x)\hat{\mathcal{T}}^{-1} = \hat{\psi}_R^a(x), \qquad \hat{\mathcal{T}}\hat{\psi}_R^a(x)\hat{\mathcal{T}}^{-1} = -\hat{\psi}_L^a(x),\\
&\hat{\mathcal{R}}\hat{\psi}_L^a(x)\hat{\mathcal{R}}^{-1} = \hat{\psi}_R^a(-x), \qquad \hat{\mathcal{R}}\hat{\psi}_R^a(x)\hat{\mathcal{R}}^{-1} = -\hat{\psi}_L^a(-x),\\
&\hat{\mathcal{T}}^2 = \hat{\mathcal{R}}^2 = \hat{\mathcal{G}}_f. \qquad (6.9)
\end{aligned}$$

One can check that in the presence of both TRS and reflection symmetry there exists no gap opening quadratic mass term within the edge theory (6.8) for any N_f. On the other hand, quartic interaction terms can fully gap out the edge states of phases with $N_f = 0 \bmod 8$. These quartic interactions are of the same form as those of the $\mathbb{Z}_2$ symmetric TSC. Thus, in the presence of interactions the classification of the 2D TCS in class DIII $+ R_{--}$ reduces from $\mathbb{Z}$ to $\mathbb{Z}_8$.

The approach that we took in the previous two examples can be summarized as follows: For a topological bulk state with a given set of symmetries, we first obtain representative edge theories (and many copies thereof when necessary), describing the gapless edge modes. As a second step, we derive interaction terms within the edge theory which gap out the edge modes and which do not break the symmetries, neither explicitly nor spontaneously. Such a microscopic stability analysis of edge theories is quite powerful in $(2+1)$D and has been applied to many SPT as well as SET phases, such as bosonic SPT phases and fractional TIs (Levin and Stern, 2009, 2012; Neupert *et al.*, 2011; Lu and Vishwanath, 2012, 2013; Hung and Wen, 2014).

As in the $(1+1)$D example of Sec. VI.B, we now present alternative derivations of the collapse of the free-fermion classification, which will give us a deeper insight into why certain edge theories are stable while others are not. To that end, we introduce three important concepts: twisting and gauging (i.e., orbifolding) symmetries, quantum anomalies, and braiding statistics.

1. Twisting and gauging symmetries

SPT phases, by definition, are topologically trivial in the absence of symmetries. In order to determine whether a given SPT phase is topological or not, it is thus necessary to probe the phase in a way that takes into account the symmetries. This can be done by many different means as described next.

First of all, quantum systems with symmetries can be probed by coupling them to an external (source) gauge field corresponding to the symmetry. This is most commonly done for unitary on-site (i.e., nonspatial) symmetries [e.g., continuous $U(1)$ symmetries] in the spirit of linear-response theory. While for discrete symmetries (e.g., nonspatial unitary $\mathbb{Z}_2$ symmetries) linear-response functions cannot be defined, the coupling to external gauge fields is in this case still a useful probe for SPT phases. The partition functions of SPT phases in the presence of external gauge fields, typically given in terms of topological terms of gauge theories, can be used to distinguish and even classify different SPT phases (Cheng and Gu, 2014; Hung and Wen, 2014; Wen, 2014; Gu, Wang, and Wen, 2015; Wang, Gu, and Wen, 2015).

A second possibility to probe the topology of an SPT phase is to *twist* the boundary conditions in space and time by elements of the symmetry group G. (Note that twisted boundary conditions can be turned into untwisted ones, by introducing background gauge fields and by applying suitable gauge transformations.) This approach, which can be applied in the presence of both interactions and disorder, is commonly used to define and compute many-body Chern numbers. Specifically, this is done by twisting the spatial boundary conditions by a $U(1)$ symmetry (Laughlin, 1981; Niu, Thouless, and Wu, 1985; Wang and Zhang, 2014).

Taking a step further, one can promote symmetries in SPT phases to gauge symmetries, by making the external gauge field dynamical. This "gauging" of symmetries was proposed and shown to be a useful method to diagnose and distinguish different SPT phases (Levin and Gu, 2012). A similar procedure is the so-called *orbifolding* (as known from conformal field theories), where one introduces twisted boundary conditions in space and time and then considers the sum (average) over all possible twisted boundary conditions (Ryu and Zhang, 2012; Sule, Chen, and Ryu, 2013). Gauging and orbifolding have a similar effect in that both procedures remove states in the original theory that are not singlets under the symmetry group G, i.e., the theory is projected onto the gauge singlet sector. Another effect of gauging and orbifolding is to introduce (i.e., "deconfine") additional topological excitations (quasiparticles).

Orbifolding and gauging can be applied not only to SPT phases with unitary nonspatial symmetries, but also to phases with unitary spatial symmetries, such as reflection. For example, twisting the boundary conditions by reflection leads to theories that are defined on nonorientied manifolds, e.g., Klein bottles, which have recently been discussed for SPT phases in $(2+1)$D and $(3+1)$D (Hsieh *et al.*, 2014; Cho *et al.*, 2015; Hsieh, Cho, and Ryu, 2016). Interestingly, this twisting procedure provides a link between SPT phases and so-called "orientifold field theories," i.e., field theories discussed in the context of unoriented superstring theory.

2. Quantum anomalies

Another diagnostic for topological phases with symmetries is *quantum anomalies*. A quantum anomaly is the breaking of a symmetry of the classical action by quantum effects. That is, an anomalous symmetry is a symmetry of the action, but not of the quantum mechanical partition function. The presence of quantum anomalies can be used for diagnosing, defining, and perhaps even classifying SPT phases. Quantum anomalies give us also a deeper insight into the properties of the edge theory of a topological phase.

For example, the edge theory of the QHE suffers from a $U(1)$ gauge anomaly, i.e., the $U(1)$ charge is not conserved by the edge theory due to quantum mechanical effects. The presence of this anomaly is directly related to the nontrivial topology of the bulk: Charge conservation is broken at the boundary, since current can leak into the bulk due to nonzero Hall conductance and hence due to the QHE. Besides the $U(1)$ charge, also energy is not conserved at the edge of the QH system. This is caused by the gravitational anomaly, i.e., by the fact that the chiral edge theory of the QH state is not

invariant under infinitesimal coordinate transformations (Alvarez-Gaume and Witten, 1984). The breaking of energy conservation at the edge signals that the bulk is topologically nontrivial, which allows leaking of energy momentum into the bulk due to the nonzero thermal Hall conductance κ_{xy} (Volovik, 1990; Read and Green, 2000; Cappelli, Huerta, and Zemba, 2002).

The $U(1)$ and gravitational anomalies discussed so far are examples of perturbative anomalies. That is, the edge theory is not invariant under infinitesimal gauge or general coordinate transformations that can be reached by successive infinitesimal transformations from the identity. On the other hand, edge theories may also possess global anomalies, in which case the quantum theory is not invariant under large gauge or large coordinate transformations that are preserved in the classical theory. Here the term "large" (or "global") refers to a transformation that cannot be continuously connected to the identity. Global gauge and global gravitational anomalies lead to anomalous phases picked up by the partition function of quantum field theories under large gauge and coordinate transformations, respectively (Witten, 1982, 1985). Note that Laughlin's gauge argument for the robustness of the QHE against disorder and interactions (Laughlin, 1981) is based on the global $U(1)$ gauge anomaly. The presence of such a global anomaly can be used as a powerful diagnostic for TR-breaking interacting topological phases with conserved particle number.

It has been shown in numerous works that quantum anomalies generically appear in the boundary theories of SPT phases (Ryu, Moore, and Ludwig, 2012; Cappelli and Randellini, 2013; Ringel and Stern, 2013; Wang and Wen, 2013; Wen, 2013; Koch-Janusz and Ringel, 2014; Santos and Wang, 2014; Cappelli and Randellini, 2015; Wang, Gu, and Wen, 2015; Wang, Santos, and Wen, 2015). Because of the presence of various types of quantum anomalies, the d-dimensional boundary theory of these SPT phases in $d+1$ dimensions cannot be realize in isolation, i.e., there exists an "obstruction" to discretize the boundary theory on a d-dimensional lattice.

a. Global gravitational anomaly and orbifolds of a $\mathbb{Z}_2$ symmetric TSC

Let us now discuss how the collapse of the noninteracting classification of the $\mathbb{Z}_2$ TSCs of example a in Sec. VI.C can be inferred from the presence or absence of global gravitational anomalies. To this end, we put the edge theory (6.8) on a flat spacetime torus $T^2 = S^1 \times S^1$ with periodic spatial and imaginary time coordinates. The geometry of the flat torus T^2 is specified by two real parameters (so-called moduli), which can be arranged into a single complex parameter $\tau = \omega_2/\omega_1$, namely, the ratio of the two periods ω_i of the torus ($\mathrm{Im}\tau > 0$). Two different modular parameters τ and τ' describe the same toroidal geometry if they are related by an integer linear transformation with unit determinant, $\tau \to \tau' = (a\tau + b)/(c\tau + d)$ with $a, b, c, d \in \mathbb{Z}$ and $ad - bc = 1$. These are large coordinate transformations on the torus T^2 and are referred to as modular transformations, which form a group. In general, any conformal field theory on T^2 that describes the continuum limit of an isolated $(1+1)$D lattice system is required to be invariant under modular transformations, and hence anomaly free (Cardy, 1986). For an edge theory, however, modular invariance is not necessarily required. That is, the inability to construct a modular-invariant partition function signals that the theory cannot be realized as an isolated $(1+1)$D system and must be realized as an edge theory of a $(2+1)$D topological bulk state.

For the edge theory (6.8) we find that the partition function is modular invariant in the absence of the $\mathbb{Z}_2 \times \mathbb{Z}_2$ symmetry. In the presence of this symmetry, however, modular invariance cannot always be achieved. To see this, we need to examine the orbifolded partition function of Eq. (6.8), i.e., the partition function summed over all possible twisted boundary conditions

$$Z(\tau, \bar{\tau}) = |G|^{-1} \sum_{g,h \in G} \epsilon(g,h) Z_h^g(\tau, \bar{\tau}), \tag{6.10}$$

where the group elements $g, h \in G = \mathbb{Z}_2 \times \mathbb{Z}_2$ specify the boundary conditions for the partition function Z_h^g in time and space directions, respectively. That is, g (h) specify if the left-moving or right-moving fermions obey periodic or antiperiodic temporal (spatial) boundary conditions. The weights $\epsilon(g,h)$ in the superposition (6.10) are constant phases with $|\epsilon(g,h)| = 1$. Now the question is whether the orbifolded partition function $Z(\tau, \bar{\tau})$ can be made modular invariant $Z(\tau, \bar{\tau}) = Z(\tau', \bar{\tau}')$ (i.e., free from global gravitational anomalies) by a suitable choice of $\epsilon(g,h)$. One can show that this is possible only when the number of Majorana fermion flavors is $N_f = 0 \bmod 8$ (Sule, Chen, and Ryu, 2013), which indicates that the noninteracting classification collapses from $\mathbb{Z} \to \mathbb{Z}_8$, thereby confirming the microscopic stability analysis of the edge theory; see example a in Sec. VI.C.

The discussed approach of studying modular invariance of orbifolded partition functions of edge theories to determine the topological character of the bulk has been successfully applied to other models, for example, 2D SPT phases (Sule, Chen, and Ryu, 2013) and 2D electron systems without any symmetries (Levin, 2013). For the examples considered by Sule, Chen, and Ryu (2013), it was shown that the orbifolded partition functions can be made modular invariant, whenever the symmetry group acts on left- and right-moving sectors of the edge theory (i.e., the holomorphic and antiholomorphic sectors of the edge CFT) in a symmetric fashion. On the other hand, modular invariance can no longer be achieved, if the symmetry group acts in an asymmetric manner on the left- and right-moving sectors. In that case the corresponding orbifolded partition function is referred to as an "asymmetric orbifold." It turns out that many nontrivial SPT phases are directly related to asymmetric orbifolds.

3. Braiding-statistics approach

By promoting the symmetry group G of an SPT phase to a gauge symmetry one can associate a topologically ordered phase to each SPT phase. As shown by Levin and Gu (2012) the topological properties of the original SPT phase can then be inferred by constructing the excitations of the gauged theory and by examining their quasiparticle braiding statistics. This provides a way to distinguish between different SPT phases: If two gauged theories have different quasiparticle

statistics, then the corresponding "ungauged" SPT phases must be distinct and cannot be continuously connected without breaking the symmetries. Moreover, using this so-called "braiding-statistics approach" one can infer the stability of the edge theory. That is, for the cases where the gauged theories are Abelian topological phases [i.e., phases that do not allow non-Abelian statistics but only Abelian (fractional) statistics], the stability of the edge theories can be diagnosed from the braiding statistics of the gauge theories. This braiding-statistics approach has recently been used to show that the noninteracting classification of the $\mathbb{Z}_2$ symmetric TSCs (example a in Sec. VI.C) collapses from $\mathbb{Z} \to \mathbb{Z}_8$ (Gu and Levin, 2014), thereby confirming the microscopic stability analysis [see also Cheng *et al.* (2015)].

As discussed, gauging and orbifolding are similar in that both procedures project the theory onto the gauge singlet (G-invariant) sector. [Although gauging means in general that the singlet condition is imposed locally (e.g., at each site of a lattice), while orbifolding enforces the projection only globally.] To make this connection between orbifolding and gauging more explicit, let us consider edge theories with symmetry group G. As in any quantum field theory we can use the global symmetries $g \in G$ to twist the boundary conditions. This leads to a "g-twisted" sector in the edge theory, which has twisted boundary conditions and whose ground state $|g\rangle$ satisfies $[\hat{\Phi}(x+\ell) - U_g \cdot \hat{\Phi}(x)]|g\rangle = 0$. Here $\hat{\Phi}(x)$ denotes a field operator that is composed of left- and right-moving Majorana fermions $\hat{\psi}_L^a$ and $\hat{\psi}_R^a$. $U_g\hat{\Phi}$ is the field operator $\hat{\Phi}$ transformed by g and ℓ is the circumference of the edge. All the states in this g-twisted sector can be constructed from the ground state $|g\rangle$. Now, by using the state-operator correspondence, we can also construct a corresponding operator, the so-called twist operator $\hat{\sigma}_g$, which implements this twisting. That is, by dragging the field operator $\hat{\Phi}$ around the twist operator $\hat{\sigma}_g$ in spacetime, $\hat{\Phi}$ gets twisted by g, i.e., $\hat{\Phi} \to U_g \cdot \hat{\Phi}$. By use of the bulk-boundary correspondence, we find that corresponding to this there exists a bulk excitation (i.e., an "anyon"). The bulk statistical properties of the gauged theory can then be read off from the operator product expansions and fusion rules obeyed by the twist operators $\hat{\sigma}_g$. Hence, by the braiding-statistics approach it follows that different ungauged SPT phases can be distinguished by studying the statistical (i.e., braiding) properties of the corresponding twist operators $\hat{\sigma}_g$, i.e., two ungauged SPT phases must be distinct if their corresponding twist operators have different statistical properties.

It is known that for Abelian edge theories (e.g., multicomponent chiral and nonchiral bosons compactified on a lattice), the braiding-statistics approach and the principle of the modular invariance of the orbifolded (gauged) edge theory give the same stability criterion for the edge theories. This follows, for example, from a self-dual condition together with an even-lattice condition that guarantees that modular invariance is achieved (Sule, Chen, and Ryu, 2013). Alternatively, this result can be derived from arguments based on braiding statistics (Levin, 2013).

In closing, we note that the braiding-statistics approach has recently been extended to $(3+1)$D SPT phases, in which case one needs to examine the statistics among loop excitations (Jian and Qi, 2014; Jiang, Mesaros, and Ran, 2014; Wang and Levin, 2014; Wang and Wen, 2015). Gauging symmetries of $(3+1)$D SPT phases was studied by Cho, Teo, and Ryu (2014), Chen *et al.* (2015), Cho *et al.* (2015), and Hsieh, Cho, and Ryu (2016).

D. Example in $(3+1)$D: Class DIII TSCs

To illustrate the collapse of a noninteracting classification in $(3+1)$D, let us now consider TR symmetric SCs in class DIII.

Example: Class DIII TSCs.—At the noninteracting level, 3D TR symmetric SCs with $\hat{\mathcal{T}}^2 = \hat{\mathcal{G}}_f$ (i.e., 3D SCs of class DIII) are classified by the 3D winding number ν (3.26), which counts the number of gapless surface Majorana cones. One example of a class DIII TSC is the B phase of ^{3}He, described by Eq. (3.45). This topological superfluid has $\nu = 1$ and supports at its surface a single Majorana cone described by the low-energy Hamiltonian

$$\hat{H} = \int dxdy\hat{\psi}^T(-i\partial_x\sigma_3 - i\partial_y\sigma_1)\hat{\psi}, \tag{6.11}$$

where $\hat{\psi}$ denotes a two-component real fermionic field satisfying $\hat{\psi}^\dagger = \hat{\psi}$. The surface Hamiltonian is invariant under TRS, which acts on $\hat{\psi}$ as $\hat{\mathcal{T}}\,\hat{\psi}\,\hat{\mathcal{T}}^{-1} = i\sigma_2\hat{\psi}$. For TSCs with $\nu = N_f$, the surface modes are described by N_f copies of the Hamiltonian (6.11).

One can verify that in the absence of interactions this surface theory is robust against perturbations for any value of $\nu = N_f$. In the presence of interactions, however, the surface theory (6.11) is unstable when $\nu = 0$ mod 16, leading to a collapse of the noninteracting classification from $\mathbb{Z}$ to $\mathbb{Z}_{16}$ (Fidkowski, Chen, and Vishwanath, 2013; Metlitski *et al.*, 2014; Wang and Senthil, 2014; Senthil, 2015). This result has been obtained by a number of different approaches. Among them are the so-called "vortex condensation approach" and a method based on symmetry-preserving surface topological order, which we review next (You and Xu, 2014; Kapustin *et al.*, 2015; Kitaev, 2015). Note that in recent works a similar collapse of noninteracting classifications was derived for $(3+1)$D crystalline TIs and TSCs (Isobe and Fu, 2015; Morimoto *et al.*, 2015b; Hsieh, Cho, and Ryu, 2016).

1. Vortex condensation approach and symmetry-preserving surface topological order

The vortex condensation approach was first developed in the context of bosonic TIs (Vishwanath and Senthil, 2013), but can also be applied to fermionic SPT phases (Metlitski *et al.*, 2014; Wang and Senthil, 2014; You, BenTov, and Xu, 2014). A crucial observation used in this approach is that the gapped surface theory of a trivial insulator is dual to a quantum disordered superfluid, which is similar to the duality between the superfluid and the Mott insulator phases of the $(2+1)$D Bose-Hubbard model. This approach hence applies most directly to SPT phases, whose symmetry group contains a $U(1)$ symmetry, for example, an S_z spin-rotation symmetry or an electromagnetic charge conservation. One then imagines driving the surface of the SPT phase into a "superfluid" phase,

which spontaneously breaks the $U(1)$ symmetry and leads to a gapped surface. The nontrivial topology of the symmetry-broken surface state can then be inferred from the properties of the topological defects of the order parameter, i.e., from the vortices of the superfluid.

One possibility is that quantum disordering the superfluid by proliferating (condensing) the vortices restores the $U(1)$ symmetry, leading to a topologically trivial gapped surface that respects all symmetries. This then indicates that the bulk phase is topologically trivial. However, this is possible only if the vortices do not have any abnormal properties. For example, if the vortices transform abnormally under the symmetries or if they have exotic exchange statistics, it may not be possible to condense the vortices, such that the surface becomes a gapped trivial state respecting all the symmetries.

Another possibility is that, while vortices may be anomalous in the above sense, vortices with vorticity > 1 (i.e., multivortices) may behave in an ordinary way. If this is the case it might be possible to condense these multivortices to form a gapped surface state that respects all symmetries. This surface state, however, inevitably exhibits an intrinsic topological order (Balents, Fisher, and Nayak, 1999; Senthil and Fisher, 2000), thereby signaling that the bulk phase is nontrivial. This surface topological order is anomalous, since it cannot be realized in an isolated $(2+1)$D system while preserving the symmetries. The existence of symmetry-preserving surface topological order may in fact be used as a nonperturbative definition of 3D SPT phases. Surface states with symmetry-preserving topological order have recently been constructed for fermionic TIs (Bonderson, Nayak, and Qi, 2013; Wang, Potter, and Senthil, 2013, 2014; Chen, Fidkowski, and Vishwanath, 2014; Metlitski, Kane, and Fisher, 2015), as well as for bosonic TIs (Metlitski, Kane, and Fisher, 2013; Vishwanath and Senthil, 2013; Wang and Senthil, 2013; Burnell *et al.*, 2014).

a. Application to class DIII TSC

Let us now discuss how the vortex condensation approach works for the 3D class DIII TSC with an even number ν of Majorana surface cones (Metlitski *et al.*, 2014; Wang and Senthil, 2014). Since ν is even, we can construct an artificial "flavor" $U(1)$ symmetry by combing Majorana cones pairwise. We then drive the surface state into a superfluid phase where this artificial $U(1)$ symmetry is spontaneously broken and the surface Majorana cones are gapped. Next, we imagine quantum disordering the superfluid by condensing the vortices. However, it turns out that for general ν the vortices are nontrivial: An elementary vortex (with vorticity 1) binds $\nu/2$ chiral Majorana modes. Hence the vortex core resembles the edge of a 1D TSC in class BDI. As discussed in Sec. VI.B, interactions can gap out these Majorana modes without breaking the symmetries when they come in multiples of 8. Thus, for $\nu = 16$ the vortices on the surface of the class DIII TSC are trivial. Hence, by condensing these vortices the $U(1)$ symmetry can be restored, which gives rise to a topologically trivial gapped surface state which respects all symmetries of class DIII. However, for smaller even ν, the elementary vortices are nontrivial and cannot condense without breaking the symmetries. This confirms the collapse of the noninteracting classification from $\mathbb{Z} \to \mathbb{Z}_{16}$, discussed previously. Fidkowski, Chen, and Vishwanath (2013) constructed symmetry-preserving gapped surface states with intrinsic topological order explicitly for this 3D TSC.

E. Proposed classification scheme of SPT phases

So far we introduced various approaches to diagnose the properties of a given interacting SPT phase. More generically, one want to obtain a comprehensive and exhaustive classification of all possible SPT phases. Here we present two approaches to this problem: the group cohomology method and the cobordism approach. For other related and complementary approaches, see also Freed (2014) and Wen (2015).

1. Group cohomology approach

The idea of using MPSs to diagnose and distinguish SPT phases discussed in Sec. VI.B.1.a can be used for ground states of generic gapped Hamiltonians in $(1+1)$D, and in fact, provides a complete classification of SPT phases in $(1+1)$D (Pollmann *et al.*, 2010, 2012; Chen, Gu, and Wen, 2011a, 2011b; Schuch, Perez-Garcia, and Cirac, 2011). Recall from Sec. VI.B.1.a that the phases $\alpha(g,h)$ of Eq. (6.7) distinguish between different projective representations of the symmetry group G and hence between different SPT phases. [Note that the set of phase functions $\alpha(g,h)$ are called 2-cocycles, since they must satisfy the so-called 2-cocycle condition $\alpha(h,k)+\alpha(g,hk)=\alpha(gh,k)+\alpha(h,k)$, which follows from associativity of the symmetry group.] Since $\hat{V}(g)$ in Eq. (6.7) is defined only up to a phase, one finds that two different projective representations with the phase functions $\alpha_1(g,h)$ and $\alpha_2(g,h)$ are equivalent, if they are related by $\alpha_2(g,h)=\alpha_1(g,h)+\beta(gh)-\beta(g)-\beta(h)$. (Here the function β is called a coboundary.) This relation defines equivalent classes, which form a group, the so-called second cohomology group of G over $U(1)$ denoted by $H^2(G,U(1))$. Different gapped $(1+1)$D phases with symmetry G are then classified by $H^2(G,U(1))$. In higher dimensions $d>1$, a large class of bosonic SPT phases can be systematically constructed using the tensor network method and path integrals on discrete spacetime using elements in $H^{d+1}(G,U(1))$ (Dijkgraaf and Witten, 1990; Chen *et al.*, 2012, 2013). For fermionic systems, group supercohomology theory has been used to classify SPT phases (Gu and Wen, 2014).

2. Cobordism approach

While the group cohomology approach is one of the most systematic and general methods to classify SPT phases, it was shown that it does not describe all possible phases (Vishwanath and Senthil, 2013; Wang and Senthil, 2013; Kapustin, 2014b). Among these is a bosonic SPT phase in $(3+1)$D (Vishwanath and Senthil, 2013). An alternative approach to classify SPT phases, based on the cobordism, was proposed (Kapustin, 2014a, 2014b; Kapustin and Thorngren, 2014a, 2014b; Kapustin *et al.*, 2015). Assuming that the low-energy effective action of the SPT phase is cobordism invariant, SPT phases with finite symmetry group G have been classified by use of the cobordism groups of the classifying spaces corresponding to G. As an

TABLE X. Classification of interacting fermionic SPT phases as a function of spatial dimension d, as derived from the cobordism approach (Kapustin *et al.*, 2015).

	d						
Symmetry	0	1	2	3	4	5	6
No symmetry (D)	$\mathbb{Z}_2$	$\mathbb{Z}_2$	$\mathbb{Z}$	0	0	0	$\mathbb{Z}^2$
$\hat{\mathcal{T}}^2 = 1$ (BDI)	$\mathbb{Z}_2$	$\mathbb{Z}_8$	0	0	0	$\mathbb{Z}_{16}$	0
$\hat{\mathcal{T}}^2 = \hat{\mathcal{G}}_f$ (DIII)	0	$\mathbb{Z}_2$	$\mathbb{Z}_2$	$\mathbb{Z}_{16}$	0	0	0
Unitary $\mathbb{Z}_2$	$\mathbb{Z}_2^2$	$\mathbb{Z}_2^2$	$\mathbb{Z}_8 \times \mathbb{Z}$	0	0	0	$\mathbb{Z}_{12} \times \mathbb{Z}^2$

example, the result of this classification for fermionic SPT phases with various symmetries is shown in Table X. Note that the classification shown in this table agrees with the results presented in the previous sections.

VII. OUTLOOK AND FUTURE DIRECTIONS

The discovery of spin-orbit-induced topological insulators has taught us that topological effects, which were long thought to occur only under extreme conditions, can profoundly affect the properties of seemingly normal materials, such as band insulators, even under ordinary conditions. Over the last few years, research on topological materials has made impressive progress starting from the experimental realizations of the quantum spin Hall and quantum anomalous Hall effects to the construction and classification of interacting SPT phases. While the basic properties of noninteracting topological systems are relatively well understood theoretically, there is much work to be done to find, design, and improve material systems that realize the theoretical models and allow one to experimentally verify the theoretical predictions.

For further progress on the theoretical front, a deeper understanding of fractional topological phases and correlated SPT phases in $d > 1$ is important. Other outstanding problems include realistic material predictions for interacting SPTs, fractional TIs, and TSCs, and the development of effective field theory descriptions. Furthermore, the full classification of noninteracting Hamiltonians in terms of all (magnetic) space-group symmetries, in particular, nonsymmorphic symmetries, remains as an important open issue for future research.

On the experimental side, perhaps the most important task is the engineering of topological electronic states. An attractive possibility is to realize topological phases in heterostructures, involving, for example, iridates or other materials with strong SOC (Xiao *et al.*, 2011), since this allows for a fine control of the interface properties and therefore of the topological state. There is already a large number of experimental studies that investigate interfaces between TIs and s-wave (M.-X. Wang *et al.*, 2012) or $d_{x^2-y^2}$-wave superconductors (Zareapour *et al.*, 2012; E. Wang *et al.*, 2013). We expect that this remains a major research direction for the foreseeable future. Another important task is the perfection of existing materials, in particular, the growth of topological materials with sufficiently high purity, such that the bulk is truly insulating.

There are numerous topics and developments which we could not mention in this review due to space limitations. These include topological field theories describing the electromagnetic, thermal, or gravitational responses of topological phases (Qi, Hughes, and Zhang, 2008; Ryu, Moore, and Ludwig, 2012; Chan *et al.*, 2013; Furusaki *et al.*, 2013), Floquet topological insulators (Kitagawa *et al.*, 2010; Lindner, Refael, and Galitski, 2011; Ezawa, 2013; Y. H. Wang *et al.*, 2013), topological phases of ultracold atoms (Goldman *et al.*, 2010, 2014; Jiang *et al.*, 2011; Sun *et al.*, 2012), photonic topological insulators (Khanikaev *et al.*, 2013; Rechtsman *et al.*, 2013), topological states in quasicrystals (Kraus *et al.*, 2012; Verbin *et al.*, 2013), and quantum phase transitions without gap closing in the presence of interactions (Amaricci *et al.*, 2015). Other interesting topics that we left out are symmetry-enriched topological phases (Cho, Lu, and Moore, 2012; Lu and Vishwanath, 2012; Chen *et al.*, 2013; Essin and Hermele, 2013; Hung and Wen, 2013; Mesaros and Ran, 2013; Barkeshli *et al.*, 2014; Teo, Hughes, and Fradkin, 2015; L. Wang *et al.*, 2015) and experimental realizations of interacting SPT phases (Lu and Lee, 2014b).

We also did not have space to discuss potential applications that utilize the conducting edge states of topological materials. Possible avenues for technological uses are low-power-consumption electronic devices based on the dissipationless edge currents of TIs. Furthermore, TSCs or heterostructures between TIs and SCs might lead to new architectures of quantum computing devices. An important first step in order to realization such devices is to control and manipulate the topological currents using, e.g., electric fields (Ezawa, 2012, 2015;Wray *et al.*, 2013), magnetic fields (Garate and Franz, 2010; Linder *et al.*, 2010; Schnyder, Timm, and Brydon, 2013), or mechanical strain (Liu *et al.*, 2011; Winterfeld *et al.*, 2013).

ACKNOWLEDGMENTS

We thank our colleagues and collaborators. We are grateful to the community for many valuable comments and encouragements. S. R., A. P. S., and J. C. Y. T. thank the ESI (Vienna) for its hospitality. C.-K. C. and A. P. S. acknowledge the support of the Max-Planck-UBC Centre for Quantum Materials. The work by S. R. was supported by the NSF under Grant No. DMR-1455296 and the Alfred P. Sloan Foundation. C.-K. C. was also supported by Microsoft and LPS-MPO-CMTC during the resubmission stage of this work at the University of Maryland.

REFERENCES

Abrahams, E., P. W. Anderson, D. C. Licciardello, and T. V. Ramakrishnan, 1979, Phys. Rev. Lett. **42**, 673.

Abramovici, G., and P. Kalugin, 2012, Int. J. Geom. Methods Mod. Phys. **09**, 1250023.

Affleck, I., 1988, in *Les Houches, Session XLIX*, edited by E. Brezin and J. Zinn-Justin (North-Holland, Amsterdam), pp. 563–640.

Akhmerov, A. R., J. P. Dahlhaus, F. Hassler, M. Wimmer, and C. W. J. Beenakker, 2011, Phys. Rev. Lett. **106**, 057001.

Alexandradinata, A., C. Fang, M. J. Gilbert, and B. A. Bernevig, 2014, Phys. Rev. Lett. **113**, 116403.

Alicea, J., 2012, Rep. Prog. Phys. **75**, 076501.

Alicea, J., Y. Oreg, G. Refael, F. von Oppen, and M. P. A. Fisher, 2011, Nat. Phys. **7**, 412.

Alpichshev, Z., J. G. Analytis, J.-H. Chu, I. R. Fisher, Y. L. Chen, Z. X. Shen, A. Fang, and A. Kapitulnik, 2010, Phys. Rev. Lett. **104**, 016401.

Altland, A., D. Bagrets, L. Fritz, A. Kamenev, and H. Schmiedt, 2014, Phys. Rev. Lett. **112**, 206602.

Altland, A., D. Bagrets, and A. Kamenev, 2015, Phys. Rev. B **91**, 085429.

Altland, A., B. D. Simons, and M. R. Zirnbauer, 2002, Phys. Rep. **359**, 283.

Altland, A., and M. R. Zirnbauer, 1997, Phys. Rev. B **55**, 1142.

Alvarez-Gaume, L., and E. Witten, 1984, Nucl. Phys. B **234**, 269.

Amaricci, A., J. C. Budich, M. Capone, B. Trauzettel, and G. Sangiovanni, 2015, Phys. Rev. Lett. **114**, 185701.

Anderson, P. W., 1958, Phys. Rev. **109**, 1492.

Anderson, P. W., and P. Morel, 1961, Phys. Rev. **123**, 1911.

Ando, T., T. Nakanishi, and R. Saito, 1998, J. Phys. Soc. Jpn. **67**, 2857.

Ando, Y., 2013, J. Phys. Soc. Jpn. **82**, 102001.

Ando, Y., and L. Fu, 2015, Annu. Rev. Condens. Matter Phys. **6**, 361.

Asahi, D., and N. Nagaosa, 2012, Phys. Rev. B **86**, 100504.

Atiyah, M., 1994, *K-Theory* (Westview Press, Boulder, CO).

Atiyah, M., R. Bott, and A. Shapiro, 1964, Topology **3**, 3.

Atiyah, M. F., and I. M. Singer, 1963, Bull. Am. Math. Soc. **69**, 422.

Balents, L., M. P. A. Fisher, and C. Nayak, 1999, Phys. Rev. B **60**, 1654.

Balian, R., and N. R. Werthamer, 1963, Phys. Rev. **131**, 1553.

Bardarson, J. H., J. Tworzydło, P. W. Brouwer, and C. W. J. Beenakker, 2007, Phys. Rev. Lett. **99**, 106801.

Barkeshli, M., P. Bonderson, M. Cheng, and Z. Wang, 2014, arXiv:1410.4540.

Beenakker, C., 2013, Annu. Rev. Condens. Matter Phys. **4**, 113.

Bellissard, J., A. van Elst, and H. Schulz-Baldes, 1994, J. Math. Phys. (N.Y.) **35**, 5373.

Benalcazar, W. A., J. C. Y. Teo, and T. L. Hughes, 2014, Phys. Rev. B **89**, 224503.

BenTov, Y. J., 2015, J. High Energy Phys. 07, 034.

Bergholtz, E. J., and Z. Liu, 2013, Int. J. Mod. Phys. B **27**, 1330017.

Béri, B., 2010, Phys. Rev. B **81**, 134515.

Berline, N., E. Getzler, and M. Vergne, 1992, *Heat Kernels and Dirac Operators* (Springer, New York).

Bernard, D., and A. LeClair, 2002, J. Phys. Soc. Jpn. **35**, 2555.

Bernevig, A. B., and T. L. Hughes, 2013, *Topological Insulators and Topological Superconductors* (Princeton University Press, Princeton, NJ).

Bernevig, B. A., T. L. Hughes, and S.-C. Zhang, 2006, Science **314**, 1757.

Bian, G., *et al.*, 2016, Phys. Rev. B **93**, 121113.

Bian, G., *et al.*, 2016, Nat. Commun. **7**, 10556.

Bocquet, M., D. Serban, and M. R. Zirnbauer, 2000, Nucl. Phys. B **578**, 628.

Bonderson, P., C. Nayak, and X.-L. Qi, 2013, J. Stat. Mech. 9, P09016.

Borisenko, S., Q. Gibson, D. Evtushinsky, V. Zabolotnyy, B. Büchner, and R. J. Cava, 2014, Phys. Rev. Lett. **113**, 027603.

Brouwer, P. W., and K. Frahm, 1996, Phys. Rev. B **53**, 1490.

Brouwer, P. W., A. Furusaki, I. A. Gruzberg, and C. Mudry, 2000, Phys. Rev. Lett. **85**, 1064.

Brouwer, P. W., C. Mudry, and A. Furusaki, 2000, Phys. Rev. Lett. **84**, 2913.

Brouwer, P. W., C. Mudry, B. D. Simons, and A. Altland, 1998, Phys. Rev. Lett. **81**, 862.

Brydon, P. M. R., A. P. Schnyder, and C. Timm, 2011, Phys. Rev. B **84**, 020501.

Budich, J. C., and E. Ardonne, 2013, Phys. Rev. B **88**, 075419.

Budich, J. C., and B. Trauzettel, 2013, Phys. Status Solidi RRL **7**, 109.

Burkov, A. A., and L. Balents, 2011, Phys. Rev. Lett. **107**, 127205.

Burkov, A. A., M. D. Hook, and L. Balents, 2011, Phys. Rev. B **84**, 235126.

Burnell, F. J., X. Chen, L. Fidkowski, and A. Vishwanath, 2014, Phys. Rev. B **90**, 245122.

Cappelli, A., M. Huerta, and G. R. Zemba, 2002, Nucl. Phys. B **636**, 568.

Cappelli, A., and E. Randellini, 2013, J. High Energy Phys. 12, 101.

Cappelli, A., and E. Randellini, 2015, J. Phys. A **48**, 105404.

Cardy, J. L., 1986, Nucl. Phys. B **270**, 186.

Castro Neto, A. H., F. Guinea, N. M. R. Peres, K. S. Novoselov, and A. K. Geim, 2009, Rev. Mod. Phys. **81**, 109.

Chaikin, P. M., and T. C. Lubensky, 2000, *Principles of Condensed Matter Physics* (Cambridge University Press, Cambridge, England).

Chan, A., T. L. Hughes, S. Ryu, and E. Fradkin, 2013, Phys. Rev. B **87**, 085132.

Chan, Y.-H., C.-K. Chiu, M. Y. Chou, and A. P. Schnyder, 2015, arXiv:1510.02759.

Chang, C.-Z., *et al.*, 2013, Science **340**, 167.

Chang, P.-Y., C. Mudry, and S. Ryu, 2014, J. Stat. Mech. 2014, P09014.

Chen, G., and M. Hermele, 2012, Phys. Rev. B **86**, 235129.

Chen, X., F. J. Burnell, A. Vishwanath, and L. Fidkowski, 2015, Phys. Rev. X **5**, 041013.

Chen, X., L. Fidkowski, and A. Vishwanath, 2014, Phys. Rev. B **89**, 165132.

Chen, X., Z.-C. Gu, Z.-X. Liu, and X.-G. Wen, 2012, Science **338**, 1604.

Chen, X., Z.-C. Gu, Z.-X. Liu, and X.-G. Wen, 2013, Phys. Rev. B **87**, 155114.

Chen, X., Z.-C. Gu, and X.-G. Wen, 2010, Phys. Rev. B **82**, 155138.

Chen, X., Z.-C. Gu, and X.-G. Wen, 2011a, Phys. Rev. B **83**, 035107.

Chen, X., Z.-C. Gu, and X.-G. Wen, 2011b, Phys. Rev. B **84**, 235128.

Chen, Y., Y.-M. Lu, and H.-Y. Kee, 2015, Nat. Commun. **6**, 6593.

Cheng, M., 2012, Phys. Rev. B **86**, 195126.

Cheng, M., Z. Bi, Y.-Z. You, and Z.-C. Gu, 2015, arXiv:1501.01313.

Cheng, M., and Z.-C. Gu, 2014, Phys. Rev. Lett. **112**, 141602.

Chiu, C.-K., 2014, arXiv:1410.1117.

Chiu, C.-K., P. Ghaemi, and T. L. Hughes, 2012, Phys. Rev. Lett. **109**, 237009.

Chiu, C.-K., M. J. Gilbert, and T. L. Hughes, 2011, Phys. Rev. B **84**, 144507.

Chiu, C.-K., D. I. Pikulin, and M. Franz, 2015a, arXiv:1502.03432.

Chiu, C.-K., D. I. Pikulin, and M. Franz, 2015b, Phys. Rev. B **91**, 165402.

Chiu, C.-K., and A. P. Schnyder, 2014, Phys. Rev. B **90**, 205136.

Chiu, C.-K., and A. P. Schnyder, 2015, J. Phys. Conf. Ser. **603**, 012002.

Chiu, C.-K., H. Yao, and S. Ryu, 2013, Phys. Rev. B **88**, 075142.

Cho, G. Y., C.-T. Hsieh, T. Morimoto, and S. Ryu, 2015, Phys. Rev. B **91**, 195142.

Cho, G. Y., Y.-M. Lu, and J. E. Moore, 2012, Phys. Rev. B **86**, 125101.

Cho, G. Y., J. C. Y. Teo, and S. Ryu, 2014, Phys. Rev. B **89**, 235103.

Chung, S. B., H. Bluhm, and E.-A. Kim, 2007, Phys. Rev. Lett. **99**, 197002.

Chung, S. B., and S.-C. Zhang, 2009, Phys. Rev. Lett. **103**, 235301.

Churchill, H. O. H., V. Fatemi, K. Grove-Rasmussen, M. T. Deng, P. Caroff, H. Q. Xu, and C. M. Marcus, 2013, Phys. Rev. B **87**, 241401.

Clarke, D. J., J. Alicea, and K. Shtengel, 2013, Nat. Commun. **4**, 1348.

Cook, A., and M. Franz, 2011, Phys. Rev. B **84**, 201105.

Darriet, J., and L. Regnault, 1993, Solid State Commun. **86**, 409.

Das, A., Y. Ronen, Y. Most, Y. Oreg, M. Heiblum, and H. Shtrikman, 2012, Nat. Phys. **8**, 887.

Das Sarma, S., C. Nayak, and S. Tewari, 2006, Phys. Rev. B **73**, 220502.

de Gennes, P. G., 1999, *Superconductivity Of Metals And Alloys* (Westview Press, Boulder, CO).

Deng, D.-L., S.-T. Wang, and L.-M. Duan, 2014, Phys. Rev. B **89**, 075126.

Deng, M. T., C. L. Yu, G. Y. Huang, M. Larsson, P. Caroff, and H. Q. Xu, 2012, Nano Lett. **12**, 6414.

De Nittis, G., and K. Gomi, 2014, J. Geom. Phys. **86**, 303.

De Nittis, G., and K. Gomi, 2015, Commun. Math. Phys. **339**, 1.

Diez, M., I. C. Fulga, D. I. Pikulin, J. Tworzydło, and C. W. J. Beenakker, 2014, New J. Phys. **16**, 063049.

Diez, M., D. I. Pikulin, I. C. Fulga, and J. Tworzydło, 2015, New J. Phys. **17**, 043014.

Dijkgraaf, R., and E. Witten, 1990, Commun. Math. Phys. **129**, 393.

Dong, X.-Y., and C.-X. Liu, 2016, Phys. Rev. B **93**, 045429.

Drüppel, M., P. Krüger, and M. Rohlfing, 2014, Phys. Rev. B **90**, 155312.

Dyson, F. J., 1953, Phys. Rev. **92**, 1331.

Dyson, F. J., 1962, J. Math. Phys. (N.Y.) **3**, 1199.

Dzero, M., K. Sun, P. Coleman, and V. Galitski, 2012, Phys. Rev. B **85**, 045130.

Dzero, M., K. Sun, V. Galitski, and P. Coleman, 2010, Phys. Rev. Lett. **104**, 106408.

Dziawa, P., *et al.*, 2012, Nat. Mater. **11**, 1023.

Efetov, K. B., 1983, Adv. Phys. **32**, 53.

Efetov, K. B., A. I. Larkin, and D. E. Kheml'Nitskiĭ, 1980, Sov. J. Exp. Theor. Phys. **52**, 568 [http://www.jetp.ac.ru/cgi-bin/e/index/e/52/3/p568?a=list].

Elliott, S. R., and M. Franz, 2015, Rev. Mod. Phys. **87**, 137.

Essin, A. M., and V. Gurarie, 2011, Phys. Rev. B **84**, 125132.

Essin, A. M., and M. Hermele, 2013, Phys. Rev. B **87**, 104406.

Essin, A. M., J. E. Moore, and D. Vanderbilt, 2009, Phys. Rev. Lett. **102**, 146805.

Evers, F., and A. D. Mirlin, 2008, Rev. Mod. Phys. **80**, 1355.

Ezawa, M., 2012, New J. Phys. **14**, 033003.

Ezawa, M., 2013, Phys. Rev. Lett. **110**, 026603.

Ezawa, M., 2015, Phys. Rev. Lett. **114**, 056403.

Fang, C., Y. Chen, H.-Y. Kee, and L. Fu, 2015, Phys. Rev. B **92**, 081201.

Fang, C., and L. Fu, 2015, Phys. Rev. B **91**, 161105.

Fang, C., M. J. Gilbert, and B. A. Bernevig, 2012, Phys. Rev. B **86**, 115112.

Fang, C., M. J. Gilbert, and B. A. Bernevig, 2013, Phys. Rev. B **87**, 035119.

Fang, C., M. J. Gilbert, and B. A. Bernevig, 2014a, Phys. Rev. Lett. **112**, 046801.

Fang, C., M. J. Gilbert, and B. A. Bernevig, 2014b, Phys. Rev. Lett. **112**, 106401.

Fang, C., M. J. Gilbert, X. Dai, and B. A. Bernevig, 2012, Phys. Rev. Lett. **108**, 266802.

Fang, C., M. J. Gilbert, S.-Y. Xu, B. A. Bernevig, and M. Z. Hasan, 2013, Phys. Rev. B **88**, 125141.

Fendley, P., 2000, arXiv:cond-mat/0006360.

Fidkowski, L., 2010, Phys. Rev. Lett. **104**, 130502.

Fidkowski, L., X. Chen, and A. Vishwanath, 2013, Phys. Rev. X **3**, 041016.

Fidkowski, L., and A. Kitaev, 2010, Phys. Rev. B **81**, 134509.

Fidkowski, L., and A. Kitaev, 2011, Phys. Rev. B **83**, 075103.

Finck, A. D. K., D. J. Van Harlingen, P. K. Mohseni, K. Jung, and X. Li, 2013, Phys. Rev. Lett. **110**, 126406.

Fischer, M. H., T. Neupert, C. Platt, A. P. Schnyder, W. Hanke, J. Goryo, R. Thomale, and M. Sigrist, 2014, Phys. Rev. B **89**, 020509.

Foster, M. S., and A. W. W. Ludwig, 2008, Phys. Rev. B **77**, 165108.

Foster, M. S., H.-Y. Xie, and Y.-Z. Chou, 2014, Phys. Rev. B **89**, 155140.

Foster, M. S., and E. A. Yuzbashyan, 2012, Phys. Rev. Lett. **109**, 246801.

Francesco, P. D., P. Mathieu, and D. Senechal, 1997, *Conformal Field Theory* (Springer-Verlag, New York).

Franz, M., and L. Molenkamp, 2013, *Topological Insulators, Contemporary Concepts of Condensed Matter Science* (Elsevier, New York).

Freed, D. S., 2014, arXiv:1406.7278.

Freed, D. S., and G. W. Moore, 2013, Ann. Henri Poincaré **14**, 1927.

Freedman, M., M. B. Hastings, C. Nayak, X.-L. Qi, K. Walker, and Z. Wang, 2011, Phys. Rev. B **83**, 115132.

Friedan, D. H., 1985, Ann. Phys. (N.Y.) **163**, 318.

Fruchart, M., and D. Carpentier, 2013, C.R. Phys. **14**, 779.

Fu, L., 2011, Phys. Rev. Lett. **106**, 106802.

Fu, L., and E. Berg, 2010, Phys. Rev. Lett. **105**, 097001.

Fu, L., and C. Kane, 2006, Phys. Rev. B **74**, 195312.

Fu, L., and C. L. Kane, 2007, Phys. Rev. B **76**, 045302.

Fu, L., and C. L. Kane, 2008, Phys. Rev. Lett. **100**, 096407.

Fu, L., and C. L. Kane, 2009, Phys. Rev. B **79**, 161408.

Fu, L., and C. L. Kane, 2012, Phys. Rev. Lett. **109**, 246605.

Fu, L., C. L. Kane, and E. J. Mele, 2007, Phys. Rev. Lett. **98**, 106803.

Fukui, T., 2010, Phys. Rev. B **81**, 214516.

Fukui, T., and T. Fujiwara, 2010, J. Phys. Soc. Jpn. **79**, 033701.

Fulga, I. C., F. Hassler, and A. R. Akhmerov, 2012, Phys. Rev. B **85**, 165409.

Fulga, I. C., F. Hassler, A. R. Akhmerov, and C. W. J. Beenakker, 2011, Phys. Rev. B **83**, 155429.

Fulga, I. C., B. van Heck, J. M. Edge, and A. R. Akhmerov, 2014, Phys. Rev. B **89**, 155424.

Furusaki, A., N. Nagaosa, K. Nomura, S. Ryu, and T. Takayanagi, 2013, C.R. Phys. **14**, 871.

Gade, R., 1993, Nucl. Phys. B **398**, 499.

Gade, R., and F. Wegner, 1991, Nucl. Phys. B **360**, 213.

Garate, I., and M. Franz, 2010, Phys. Rev. Lett. **104**, 146802.

Goldman, N., G. Juzeliūnas, P. Öhberg, and I. B. Spielman, 2014, Rep. Prog. Phys. **77**, 126401.

Goldman, N., I. Satija, P. Nikolic, A. Bermudez, M. A. Martin-Delgado, M. Lewenstein, and I. B. Spielman, 2010, Phys. Rev. Lett. **105**, 255302.

Goswami, P., and L. Balicas, 2013, arXiv:1312.3632.

Goswami, P., and S. Chakravarty, 2011, Phys. Rev. Lett. **107**, 196803.

Gottesman, D., and M. B. Hastings, 2010, New J. Phys. **12**, 025002.

Graf, G. M., and M. Porta, 2013, Commun. Math. Phys. **324**, 851.

Groth, C. W., M. Wimmer, A. R. Akhmerov, J. Tworzydło, and C. W. J. Beenakker, 2009, Phys. Rev. Lett. **103**, 196805.

Gruzberg, I. A., A. W. W. Ludwig, and N. Read, 1999, Phys. Rev. Lett. **82**, 4524.

Gruzberg, I. A., N. Read, and S. Vishveshwara, 2005, Phys. Rev. B **71**, 245124.

Gu, Z.-C., and M. Levin, 2014, Phys. Rev. B **89**, 201113.

Gu, Z.-C., J. C. Wang, and X.-G. Wen, 2015, arXiv:1503.01768.
Gu, Z.-C., and X.-G. Wen, 2009, Phys. Rev. B **80**, 155131.
Gu, Z.-C., and X.-G. Wen, 2014, Phys. Rev. B **90**, 115141.
Guo, H.-M., G. Rosenberg, G. Refael, and M. Franz, 2010, Phys. Rev. Lett. **105**, 216601.
Gurarie, V., 2011, Phys. Rev. B **83**, 085426.
Gurarie, V., and J. T. Chalker, 2002, Phys. Rev. Lett. **89**, 136801.
Gurarie, V., and J. T. Chalker, 2003, Phys. Rev. B **68**, 134207.
Gurarie, V., and L. Radzihovsky, 2007, Phys. Rev. B **75**, 212509.
Haldane, F. D. M., 1983a, Phys. Lett. A **93**, 464.
Haldane, F. D. M., 1983b, Phys. Rev. Lett. **50**, 1153.
Haldane, F. D. M., 1988, Phys. Rev. Lett. **61**, 2015.
Halperin, B. I., 1982, Phys. Rev. B **25**, 2185.
Hasan, M. Z., and C. L. Kane, 2010, Rev. Mod. Phys. **82**, 3045.
Hasan, M. Z., and J. E. Moore, 2011, Annu. Rev. Condens. Matter Phys. **2**, 55.
Hasan, M. Z., S.-Y. Xu, and G. Bian, 2015, Phys. Scr. **T164**, 014001.
Hastings, M. B., 2007, J. Stat. Mech. 8, P08024.
Hastings, M. B., and T. A. Loring, 2011, Ann. Phys. (Amsterdam) **326**, 1699.
Hatcher, A., 2001, *Algebraic Topology* (Cambridge University Press, Cambridge, England).
Hatsugai, Y., 1993, Phys. Rev. Lett. **71**, 3697.
Heeger, A. J., S. Kivelson, J. R. Schrieffer, and W. P. Su, 1988, Rev. Mod. Phys. **60**, 781.
Helgason, S., 1978, *Differential geometry, Lie groups, and symmetric spaces* (American Mathematical Society, Providence, RI).
Hor, Y. S., A. J. Williams, J. G. Checkelsky, P. Roushan, J. Seo, Q. Xu, H. W. Zandbergen, A. Yazdani, N. P. Ong, and R. J. Cava, 2010, Phys. Rev. Lett. **104**, 057001.
Hořava, P., 2005, Phys. Rev. Lett. **95**, 016405.
Hosur, P., P. Ghaemi, R. S. K. Mong, and A. Vishwanath, 2011, Phys. Rev. Lett. **107**, 097001.
Hosur, P., and X. Qi, 2013, C.R. Phys. **14**, 857.
Hosur, P., S. Ryu, and A. Vishwanath, 2010, Phys. Rev. B **81**, 045120.
Hsieh, C.-T., G. Y. Cho, and S. Ryu, 2016, Phys. Rev. B **93**, 075135.
Hsieh, C.-T., T. Morimoto, and S. Ryu, 2014, Phys. Rev. B **90**, 245111.
Hsieh, C.-T., O. M. Sule, G. Y. Cho, S. Ryu, and R. G. Leigh, 2014, Phys. Rev. B **90**, 165134.
Hsieh, D., D. Qian, L. Wray, Y. Xia, Y. S. Hor, R. J. Cava, and M. Z. Hasan, 2008, Nature (London) **452**, 970.
Hsieh, D., *et al.*, 2009, Nature (London) **460**, 1101.
Hsieh, T. H., H. Lin, J. Liu, W. Duan, A. Bansil, and L. Fu, 2012, Nat. Commun. **3**, 982.
Hsieh, T. H., J. Liu, and L. Fu, 2014, Phys. Rev. B **90**, 081112.
Huang, S.-M., *et al.*, 2015, Nat. Commun. **6**, 7373.
Huang, X., *et al.*, 2015, Phys. Rev. X **5**, 031023.
Hughes, T. L., E. Prodan, and B. A. Bernevig, 2011, Phys. Rev. B **83**, 245132.
Hughes, T. L., H. Yao, and X.-L. Qi, 2014, Phys. Rev. B **90**, 235123.
Hung, H.-H., P. Ghaemi, T. L. Hughes, and M. J. Gilbert, 2013, Phys. Rev. B **87**, 035401.
Hung, L.-Y., and X.-G. Wen, 2013, Phys. Rev. B **87**, 165107.
Hung, L.-Y., and X.-G. Wen, 2014, Phys. Rev. B **89**, 075121.
Ishikawa, K., and T. Matsuyama, 1987, Nucl. Phys. B **280**, 523.
Isobe, H., and L. Fu, 2015, Phys. Rev. B **92**, 081304.
Ivanov, D. A., 2001, Phys. Rev. Lett. **86**, 268.
Jackiw, R., and C. Rebbi, 1976, Phys. Rev. D **13**, 3398.
Jackiw, R., and P. Rossi, 1981, Nucl. Phys. B **190**, 681.
Jadaun, P., D. Xiao, Q. Niu, and S. K. Banerjee, 2013, Phys. Rev. B **88**, 085110.
Jang, J., D. G. Ferguson, V. Vakaryuk, R. Budakian, S. B. Chung, P. M. Goldbart, and Y. Maeno, 2011, Science **331**, 186.
Jeon, S., B. B. Zhou, A. Gyenis, B. E. Feldman, I. Kimchi, A. C. Potter, Q. D. Gibson, R. J. Cava, A. Vishwanath, and A. Yazdani, 2014, Nat. Mater. **13**, 851.
Jian, C.-M., and X.-L. Qi, 2014, Phys. Rev. X **4**, 041043.
Jiang, L., T. Kitagawa, J. Alicea, A. R. Akhmerov, D. Pekker, G. Refael, J. I. Cirac, E. Demler, M. D. Lukin, and P. Zoller, 2011, Phys. Rev. Lett. **106**, 220402.
Jiang, S., A. Mesaros, and Y. Ran, 2014, Phys. Rev. X **4**, 031048.
Juričić, V., A. Mesaros, R.-J. Slager, and J. Zaanen, 2012, Phys. Rev. Lett. **108**, 106403.
Kane, C. L., and M. P. A. Fisher, 1997, Phys. Rev. B **55**, 15832.
Kane, C. L., and T. C. Lubensky, 2014, Nat. Phys. **10**, 39.
Kane, C. L., and E. J. Mele, 2005a, Phys. Rev. Lett. **95**, 226801.
Kane, C. L., and E. J. Mele, 2005b, Phys. Rev. Lett. **95**, 146802.
Kapustin, A., 2014a, arXiv:1404.6659.
Kapustin, A., 2014b, arXiv:1403.1467.
Kapustin, A., and R. Thorngren, 2014a, arXiv:1404.3230.
Kapustin, A., and R. Thorngren, 2014b, Phys. Rev. Lett. **112**, 231602.
Kapustin, A., R. Thorngren, A. Turzillo, and Z. Wang, 2015, J. High Energy Phys. 12, 52.
Kariyado, T., and M. Ogata, 2011, J. Phys. Soc. Jpn. **80**, 083704.
Karoubi, M., 1978, *K-Theory: An Introduction* (Springer, New York).
Kennedy, R., and M. R. Zirnbauer, 2016, Commun. Math. Phys. **342**, 909.
Keselman, A., L. Fu, A. Stern, and E. Berg, 2013, Phys. Rev. Lett. **111**, 116402.
Khanikaev, A. B., S. Hossein Mousavi, W.-K. Tse, M. Kargarian, A. H. MacDonald, and G. Shvets, 2013, Nat. Mater. **12**, 233.
Khmel'Nitskiĭ, D. E., 1983, Sov. J. Exp. Theor. Phys. Lett. **38**, 552 [http://adsabs.harvard.edu/abs/1983JETPL..38..552K].
Kim, Y., B. J. Wieder, C. L. Kane, and A. M. Rappe, 2015, Phys. Rev. Lett. **115**, 036806.
King-Smith, R. D., and D. Vanderbilt, 1993, Phys. Rev. B **47**, 1651.
Kitaev, A., 2001, Phys. Usp. **44**, 131.
Kitaev, A., 2006, Ann. Phys. (Amsterdam) **321**, 2.
Kitaev, A., 2009, AIP Conf. Proc. **1134**, 22.
Kitaev, A., 2015, talk at the IPAM workshop "Symmetry and Topology in Quantum Matter".
Kitaev, A., and J. Preskill, 2006, Phys. Rev. Lett. **96**, 110404.
Kitagawa, T., E. Berg, M. Rudner, and E. Demler, 2010, Phys. Rev. B **82**, 235114.
Klitzing, K. v., G. Dorda, and M. Pepper, 1980, Phys. Rev. Lett. **45**, 494.
Knez, I., R.-R. Du, and G. Sullivan, 2011, Phys. Rev. Lett. **107**, 136603.
Kobayashi, K., T. Ohtsuki, K.-I. Imura, and I. F. Herbut, 2014, Phys. Rev. Lett. **112**, 016402.
Kobayashi, S., and M. Sato, 2015, arXiv:1504.07408.
Kobayashi, S., K. Shiozaki, Y. Tanaka, and M. Sato, 2014, Phys. Rev. B **90**, 024516.
Koch-Janusz, M., and Z. Ringel, 2014, Phys. Rev. B **89**, 075137.
Kohmoto, M., 1985, Ann. Phys. (N.Y.) **160**, 343.
Kong, L., and X.-G. Wen, 2014, arXiv:1405.5858.
Konig, M., S. Wiedmann, C. Brune, A. Roth, H. Buhmann, L. W. Molenkamp, X.-L. Qi, and S.-C. Zhang, 2007, Science **318**, 766.
König, M., H. Buhmann, L. W. Molenkamp, T. Hughes, C.-X. Liu, X.-L. Qi, and S.-C. Zhang, 2008, J. Phys. Soc. Jpn. **77**, 031007.
Kotetes, P., 2013, New J. Phys. **15**, 105027.

Kraus, Y. E., Y. Lahini, Z. Ringel, M. Verbin, and O. Zilberberg, 2012, Phys. Rev. Lett. **109**, 106402.

Kurter, C., A. D. K. Finck, P. Ghaemi, Y. S. Hor, and D. J. Van Harlingen, 2014, Phys. Rev. B **90**, 014501.

Landau, L. D., E. M. Lifshitz, and M. Pitaevskii, 1999, *Statistical Physics* (Butterworth-Heinemann, New York).

Lapa, M. F., J. C. Y. Teo, and T. L. Hughes, 2016, Phys. Rev. B **93**, 115131.

Laughlin, R. B., 1981, Phys. Rev. B **23**, 5632.

Lawson, H. B., and M.-L. Michelsohn, 1990, *Spin Geometry* (Princeton University Press, Princeton, NJ).

Lee, E. J. H., X. Jiang, M. Houzet, R. Aguado, C. M. Lieber, and S. De Franceschi, 2014, Nat. Nanotechnol. **9**, 79.

Lee, S.-S., and S. Ryu, 2008, Phys. Rev. Lett. **100**, 186807.

Leggett, A. J., 1975, Rev. Mod. Phys. **47**, 331.

Leggett, A. J., 2006, *Quantum Liquids: Bose Condensation and Cooper Pairing in Condensed-Matter Systems* (Oxford University Press, New York).

Levin, M., 2013, Phys. Rev. X **3**, 021009.

Levin, M., and Z.-C. Gu, 2012, Phys. Rev. B **86**, 115109.

Levin, M., and A. Stern, 2009, Phys. Rev. Lett. **103**, 196803.

Levin, M., and A. Stern, 2012, Phys. Rev. B **86**, 115131.

Li, J., R.-L. Chu, J. K. Jain, and S.-Q. Shen, 2009, Phys. Rev. Lett. **102**, 136806.

Li, Q., D. E. Kharzeev, C. Zhang, Y. Huang, I. Pletikosic, A. V. Fedorov, R. D. Zhong, J. A. Schneeloch, G. D. Gu, and T. Valla, 2016, Nat. Phys. **12**, 550.

Liang, T., Q. Gibson, M. N. Ali, M. Liu, R. J. Cava, and N. P. Ong, 2015, Nat. Mater. **14**, 280.

Linder, J., Y. Tanaka, T. Yokoyama, A. Sudbø, and N. Nagaosa, 2010, Phys. Rev. Lett. **104**, 067001.

Lindner, N. H., E. Berg, G. Refael, and A. Stern, 2012, Phys. Rev. X **2**, 041002.

Lindner, N. H., G. Refael, and V. Galitski, 2011, Nat. Phys. **7**, 490.

Liu, C., T. L. Hughes, X.-L. Qi, K. Wang, and S.-C. Zhang, 2008, Phys. Rev. Lett. **100**, 236601.

Liu, C.-X., X.-L. Qi, X. Dai, Z. Fang, and S.-C. Zhang, 2008, Phys. Rev. Lett. **101**, 146802.

Liu, C.-X., X.-L. Qi, and S.-C. Zhang, 2012, Physica E (Amsterdam) **44**, 906.

Liu, C.-X., P. Ye, and X.-L. Qi, 2013, Phys. Rev. B **87**, 235306.

Liu, C.-X., R.-X. Zhang, and B. K. VanLeeuwen, 2014, Phys. Rev. B **90**, 085304.

Liu, J., W. Duan, and L. Fu, 2013, Phys. Rev. B **88**, 241303.

Liu, J., T. H. Hsieh, P. Wei, W. Duan, J. Moodera, and L. Fu, 2014, Nat. Mater. **13**, 178.

Liu, W., X. Peng, C. Tang, L. Sun, K. Zhang, and J. Zhong, 2011, Phys. Rev. B **84**, 245105.

Liu, X.-J., J. J. He, and K. T. Law, 2014, Phys. Rev. B **90**, 235141.

Liu, Z. K., *et al.*, 2014a, Nat. Mater. **13**, 677.

Liu, Z. K., *et al.*, 2014b, Science **343**, 864.

Loring, T. A., and M. B. Hastings, 2010, Europhys. Lett. **92**, 67004.

Lu, L., C. Fang, L. Fu, S. G. Johnson, J. D. Joannopoulos, and M. Soljacic, 2016, Nat. Phys. **12**, 337.

Lu, L., L. Fu, J. D. Joannopoulos, and M. Soljacic, 2013, Nat. Photonics **7**, 294.

Lu, L., Z. Wang, D. Ye, L. Ran, L. Fu, J. D. Joannopoulos, and M. Soljačić, 2015, Science **349**, 622.

Lu, Y.-M., and D.-H. Lee, 2014a, arXiv:1403.5558.

Lu, Y.-M., and D.-H. Lee, 2014b, Phys. Rev. B **89**, 184417.

Lu, Y.-M., and A. Vishwanath, 2012, Phys. Rev. B **86**, 125119.

Lu, Y.-M., and A. Vishwanath, 2013, arXiv:1302.2634.

Ludwig, A. W. W., M. P. A. Fisher, R. Shankar, and G. Grinstein, 1994, Phys. Rev. B **50**, 7526.

Luke, G. M., *et al.*, 1998, Nature (London) **394**, 558.

Lutchyn, R. M., J. D. Sau, and S. Das Sarma, 2010, Phys. Rev. Lett. **105**, 077001.

Luttinger, J. M., 1964, Phys. Rev. **135**, A1505.

Lv, B. Q., *et al.*, 2015, Phys. Rev. X **5**, 031013.

Maciejko, J., and G. A. Fiete, 2015, Nat. Phys. **11**, 385.

Maciejko, J., X.-L. Qi, A. Karch, and S.-C. Zhang, 2010, Phys. Rev. Lett. **105**, 246809.

Maeno, Y., S. Kittaka, T. Nomura, S. Yonezawa, and K. Ishida, 2012, J. Phys. Soc. Jpn. **81**, 011009.

Maeno, Y., T. M. Rice, and M. Sigrist, 2001, Phys. Today **54**, 42.

Mañes, J. L., F. Guinea, and M. A. H. Vozmediano, 2007, Phys. Rev. B **75**, 155424.

Matsuura, S., P.-Y. Chang, A. P. Schnyder, and S. Ryu, 2013, New J. Phys. **15**, 065001.

Mendler, D., P. Kotetes, and G. Schön, 2015, Phys. Rev. B **91**, 155405.

Mesaros, A., and Y. Ran, 2013, Phys. Rev. B **87**, 155115.

Metlitski, M. A., L. Fidkowski, X. Chen, and A. Vishwanath, 2014, arXiv:1406.3032.

Metlitski, M. A., C. L. Kane, and M. P. A. Fisher, 2013, Phys. Rev. B **88**, 035131.

Metlitski, M. A., C. L. Kane, and M. P. A. Fisher, 2015, Phys. Rev. B **92**, 125111.

Milnor, J., 1963, *Morse Theory* (Princeton University Press, Princeton, NJ).

Mizushima, T., Y. Tsutsumi, M. Sato, and K. Machida, 2015, J. Phys. Condens. Matter **27**, 113203.

Mong, R. S. K., J. H. Bardarson, and J. E. Moore, 2012, Phys. Rev. Lett. **108**, 076804.

Moore, J. E., 2010, Nature (London) **464**, 194.

Moore, J. E., and L. Balents, 2007, Phys. Rev. B **75**, 121306.

Moore, J. E., Y. Ran, and X.-G. Wen, 2008, Phys. Rev. Lett. **101**, 186805.

Morimoto, T., and A. Furusaki, 2013, Phys. Rev. B **88**, 125129.

Morimoto, T., and A. Furusaki, 2014, Phys. Rev. B **89**, 235127.

Morimoto, T., A. Furusaki, and C. Mudry, 2015a, Phys. Rev. B **91**, 235111.

Morimoto, T., A. Furusaki, and C. Mudry, 2015b, Phys. Rev. B **92**, 125104.

Mourik, V., K. Zuo, S. M. Frolov, S. R. Plissard, E. P. A. M. Bakkers, and L. P. Kouwenhoven, 2012, Science **336**, 1003.

Mudry, C., C. Chamon, and X.-G. Wen, 1996, Nucl. Phys. B **466**, 383.

Murakami, S., 2007, New J. Phys. **9**, 356.

Murakawa, S., *et al.*, 2009, Phys. Rev. Lett. **103**, 155301.

Murakawa, S., *et al.*, 2011, J. Phys. Soc. Jpn. **80**, 013602.

Nadj-Perge, S., I. K. Drozdov, J. Li, H. Chen, S. Jeon, J. Seo, A. H. MacDonald, B. A. Bernevig, and A. Yazdani, 2014, Science **346**, 602.

Nagaosa, N., J. Sinova, S. Onoda, A. H. MacDonald, and N. P. Ong, 2010, Rev. Mod. Phys. **82**, 1539.

Nakahara, M., 2003, *Geometry, Topology and Physics, Second Edition*, Graduate Student Series in Physics (Taylor & Francis, London).

Nayak, C., S. H. Simon, A. Stern, M. Freedman, and S. Das Sarma, 2008, Rev. Mod. Phys. **80**, 1083.

Nelson, D. R., 2002, *Defects and Geometry in Condensed Matter Physics* (Cambridge University Press, Cambridge, England).

Nersesyan, A. A., A. M. Tsvelik, and F. Wenger, 1994, Phys. Rev. Lett. **72**, 2628.

Neupane, M., *et al.*, 2014, Nat. Commun. **5**, 3786.
Neupert, T., C. Chamon, C. Mudry, and R. Thomale, 2014, Phys. Rev. B **90**, 205101.
Neupert, T., L. Santos, S. Ryu, C. Chamon, and C. Mudry, 2011, Phys. Rev. B **84**, 165107.
Nielsen, H., and M. Ninomiya, 1981, Nucl. Phys. B **185**, 20.
Ning, S.-Q., H.-C. Jiang, and Z.-X. Liu, 2015, Phys. Rev. B **91**, 241105.
Niu, Q., D. J. Thouless, and Y.-S. Wu, 1985, Phys. Rev. B **31**, 3372.
Nomura, K., M. Koshino, and S. Ryu, 2007, Phys. Rev. Lett. **99**, 146806.
Nomura, K., S. Ryu, A. Furusaki, and N. Nagaosa, 2012, Phys. Rev. Lett. **108**, 026802.
Novak, M., S. Sasaki, K. Segawa, and Y. Ando, 2015, Phys. Rev. B **91**, 041203.
Obuse, H., A. Furusaki, S. Ryu, and C. Mudry, 2007, Phys. Rev. B **76**, 075301.
Obuse, H., A. Furusaki, S. Ryu, and C. Mudry, 2008, Phys. Rev. B **78**, 115301.
Obuse, H., S. Ryu, A. Furusaki, and C. Mudry, 2014, Phys. Rev. B **89**, 155315.
Okada, Y., *et al.*, 2013, Science **341**, 1496.
Oreg, Y., G. Refael, and F. von Oppen, 2010, Phys. Rev. Lett. **105**, 177002.
Ostrovsky, P. M., I. V. Gornyi, and A. D. Mirlin, 2007, Phys. Rev. Lett. **98**, 256801.
Ostrovsky, P. M., I. V. Gornyi, and A. D. Mirlin, 2010, Phys. Rev. Lett. **105**, 036803.
Parameswaran, S. A., T. Grover, D. A. Abanin, D. A. Pesin, and A. Vishwanath, 2014, Phys. Rev. X **4**, 031035.
Parameswaran, S. A., R. Roy, and S. L. Sondhi, 2012, Phys. Rev. B **85**, 241308.
Parameswaran, S. A., A. M. Turner, D. P. Arovas, and A. Vishwanath, 2013, Nat. Phys. **9**, 299.
Pletikosić, I., G. D. Gu, and T. Valla, 2014, Phys. Rev. Lett. **112**, 146403.
Pollmann, F., E. Berg, A. M. Turner, and M. Oshikawa, 2012, Phys. Rev. B **85**, 075125.
Pollmann, F., A. M. Turner, E. Berg, and M. Oshikawa, 2010, Phys. Rev. B **81**, 064439.
Prange, R. E., and S. M. Girvin, 1990, Eds., *The Quantum Hall effect* (Springer-Verlag, Berlin).
Prodan, E., 2009, Phys. Rev. B **80**, 125327.
Prodan, E., 2011, Phys. Rev. B **83**, 235115.
Prodan, E., 2014, Topological Quantum Matter **1**, 1.
Prodan, E., B. Leung, and J. Bellissard, 2013, J. Phys. A **46**, 485202.
Prodan, E., and H. Schulz-Baldes, 2014, arXiv:1402.5002.
Pruisken, A. M. M., 1984, Nucl. Phys. B **235**, 277.
Qi, X.-L., 2013, New J. Phys. **15**, 065002.
Qi, X.-L., T. L. Hughes, S. Raghu, and S.-C. Zhang, 2009, Phys. Rev. Lett. **102**, 187001.
Qi, X.-L., T. L. Hughes, and S.-C. Zhang, 2008, Phys. Rev. B **78**, 195424.
Qi, X.-L., T. L. Hughes, and S.-C. Zhang, 2010, Phys. Rev. B **81**, 134508.
Qi, X.-L., and S.-C. Zhang, 2011, Rev. Mod. Phys. **83**, 1057.
Qiao, Z., S. A. Yang, W. Feng, W.-K. Tse, J. Ding, Y. Yao, J. Wang, and Q. Niu, 2010, Phys. Rev. B **82**, 161414.
Raghu, S., A. Kapitulnik, and S. A. Kivelson, 2010, Phys. Rev. Lett. **105**, 136401.
Ran, Y., 2010, arXiv:1006.5454.
Ran, Y., Y. Zhang, and A. Vishwanath, 2009, Nat. Phys. **5**, 298.
Read, N., and D. Green, 2000, Phys. Rev. B **61**, 10267.
Rechtsman, M. C., J. M. Zeuner, Y. Plotnik, Y. Lumer, D. Podolsky, F. Dreisow, S. Nolte, M. Segev, and A. Szameit, 2013, Nature (London) **496**, 196.
Renard, J. P., M. Verdaguer, L. P. Regnault, W. A. C. Erkelens, J. Rossat-Mignod, and W. G. Stirling, 1987, Europhys. Lett. **3**, 945.
Repellin, C., B. A. Bernevig, and N. Regnault, 2014, Phys. Rev. B **90**, 245401.
Resta, R., 1994, Rev. Mod. Phys. **66**, 899.
Rice, T. M., and M. Sigrist, 1995, J. Phys. Condens. Matter **7**, L643.
Rieder, M.-T., and P. W. Brouwer, 2014, Phys. Rev. B **90**, 205404.
Ringel, Z., Y. E. Kraus, and A. Stern, 2012, Phys. Rev. B **86**, 045102.
Ringel, Z., and A. Stern, 2013, Phys. Rev. B **88**, 115307.
Rokhinson, L. P., X. Liu, and J. K. Furdyna, 2012, Nat. Phys. **8**, 795.
Rosch, A., 2012, Phys. Rev. B **86**, 125120.
Roushan, P., J. Seo, C. V. Parker, Y. S. Hor, D. Hsieh, D. Qian, A. Richardella, M. Z. Hasan, R. J. Cava, and A. Yazdani, 2009, Nature (London) **460**, 1106.
Roy, R., 2009a, Phys. Rev. B **79**, 195322.
Roy, R., 2009b, Phys. Rev. B **79**, 195321.
Roy, R., 2012, arXiv:1212.2944.
Ryu, S., and Y. Hatsugai, 2002, Phys. Rev. Lett. **89**, 077002.
Ryu, S., and Y. Hatsugai, 2006, Phys. Rev. B **73**, 245115.
Ryu, S., J. E. Moore, and A. W. W. Ludwig, 2012, Phys. Rev. B **85**, 045104.
Ryu, S., C. Mudry, A. W. W. Ludwig, and A. Furusaki, 2012, Phys. Rev. B **85**, 235115.
Ryu, S., C. Mudry, H. Obuse, and A. Furusaki, 2007, Phys. Rev. Lett. **99**, 116601.
Ryu, S., C. Mudry, H. Obuse, and A. Furusaki, 2010, New J. Phys. **12**, 065005.
Ryu, S., and K. Nomura, 2012, Phys. Rev. B **85**, 155138.
Ryu, S., A. P. Schnyder, A. Furusaki, and A. W. W. Ludwig, 2010, New J. Phys. **12**, 065010.
Ryu, S., and S.-C. Zhang, 2012, Phys. Rev. B **85**, 245132.
Safaei, S., P. Kacman, and R. Buczko, 2013, Phys. Rev. B **88**, 045305.
Salomaa, M. M., and G. E. Volovik, 1985, Phys. Rev. Lett. **55**, 1184.
Santos, L. H., and J. Wang, 2014, Phys. Rev. B **89**, 195122.
Sato, M., 2006, Phys. Rev. B **73**, 214502.
Sato, M., A. Yamakage, and T. Mizushima, 2014, Physica E (Amsterdam) **55**, 20.
Sau, J. D., R. M. Lutchyn, S. Tewari, and S. Das Sarma, 2010, Phys. Rev. Lett. **104**, 040502.
Schnyder, A. P., and P. M. R. Brydon, 2015, J. Phys. Condens. Matter **27**, 243201.
Schnyder, A. P., P. M. R. Brydon, and C. Timm, 2012, Phys. Rev. B **85**, 024522.
Schnyder, A. P., and S. Ryu, 2011, Phys. Rev. B **84**, 060504.
Schnyder, A. P., S. Ryu, A. Furusaki, and A. W. W. Ludwig, 2008, Phys. Rev. B **78**, 195125.
Schnyder, A. P., S. Ryu, A. Furusaki, and A. W. W. Ludwig, 2009, AIP Conf. Proc. **1134**, 10.
Schnyder, A. P., C. Timm, and P. M. R. Brydon, 2013, Phys. Rev. Lett. **111**, 077001.
Schuch, N., D. Perez-Garcia, and I. Cirac, 2011, Phys. Rev. B **84**, 165139.
Schuch, N., M. M. Wolf, F. Verstraete, and J. I. Cirac, 2008, Phys. Rev. Lett. **100**, 030504.
Schulz-Baldes, H., J. Kellendonk, and T. Richter, 2000, J. Phys. A **33**, L27.
Senthil, T., 2015, Annu. Rev. Condens. Matter Phys. **6**, 299.
Senthil, T., and M. P. A. Fisher, 2000, Phys. Rev. B **62**, 7850.

Senthil, T., M. P. A. Fisher, L. Balents, and C. Nayak, 1998, Phys. Rev. Lett. **81**, 4704.

Senthil, T., J. B. Marston, and M. P. A. Fisher, 1999, Phys. Rev. B **60**, 4245.

Serbyn, M., and L. Fu, 2014, Phys. Rev. B **90**, 035402.

Shekhar, C., *et al.*, 2015, Nat. Phys. **11**, 645.

Shen, S.-Q., 2012, *Topological insulators*, Springer Series in Solid-State Sciences, Vol. 174 (Springer, New York).

Sheng, D. N., Z.-C. Gu, K. Sun, and L. Sheng, 2011, Nat. Commun. **2**, 389.

Shindou, R., and S. Murakami, 2009, Phys. Rev. B **79**, 045321.

Shindou, R., R. Nakai, and S. Murakami, 2010, New J. Phys. **12**, 065008.

Shiozaki, K., and M. Sato, 2014, Phys. Rev. B **90**, 165114.

Shiozaki, K., M. Sato, and K. Gomi, 2015, Phys. Rev. B **91**, 155120.

Shitade, A., H. Katsura, J. Kuneš, X.-L. Qi, S.-C. Zhang, and N. Nagaosa, 2009, Phys. Rev. Lett. **102**, 256403.

Sigrist, M., and K. Ueda, 1991, Rev. Mod. Phys. **63**, 239.

Slager, R.-J., A. Mesaros, V. Juricic, and J. Zaanen, 2013, Nat. Phys. **9**, 98.

Soluyanov, A. A., D. Gresch, Z. Wang, Q. Wu, M. Troyer, X. Dai, and B. A. Bernevig, 2015, Nature (London) **527**, 495.

Soluyanov, A. A., and D. Vanderbilt, 2011, Phys. Rev. B **83**, 035108.

Stanescu, T. D., and S. Tewari, 2013, J. Phys. Condens. Matter **25**, 233201.

Stone, M., 2012, Phys. Rev. B **85**, 184503.

Stone, M., C.-K. Chiu, and A. Roy, 2011, J. Phys. A **44**, 045001.

Stone, M., and R. Roy, 2004, Phys. Rev. B **69**, 184511.

Su, W. P., J. R. Schrieffer, and A. J. Heeger, 1980, Phys. Rev. B **22**, 2099.

Sule, O. M., X. Chen, and S. Ryu, 2013, Phys. Rev. B **88**, 075125.

Sun, K., W. V. Liu, A. Hemmerich, and S. Das Sarma, 2012, Nat. Phys. **8**, 67.

Swingle, B., M. Barkeshli, J. McGreevy, and T. Senthil, 2011, Phys. Rev. B **83**, 195139.

Takane, Y., 2004a, J. Phys. Soc. Jpn. **73**, 2366.

Takane, Y., 2004b, J. Phys. Soc. Jpn. **73**, 9.

Takane, Y., 2004c, J. Phys. Soc. Jpn. **73**, 1430.

Tanaka, Y., Z. Ren, T. Sato, K. Nakayama, S. Souma, T. Takahashi, K. Segawa, and Y. Ando, 2012, Nat. Phys. **8**, 800.

Tanaka, Y., M. Sato, and N. Nagaosa, 2012, J. Phys. Soc. Jpn. **81**, 011013.

Tanaka, Y., T. Yokoyama, and N. Nagaosa, 2009, Phys. Rev. Lett. **103**, 107002.

Tang, E., and X.-G. Wen, 2012, Phys. Rev. Lett. **109**, 096403.

Teo, J. C. Y., L. Fu, and C. L. Kane, 2008, Phys. Rev. B **78**, 045426.

Teo, J. C. Y., and T. L. Hughes, 2013, Phys. Rev. Lett. **111**, 047006.

Teo, J. C. Y., T. L. Hughes, and E. Fradkin, 2015, Ann. Phys. (Amsterdam) **360**, 349.

Teo, J. C. Y., and C. L. Kane, 2010a, Phys. Rev. Lett. **104**, 046401.

Teo, J. C. Y., and C. L. Kane, 2010b, Phys. Rev. B **82**, 115120.

Tewari, S., C. Zhang, S. Das Sarma, C. Nayak, and D.-H. Lee, 2008, Phys. Rev. Lett. **100**, 027001.

Thiang, G. C., 2016, Ann. Henri Poincaré **17**, 757.

Thouless, D. J., 1983, Phys. Rev. B **27**, 6083.

Thouless, D. J., M. Kohmoto, M. P. Nightingale, and M. den Nijs, 1982, Phys. Rev. Lett. **49**, 405.

Titov, M., P. W. Brouwer, A. Furusaki, and C. Mudry, 2001, Phys. Rev. B **63**, 235318.

Tsvelik, A. M., 1995, Phys. Rev. B **51**, 9449.

Turner, A. M., F. Pollmann, and E. Berg, 2011, Phys. Rev. B **83**, 075102.

Turner, A. M., and A. Vishwanath, 2013, arXiv:1301.0330.

Turner, A. M., Y. Zhang, R. S. K. Mong, and A. Vishwanath, 2012, Phys. Rev. B **85**, 165120.

Turner, A. M., Y. Zhang, and A. Vishwanath, 2010, Phys. Rev. B **82**, 241102.

Ueno, Y., A. Yamakage, Y. Tanaka, and M. Sato, 2013, Phys. Rev. Lett. **111**, 087002.

Vaezi, A., 2013, Phys. Rev. B **87**, 035132.

Vafek, O., and A. Vishwanath, 2014, Annu. Rev. Condens. Matter Phys. **5**, 83.

Vanderbilt, D., and R. D. King-Smith, 1993, Phys. Rev. B **48**, 4442.

Vazifeh, M. M., and M. Franz, 2013, Phys. Rev. Lett. **111**, 027201.

Verbaarschot, J., 1994, Phys. Rev. Lett. **72**, 2531.

Verbin, M., O. Zilberberg, Y. E. Kraus, Y. Lahini, and Y. Silberberg, 2013, Phys. Rev. Lett. **110**, 076403.

Vishwanath, A., and T. Senthil, 2013, Phys. Rev. X **3**, 011016.

Volovik, G. E., 1990, Sov. J. Exp. Theor. Phys. Lett. **51**, 125 [http://www.jetpletters.ac.ru/ps/1136/article_17200.shtml].

Volovik, G. E., 1992, JETP Lett. **55**, 368 [http://www.jetpletters.ac.ru/ps/1273/article_19263.shtml].

Volovik, G. E., 1999, JETP Lett. **70**, 609.

Volovik, G. E., 2003, *Universe in a helium droplet* (Oxford University Press, Oxford, UK).

Volovik, G. E., 2011, JETP Lett. **93**, 66.

Volovik, G. E., 2013, *Topology of quantum vacuum*, Lecture Notes in Physics, Vol. 870 (Springer, Berlin).

Wada, Y., S. Murakawa, Y. Tamura, M. Saitoh, Y. Aoki, R. Nomura, and Y. Okuda, 2008, Phys. Rev. B **78**, 214516.

Wan, X., A. M. Turner, A. Vishwanath, and S. Y. Savrasov, 2011, Phys. Rev. B **83**, 205101.

Wang, C., and M. Levin, 2014, Phys. Rev. Lett. **113**, 080403.

Wang, C., A. C. Potter, and T. Senthil, 2013, Phys. Rev. B **88**, 115137.

Wang, C., A. C. Potter, and T. Senthil, 2014, Science **343**, 629.

Wang, C., and T. Senthil, 2013, Phys. Rev. B **87**, 235122.

Wang, C., and T. Senthil, 2014, Phys. Rev. B **89**, 195124.

Wang, E., *et al.*, 2013, Nat. Phys. **9**, 621.

Wang, J., J. Liu, Y. Xu, J. Wu, B.-L. Gu, and W. Duan, 2014, Phys. Rev. B **89**, 125308.

Wang, J., and X.-G. Wen, 2013, arXiv:1307.7480.

Wang, J. C., Z.-C. Gu, and X.-G. Wen, 2015, Phys. Rev. Lett. **114**, 031601.

Wang, J. C., L. H. Santos, and X.-G. Wen, 2015, Phys. Rev. B **91**, 195134.

Wang, J. C., and X.-G. Wen, 2015, Phys. Rev. B **91**, 035134.

Wang, L., A. Essin, M. Hermele, and O. Motrunich, 2015, Phys. Rev. B **91**, 121103.

Wang, M.-X., *et al.*, 2012, Science **336**, 52.

Wang, Q.-Z., X. Liu, H.-J. Zhang, N. Samarth, S.-C. Zhang, and C.-X. Liu, 2014, Phys. Rev. Lett. **113**, 147201.

Wang, S.-T., D.-L. Deng, J. E. Moore, K. Sun, and L.-M. Duan, 2015, Phys. Rev. B **91**, 035108.

Wang, Y. H., H. Steinberg, P. Jarillo-Herrero, and N. Gedik, 2013, Science **342**, 453.

Wang, Z., X.-L. Qi, and S.-C. Zhang, 2010, New J. Phys. **12**, 065007.

Wang, Z., X.-L. Qi, and S.-C. Zhang, 2011, Phys. Rev. B **84**, 014527.

Wang, Z., X.-L. Qi, and S.-C. Zhang, 2012, Phys. Rev. B **85**, 165126.

Wang, Z., Y. Sun, X.-Q. Chen, C. Franchini, G. Xu, H. Weng, X. Dai, and Z. Fang, 2012, Phys. Rev. B **85**, 195320.

Wang, Z., H. Weng, Q. Wu, X. Dai, and Z. Fang, 2013d, Phys. Rev. B **88**, 125427.

Wang, Z., and S.-C. Zhang, 2012, Phys. Rev. X **2**, 031008.

Wang, Z., and S.-C. Zhang, 2014, Phys. Rev. X **4**, 011006.

Wegner, F., 1979, Z. Phys. B **35**, 207.

Weinberg, E. J., 1981, Phys. Rev. D **24**, 2669.
Wen, X. G., 1990, Int. J. Mod. Phys. B **04**, 239.
Wen, X.-G., 2002, Phys. Rev. B **65**, 165113.
Wen, X.-G., 2012, Phys. Rev. B **85**, 085103.
Wen, X.-G., 2013, Phys. Rev. D **88**, 045013.
Wen, X.-G., 2014, Phys. Rev. B **89**, 035147.
Wen, X.-G., 2015, Phys. Rev. B **91**, 205101.
Wen, X.-G., and Q. Niu, 1990, Phys. Rev. B **41**, 9377.
Weng, H., C. Fang, Z. Fang, B. A. Bernevig, and X. Dai, 2015, Phys. Rev. X **5**, 011029.
Weng, H., Y. Liang, Q. Xu, R. Yu, Z. Fang, X. Dai, and Y. Kawazoe, 2015, Phys. Rev. B **92**, 045108.
Williams, J. R., A. J. Bestwick, P. Gallagher, S. S. Hong, Y. Cui, A. S. Bleich, J. G. Analytis, I. R. Fisher, and D. Goldhaber-Gordon, 2012, Phys. Rev. Lett. **109**, 056803.
Wilson, K. G., and J. B. Kogut, 1974, Phys. Rep. **12**, 75.
Winterfeld, L., L. A. Agapito, J. Li, N. Kioussis, P. Blaha, and Y. P. Chen, 2013, Phys. Rev. B **87**, 075143.
Witczak-Krempa, W., G. Chen, Y. B. Kim, and L. Balents, 2014, Annu. Rev. Condens. Matter Phys. **5**, 57.
Witczak-Krempa, W., and Y. B. Kim, 2012, Phys. Rev. B **85**, 045124.
Witten, E., 1982, Phys. Lett. B **117**, 324.
Witten, E., 1985, Commun. Math. Phys. **100**, 197.
Wojek, B. M., *et al.*, 2013, Phys. Rev. B **87**, 115106.
Wolgast, S., C. Kurdak, K. Sun, J. W. Allen, D.-J. Kim, and Z. Fisk, 2013, Phys. Rev. B **88**, 180405.
Wrasse, E. O., and T. M. Schmidt, 2014, Nano Lett. **14**, 5717.
Wray, L. A., S. Xu, M. Neupane, A. V. Fedorov, Y. S. Hor, R. J. Cava, and M. Z. Hasan, 2013, J. Phys. Conf. Ser. **449**, 012037.
Wray, L. A., S.-Y. Xu, Y. Xia, Y. S. Hor, D. Qian, A. V. Fedorov, H. Lin, A. Bansil, R. J. Cava, and M. Z. Hasan, 2010, Nat. Phys. **6**, 855.
Xia, J., Y. Maeno, P. T. Beyersdorf, M. M. Fejer, and A. Kapitulnik, 2006, Phys. Rev. Lett. **97**, 167002.
Xia, Y., *et al.*, 2009, Nat. Phys. **5**, 398.
Xiao, D., J. Shi, D. P. Clougherty, and Q. Niu, 2009, Phys. Rev. Lett. **102**, 087602.
Xiao, D., W. Zhu, Y. Ran, N. Nagaosa, and S. Okamoto, 2011, Nat. Commun. **2**, 596.
Xie, H.-Y., Y.-Z. Chou, and M. S. Foster, 2015, Phys. Rev. B **91**, 024203.
Xie, L. S., L. M. Schoop, E. M. Seibel, Q. D. Gibson, W. Xie, and R. J. Cava, 2015, APL Mater. **3**, 083602.
Xu, C., and A. W. W. Ludwig, 2013, Phys. Rev. Lett. **110**, 200405.
Xu, G., J. Wang, C. Felser, X.-L. Qi, and S.-C. Zhang, 2015, Nano Lett. **15**, 2019.
Xu, G., H. Weng, Z. Wang, X. Dai, and Z. Fang, 2011, Phys. Rev. Lett. **107**, 186806.
Xu, J.-P., *et al.*, 2014a, Phys. Rev. Lett. **112**, 217001.
Xu, S.-Y., *et al.*, 2012, Nat. Commun. **3**, 1192.
Xu, S.-Y., *et al.*, 2014, Nat. Phys. **10**, 943.
Xu, S.-Y., *et al.*, 2015a, Nat. Phys. **11**, 748.
Xu, S.-Y., *et al.*, 2015b, Science **349**, 613.
Xu, S.-Y., *et al.*, 2015c, Science **347**, 294.
Xu, Y., F. Zhang, and C. Zhang, 2015, Phys. Rev. Lett. **115**, 265304.
Yamakage, A., K. Nomura, K.-I. Imura, and Y. Kuramoto, 2011, J. Phys. Soc. Jpn. **80**, 053703.
Yamakage, A., K. Nomura, K.-I. Imura, and Y. Kuramoto, 2013, Phys. Rev. B **87**, 205141.
Yamakage, A., M. Sato, K. Yada, S. Kashiwaya, and Y. Tanaka, 2013, Phys. Rev. B **87**, 100510.
Yamakage, A., Y. Yamakawa, Y. Tanaka, and Y. Okamoto, 2015, arXiv:1510.00202.
Yang, B.-J., T. Morimoto, and A. Furusaki, 2015, Phys. Rev. B **92**, 165120.
Yang, B.-J., and N. Nagaosa, 2014, Nat. Commun. **5**, 4898.
Yang, S. A., H. Pan, and F. Zhang, 2014, Phys. Rev. Lett. **113**, 046401.
Yao, H., and S. Ryu, 2013, Phys. Rev. B **88**, 064507.
Ye, M., J. W. Allen, and K. Sun, 2013, arXiv:1307.7191.
You, Y.-Z., Y. BenTov, and C. Xu, 2014, arXiv:1402.4151.
You, Y.-Z., and C. Xu, 2014, Phys. Rev. B **90**, 245120.
Young, M. W., S.-S. Lee, and C. Kallin, 2008, Phys. Rev. B **78**, 125316.
Young, S. M., and C. L. Kane, 2015, Phys. Rev. Lett. **115**, 126803.
Young, S. M., S. Zaheer, J. C. Y. Teo, C. L. Kane, E. J. Mele, and A. M. Rappe, 2012, Phys. Rev. Lett. **108**, 140405.
Yu, R., X. L. Qi, A. Bernevig, Z. Fang, and X. Dai, 2011, Phys. Rev. B **84**, 075119.
Yu, R., H. Weng, Z. Fang, X. Dai, and X. Hu, 2015, Phys. Rev. Lett. **115**, 036807.
Yu, R., W. Zhang, H.-J. Zhang, S.-C. Zhang, X. Dai, and Z. Fang, 2010, Science **329**, 61.
Zahid Hasan, M., S.-Y. Xu, and M. Neupane, 2014, arXiv:1406.1040.
Zak, J., 1989, Phys. Rev. Lett. **62**, 2747.
Zareapour, P., *et al.*, 2012, Nat. Commun. **3**, 1056.
Zeng, M., C. Fang, G. Chang, Y.-A. Chen, T. Hsieh, A. Bansil, H. Lin, and L. Fu, 2015, arXiv:1504.03492.
Zhang, C., *et al.*, 2015, arXiv:1503.02630.
Zhang, F., and C. L. Kane, 2014a, Phys. Rev. B **90**, 020501.
Zhang, F., and C. L. Kane, 2014b, Phys. Rev. Lett. **113**, 036401.
Zhang, F., C. L. Kane, and E. J. Mele, 2013a, Phys. Rev. Lett. **111**, 056403.
Zhang, F., C. L. Kane, and E. J. Mele, 2013b, Phys. Rev. Lett. **111**, 056402.
Zhang, H., H. Huang, K. Haule, and D. Vanderbilt, 2014, Phys. Rev. B **90**, 165143.
Zhang, Q., Y. Cheng, and U. Schwingenschlögl, 2015, Sci. Rep. **5**, 8379.
Zhang, R.-X., and C.-X. Liu, 2015, Phys. Rev. B **91**, 115317.
Zhao, Y. X., and Z. D. Wang, 2013, Phys. Rev. Lett. **110**, 240404.
Zhao, Y. X., and Z. D. Wang, 2014, Phys. Rev. B **89**, 075111.
Zirnbauer, M. R., 1992, Phys. Rev. Lett. **69**, 1584.
Zirnbauer, M. R., 1996, J. Math. Phys. (N.Y.) **37**, 4986.
Zyuzin, A. A., and A. A. Burkov, 2012, Phys. Rev. B **86**, 115133.